CIVIL ENGINEERING STUDIES
HYDRAULIC ENGINEERING SERIES NO. 13

EXPERIMENTAL AND THEORETICAL STUDY OF MOTION OF A BARGE AS MOORED IN OCEAN WAVES

by
BRUCE J. MUGA

sponsored by
U. S. NAVAL CIVIL ENGINEERING LABORATORY
PORT HUENEME, CALIFORNIA

DEPARTMENT OF CIVIL ENGINEERING
UNIVERSITY OF ILLINOIS
URBANA, ILLINOIS
January 1967

EXPERIMENTAL AND THEORETICAL STUDY OF MOTION OF A BARGE AS MOORED IN OCEAN WAVES

BY

BRUCE J. MUGA

Sponsored by
U. S. NAVAL CIVIL ENGINEERING LABORATORY
PORT HUENEME, CALIFORNIA

DEPARTMENT OF CIVIL ENGINEERING
UNIVERSITY OF ILLINOIS
URBANA, ILLINOIS

October 1966

ACKNOWLEDGMENTS

The author wishes to acknowledge the interest and encouragement of Mr. J. T. O'Brien of the U. S. Naval Civil Engineering Laboratory, Port Hueneme, California; of Mr. M. L. Hilleger of the Naval Ordnance Test Station, Pasadena, California, who was instrumental in initiating this study; of Professor J. M. Robertson who reviewed the manuscript; and of Dr. Ven Te Chow, graduate adviser and doctoral committee chairman, who participated in many stimulating discussions and guided the preparation of a doctoral thesis which constitutes this report.

The author expresses his appreciation to the following colleagues: Messrs. Kenneth Mears, Floyd Nelson, and Wilber Hoffman of the U. S. Naval Civil Engineering Laboratory, for installing the instruments on and collecting the data from the Fishhook prototype barge; and Mr. Naresh Maniar for conducting the model tests and collecting the data therefrom.

The author wishes to thank Messrs. Glen Stout and Marvin Clevinger of the Meteorology Laboratory, Illinois State Water Survey, for use of the prototype data reduction equipment. He wishes to thank Messrs. Fred Lehnhardt and Nathan Shoemaker and Mrs. Melba J. McFarland of the U. S. Naval Civil Engineering Laboratory for the laborious correction of the model data.

The author wishes to acknowledge the use of the computer facilities provided for this study by the University of Illinois Graduate College Research Board and the U. S. Naval Civil Engineering Laboratory, whose generous support made the study possible.

TABLE OF CONTENTS

LIST OF ILLUSTRATIONS

LIST OF TABLES

INTRODUCTION

The problems associated with raising and lowering heavy loads in the deep ocean have received increasing attention during recent years as a result of the need to carry out a wide range of operations demanding varied capabilities in the deep ocean environment. This attention stems from two factors: the numerous successful drilling operations conducted from surface ships over the past 10 years, including the preliminary "Project Mohole" activities, and second, the difficulties encountered or anticipated in the placement and recovery of instrumented packages, including nuclear reactors, and other military systems on the ocean floor.

For studies reflecting this interest in deep sea operations, it is useful to classify the hydrodynamic problems of raising and lowering heavy loads into the arbitrary categories of (1) surface and near-surface, (2) intermediate-depth, and (3) bottom and near-bottom.

Bottom and near-bottom problems include the placement and recovery of the load with a definite degree of precision and safety on or from a semiplastic or rigid foundation. Terminal velocities and the oscillation of a body are suggestive of intermediate-depth problems. Surface and near-surface problems consist of those related to the submergence and withdrawal of an object of arbitrary shape from a fluid bounded by a randomly moving free surface. The purpose of this study is to investigate one of the problems in this latter category, namely, to determine the response of a construction-type barge to irregular waves when moored in the open ocean.

Ships of conventional design seldom operate at practically zero speed in significant waves. Routine operation of this kind is restricted mainly to weather and survey vessels engaged in making certain observations and measurements. As a consequence, only a trivial amount of data has been published on the motions of ships in general at zero speed. Zero-speed studies of models in the laboratory are difficult to conduct because of the requirement to eliminate wave reflections from the tank sides. Data on the behavior of moored ships, barges, and special-purpose platforms is scarcer even than that for models. Nevertheless, the recent demands for deep ocean construction underline the need for knowledge in this area. The present study is intended to contribute pertinent information.

Since it was necessary to arrive at some preliminary engineering estimates on the behavioral response of the barge being considered as a subject as well as to determine how far these estimates might be in error, it was decided to conduct a combination prototype, model, and theoretical study. The need to compare the results of prototype measurements with those obtained from model or theoretical calculations is obvious. On the other hand, the need for conducting both a model and a theoretical study is perhaps not obvious and requires additional comment. Direct comparison of the model and theoretical results yields an indication of the limits of the linear theory of the overall investigation. Furthermore, both

the model and the theoretical study permit predictions to be made under carefully controlled conditions over a wide range of characterizing parameters, whereas the prototype study is necessarily limited to only a few situations of interest.

In summary, the present study consists of:

1. Analysis of the measurements of the motions and forces induced on an instrumented prototype barge by irregular waves as moored in the open Pacific Ocean in approximately 160 feet of water off San Clemente Island.
2. Analysis of the measurements of the motions and forces induced on a dynamically similar reduced-scale model barge by irregular waves as moored in tank No. 2 (75 by 75 feet) at Stevens Institute of Technology, Hoboken, New Jersey.
3. Theoretical determination of the response of the barge to representative sea states by application of the linear theory of ships' motions.

A study of the motion of a ship with 6 degrees of physical freedom excited by waves is a formidable problem for which a complete solution has not yet been achieved. Moreover, maintenance of the historical position of the barge by means of the mooring restraints further complicates the immediate motion problem.

The endurance life of the moorings is dependent upon the long-term distribution of the stress variations. Therefore, a determination of the probable environmental level (excitation) to which the barge will be subjected over a specified period will permit an estimate of the "maximum load response spectrum" to be made. This information together with a knowledge of the load endurance capability of the moorings provides a basis from which the service life of the moorings can be evaluated.

The present study is, therefore, a determination and comparison of the response of a construction-type barge moored in irregular waves as obtained from (1) prototype measurements, (2) model measurements, and (3) theory. It also includes a prediction of the probable excitation as obtained from the historical weather data and an evaluation of the performance of the moorings.

THE PROTOTYPE

The craft studied is a special-purpose construction-type platform serving as a missile recovery vessel at the Polaris "Pop-Up" Variable Depth Launch Facility. This test facility is located on the northwest coast of San Clemente Island 65 miles off the coast of Southern California (Figure 1). Under the management of the Naval Ordnance Test Station (NOTS), it provides means for conducting instrumented launching and retrieval of the missile in flight. NOTS has designated the craft, the subject of this study, as Fishhook.

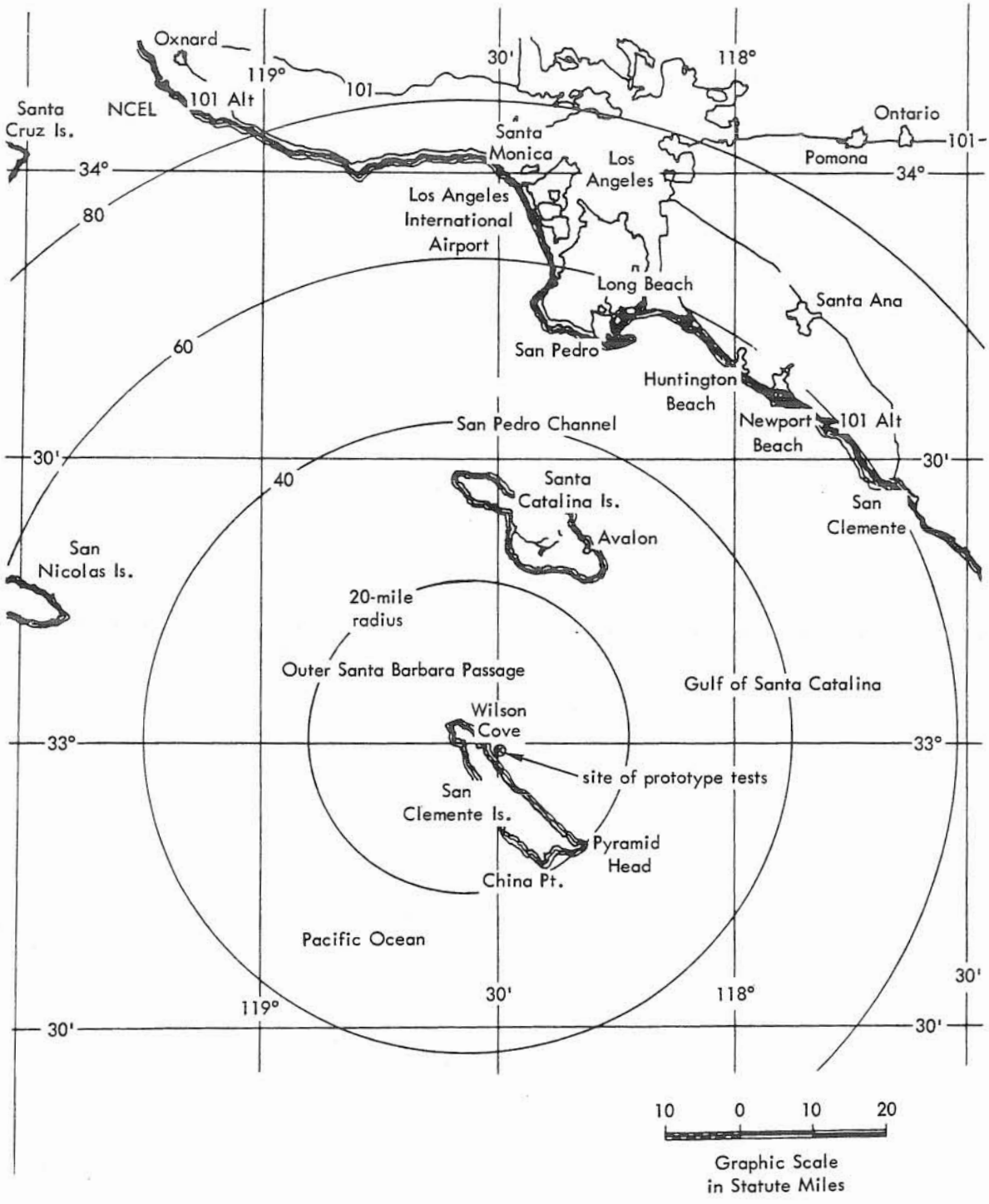

Figure 1. General location plan.

The Fishhook, details of which are shown in Figures 2 and 3, was built at the Long Beach Naval Shipyard, Long Beach, California. The hull outline is that of two standard (34 by 110 feet) Navy lighter barges (YFNB) separated by a distance of 22 feet. Forward (toward the bow) of Frame 5*, there is a catamaran center section which provides additional buoyancy, while aft (toward the stern) of Frame 5 the barges are tied together by the structural framework supporting the recovery mechanism. This open framework provides a center well which permits the measurement of water level variation near the center of gravity. The composite platform supports a 185-foot recovery tower whose mass distribution gives the Fishhook some unusual, if not unique, architectural characteristics. As shown in Figure 2, the Fishhook has a length of 110 feet, an extreme breadth of 90 feet, and a mean draft of 5 feet. Other characteristics of the moored-barge system, including displacement (850 long tons), are given in Table 1.

The craft is moored in approximately 163 feet of water by four 2-1/2-inch die-lock chains. These chains, which vary in length from 496 feet to 736 feet, are anchored to stake piles implanted in the ocean floor by drilling and grouting. In addition, an 18,500-pound cast-iron sinker has been attached to each mooring chain by means of a ground ring located at a point about one-third of the distance from the stake pile to the barge. The geometry of the moorings is given in Figure 4 and summarized in Table 2. (The dominant wind and wave directions for the periods selected for analysis are also given in Figure 4.) The 2-1/2-inch die-lock chain has a proof breaking load when new of approximately 492 kips. (Further data on the mooring chains is presented in Figure 53.) It is sufficient to point out here that from measurements of the chain geometry, the total tension in the chains can be calculated for the equilibrium position and compared to that measured when the craft is in essentially calm water. From these calculations, the craft can be displaced analytically, and the restoring forces and moments calculated. The moorings are ineffective against heave, pitch, and roll. A photograph of the Fishhook on location is shown in Figure 5.

Data Pickup

The location of all recording instruments is indicated in Figure 2. Pickups were as follows: four chain tensions, seven accelerations, two angular displacements (roll and pitch), one wind velocity, three water levels, and three water pressures.

*To aid in identifying locations on marine craft, it is customary to assign frame numbers to the main structural ribs, beginning with 0 at the bow and numbering sequentially toward the stern. Distance between frame numbers (as shown in Figure 2) is approximately 7 feet.

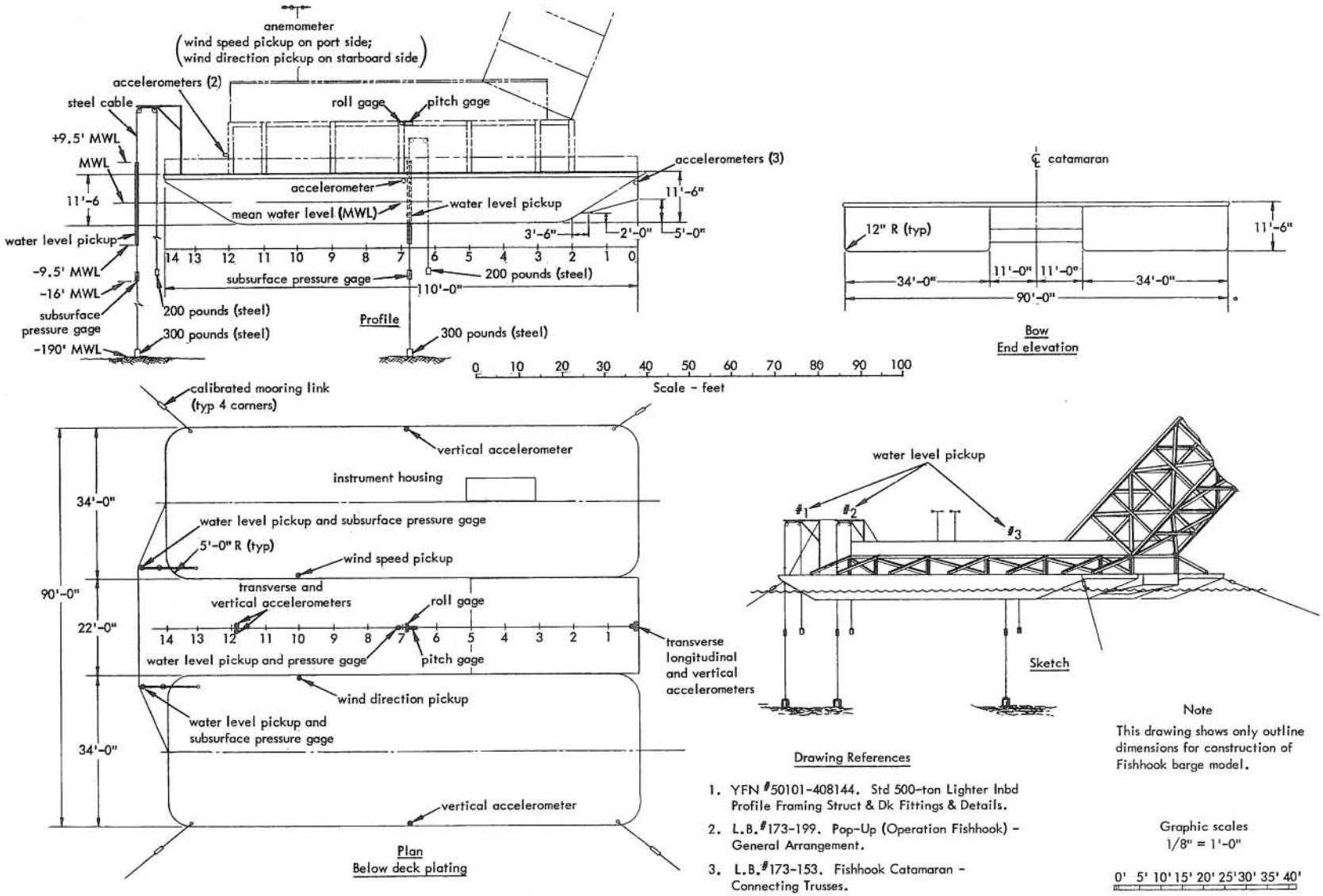

Drawing References

1. YFN #50101-408144. Std 500-ton Lighter Inbd Profile Framing Struct & Dk Fittings & Details.
2. L.B.#173-199. Pop-Up (Operation Fishhook) - General Arrangement.
3. L.B.#173-153. Fishhook Catamaran - Connecting Trusses.

Note

This drawing shows only outline dimensions for construction of Fishhook barge model.

Graphic scales
1/8" = 1'-0"

0' 5' 10' 15' 20' 25' 30' 35' 40'

Figure 2. Fishhook prototype barge - plan and elevation.

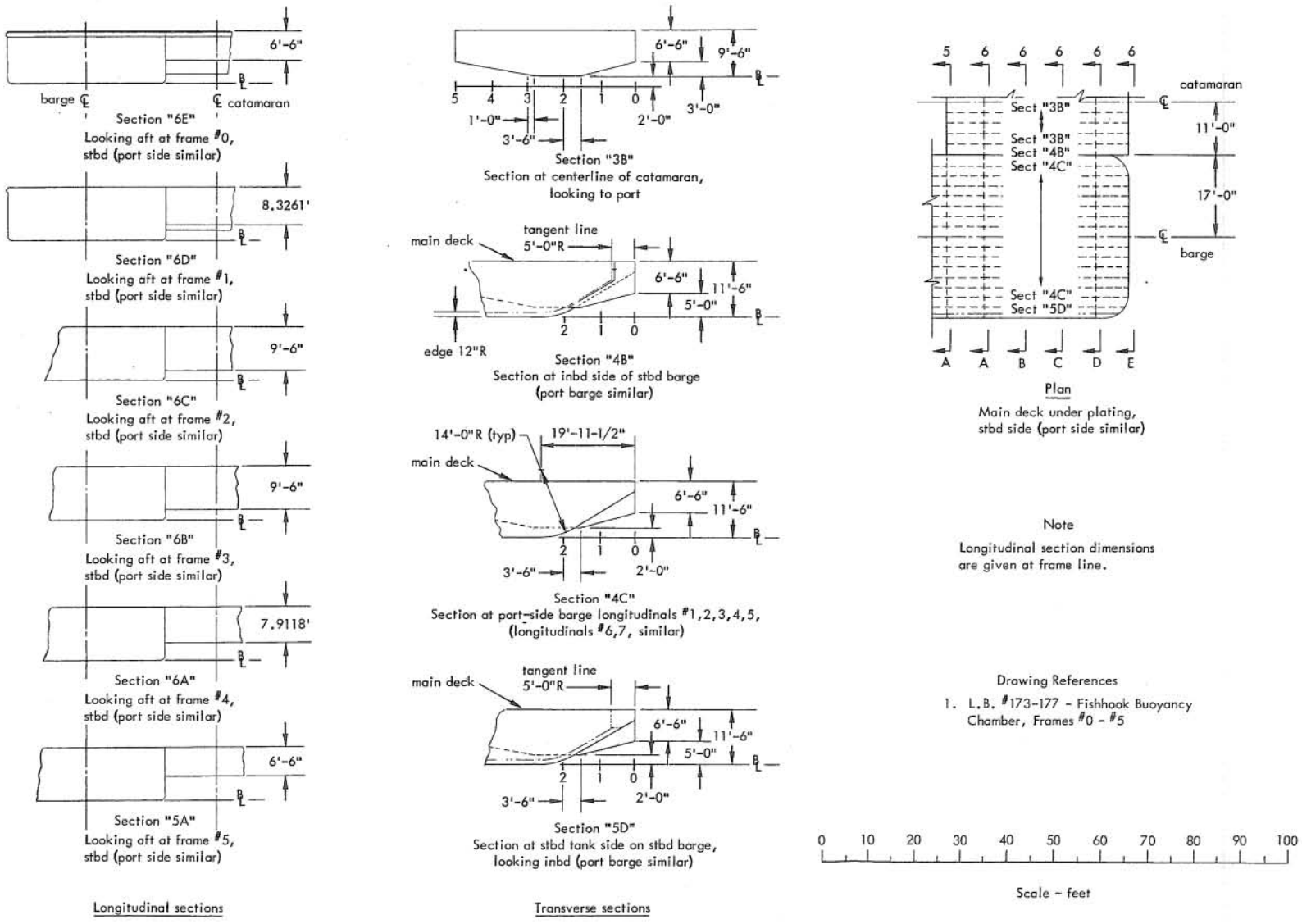

Figure 3. Fishhook prototype barge - transverse and longitudinal sections.

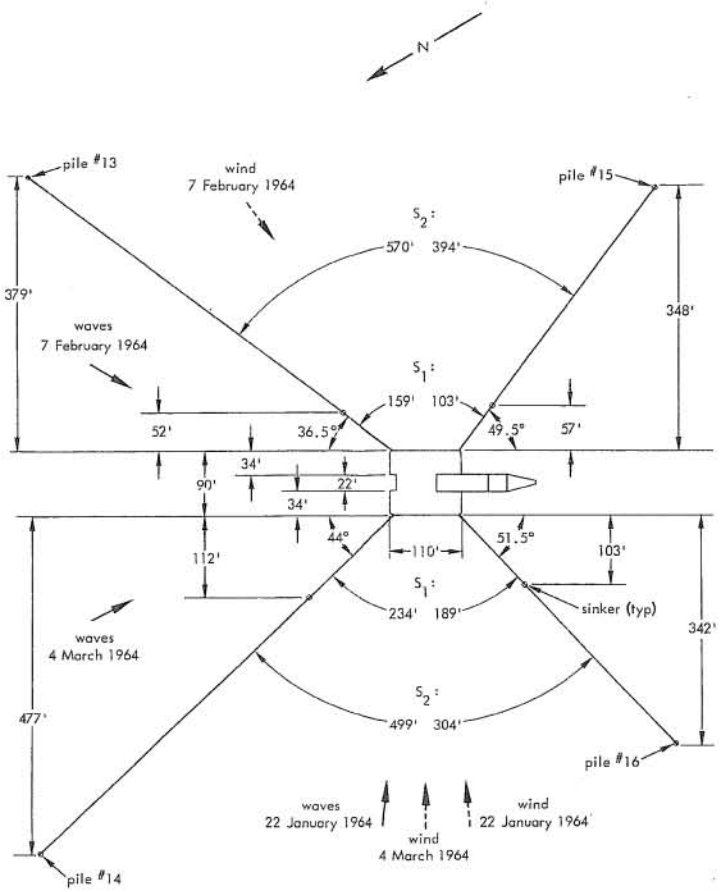

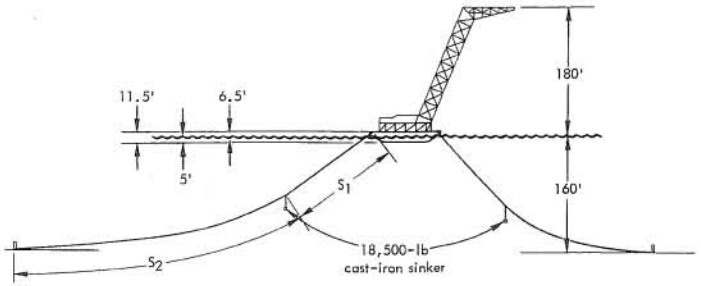

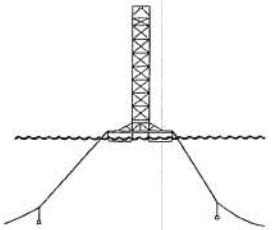

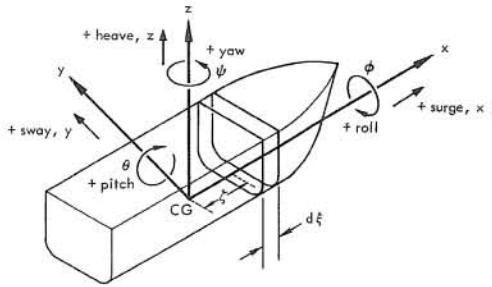

Coordinate system employed in study
(right-hand notation)

S_1 = upper chain length
S_2 = lower chain length

0 100 200 300 400 500
Scale - feet

Figure 4. Mooring plan, exciting wind and wave directions, and sketches of coordinate system and catenary profile of Fishhook prototype barge as moored off San Clemente Island.

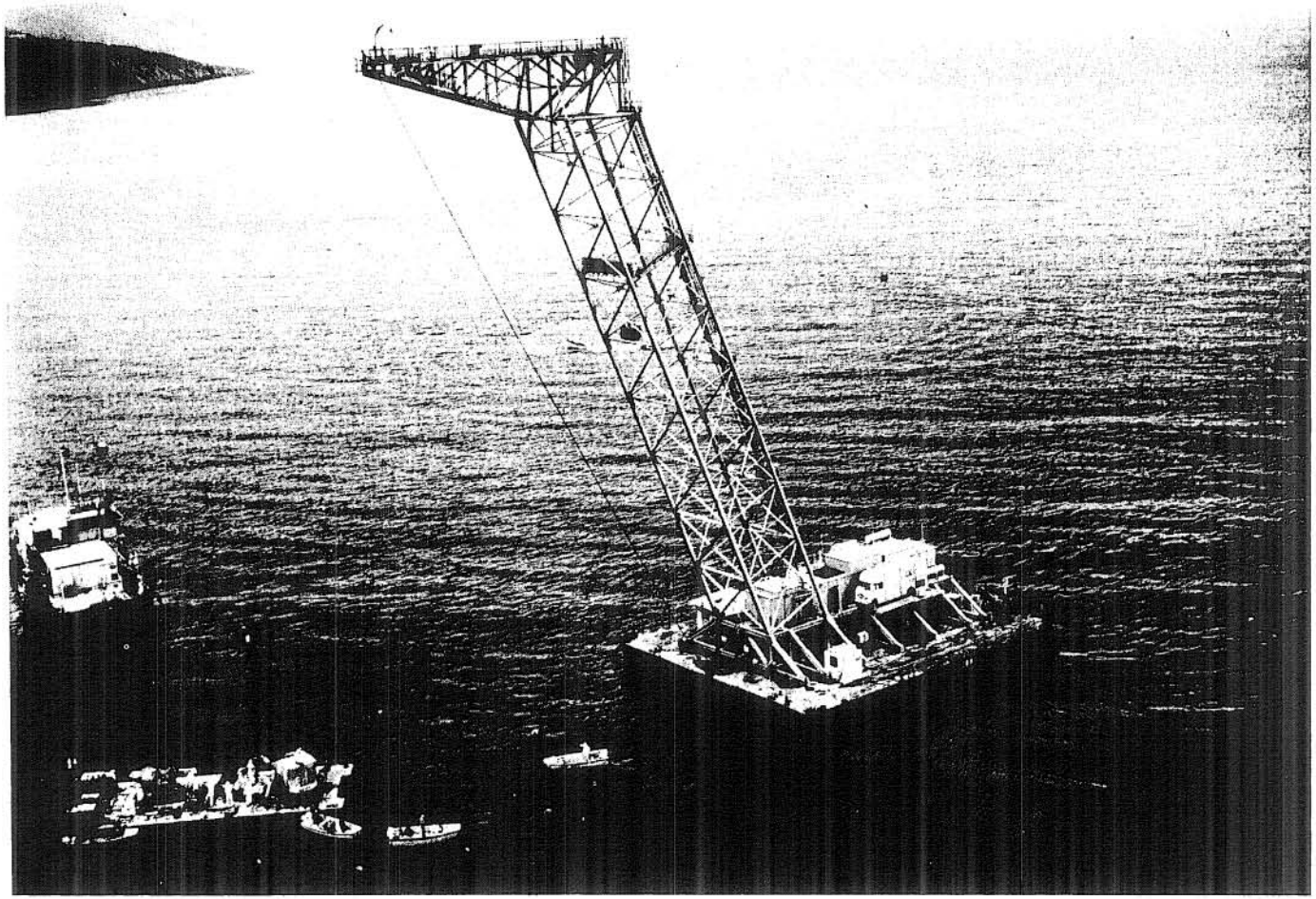

Figure 5. Fishhook prototype barge on location.

Table 1. Numerical Values of the Moored-Barge System

Characteristic	Measure
Length, L	110.00 ft
Beam, B	90.00 ft
Draft, mean	5.00 ft
Vertical distance from center of buoyancy to center of gravity	17.28 ft
Vertical distance from free surface to center of gravity	14.95 ft
Vertical distance from center of gravity to keel	19.95 ft
Longitudinal metacentric height	167.50 ft
Transverse metacentric height	180.00 ft
Displacement	850.00 long tons
Weight, W	1.870×10^6 lb
Mass, m	58.075×10^3 slugs
Pitch moment of inertia, $I_{y_o} = mk_{yo}^2$	1.296×10^8 slugs-ft^2
Yaw moment of inertia, $I_{z_o} = mk_{zo}^2$	1.130×10^8 slugs-ft^2
Roll moment of inertia, $I_{x_o} = mk_{xo}^2$	9.590×10^7 slugs-ft^2
Total roll moment of inertia (including added inertia due to fluid), I_{x_t}	3.160×10^8 slugs-ft^2
Surge period, T_{surge}	≈36.0 sec (model)
Sway period, T_{sway}	≈36.0 sec (model)
Heave period, T_{heave}	6.1 sec
Pitch period, T_{pitch}	6.5 sec
Natural roll period, T_{roll}	6.1 sec
Effective mooring system spring constants:	
Surge, k_x	3.073 kips/ft
Sway, k_y	3.576 kips/ft
Yaw, k_ψ	8.940×10^3 kips-ft/rad
Depth of barge	5.00 ft

Table 2. Summary of Mooring Dimensions

Stake Pile No.	Connects to	Upper Chain Length S_1 (ft)	Lower Length Chain S_2 (ft)	Total Chain Length L* (ft)	Coordinate Horizontal Distance x (ft)	Coordinate Vertical Distance y (ft)	Measured Initial** Tension (kips)	Computed Initial Tension (kips)	Horizontal Force Components (kips)			Vertical Component F_v (kips)
									F_x (total)	F_x Surge	F_x Sway	
13	Port aft	159	570	732	676.4	191	36.2	36.7	26.6	-19.6	+18.3	25.2
14	Stbd aft	234	499	736	685.3	166	30.9	29.8	21.1	-15.2	-14.7	21.1
15	Port fwd	103	394	500	446.9	178	32.8	34.6	25.0	+17.0	+18.3	23.9
16	Stbd fwd	189	304	496	433.3	178	46.0	40.5	28.2	+17.8	-21.9	29.0

* L is the total length of the chain, ($L = S_1 + S_2 + 3$ feet); the ground ring has a nominal diameter of 3 feet.

** Tensions were measured during periods of calm, but currents may have been present. Measured tensions are not in equilibrium.

Sea State

Sea state was measured at three locations (see Figure 2) relative to the barge by both water level gages and subsurface pressure pickups. The locations were those designated starboard stern, port stern, and center well. The water level gages consisted of two parallel 1/16-inch-diameter steel wires spaced 1 foot apart. These wires extended vertically from an anchor on the ocean bottom through two sheaves to a suspended counterweight. As part of an energized electrical circuit, the wires sensed changes in capacitance due to variations in water level. Calibration was accomplished by raising and lowering the anchor wire assembly by certain fixed increments in calm water. The subsurface pressure pickups each consisted of a potentiometer-transducer as a pressure sensor to convert subsurface pressure fluctuations into an electrical signal. These pickups were suspended approximately 20 feet below the mean water level from the anchor wire assembly. Conventional in type, they responded to variations in the water level with an attenuation of certain components of the wave spectrum which is dependent on depth and easily determined from the calibration curve. Wave direction was not measured; rather, it was observed visually from the shore and neighboring barges.

Ship Motion

The angular displacements, roll and pitch, were measured by pickups each consisting of a wiper fastened to a free pendulum backed by a potentiometer such that, as the ship rolled or pitched, the pendulum tended to remain stationary while the potentiometer rode back and forth across the wiper. The wiper-potentiometer constituted an electrical circuit which when energized produced an electrical output proportional to the angular displacement. The pickups were located amidships, in the center well section near the vertical line passing through the center of gravity which is located 52.73 feet aft of the bow and 19.95 feet above the bottom of the craft.

Ship Acceleration

Acceleration was measured by seven linear accelerometers mounted in gimbals. Three were installed along the barge centerline 52.5 feet forward of the center of gravity to measure, respectively, acceleration in the vertical, longitudinal, and transverse directions. Two were installed on the centerline 42.4 feet aft of the center of gravity to measure acceleration in the vertical and transverse directions. Data from the pair of vertical and transverse accelerometers have been used to obtain the heave and pitch and sway and yaw spectra, respectively. Since the accelerometers were located on the centerline and mounted in gimbals, data from the longitudinal accelerometer could be used to obtain the surge spectra. Contributions to longitudinal acceleration from pitching and yawing motions may be considered trivial.

Two more accelerometers were installed on the port and starboard amidships centerline to measure acceleration in the vertical. Data from these two pickups have been used to obtain the heave and roll spectra, with the pitch contribution to vertical acceleration assumed to be negligible (i. e., the pitch point being assumed as constant and located at the amidships centerline). The accelerometers were mounted on plates welded directly to the inside skin plate of the barge or to the structural framework as shown in Figure 2. In theory, all accelerometers are continuously sensitive over their design range. In practice, however, accelerations less than approximately ±0. 01 g are hidden within the spurious "noise" signals of other instrument components.

Mooring Forces

Forces in the mooring chains were measured by calibrated links (2-1/2-inch die-lock) inserted in the chains (see Figure 6). Four strain gages were bonded to each link and so arranged as to form an electrical bridge. The instrumented link was made part of a three-link assembly consisting of two detachable links and the instrumented link in the center. This assembly after waterproofing and calibration in a static testing machine was incorporated in the mooring chain. Calibration indicated that the relationship between electrical output and load was significantly linear over the range of forces encountered in this study. Periodically, the mooring lines were slackened by a barge crane to obtain a no-load reading as a means of defining the zero point on the mooring force record.

The inclination of the chain from the vertical was not recorded continuously. However, it was measured periodically by means of a plumb bob and an ordinary carpenter-type level.

Wind Velocity

Wind velocity was measured by means of a recording selsyn-type anemograph located above the instrument housing as shown in Figure 2. The speed-measuring component is a ring to which are fastened cups such that the incident wind causes a slight torque in the shaft holding the ring. This torque is reflected as a speed output in an electrical circuit. A conventional vane is used as a wind-direction pickup with its output part of the same electrical circuit as the speed output.

Current Velocity

Current speed was measured periodically with a Roberts meter. Current velocity at the surface was measured periodically both by visual means and by photography which recorded observations on floating debris such as garbage and wooden blocks.

Data Transmission and Recording

Data Transmission. Data transmission from all pickups, except wind, was by means of multiconductor waterproof electrical cables. These generally ran under the barge or through the flotation chambers to the center well and thence to the instrument housing. Data transmission from the wind pickup was self-contained within the anemograph (Bendix-Frieze).

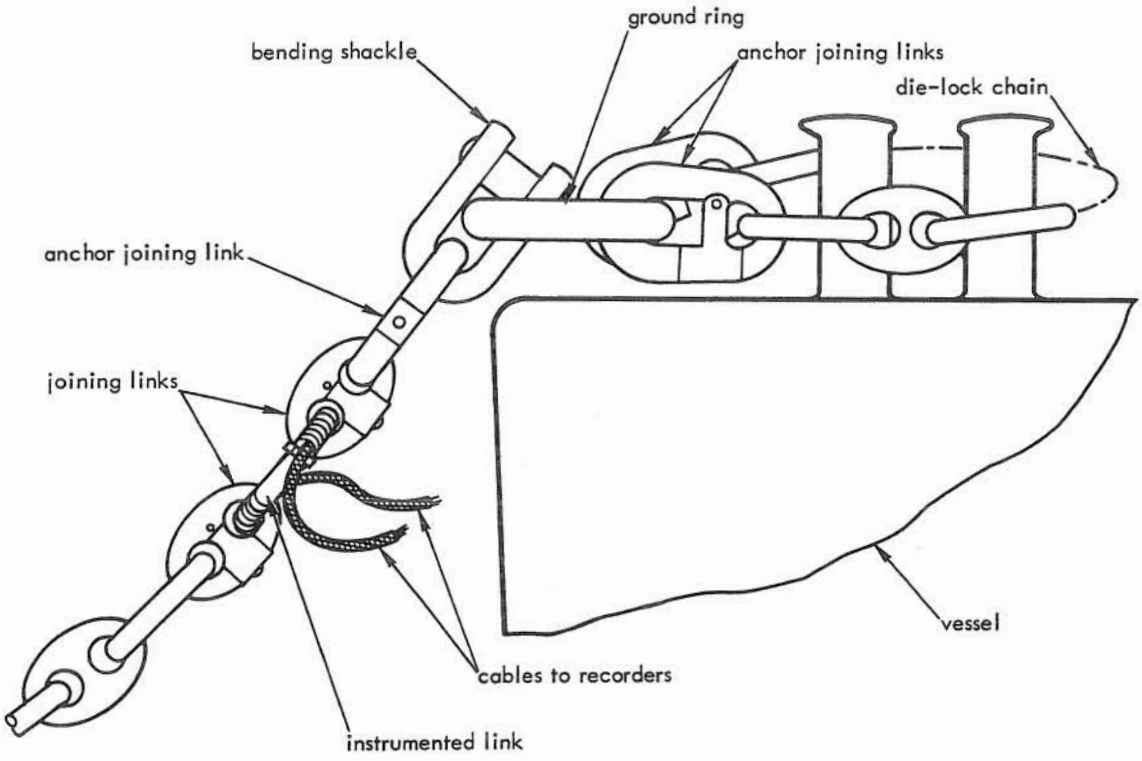

Figure 6. Sketch of mooring-chain tension pickup.

Data Recording. The data output of the wind velocity pickup was recorded on a direct writing-type oscillograph which was part of the anemograph. A facsimile of the wind data output is shown in Figure 7. The data output of the remainder of the pickups was recorded on two standard photographic-type recorders, a facsimile of which is shown in Figure 8. The oscillographs were operated during periods of high wave excitation and recorded up to 19 channels of information to the same time base.

THE MODEL

Description

Moored model tests of the Fishhook barge were performed to obtain the time history records of motions, accelerations, and mooring line tensions under the action of surface gravity-type irregular water waves. A 1:32-scale model of the barge, shown in Figure 9, was built to the full-scale characteristics given in Table 3.

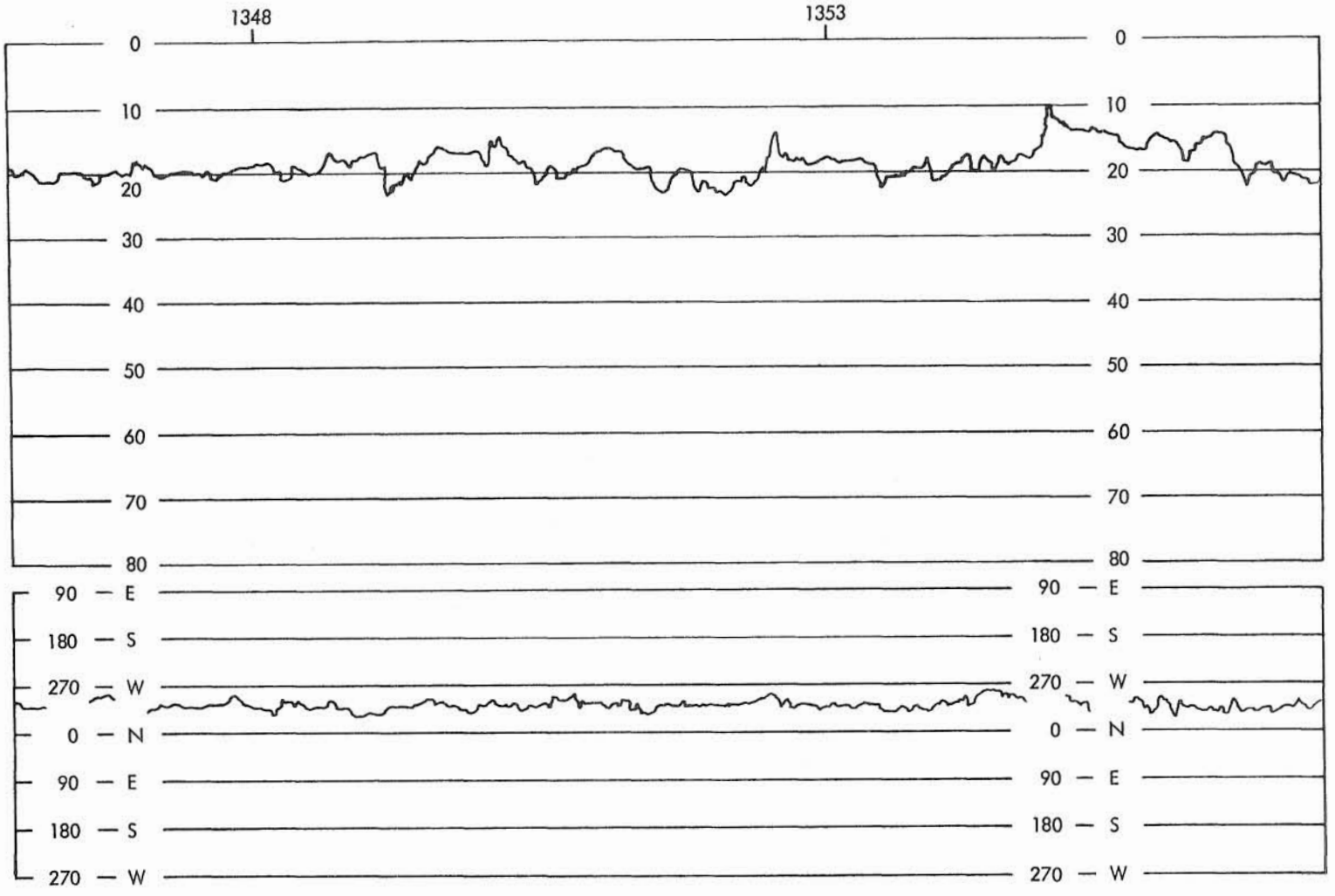

Figure 7. Facsimile of wind speed and direction oscillogram for 4 March 1964.

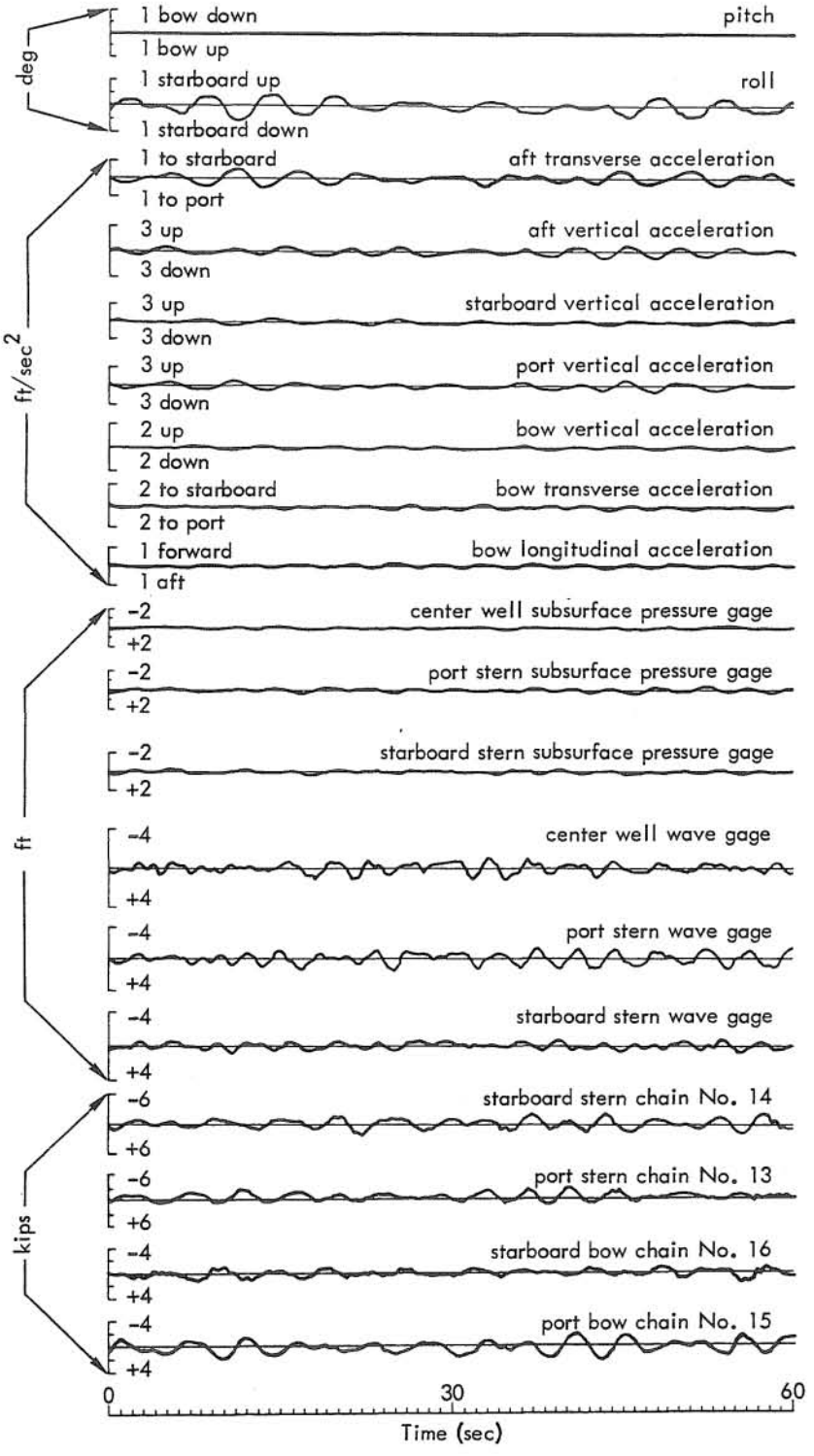

Figure 8. Facsimile of oscillogram of motions and forces for 7 February 1964.

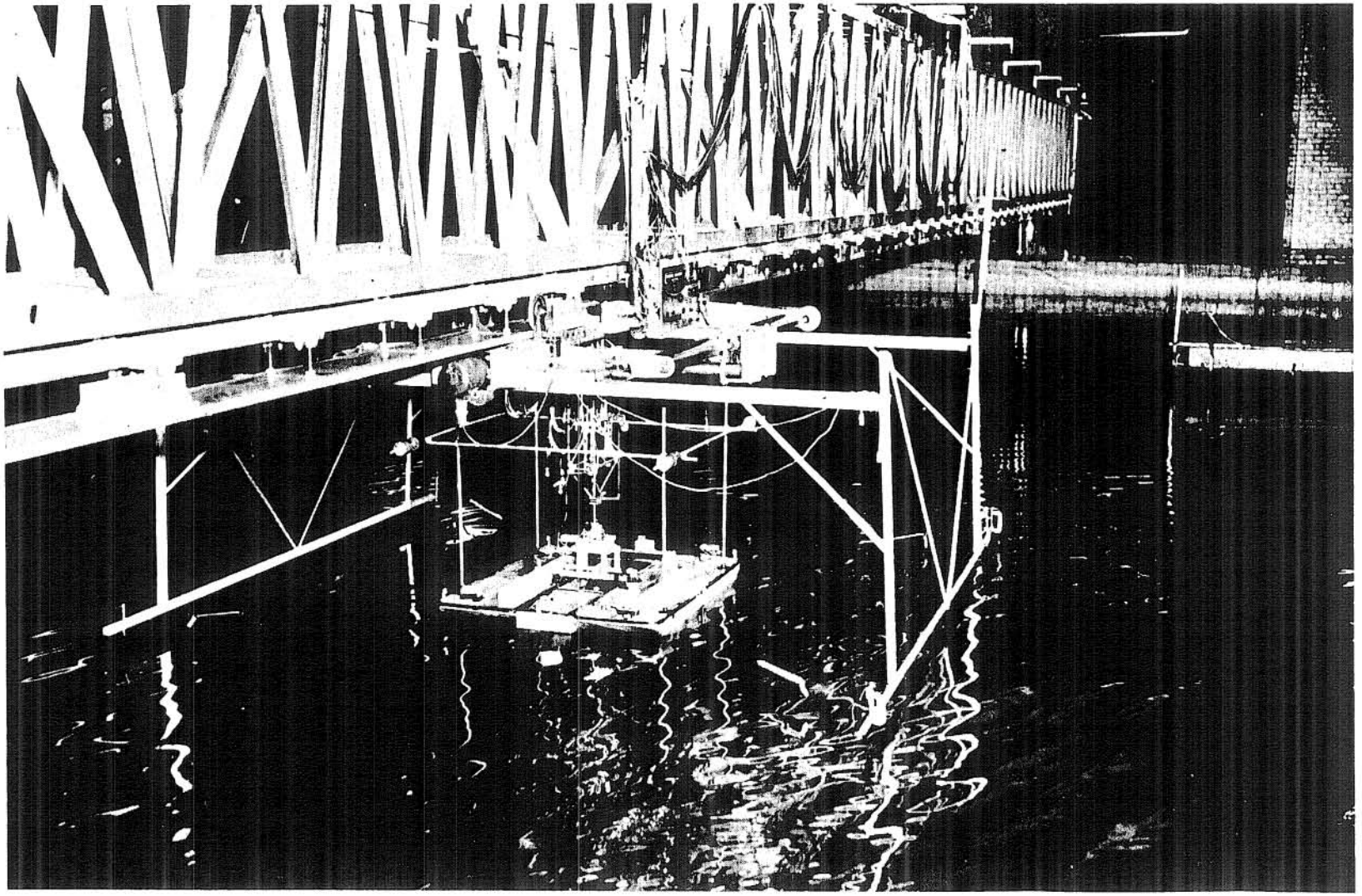

Figure 9. Scale model (1:32) of Fishhook prototype barge, wave tank No. 2, Stevens Institute of Technology, Hoboken, New Jersey. (Photograph courtesy of Davidson Laboratory, Stevens Institute of Technology.)

Table 3. Characteristics of Fishhook Prototype Barge to Which the Model was Constructed and Ballasted

Model Scale: 1:32	
Length on 14 stations	110.0 ft
Beam overall	90.0 ft
Beam on single hull	34.0 ft
Hull spacing	22.0 ft
Depth	11.5 ft
Displacement (salt water)	853 long tons
Mean draft	5.0 ft
Longitudinal center of gravity from bow	52.67 ft
Vertical center of gravity from barge bottom	27.73 ft (required: 19.95 ft)
Natural period of roll	6.1 sec
Natural period of pitch	6.1 sec (required: 6.5 sec)

It should be noted that the vertical center of gravity (VCG), the longitudinal gyradius, and the natural pitch period do not agree with those required to simulate the full-scale prototype. Originally, the model was ballasted to the required VCG and the longitudinal gyradius; however, in that condition the natural pitch period was much lower than required. It was decided to sacrifice the VCG and the longitudinal gyradius requirements and to ballast the model to the required period. Due to physical limitations in locating the ballast weights, a slightly lower pitch period than required was accepted. The locations of the accelerometers on the model are given in Table 4.

Tests

The model was tested in three positions with the waves approaching stern-on, off the starboard beam, and four points (45 degrees) abaft the port beam. Model positions and layout of the mooring lines with their spring constants and initial tensions are given in Figure 10.

Due to limitations in positioning the bridge carrying the model carriage, the model could not be located so that the waves approached from four points abaft the starboard beam. It had to be located so that the waves approached from the port side. In order to simulate the conditions of waves approaching from starboard as far as the mooring lines were concerned, the locations of the port and starboard lines were interchanged. The locations of the model and the wave probes are given in Figure 11.

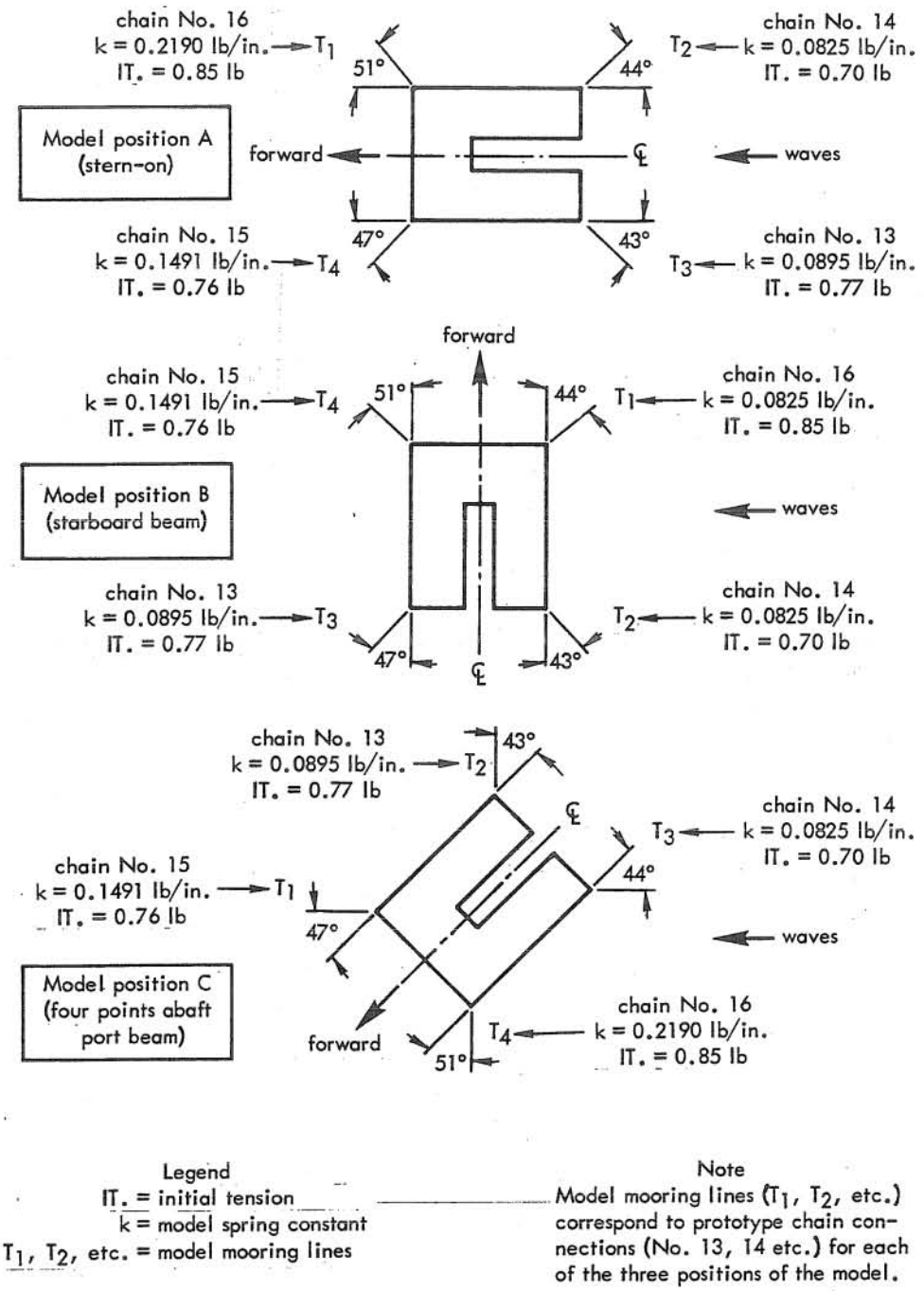

Figure 10. Mooring-line layout for the three positions of the model.

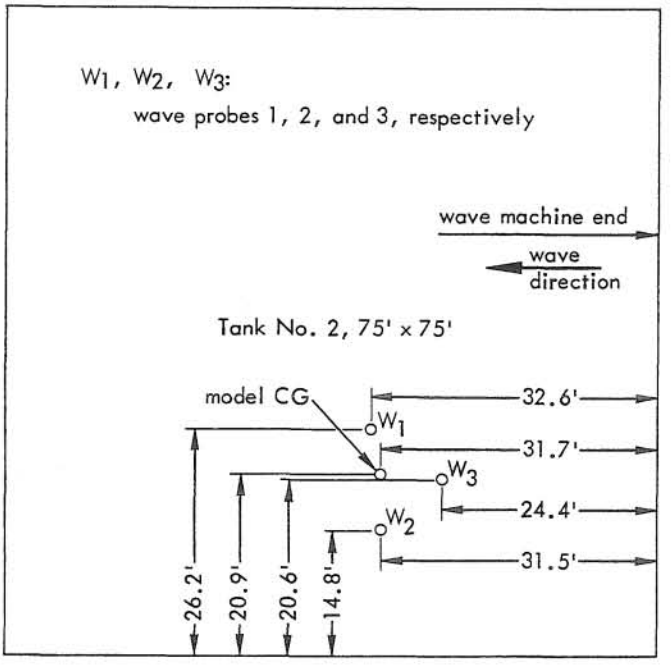

Figure 11. Location of model and wave probes in tank No. 2, Stevens Institute of Technology, Hoboken, New Jersey.

Table 4. Locations of Accelerometers on the Model

Acceleration	Longitudinal Position From Midship (in.)	Transverse Position From Centerline (in.)	Vertical Position Above Deck (in.)
Bow vertical	19.53 fwd	on centerline	0.8
Stern vertical	19.68 aft	on centerline	0.8
Port vertical	1.40 fwd	16.23 port	0.8
Bow longitudinal	18.88 fwd	on centerline	1.25
Stern longitudinal	18.48 aft	on centerline	1.00
Port longitudinal	1.33 aft	16.23 port	0.50
Bow transverse	20.13 fwd	1.3 port	1.25
Stern transverse	20.08 aft	1.3 port	1.00
Port transverse	0.28 aft	15.18 port	0.50

The irregular waves used in the test had an average equivalent prototype height of 3.1 feet and a period of 6.2 seconds. This corresponded to a sea state 4 (Neumann wind velocity model). Measurements were recorded by a direct-writing eight-channel oscillograph and on a nine-channel magnetic tape recorder. A facsimile of the oscillogram for one run is shown in Figure 12. Calibration constants were noted directly on the oscillogram paper and on the voice channel (Channel No. 1) of the magnetic tape. Since 22 measurements were required (3 wave probes, 6 linear displacement pickups, 4 dynamometers, and 9 accelerometers), it was necessary to reproduce the identical wave record. To provide a check on the reproducibility of the generated random irregular exciting wave, two of the wave probes and the heave pickup were monitored during each run. Four runs were required to record each of the pickups at least once.

Motion picture film (16-mm) was taken of the model with the waves approaching from four points abaft the port beam.

ANALYSIS OF PROTOTYPE AND MODEL DATA

The time series technique is the basis for the analysis of the experimental data. Though complicated, this technique is widely documented in the related literature. The calculation of spectra and cross-spectra constitutes an essential first step in the analysis of any time series data. Any further reduction of the data can be referred to this basic calculation. Therefore, only a brief outline of the formulation of the method is given here.

Consider a set of functions of time, $x(t)$, $y(t)$, $z(t)$, . . . In the immediate problem, these are water level variations, chain tensions, accelerations . . . The series to be considered is not the continuous functions $x(t)$, $y(t)$, $z(t)$, but rather certain discrete sets of observations obtained from them, one observation for every time unit, which in this problem is approximately one observation per second in real time. Thus, consider a set of p series of n observations. Initially, the means, $\langle x \rangle$, $\langle y \rangle$, $\langle z \rangle$, . . . , of the series are calculated. Then the lagged auto- and cross-covariances of the series are calculated.

Auto-covariance for lag, $\ell = 0, 1, 2, \ldots m$, is

$$c_{xx}(\ell) = \frac{1}{n} \sum_{s} (x_s - \langle x \rangle)(x_{s+\ell} - \langle x \rangle)$$

Cross-covariance of $x(t)$, $y(t)$, for lag, $\ell = 0, 1, 2, \ldots m$, is

$$c_{xy}(\ell) = \frac{1}{n} \sum_{s} (x_s - \langle x \rangle)(y_{s+\ell} - \langle y \rangle)$$

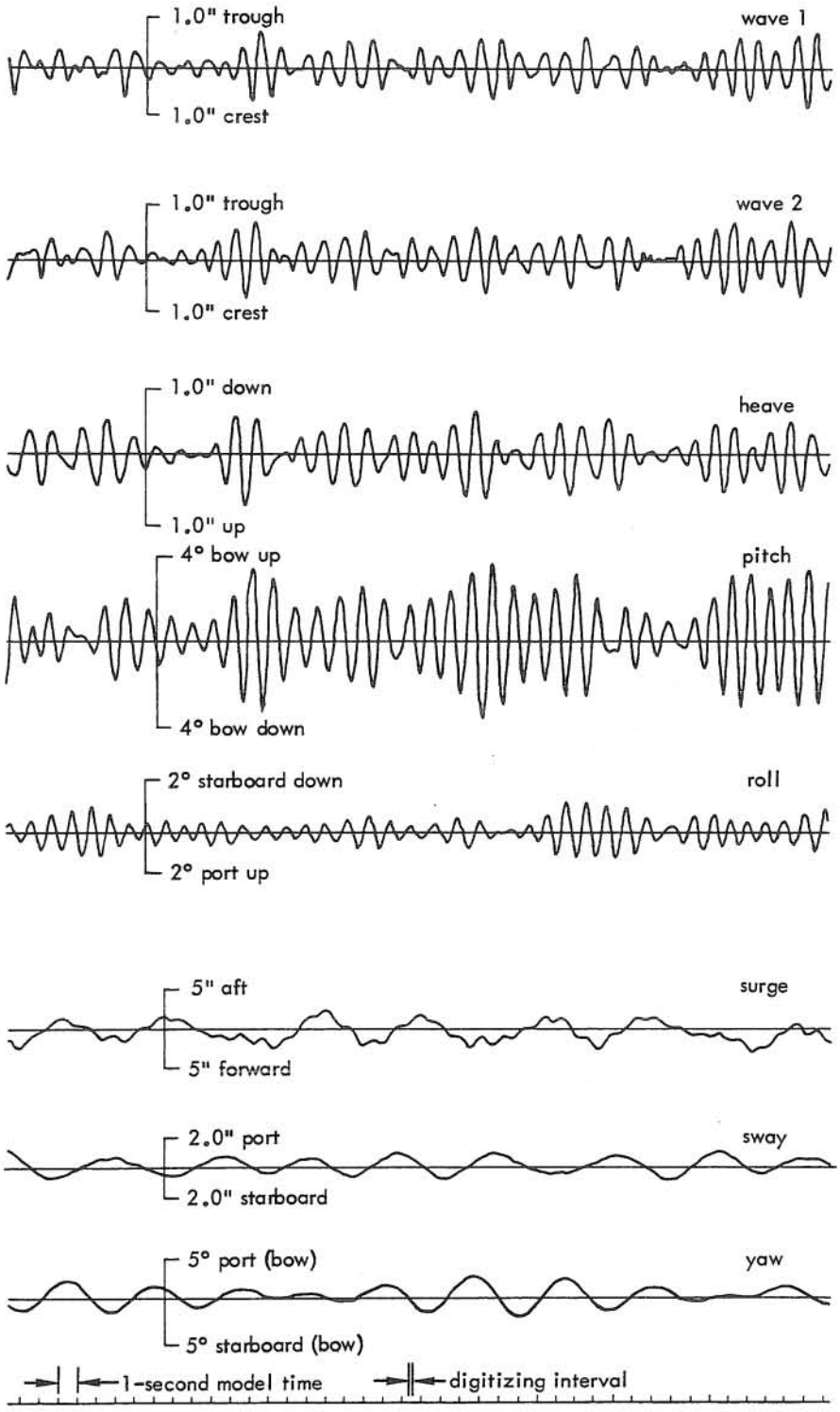

Figure 12. Facsimile of oscillogram of model measurements.

From the auto-covariance, the spectra may be calculated

$$X(k) = \frac{\delta(k)}{m}\left\{c_{xx}(o) + \sum_{1}^{m-1}\left[c_{xx}(\ell)\left(1 + \cos\frac{\pi\ell}{m}\right)\cos\frac{\pi k\ell}{m}\right]\right\}$$

which is seen to be the Fourier transform of the auto-covariance.

From the cross-covariance, the cospectrum and quadrature cross-spectrum may be calculated, as from Goodman (1957),

$$C_{xy}(k) = \frac{\delta(k)}{m}\left\{c_{xy}(o) + \sum_{1}^{m-1}\frac{1}{2}\left[\left(1 + \cos\frac{\pi\ell}{m}\right)\cos\frac{\pi k\ell}{m}\right]\left[c_{xy}(\ell) + c_{yx}(\ell)\right]\right\}$$

$$Q_{xy}(k) = \frac{1}{m}\left\{\sum_{1}^{m-1}\left[\frac{1}{2}\left(1 + \cos\frac{\pi\ell}{m}\right)\sin\frac{\pi k\ell}{m}\right]\left[c_{xy}(\ell) - c_{yx}(\ell)\right]\right\}$$

where $\delta(k) = 1/2$ when $k = 0$ and is unity otherwise.

The cospectrum is thus the cosine transformation of the real part of the cross-covariance, while the quadrature spectrum is the sine transformation of the imaginary part of the cross-covariance. Thus, the spectra and cross-spectra may be computed for $k = 0, \ldots m$.

A fundamental assumption of the method is that the process is stationary (i. e., an ensemble of time functions - or random processes - is said to be stationary if any translation of the time origin leaves its statistical properties unaffected). However, it has been emphasized by others (e. g., Tukey, 1961) that the method is insensitive to departures from stationary. In any event, the quantities can be computed and the question of the meaning of these quantities (i. e., in relation to the true quantities) will not be discussed in detail.

It is sufficient to point out that $X(k)$ measures the proportion of the total variance (power) of x_t due to frequencies in a band, centered about $k/2m$ cycles per time interval. The cospectrum and quadrature cross-spectrum are used to obtain the coherence $R(k)$ and the phase $\theta(k)$ defined by

$$R(k) = \left\{\frac{\left[C^2(k) + Q^2(k)\right]}{\left[X(k)\,\gamma(k)\right]}\right\}^{1/2}$$

$$\theta(k) = \arctan\left[\frac{Q(k)}{C(k)}\right]$$

R(k) is a measure of the strength of association between the two series in the kth band in a fashion analogous to that in which a correlation describes the strength of association between two random variables. The phase $\theta(k)$ describes the phase lead or lag of the y series relative to the x series at the frequency k/2m.

In summary, the principle of linear superposition is used as a device for breaking down the complex records into simple elements. The irregular records are regarded as approximately the sum of a number of regular sinusoidal components in random phase relationship. By use of the proper "correlation" functions and transforms, the variance in an irregular wave record is isolated into particular frequency bands. Since the analysis is statistical in nature, answers are obtained only with a certain probability. Thus, Blackman and Tukey (1958) give the probable distribution (chi-square) of the X(k) if the x(t) are independently distributed according to a standard normal distribution. This distribution is used to obtain the well-known confidence limits.

Prototype Data

Continuous measurements on the instrumented Fishhook barge of 60, 30, and 55 minutes' duration recorded, respectively, on January 22, February 7, and March 4, 1964, were selected for analysis. Preliminary calculations indicated that the Nyquist or folding frequency was slightly greater than 2 seconds. Thus, a digitizing interval of 1 second was employed for the reduction of the prototype data. This resulted in 3,601, 1,801, and 3,301 time stations for the January 22, February 7, and March 4 records, respectively. Excluding the wind records, 19 channels were recorded on January 22 and February 7, while 15 were recorded on March 4. The number of data points to be handled simultaneously was 68,411, 27,015, and 62,719 for the January 22, February 7, and March 4 data, respectively.

To clarify the magnitude of the computations required to determine the minimal information necessary to specify the resulting 19-component, matrix-valued, cross-spectral density function, the following enumeration of solution cases is cited. The complete solution for each wave length requires a total of 19 x 19 = 361 solution-numbers. Since the data recorded included three different headings of the barge relative to the oncoming waves as well as three different sea states, and since resolution required computation for 60 different wave lengths, the solution-numbers total 3 x 3 x 60 x 361 = 194,940. This manner of stating the task suggests that time series analysis of records of this magnitude should be attempted only on the very fastest computing systems.

Model Data

Limitations in the recording system for the model tests required four separate test periods for each direction of barge heading. Each test period was of the order of 10 minutes' duration. From the 13 test runs (one extra for the wave measurement without the barge), approximately 3,000 time stations of eight channels each were selected for analysis. As in the case of the prototype, the magnitude of the data processing effort appears to have been without

precedent, at least in the case of ship motion studies. Information was recorded on a direct-writing brush recorder as well as on magnetic tape in analog fashion. The magnetic tapes were then digitized through the courtesy of the Statistical Research Laboratory, New York University. An unfortunate misunderstanding of the desired digitizing interval as well as a misinterpretation of the calibration signal for the range of data required a laborious hand correction of the peaks in certain of the time histories. Eventually, it became necessary to discard 90 percent of the digitized data, since the digitizing interval was excessively fine. From this remaining raw data, all possible spectra and cross-spectra were obtained, of which only a small percentage is reported on herein.

BASIS OF THEORETICAL ANALYSIS

General

The model used in the theoretical analysis was assumed to be a rigid body with zero forward speed, spread moored by the four mooring lines. It was considered as being situated in a currentless, windless sea, 165 feet deep, and exposed to regular long-crested sinusoidal waves of unit amplitude with fixed frequency and selected headings. Waves with the frequency, period, and length indicated in Table 5 were considered.

The theory used is a modification of the deep water theory proposed by Kaplan and Putz (1962). The craft had the usual 6 degrees of freedom: 3 translational (surge, sway, and heave) and 3 rotational (roll, pitch, and yaw). A complete development of the theory and its application to the barge under analysis is given in Appendixes A, B, and C.

Basic Assumption

The basic assumption is that of linearity. Specifically, it is assumed that in the absence of excitation the ship motion can be described in terms of homogeneous, second-order, linear, differential equations with time as the independent variable. An excitation term is added to the homogeneous equations as a "right-hand-side term," which in the present case is sinusoidal.

In accordance with the linear theory, it is assumed that there is no coupling between the variables in the two planes of motion; that is, those longitudinally in heave, pitch, and surge and those laterally in sway, yaw, and roll. However, the longitudinal motions are coupled with each other and, similarly, the lateral motions are coupled with each other.

A fundamental analytical tool in carrying out the prediction of the motions of moored-ship systems is the slender body theory. Essentially, this theory makes the assumption that, for an elongated body where a transverse dimension is small compared to its length, the fluid flow at any cross section is independent of the flow at any other section; therefore, the flow problem is reduced to a two-dimensional problem in the transverse plane. The force is found by integrating the pressure over the length of the body.

Table 5. Wave Period, Frequency, and Length Used in Theory

Wave Frequency, ω (rad/sec)	Wave Period, T (sec)	Wave Length, λ (ft)
2.84	2.21	25
2.01	3.12	50
1.64	3.83	75
1.42	4.42	100
1.16	5.41	150
0.90	6.98	250
0.76	8.27	350
0.66	9.51	450

Equations are formulated by the balance of inertial, damping, restoring, exciting, and coupling forces and moments. Hydrodynamic and hydrostatic fluid effects, together with body inertia and mooring influences, are included in the analysis.

Inertial Forces

The forces exerted by the ship in accelerating the surrounding water give rise to equal and opposite forces by the water on the ship. These are termed inertial forces and, correspondingly, inertial moments. Since they are proportional to acceleration, they are usually expressed in terms of a fictitious added mass. The total inertial force has components in all three directions of translation and rotation.

Damping Forces

Damping forces involve the dissipation of energy and are due to wave generation, viscosity, and eddy-making. Except in the case of roll, damping due to wave generation only is considered in this study. Total damping force, like inertial force, has components in all three directions of translation and rotation.

Hydrostatic Restoring Forces

Hydrostatic restoring forces result from the buoyancy effect arising from static displacements. Total hydrostatic restoring force has a component only in the vertical, or heave, direction. The hydrostatic restoring moment has components only in the roll and pitch directions.

Mooring Restoring Forces

The mooring type of restoring force has been added, in the case of the moored barge under analysis, in addition to the hydrostatic restoring force which is always present in the case of a barge in water. The mooring restoring force is effective only in surge, sway, and

yaw. While it is present in the three remaining modes (heave, pitch, and roll), it is not generally significant in relation to the hydrostatic restoring forces. The mooring restoring forces and moments are assumed to be linear functions of displacement in surge and sway as well as in yaw, respectively. This assumption of linearity is a proper one for the small displacements encountered in the prototype tests. It is valid so long as the level of excitation is relatively low. However, when the excitation attains a certain level and the displacement becomes large, the nonlinear character of the restoring forces is responsible for the appearance of the phenomenon of subharmonic response. Under these conditions, the basic assumption of this theoretical study, i. e., linearity, is no longer valid.

Excitation Forces

The excitation forces are due to the waves which excite the barge and generate all of the preceding forces and moments. They are assumed to be sinusoidal in nature and have components in all three directions of translation and rotation, although some of these components vanish at certain headings of the barge relative to the incident wave direction. Since the barge was assumed to be situated in a currentless, windless sea, only surface gravity waves were considered.

Equations of Motion

The foregoing paragraphs describe four main categories of forces considered in the analysis: inertial, damping, excitation, and restoring. In case of the latter, the hydrostatic and mooring forces are combined. On this basis, six equations of motion, one for each degree of freedom, are written as follows:

$$m\ddot{x} = F_x^{\,i} + F_x^{\,d} + F_x^{\,m} + F_x^{\,w} \qquad \text{(surge)}$$

$$m\ddot{y} = F_y^{\,i} + F_y^{\,d} + F_y^{\,m} + F_y^{\,w} \qquad \text{(sway)}$$

$$m\ddot{z} = F_z^{\,i} + F_z^{\,d} + F_z^{\,h} + F_z^{\,w} \qquad \text{(heave)}$$

$$I_x\ddot{\phi} = M_\phi^{\,i} + M_\phi^{\,d} + M_\phi^{\,h} + M_\phi^{\,w} \qquad \text{(roll)}$$

$$I_y\ddot{\theta} = M_\theta^{\,i} + M_\theta^{\,d} + M_\theta^{\,h} + M_\theta^{\,w} \qquad \text{(pitch)}$$

$$I_z\ddot{\psi} = M_\psi^{\,i} + M_\psi^{\,d} + M_\psi^{\,m} + M_\psi^{\,w} \qquad \text{(yaw)}$$

where m(I) = mass (inertial moment) of the ship

F = force

M = moment

with subscripts on the F's and M's indicating components, and superscripts indicating the type of force or moment according to the following notation:

i = inertial

d = damping

h = hydrostatic restoring

m = mooring restoring

w = wave

x = surge

y = sway

z = heave

ϕ = roll angle

θ = pitch angle

ψ = yaw angle

Acceleration is indicated by the second derivative symbol $(\cdot\cdot)$ above the motion symbol, for example, $\ddot{x}$.

The equations of motion consist of linear combinations of terms which vary in time and are proportional to acceleration, velocity, and displacement. Each of the terms contains certain coefficients which require evaluation.

Solution of the Equations of Motion

Through appropriate manipulation, the simultaneous equations for the longitudinal motions (heave, pitch and surge) are evolved in the form of a matrix equation with complex entries. Solution for motions in 3 degrees of freedom is obtained by multiplying an inverted 3 by 3 frequency-dependent matrix by the matrix representing the excitation, which is both frequency- and direction-dependent. By varying the value of the frequency and direction, responses are calculated in the form of amplitude and phase relative to a unit amplitude of excitation. When these responses are expressed as a function of frequency, they are known as "linear directional complex response operators" or simply "response operators."

The same procedure is followed in the case of the lateral motions.

The complex form of the response operators permits calculation of the phase relationship as well as the relative absolute amplitude.

Results of the theoretical analysis are given in the appendixes and also in the section which compares prototype, model, and theoretical results.

RESULTS OF THEORETICAL ANALYSIS

The complex response operators for the longitudinal motions are shown in Figure 13. Those for the lateral motions appear in Figure 14.

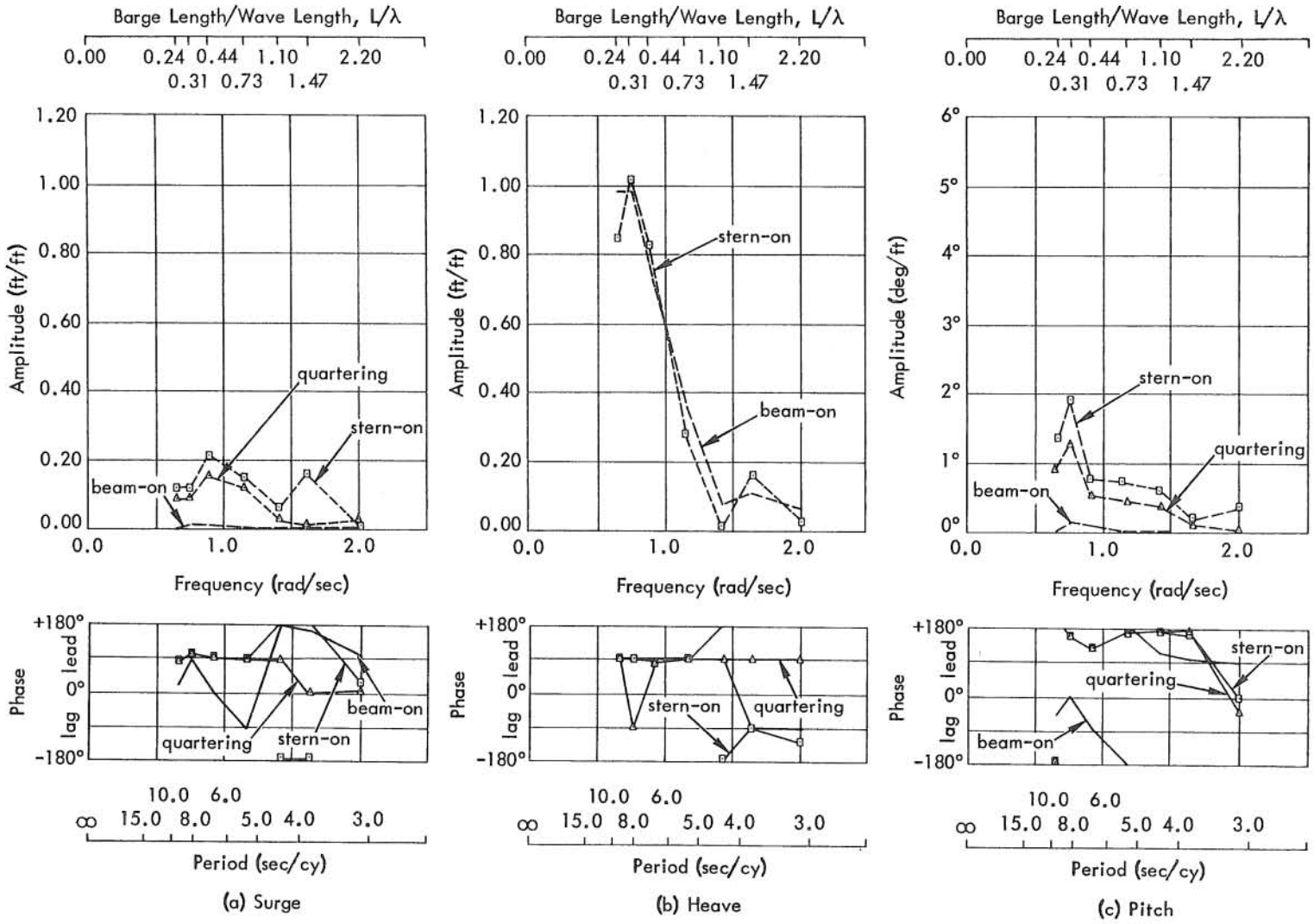

Figure 13. Complex response operators for longitudinal motions from linear theory.

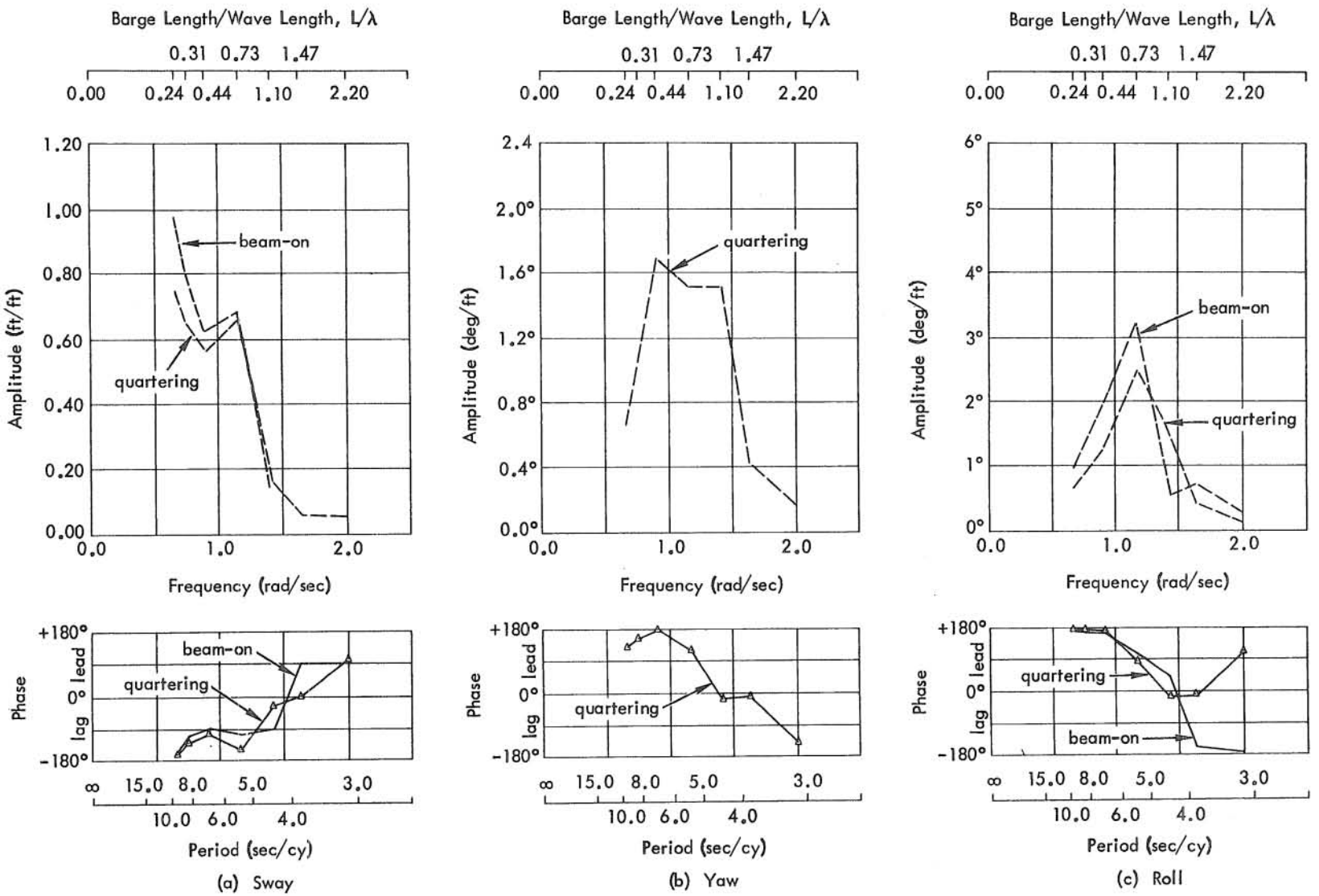

Figure 14. Complex response operators for lateral motions from linear theory.

Detailed comments concerning the amplitude results are presented in the next section, Comparison of Prototype, Model, and Theoretical Results. Only the phase results are discussed at this point. Within the normal frequency range of sea and swell, peak amplitudes in the time histories of surge and heave are shown to lead peak amplitudes (crests) in the time history of the surface water displacement by approximately 90 degrees.

Pitch, on the other hand, is shown to lead the wave crest by from 135 to 180 degrees. This agrees with the results obtained from other ship motion studies, notably that of Canham et al. (1962).

For the lateral motions in beam-on seas, sway tends to lag wave crest by from 160 to 90 degrees, and then lead wave crest at a rather constant 90 degrees at the higher frequencies. Roll tends to lead and then lag the wave crest by a rather constant angle of 165 degrees except at a barge length-wave length ratio near 1.0, where the phase angle changes from lead to lag.

In quartering seas, maximum yaw tends to first lead and then lag the wave crest, again changing from lead to lag at a barge length-wave length ratio of approximately 1.0.

COMPARISON OF PROTOTYPE, MODEL, AND THEORETICAL RESULTS

General

A comparison of prototype, model, and theoretical results is presented in this section. The categories for which comparison is made are (1) excitation, (2) response, (3) response operators, and (4) phase and coherence.

Excitation

Prototype. Excitation in the prototype consisted of winds, currents, and surface gravity waves. Of these, waves were the dominant means of inducing motion of the barge.

A summary of the wind data for the three periods under study is given in Table 6. The wind record for January 22 is very similar to that for March 4, a facsimile of which is shown in Figure 7. The wind record for both these days contained many gusts in contrast to the record for February 7, which indicated an almost steady wind speed of 6 knots. The mean wind speeds for January 22 and March 4 were 17.0 and 20.7 knots, respectively. Spectral distributions for the wind records are shown in Figure 15. These computations were based on a lengthy record (up to 4 hours) digitized at a 4-second interval.

The wind gust period band is generally in excess of 1 minute. The amplitudes of the gusts are small relative to the mean wind speed and hence unimportant. (In this context, "gust" is used to indicate instantaneous departures of the wind speed from its mean. The gust period is a measure of the length of time between successive ordinate up - or down - crossings of the instantaneous wind speed with the mean.) The standard deviations are 3.0 and 2.0 knots for January 22 and March 4, respectively. Since the wind pickups (direction and speed) were mounted on the barge, the records also contain a factor based on the relative motion of the barge.

Table 6. Summary of Wind Data

Date	Mean Wind Speed (knots)	Incident Direction Azimuth (deg)	Standard Deviation (knots)
January 22	17.0	300	3.06
February 7	6.0	90	0.00
March 4	20.7	315	2.03

The drag force induced on the tower and barge by the winds is unknown, but is likely to be considerable. The effect of the mean wind velocity is simply to displace the craft from its equilibrium position, thereby changing the initial tensions in the mooring chains. The effect of the gusts, however, is to induce not only changes in the mooring chain tensions, but the motions as well, notably roll and pitch and either sway or surge. Fortunately, the gust period is decidedly different from the wave period. Additional discussion on these effects will be given later.

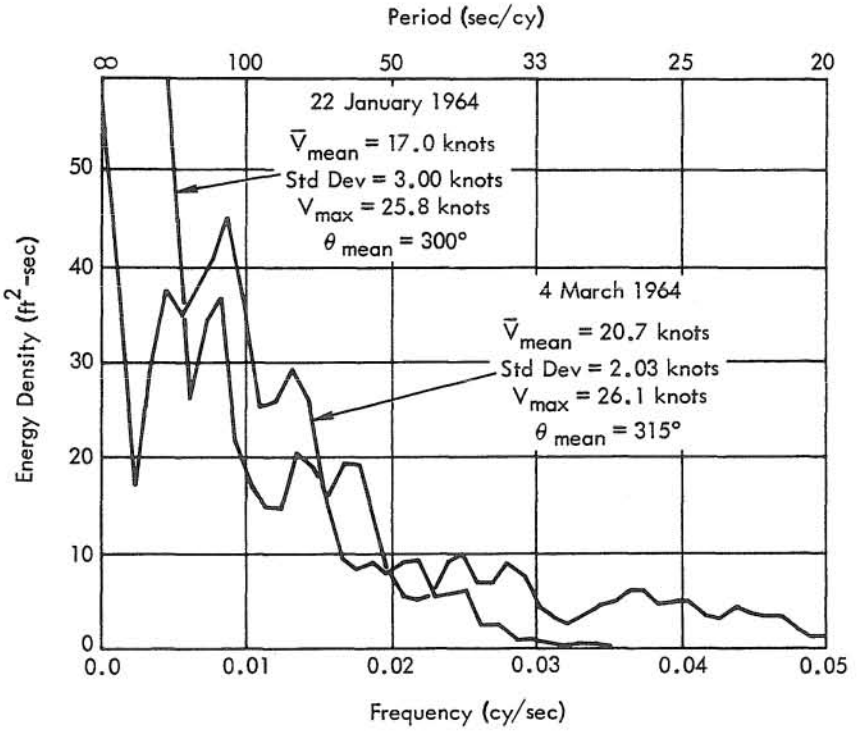

Figure 15. Spectra of wind speeds.

Currents were not measured since the barge was evacuated during periods of relatively high wave disturbance that occurred during the periods selected for analysis. However, during periods of relative calm, maximum currents of up to 3 knots were measured. Current measurements could be related generally to the tides. No quantitative data is given here; periodic observations were entered in the rough log only. The effect of the currents was to displace the barge from its equilibrium position, thereby changing the initial tensions. Since the maximum duration of the test periods was 55 minutes, the relatively slow changes in the currents had little effect on the other measurements.

The spectral distributions of the measured water surface variation (waves) are given in Figure 16a through c for January 22, February 7, and March 4, respectively. The three curves for January 22 and February 7 represent the spectra computed for measurements recorded from pickups at the three different locations (i. e., port stern, starboard stern, and center well). Only the center well wave gage was operative on March 4. The dominant directions in azimuth angle and relative to the barge, β ($\beta = 0^\circ$ corresponds to stern-on), are noted on the graphs of the figure. For comparative purposes, the spectra for sea states 3 and 4 according to the Neumann model for wind velocities are given in Figure 16e. The excitation for all days was relatively low, never being above a sea state 3. It is obvious that these spectra are only qualitative estimates of the excitation since the continuous water level variations upon which they are based also contain the reflected waves generated by the barge. The separation of these two wave systems was precluded by an incomplete knowledge of the barge damping characteristics as well as by certain limitations imposed by the computing scheme.

January 22 Data: The range of significant periods is from approximately 2.5 to 8 seconds, with the period of maximum energy (peak) varying from 3.8 to 4.6 seconds. The shapes of the spectra are ill defined; their broadbandedness is indicative of a confused sea. From the pertinent wind record, the wind velocity is of the order of 17.0 knots from an azimuth of 300 degrees. The waves were observed visually to be approaching from an azimuth of approximately 320 degrees. Putting these facts together, it may be concluded that the sea, as described by Marks (Kaplan and Putz, 1962), was between states 1 and 2.

February 7 and March 4 Data: These spectra exhibit marked narrowbandedness with peaks concentrated at approximately 3.5 seconds' period. The shapes of the spectra are well defined and suggest that the wave system was highly directionalized. The wind velocity was 6.0 knots from a direction of 90 degrees on February 7 and 20.7 knots from a direction of 315 degrees on March 4. The waves were observed to be approaching from an azimuth of 50 degrees on February 7 and from 360 degrees on March 4. Sea on both days may be considered as state 2.

Although the level of excitation was low, the response operators to be derived from these measurements are invariant relative to the excitation level according to the linearized theory. Thus, the prototype measurements taken during these relatively low levels of excitation are equally as useful as those taken during periods of intense activity.

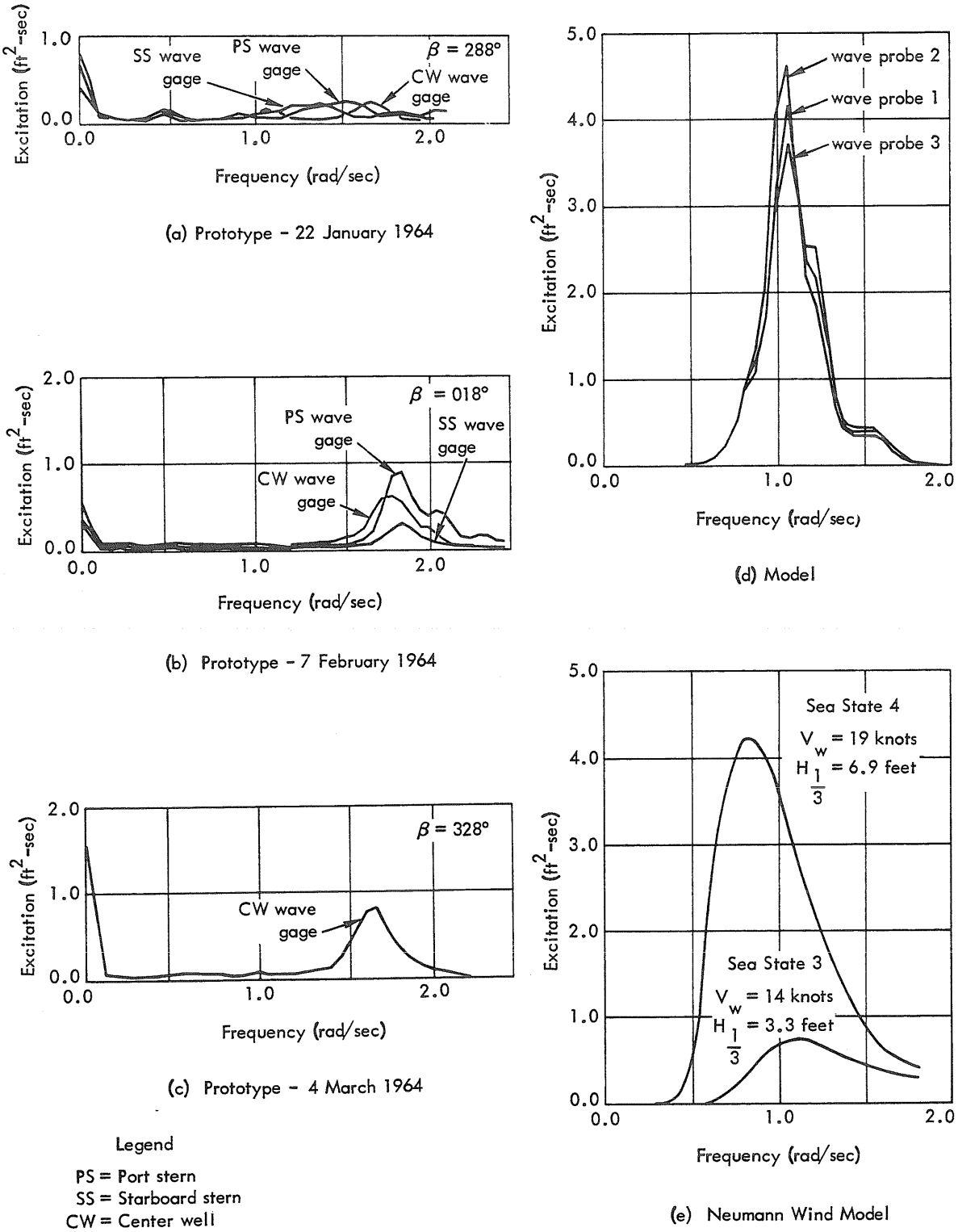

Figure 16. Spectral energy densities for wave excitation.

The foregoing deals with storm waves in the usual frequency band of interest. Previous mooring force studies (O'Brien and Muga, 1963 and 1964) indicated that long-period waves might induce mooring line tensions of considerable importance. Pursuant to this possibility, subsurface pressure pickups were installed at the locations indicated by Figure 2. The spectra of the time history records are shown in Figure 17. Note that certain long-period waves are indeed present, although of low amplitude. Since the high-frequency components of the wave spectrum are attenuated with depth, the long-period wave components are accentuated, even though the resolution at these frequencies is inadequate.

The long-period waves (greater than 2 minutes) are usually associated with the harmonics of the natural period of oscillation of the offshore basin.

Model. Excitation in the model consisted only of surface gravity waves. Spectral distributions of the time history records for the three measurement locations are shown in Figure 16d. The time history records were first extrapolated to prototype conditions according to the Froude scaling laws. The spectra of the model when compared with Figure 16e correspond to a sea state 4. No long-period wave was present during the model tests.

Theory. The excitation employed in the theoretical model is assumed to consist of unidirectional long-crested waves of unit amplitude. No winds or currents are considered.

In summary, the relative excitation due to waves was much higher in the model (sea state 4) than in the prototype (sea state 3). The character of the excitation was different in that the prototype was excited by long-period waves whereas the model was not. In addition, the prototype was subject to excitation by winds and currents, whereas the model was excited only by surface gravity waves.

Motion Response

The motion response of the barge to the excitation in the various modes is indicated by the spectra of the time histories. These records correspond exactly in time to those used in computing the spectra of the excitation. Since the motions are functions of the exciting wave direction, and since the incident wave direction varied from test period to test period, comparisons of the response motions without due regard for both the wave direction and intensity level of excitation are meaningless. The spectra of the response measurements are presented mainly to give a broad perspective of the order of magnitude of the amplitudes and periods of motion of the barge.

In the case of the prototype, the spectra of the motions in heave, sway, and yaw can be determined only indirectly from selected pairs of acceleration records as derived in Appendix C. The surge motion is also determined indirectly from the spectra of the longitudinal acceleration record by dividing each ordinate by ω^4. Cartwright (1963) notes that this procedure may be deficient.

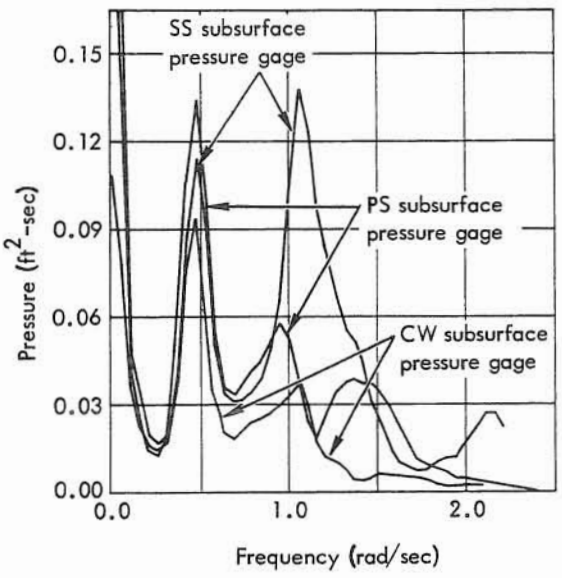

(a) 22 January 1964

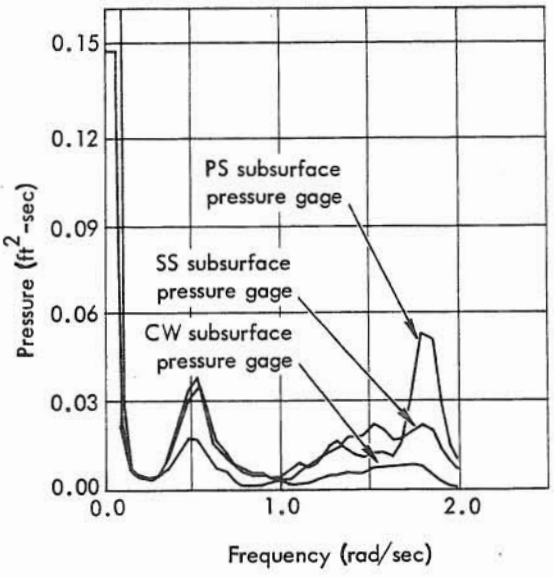

(b) 7 February 1964

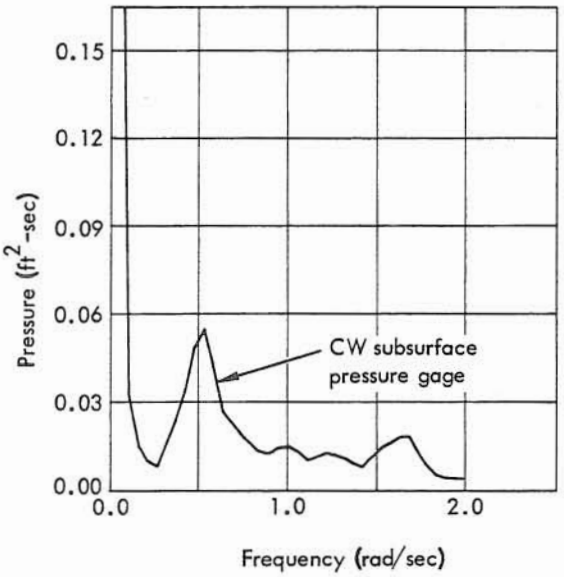

(c) 4 March 1964

Note

All gages were located approximately 16 feet below mean water level (MWL).

Legend

PS = Port stern
SS = Starboard stern
CW = Center well

Figure 17. Spectra of subsurface pressure measurements.

Surge - Prototype. The prototype spectra of longitudinal acceleration in surge for the 3 days are shown in Figure 18. The sharp spike near the origin is due to a long-period oscillation in the acceleration record. Since the record was of finite duration, adequate resolution in this period band could not be obtained. In addition, background noise of the recording system constituted a large percentage of the measured response.

In some cases a sharp spike near the origin is due to a sinusoidal or linear drift in the electronics. This possibility was eliminated as a causative factor by careful monitoring of the power source during recording periods. In order to account for the presence of long-period oscillations, it is useful to review certain kinds of motion.

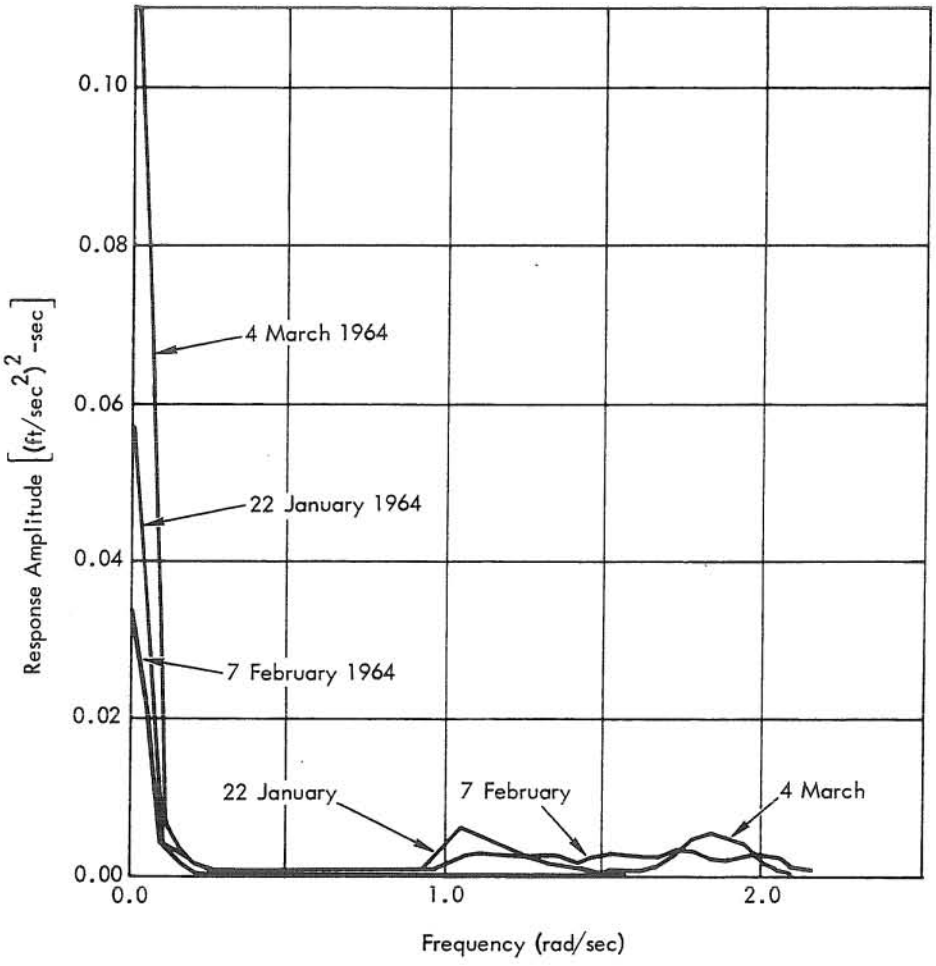

Figure 18. Response spectra of longitudinal acceleration measurements (bow), Fishhook prototype barge.

From the resume, in the form of a table, prepared by Stoker (1950) which compares the characteristics and properties of linear and nonlinear systems, the following salient facts concerning the motion of the barge under various assumptions have been extracted. Various special cases are not included.

I. Linear Systems
   A. Without damping
      1. Free oscillation: Motion is simple harmonic.
      2. Forced oscillation: Motion is a superposition of simple harmonic (free) and a forced oscillation having the same period as forcing function. If free and forced periods are equal, resonance results.
   B. With damping
      1. Free oscillation: Motion is damped out exponentially.
      2. Forced oscillation: Motion is a superposition of a free oscillation which is damped out exponentially and a forced oscillation with a frequency equal to that of the forcing function.

II. Nonlinear Systems
   A. Without damping
      1. Free oscillation: Motion is periodic but not simple harmonic.
      2. Forced oscillation: General motion is unknown, but many types of periodic motion (subharmonics, etc.) exist.
   B. With damping
      1. Free oscillation: Motion is damped out.
      2. Forced oscillation: General motion is unknown.

Thus, in the case of linear systems without damping, the craft tends to: (1) oscillate about its own natural period when freely excited, or (2) oscillate about a superposition of its natural period and the forcing period under forced excitation. In the latter case, when damping is present, the craft tends to oscillate about a superposition of the free oscillation, which is damped out exponentially, and of the forced oscillation. As the time, t, increases, the response period approaches and eventually is equal to the period of the forcing function.

In the case of nonlinear forced systems with and without damping, the general motion is unknown, but many different types of periodic and nonperiodic motions have been observed. One particular motion of interest is that of subharmonic response, as described for example by von Kármán (1940), Den Hartog (1947), and Stoker (1950).

In the Fishhook prototype barge, the mooring restoring forces are nonlinear functions of displacement; hence, the system is nonlinear. In addition, certain long-period wave components were known to be present as detected by the subsurface pressure pickups. Thus, the long-period spike in the acceleration spectra, Figure 18, is due to (1) linear response of the barge to surface gravity waves of long period characteristic of the offshore basin and (2) subharmonic (nonlinear) response of the barge to surface gravity waves having periods in the normal range of sea and swell.

The spectra of the prototype response in surge displacement are obtained by dividing the longitudinal acceleration spectra by ω^4. The acceleration spectra should be highly resolved by passing them through a narrow-band filter before carrying out the division. However, the volume of data to be analyzed within the budgeted time and cost frame dictated a compromise in the degree of resolution.

Thus, since the recording periods were of finite duration, emphasis was placed on obtaining a satisfactory degree of resolution applicable to the frequency band corresponding to the dominant exciting wave period and compatible with the digitizing interval. With this in mind, the displacement spectra in surge for only the frequency band of interest shown in Figure 19 were obtained. The period of maximum energy was approximately 5.9 seconds. The spectra tend to be narrow banded and similar for at least two of the days. The greatest response in surge occurred when the excitation was lowest (January 22) and when the waves were observed to be almost beam-on. The stern-on waves (February 7) produced almost no surge motion. No rational explanation could be found for this apparent discrepancy.

Surge - Model. The spectra of the surge response motion for the model for the three conditions of barge orientation with respect to the incident wave are presented in Figure 20a. Note that the spectra are binodal and that most of the energy is distributed in the long-period or low-frequency portions. No comparable long-period surface gravity waves were generated in the model basin. In addition, the coil springs employed to simulate the moorings were linear for up to 6 inches' amplitude about the mean (initial) tensions. Maximum amplitude experienced in the test runs amounted to only approximately 3 inches. Thus, the mooring restoring forces in the model were definitely linear. The barge tended to respond in the surge, sway, and yaw motions about a frequency characteristic of the mooring configuration. This characteristic period was from four to nine times the period of the fundamental exciting wave ($(27 \leq 36 \leq 54)$ versus $(6.1 \leq 6.4 \leq 6.8)$). The resolution in terms of period at the lower frequencies is not precise, as shown above. The characteristic period of the model barge in surge is thus found to be 36 ($27 \leq 36 \leq 54$) seconds. This compares with a prototype period of approximately 30 seconds as obtained from the chain tension response operators.

The prototype was known to have nonlinear restoring forces whereas the model had linear restoring forces. The damping forces are due to wave generation, eddy-making, and/or viscous (or other drag-related) effects. The contribution from viscous damping (for all motions) is generally considered to be negligible for most normal ship forms. However, for large beam-draft ratios, it seems reasonable to assume that viscous effects acquire greater importance, particularly in the present case. Since the absolute velocities are smaller in the model than in the prototype, the viscous-damping coefficients and hence the forces tend to be relatively larger in the model. In addition, if the viscous-damping forces were nonlinear, they would be relatively more pronounced in the model than in the prototype. In either case, linear or nonlinear, a rational explanation for the response at a frequency

other than the frequency of the exciting forces may be developed. In undamped or slightly damped linear systems, it is due to the characteristic period of the mooring configuration. In damped or undamped nonlinear systems, it is due to the phenomenon of subharmonic response.

The influence of these differences in damping and restoring forces is difficult to assess. The damping forces, if nonlinear, tend to be more pronounced in the model than in the prototype. On the other hand, the mooring restoring forces were definitely nonlinear in the prototype but not in the model.

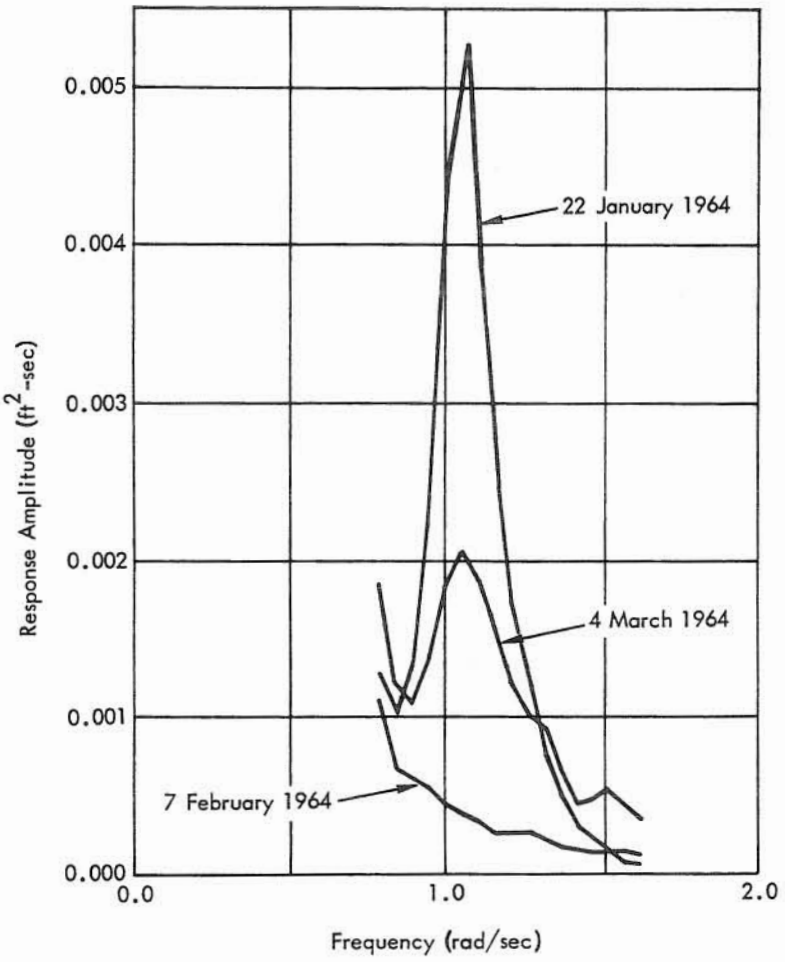

Figure 19. Response spectra of surge displacement, Fishhook prototype barge.

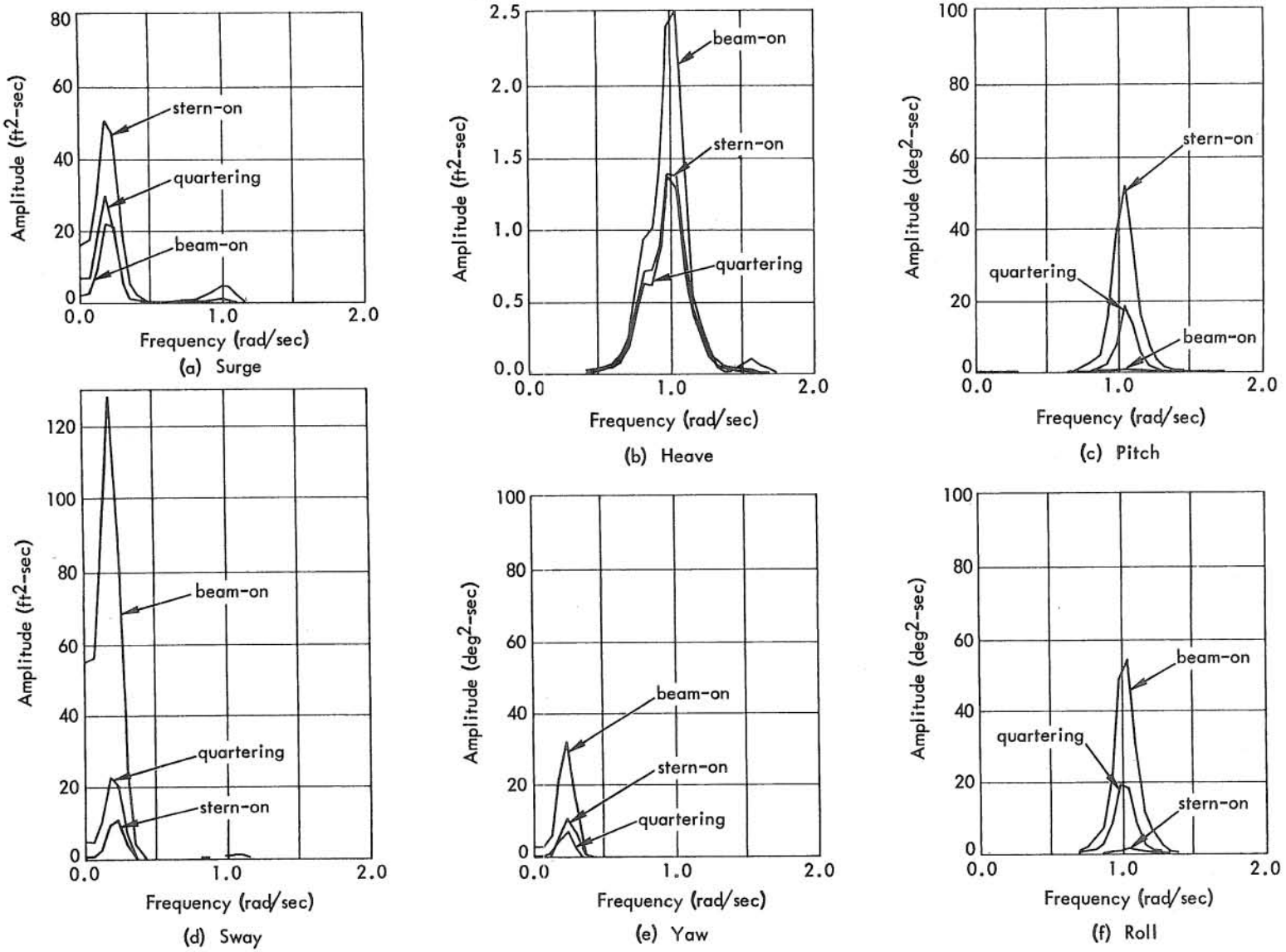

Figure 20. Motion response spectra from model measurements.

Previous studies (O'Brien and Muga, 1964) have postulated the existence of undetected long-period low-amplitude exciting waves to account for the long-period oscillations in certain motions. It is now definitely established that such long-period oscillations may arise in both linear and nonlinear systems in the absence of exciting waves of corresponding period.

The influence of exciting wave direction may be observed in Figure 20a. The stern-on waves produced greatest response in surge, beam-on waves the least. In contrast to the prototype observations (January 22 and February 7), this result is the one normally expected.

Heave - Prototype. The prototype barge response spectra for heave for the 3 days are shown in Figure 21. Two sets of records are available: one is derived from the pair of bow and stern vertical accelerometer records, the other set from the pair of port and starboard vertical accelerometers. In the former, pitch is coupled with heave, whereas in the latter roll is coupled with heave. Thus, for the first time in the history of ship motion studies, a check on the method of obtaining the heave spectra is available. Considering the low level of excitation and the signal noise of the recording system, the comparison is extremely good. Roll and pitch may be checked independently against the spectra of time histories of roll and pitch as measured by the pendulum-type gages. The same comments given on the method of obtaining the displacement spectra from the acceleration spectra in the case of surge also apply in the case of heave. The pair of bow-aft accelerometers consistently yielded larger values of the spectral ordinates than did the starboard-port accelerometers.

The period of peak maximum energy in heave for January 22 and March 4 is approximately 6.0 seconds, which compares with the natural period in heave of 6.1 seconds. A secondary peak of approximately 4.2-seconds' period is shown by the spectra of March 4. This period band corresponds to the period of maximum peak energy for the February 7 record. The differing directions of the incident waves do not seem to explain this behavior except indirectly. The level of response in heave was substantially lower for February 7 than for the other 2 days in spite of the fact that the level of excitation did not follow the same trend. Thus, no definite explanation for the response in heave at a period of approximately 4.2 seconds for February 7 could be established.

Heave - Model. The heave spectra obtained from the model results are given in Figure 20b. The period of peak energy density is approximately the same as for the prototype; i.e., 6.0 seconds. The shape of the model spectra in heave is very similar in appearance to that of the prototype spectra. Whereas no definite conclusions can be formulated regarding trends of response versus wave propagation direction in the prototype, the model results suggest that the beam-on waves tend to induce the greatest response. Since the heave motion is not greatly affected by the moorings, no long-period components are present in the response spectra. This contrasts sharply with response of the craft in surge.

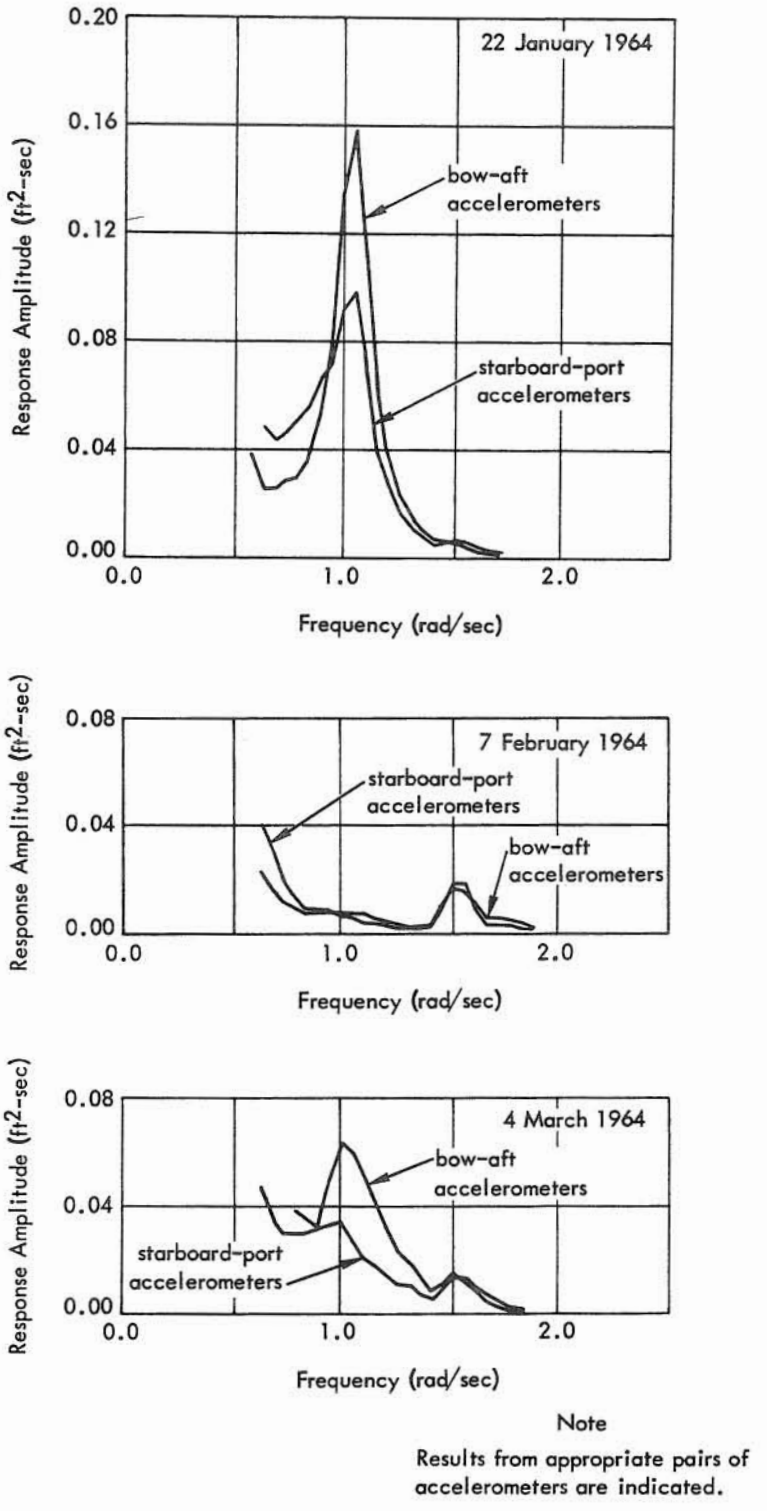

Figure 21. Response spectra of heave displacement, Fishhook prototype barge.

Pitch - Prototype. The prototype response spectra in the pitch mode as obtained from the accelerometers and pendulum-type gage attached to the prototype barge are given in Figure 22. Note that the spectra indicate that the gage was almost insensitive. This was confirmed by field observations, and although the gage was overhauled on numerous occasions, it continued to remain relatively insensitive to the barge motion in pitch. Figure 23 compares the pitch spectra as obtained from the acceleration records. The influence of incident wave direction casts some doubt on the credibility of the field observations relative to wave direction. The greatest response (January 22) occurred when the waves approached from the beam-on direction (when the excitation was lowest). Minimum response (February 7) occurred when the waves approached from a stern-on direction. The period of maximum energy (6.3 seconds) for all 3 days was very close to the natural period in pitch of 6.5 seconds.

Pitch - Model. The model response spectra in pitch are shown in Figure 20c. The trend of response is decidedly different from that of the prototype. The stern-on seas produce the greatest response and the beam-on seas the least. The influence of direction is apparent. The period of peak energy is 6.1 seconds, which is slightly lower than that in the prototype. However, it should be recalled that the natural period in pitch of the model was accepted as 6.1 seconds instead of the prescribed 6.5 seconds because of the difficulty (physical limitations) in locating the ballast weights. Thus, what appears to be a slight discrepancy is in reality a confirmation of the accuracy and care of the experimental work in the laboratory, including the computations and measurements. No long-period waves were present in any of the pitch spectra.

Sway - Prototype. The spectra of prototype response in sway acceleration are given in Figure 24a. These spectra were obtained along with the yaw acceleration spectra from the transverse pair of accelerometers located at the bow and the stern. Thus, the method of obtaining the sway and yaw acceleration spectra is similar to that employed in the case of heave and pitch and heave and roll. It differs from the case of surge motion where a strategically placed accelerometer measured the surge acceleration directly. However, the sway displacement response spectra, Figure 24b, are very similar to the surge displacement response spectra (Figure 19), and the remarks given for surge response apply also to sway response. Notice that a sharp spike appears near the origin of the sway acceleration response spectra, Figure 24a. Since this portion of the acceleration spectra is inadequately resolved, only a portion of the displacement spectra is shown in Figure 24b. This portion corresponds to the frequency band of the dominant exciting waves.

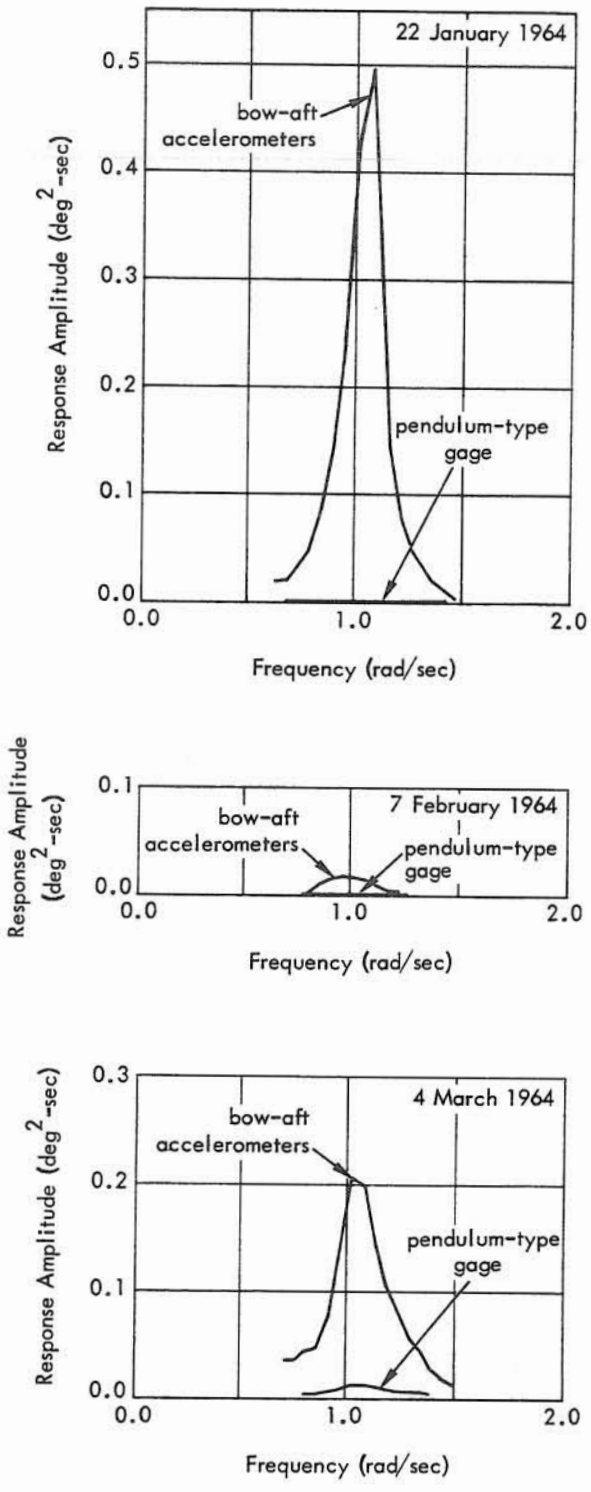

Figure 22. Response spectra of pitch as obtained from accelerometers and pendulum-type gage, Fishhook prototype barge.

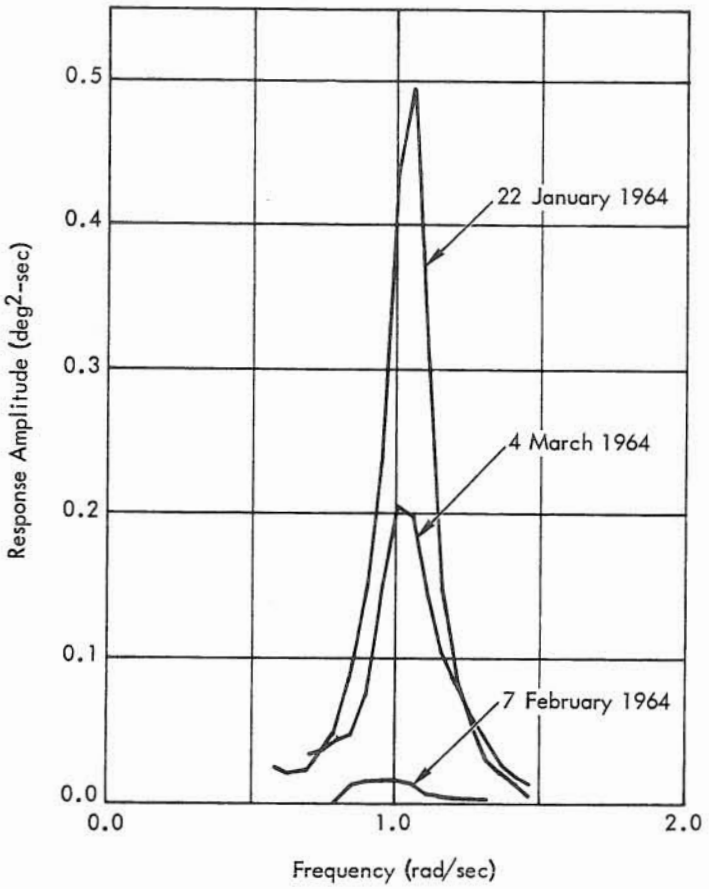

Figure 23. Response spectra of pitch as obtained from accelerometers only, Fishhook prototype barge.

As in the case of surge, the low-frequency long-period oscillations which appear in the acceleration record result from: (1) linear response of the barge to long-period surface gravity waves which are characteristic of the offshore basin, and (2) nonlinear subharmonic response of the barge (caused by nonlinear mooring restoring forces) to waves within the normal frequency band of sea and swell.

As in the case for surge and pitch, the influence of incident wave direction presents an interesting anomaly. The greatest response (in the acceleration spectra) occurred when the waves were stern-on instead of beam-on as would normally be expected.

The sway displacement spectra indicate that the period of maximum energy varied from 5.0 to 6.0 seconds. This corresponds to the period of the dominant exciting wave system.

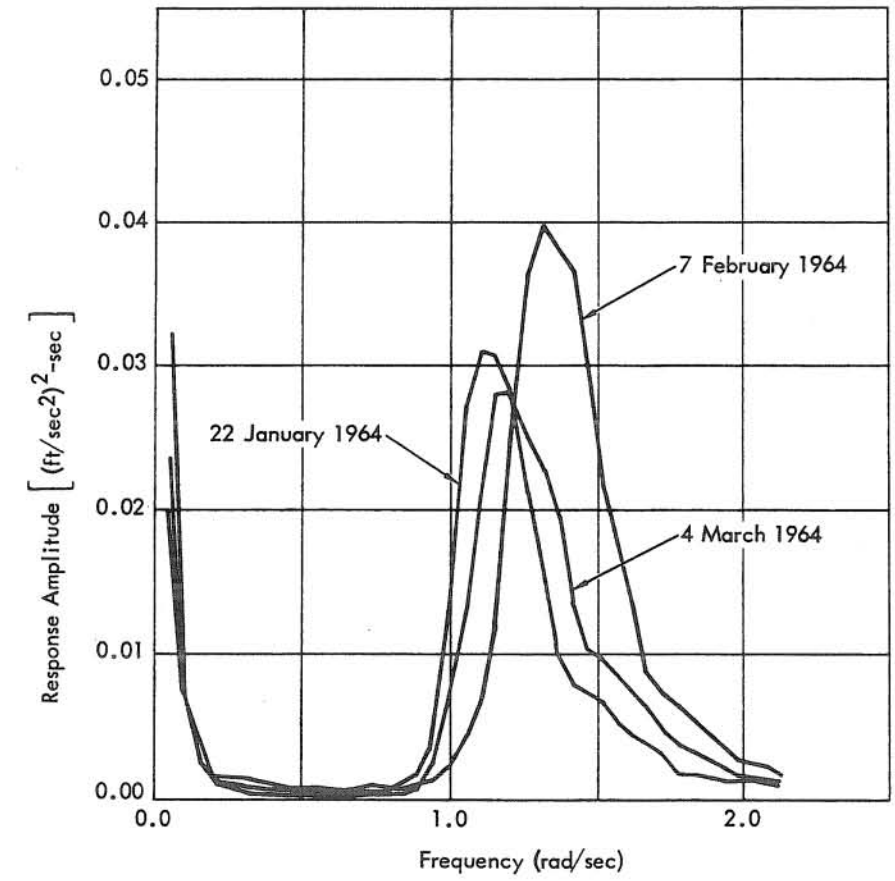

(a) Sway - acceleration

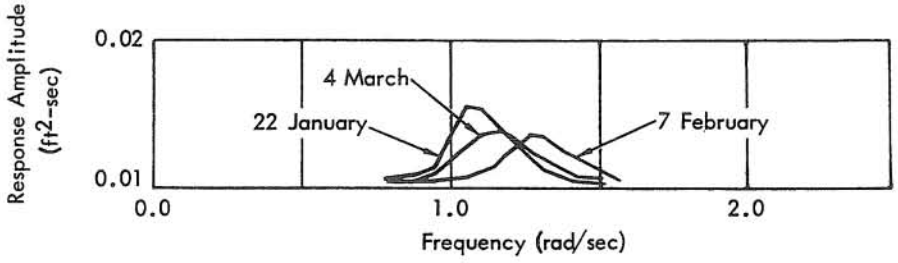

(b) Sway - displacement

Figure 24. Response spectra of sway acceleration and displacement, Fishhook prototype barge.

Sway - Model. The sway response spectra obtained from the model measurements are shown in Figure 20d. Note that the long-period components completely dominate the spectra. Since no long-period exciting waves were present and since the mooring restoring forces were linear over the range of displacements encountered during the tests, the response may be considered the tendency of the craft to oscillate about the characteristic period of the moored-barge system. The situation for sway is almost identical to that for surge. The influence of incident wave direction is again obvious, in sharp contrast to the prototype observations. Beam-on waves resulted in the greatest response, and stern-on the least. The characteristic period of the moored-barge system in sway as determined from the model tests is found to be 36 seconds. This compares with a period of 30 seconds as determined from the spectra of chain tension response. Again, viscous damping in the model is proportionately greater than that in the prototype. The discussion following surge response is also applicable to sway response.

Yaw - Prototype. The response spectra of yaw motion are shown in Figure 25. The yaw spectra of angular displacement were obtained from spectra of angular acceleration. The yaw acceleration spectra, not shown, are very similar in appearance to the acceleration spectra for surge and sway. They have the characteristic sharp spike near the origin where adequate resolution could not be obtained for the limited period of observation. Thus, only that portion of the yaw displacement spectra is shown in the frequency band corresponding to the dominant exciting wave period. The remarks on surge and sway apply also to the yaw motion. The period of peak yaw motion varied from 5.0 to 6.0 seconds. The influence of exciting wave direction and intensity level are not apparent. The lowest level of excitation approaching from the beam-on direction (January 22) was responsible for the highest measured response. On the other hand, the waves approaching from the stern-on direction (February 7) produced the lowest measured response. If the barge were truly symmetrical, and if the waves approached from precisely the stern-on and beam-on directions, the contribution to yaw should be negligible. However, neither condition was prevalent in the present case.

Yaw - Model. The spectra of yaw response as obtained from the model test are given in Figure 20e. Only the long-period (27 seconds) component is present. The trend of the responses (in the long-period frequency band) differs markedly from that in the prototype (in the short-period band corresponding to sea and swell). Beam-on seas produced the greatest response and quartering seas the least.

Roll - Prototype. The spectra of prototype measurements of roll are shown in Figure 26. For each day, the spectra obtained from the accelerometer records and the pendulum-type gage record are herein compared. The comparison indicates that the accelerometers were much more sensitive than the pendulum-type gage. Since roll for the subject craft, like pitch, is a highly tuned motion, there is a tendency for the period of peak energy to coincide with the natural period in roll, irrespective of the exciting periods. The

response period in roll is approximately the same for January 22 and March 4, being approximately 6.0 seconds, which is close to the natural period in roll of 6.1 seconds. The period of maximum energy for February 7 is 5.0 seconds. This apparent shift in the peak period of maximum energy may be due more to the different character of excitation than to either excitation level or wave direction.

On January 22, the exciting wave spectrum was notably broadbanded (i.e., all frequency components were present in approximately equal proportions), whereas on February 7 the exciting wave system was narrow banded (i.e., one frequency tended to dominate the system). The March 4 exciting wave spectrum appeared to be a mixture of both extremes. Thus, the sea (January 22) tended to produce a period closer to the natural period (6.1 seconds) of the barge in roll than did the swell (February 7). It may be parenthetically remarked that the natural period of 6.1 seconds in roll was that observed in the absence of the moorings. This appears to be a reasonable trend.

Roll - Model. The spectra of roll response as obtained from the model measurements for the three incident wave directions is shown in Figure 20f. The period of maximum energy is 6.1 seconds, which corresponds exactly to the natural period in roll. The influence of incident wave direction is obvious. Beam-on waves produced the greatest response and stern-on the least. There were no long-period oscillations present in the roll response motion.

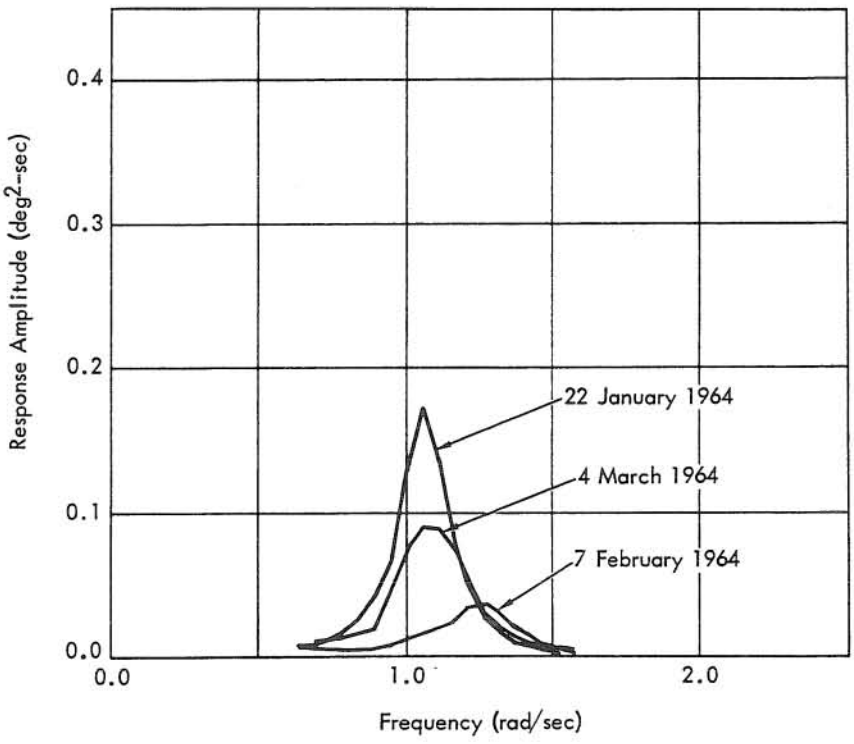

Figure 25. Response spectra of yaw, Fishhook prototype barge.

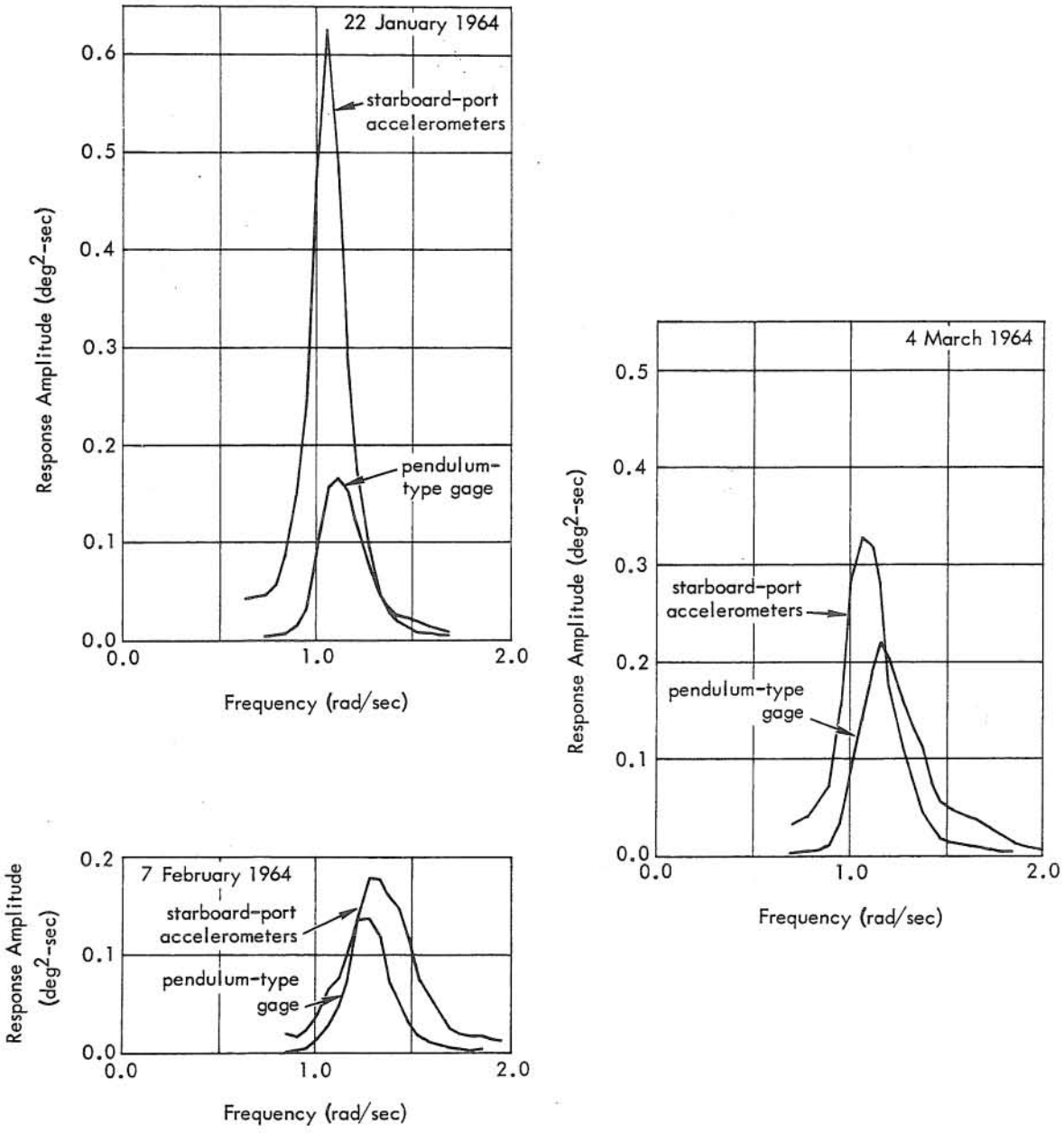

Figure 26. Response spectra of roll, Fishhook prototype barge.

Chain Response

The response of the chains in both the prototype and the model are given in terms of the spectra of the time histories. The response of any given chain is a function of the magnitude and direction of the exciting wave. Unlike the prototype displacement motion, chain response was recorded directly, and thus a greater degree of resolution at the lower frequencies (near the origin) of the spectra was obtained. Therefore, spectral ordinates for the entire range of frequencies are included.

Prototype. The spectra for prototype chain response are given in Figure 27. All are plotted to the same scale with the exception of chain No. 14 on January 22. Each of the spectra contains a peak within the normal period range of the exciting waves (i. e., 3 to 15 seconds) and a sharp spike or peak near the origin. Energy within the dominant period range (3 to 15 seconds) is due to exciting waves of the same range. Within the normal range of sea and swell, the dominant period is approximately 6. 0 seconds for all the chains. A lower secondary peak of approximately 4. 0 seconds occurs for March 4. The dominant period for the February 7 data is consistently lower, varying between 4. 0 and 5. 0 seconds for all the chains. This behavior is compatible with that noted for sway, yaw, and roll (i. e., for each motion, the peak response period for February 7 was lower than for any such period of the other 2 days).

Energy distributed within the peak or spike near the origin may be due to (1) linear response of the moorings to long-period surface gravity waves characteristic of the offshore basin, (2) linear response of the barge and moorings to wind gusts, and (3) nonlinear (subharmonic) response of the moorings to surface gravity waves within the normal frequency band of sea and swell.

Model. The response spectra of chain tension for each of the three conditions of barge orientation are shown in Figure 28. The ordinate scale is varied for each chain to accommodate the low-frequency peak of the spectra. The major trend is that beam-on seas induce greatest forces in the chain, and quartering seas the least. Considering only the frequency band of the exciting wave system, the trend is different although not reversed. Here, the greatest forces are induced by the stern-on seas, and again, quartering seas induce the least. The period of peak chain tension response coincides with the period of peak response in surge, sway, and yaw.

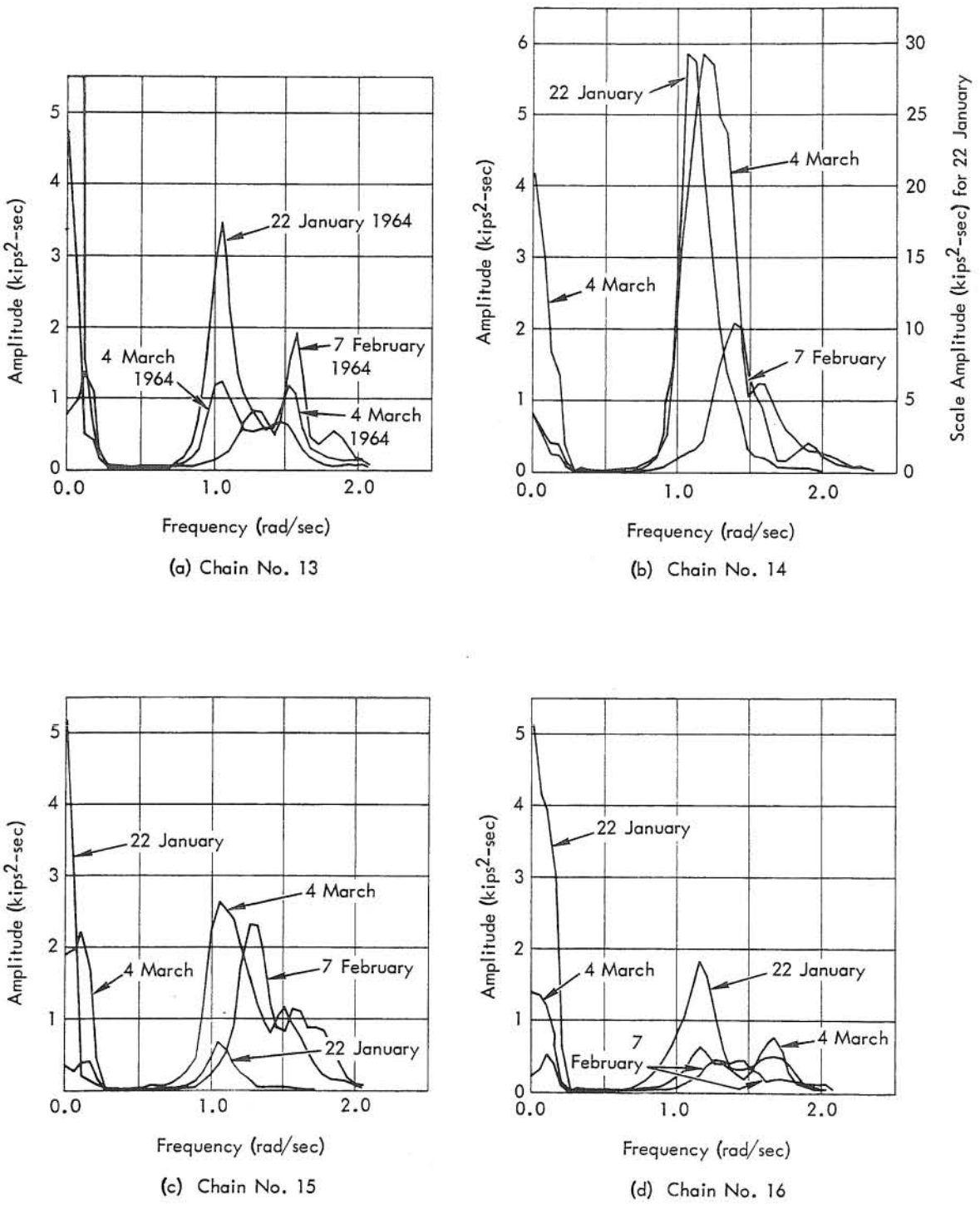

Figure 27. Response spectra from prototype chain tension measurements.

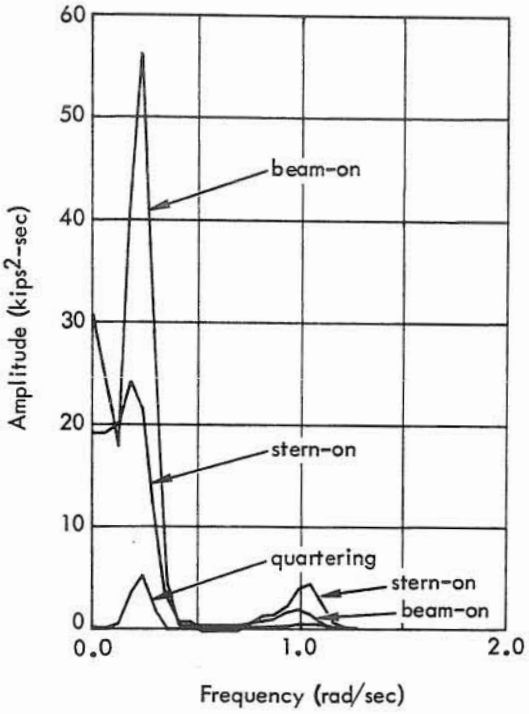

(a) Chain No. 13

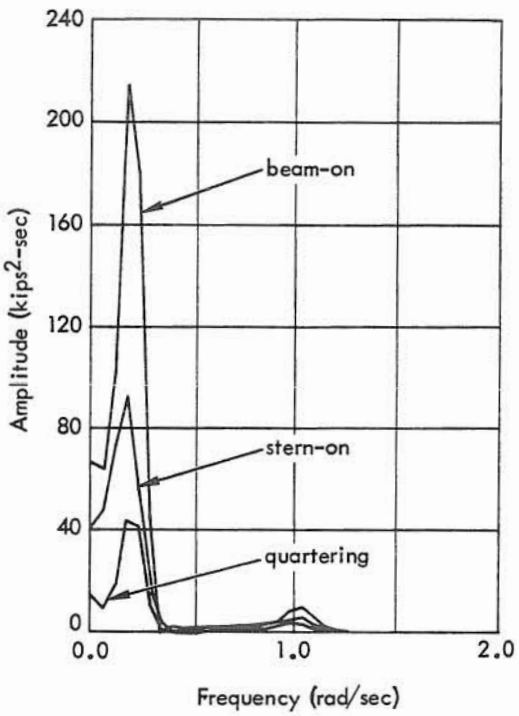

(b) Chain No. 14

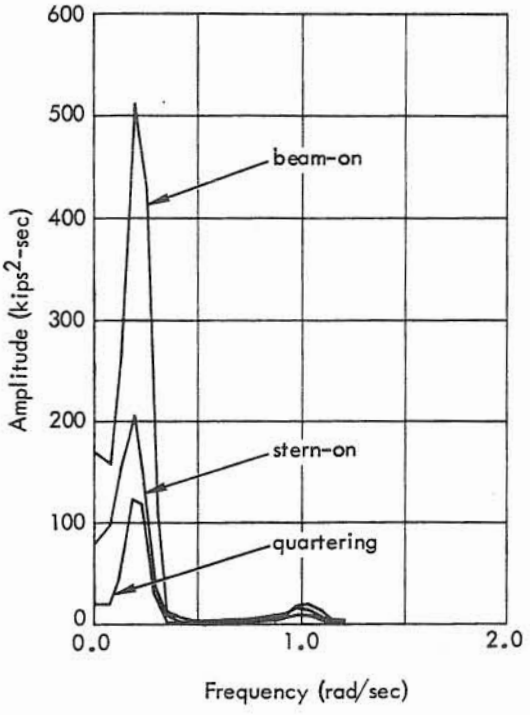

(c) Chain No. 15

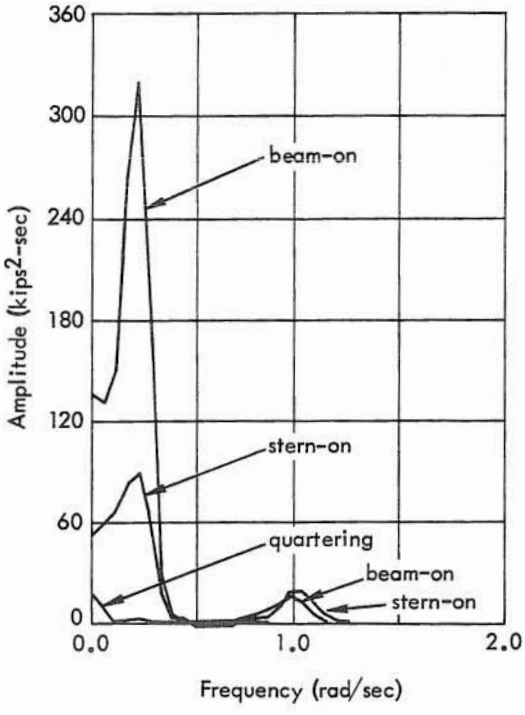

(d) Chain No. 16

Figure 28. Response spectra of chain tension (horizontal component) from model measurements.

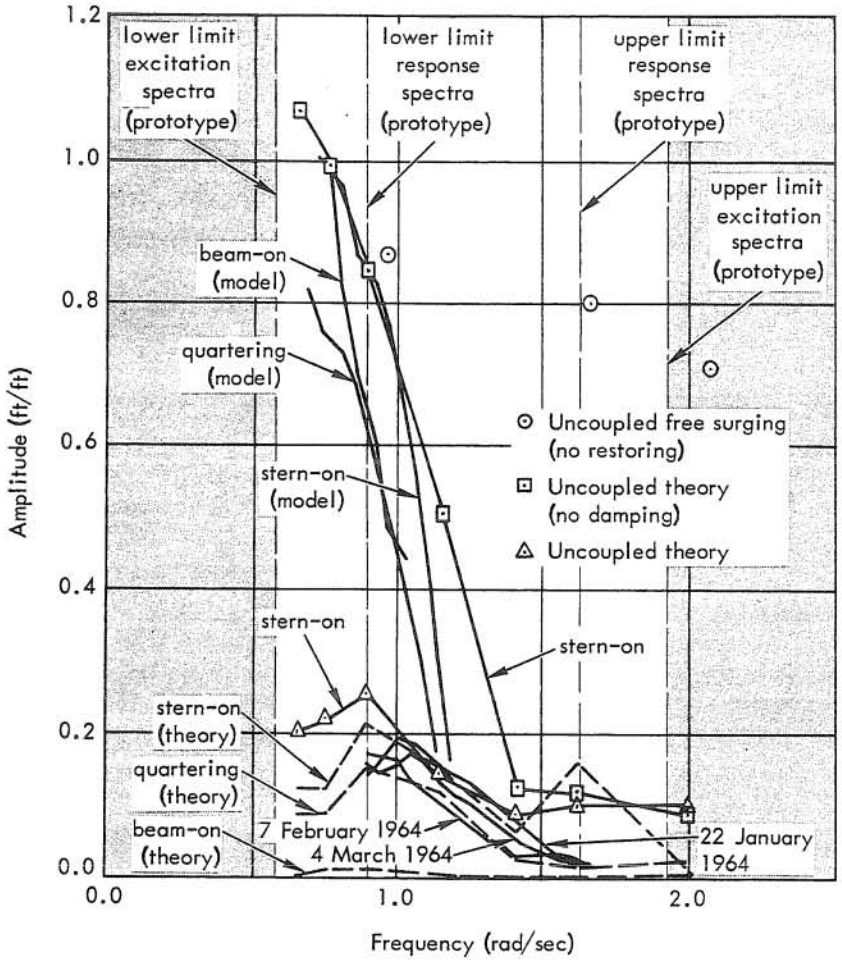

Figure 29. Comparison of surge amplitude response operators as obtained from model and prototype measurements and theory.

Response Operators

Surge. The surge amplitude response operators as derived from the prototype and model measurements and from the linear theory described in Appendix A are shown in Figure 29. In the case of the operators derived from the model and prototype tests, only a portion of the values is presented. Even these values may not be considered reliable since the ordinates of either the exciting wave spectrum or the response spectrum were within the signal "noise" level at these frequencies. The upper and lower limits of the significant

frequency range for both exciting and response spectra are indicated. The values shown in Figure 29 were further restricted by including only the calculations involving the center-well wave gage in the prototype and wave probe 2 in the model. The center of gravity of the barge is represented by these locations.

Considering values of the surge amplitude response operator which are known to be reliable, only one discrepancy exists - that between theory and model for stern-on and quartering seas at frequencies less than 1.0 radian/second. This is believed to result from the large value of the surge damping coefficient, N_x, employed in the theory. The coupled equations are far too complicated for simple analysis. However, at least two comparisons may be made. In the first, some insight into the behavior of the barge in both prototype and model forms may be gained by examining the uncoupled equation for the free surging of an unmoored ship in regular waves (approaching stern-on as given by Wilson, 1959). This equation, derived by likening a ship to a rectangular block, is

$$\frac{X}{A} = \frac{g}{\omega^2 D} \frac{\sinh kd - \sinh kS}{\cosh kD} \left(\frac{\sin 0.5\ kL}{0.5\ kL} \right) \sin (\omega t + \epsilon)$$

where X = surge amplitude
A = wave amplitude
D = draft
$\omega = 2\pi/T$ = frequency
T = wave period
$k = 2\pi/\lambda$
D = water depth
S = clearance between sea bed and ship keel = $d - D$
ϵ = phase angle
t = time, as a variable
L = ship length
λ = wave length

The above equation neglects the term bearing a second harmonic overtone which Wilson admits is unimportant. Wilson notes that the motion will be maximum when the ratio L/λ is such as to make $\sin (0.5\ kL) = \pm 1$. This occurs when $L/\lambda = 1/2,\ 3/2,\ 5/2 \ldots$, where $L = 110$ feet, that is, when the values of the wave frequency, ω, are 0.96, 1.66, 2.14 .... The amplitudes of surge response calculated for these frequencies according to the above equation are 0.87, 0.80, and 0.71, as shown in Figure 29. Thus, the uncoupled equation for the unmoored freely surging vessel predicts values for the surge response operator greatly in excess of the prototype and model tests.

The second comparison is obtained by examining the amplitude response operator when the coupling term(s) is omitted. Consistent with the notation employed and explained in Appendix A, the "uncoupled" amplitude response operator, a_x, for surge is given by

$$a_x = \frac{\sqrt{\left(A_x^w\right)^2 + \left(B_x^w\right)^2}}{\sqrt{\left(k_x - m\omega^2\right)^2 + \left(\omega C_x N_x\right)^2}} \tag{1}$$

where

$$\sqrt{\left(A_x^w\right)^2 + \left(B_x^w\right)^2} = \frac{\sin\frac{\pi B}{2}}{\frac{\pi B}{\lambda}} e^{\frac{-2\pi h}{\lambda}} \sqrt{\left(m\omega^2\right)^2}$$

for waves incident stern-on. Values of a_x for stern-on seas were computed and are shown by the small triangle symbols in Figure 29. The effect of including the coupling term(s) (pitch in this case) is almost negligible. Next, the damping term, N_x, in Equation 1 was set equal to zero, and values of the response amplitude operator were computed. These results, shown by the small squares in Figure 29, agree quite well with the model results in the low-frequency range (0.6 to 1.4 radians/second) and with the prototype results in the high-frequency range (>1.4 radians/second). Thus, substantial agreement between theory, prototype, and model results can be achieved through judicious selection of the values of the surge damping coefficient, N_x.

At this point, certain important differences in the model and prototype tests need to be restated. First, the moorings in the model were decidedly linear over the range of deflections encountered in the study. The prototype moorings were nonlinear. Thus, the motions per unit amplitude wave tended to be somewhat greater in the model than in the prototype. Second, differences in incident wave directions as observed in the prototype were much smaller than in the model tests. In the model tests, incident wave directions were almost exactly beam-on, quartering, or stern-on (except for instantaneous changes in attitude). In the prototype tests, wave directions were observed to be from an approximate heading, β, of 015, 275, and 330 degrees relative to the barge, where β = 0 degrees indicates a wave approaching from stern-on and positive angles are measured counter-clockwise. It has been previously noted that the prototype barge was excited by winds and currents as well as waves. The model barge was excited by waves only.

Third, the excitations as measured in the prototype contained the reflected waves generated by the barge. The excitations employed in the reduction of the model data were measured with the barge removed from the tank, and thus contained no such reflected waves.

Fourth, the excitation in the model was "narrow" banded whereas that in the prototype tended to be not quite so "narrow." Finally, the level of excitation was proportionately greater in the model tests than in the prototype tests. Sea state 4 was simulated in the model tests whereas measurements of the prototype were never taken in a sea state higher than 3.

In summary, only one discrepancy appears to exist in the surge amplitude response operators as obtained from model and prototype tests and from theory. This concerns the difference between model tests and theory at a frequency less than 1.0 radian/second. The discrepancy is believed to be due to the large value of the surge-damping coefficient, N_X, used in the theoretical calculations.

Heave. The amplitude response operators for heave are shown in Figure 30. The prototype results are not valid throughout the frequency range represented there. Values of the excitation and response ordinates were submerged within the signal "noise" level of the recording system at the lower frequencies. Nevertheless, the amplitude response operators are shown to indicate consistency in trends. The prototype response operators were almost identical for each test period. Only those obtained from the January 22 and February 7 data (center-well wire wave gage) are shown in Figure 30.

At a frequency of approximately 1.0 radian/second, a response greater than 1.0 foot/foot is indicated. This apparent peak is close to the observed natural period in heave of 6.1 seconds. Physically, such behavior is not likely. In addition to the "noise" problem referred to previously, that behavior may be attributed to statistical variability associated with a record of finite length. The spectral ordinates from which Figure 30 was derived have a chi-square distribution (Blackman and Tukey, 1958) based on the number of degrees of statistical freedom. The spectral ordinates for which the amplitude response exceeds a value of 1.0 foot/foot were based on a prototype record containing 3,601 data points. Pierson and Marks (1952) give the following approximate formula for calculating the number of degrees of freedom, f:

$$f = \frac{N - \frac{1}{4}m}{\frac{1}{2}m}$$

where N = number of data points and m = number of lags. On this basis, the number of degrees of freedom, f, is found to be 165. From any standard statistical table in chi-square distributions, it is found that the 90-percent confidence intervals for 165 degrees of freedom are 1.15 and 0.85 times the mean. Thus, the spectral ordinates obtained from a finite length of record would have a true value of from 0.85 to 1.15 times its mean at least 90 percent of the time. The response operator is obtained by dividing one ordinate by another, each of which has a chi-square distribution. The confidence limits for the response operator ordinates are not known, but Canham et al. (1962) indicate that there should be greater confidence in the operators than in the excitation and response from which they were derived.

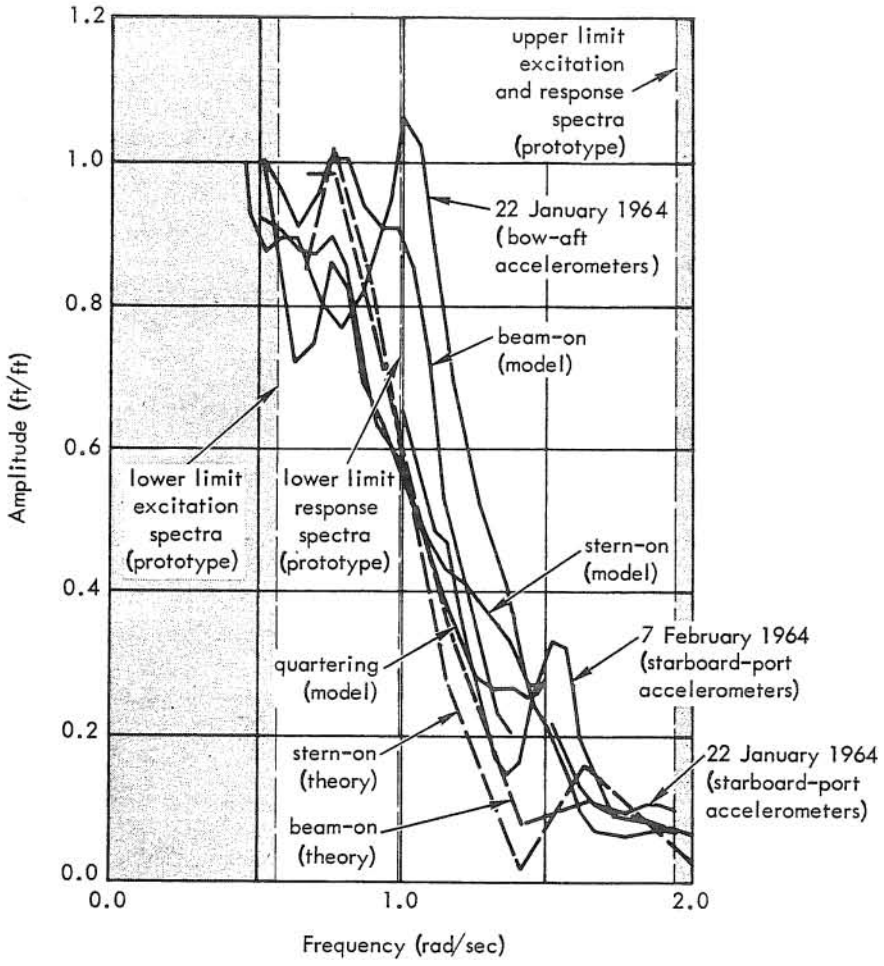

Figure 30. Comparison of heave amplitude response operators as obtained from model and prototype measurements and theory.

In order to evaluate the effect of the coupling terms, the amplitude response operators were computed as given by the following equation (coupling terms omitted):

$$a_z = \frac{\sqrt{\left(A_z{}^w\right)^2 + \left(B_z{}^w\right)^2}}{\sqrt{\left[\rho g \int B^* d\xi - \left(m + \int A_{33}' d\xi\right)\omega^2\right]^2 + \left(\omega C_z N_z\right)^2}} \qquad (2)$$

where for beam-on waves, the numerator $\sqrt{\left(A_z{}^w\right)^2 + \left(B_z{}^w\right)^2}$ is given by the following expression:

$$\frac{\sin\frac{\pi B}{\lambda}}{\frac{\pi B}{\lambda}} e^{\frac{-2\pi h}{\lambda}} \sqrt{\left[\left(m + \int A_{33}' d\xi\right)\omega^2 - \left(\rho g \tanh\frac{2\pi d}{\lambda} e^{\frac{2\pi h}{\lambda}} \int B^* d\xi\right)\right]^2 + \left(\omega C_z N_z\right)^2}$$

The results (not shown in Figure 30) indicated that the coupling terms have virtually no effect on the heave amplitude response operators. Referring to Equation 2, the terms

$$\frac{\sin\frac{\pi B}{\lambda}}{\frac{\pi B}{\lambda}} e^{\frac{-2\pi h}{\lambda}} \text{ and } \tanh\frac{2\pi d}{\lambda}$$

are equal to unity for large values of wave length, λ. Thus, for long wave periods, T, or low frequencies, ω, the response operator a_z approaches a value of one. Departures from a value of one for decreasing values of wave length, λ, depend upon the effect of each of these terms in relation to the other terms, two of which are themselves frequency-dependent, namely, the damping coefficient, N_z, and the added mass coefficient, A_{33}'. Thus, it is possible that absolute values of the damping coefficients, N_z, which were used in the theory may have contributed to small differences between theory, prototype, and model results.

Comparison of the heave amplitude response operators as obtained from the prototype measurements and theoretical calculations is very good within the frequency band (1.5 to 2.0 radians/second) in which the prototype results are valid. Comparison of the model results with the theoretical calculations is very good within the frequency band in which the model results are valid. In addition, the trends indicated by the model and prototype results are in substantial agreement.

In summary, no anomalies are present in the heave amplitude response operators.

Pitch. The amplitude response operators for pitch are shown in Figure 31. For the case of stern-on waves, the amplitude response operator attained a maximum value of 1.9, 3.2, and 1.9 degrees/foot from the prototype and model tests and from the theory, respectively. The general shapes of all the curves are very similar. The prototype and model results show a peak at a period of approximately 6.3 seconds, which is close to the observed natural periods of 6.5 and 6.1 seconds in the prototype and model, respectively. The theoretical calculations, on the other hand, indicate a peak at a period of approximately 8.6 seconds. In order to determine reasons for this difference in peak response period, the uncoupled equation for the pitch amplitude reponse operator was examined. The appropriate equation is

$$a_\theta = \frac{\sqrt{\left(A_\theta{}^w\right)^2 + \left(B_\theta{}^w\right)^2}}{\sqrt{\left[\rho g \int B^* \xi^2 d\xi - \left(I_y + \int A_{33}' \xi^2 d\xi\right)\omega^2\right]^2 + \left(\omega C_\theta N_\theta\right)^2}} \qquad (3)$$

where for waves incident stern-on, the numerator $\sqrt{\left(A_\theta{}^w\right)^2 + \left(B_\theta{}^w\right)^2}$ is given by the following expression:

$$\frac{\sin\frac{\pi B}{\lambda}}{\frac{\pi B}{\lambda}} \; e^{\frac{-2\pi h}{\lambda}} \sqrt{\left\{\left[\int\left(\rho s + A_{33}'\right)\xi d\xi\right]\omega^2 - \left(\rho g \tanh\frac{2\pi d}{\lambda}\, e^{\frac{2\pi h}{\lambda}} \int B^* \xi d\xi\right)\right\}^2 + \left(\omega C_\theta N_\theta\right)^2}$$

The results shown by the small triangles in Figure 31 indicate that the coupling terms increase the amplitude of the response but do not change the period of peak unit response.

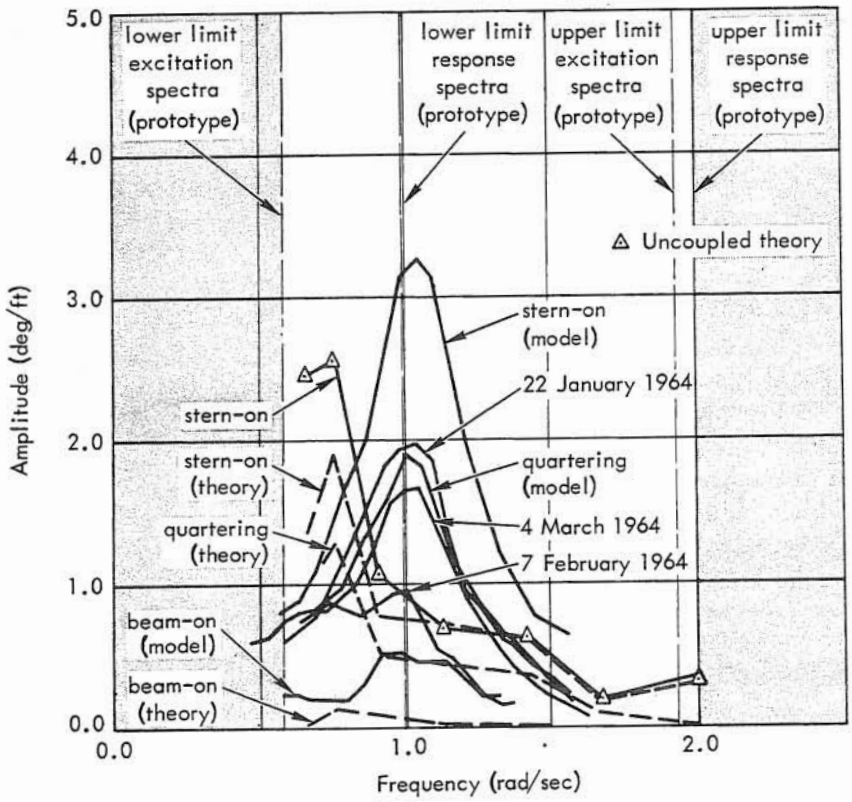

Figure 31. Comparison of pitch amplitude response operators as obtained from model and prototype measurements and theory.

The results shown by the small triangles in Figure 31 indicate that the coupling terms increase the amplitude of the response but do not change the period of peak unit response.

To study the effect of damping, values of a_θ were computed from Equation 3 with the damping coefficient, N_θ, set equal to zero. The results, not shown, indicated that the period of peak unit response was independent of the damping coefficient. The only remaining frequency-dependent coefficients in Equation 3 are the added mass coefficient, A_{33}', and the correction (or approximating) factors for (1) slender body approximation

$$\frac{\sin \frac{\pi B}{\lambda}}{\frac{\pi B}{\lambda}},$$

(2) shallow water waves, $\tanh 2\pi d/\lambda$, and (3) mean half-draft velocity approximation, $e^{-2\pi h/\lambda}$. With substantial faith in the latter, it appears that values of the added mass coefficient in heave, A_{33}', which were employed in the theory cause the pitch amplitude response operator to peak at a period of 8.6 seconds rather than at the observed natural period in pitch of 6.5 seconds.

Differences in magnitude of the pitch amplitude response operator as obtained from the model and prototype results are believed to be associated with physical differences between the model and prototype tests. In addition to those differences previously noted, the vertical components of the mooring restoring forces, and thus the important moments in the case of pitch and roll, were not simulated in the model. This rationale may be used to explain similar differences in the roll amplitude response operator. For both motions, the amplitude response operator obtained from the model tests was smaller than that obtained from the prototype tests; hence, the trend is consistent.

In summary, deviations of the period of peak unit response as obtained from the prototype and model tests and the theory are believed due to improper values of the added mass coefficient in heave, A_{33}', which were employed in the theory. Amplitude differences are believed to be accounted for by (1) inherent physical differences between the model and test installations, and (2) improper values of the damping and coupling terms employed in the theory.

Sway. The amplitude response operators for sway are shown in Figure 32. For beam-on seas, the theory agrees quite well with the model results in the frequency range 0.6 to 1.4 radians/second and with the prototype results in the frequency range above 1.4 radians/second. These frequency ranges correspond to the validity limits of the prototype and model results. However, the prototype operators are extended beyond these limiting frequency ranges to show that the trend of the operators even in the presence of high background "noise" is as expected and similar to the model results.

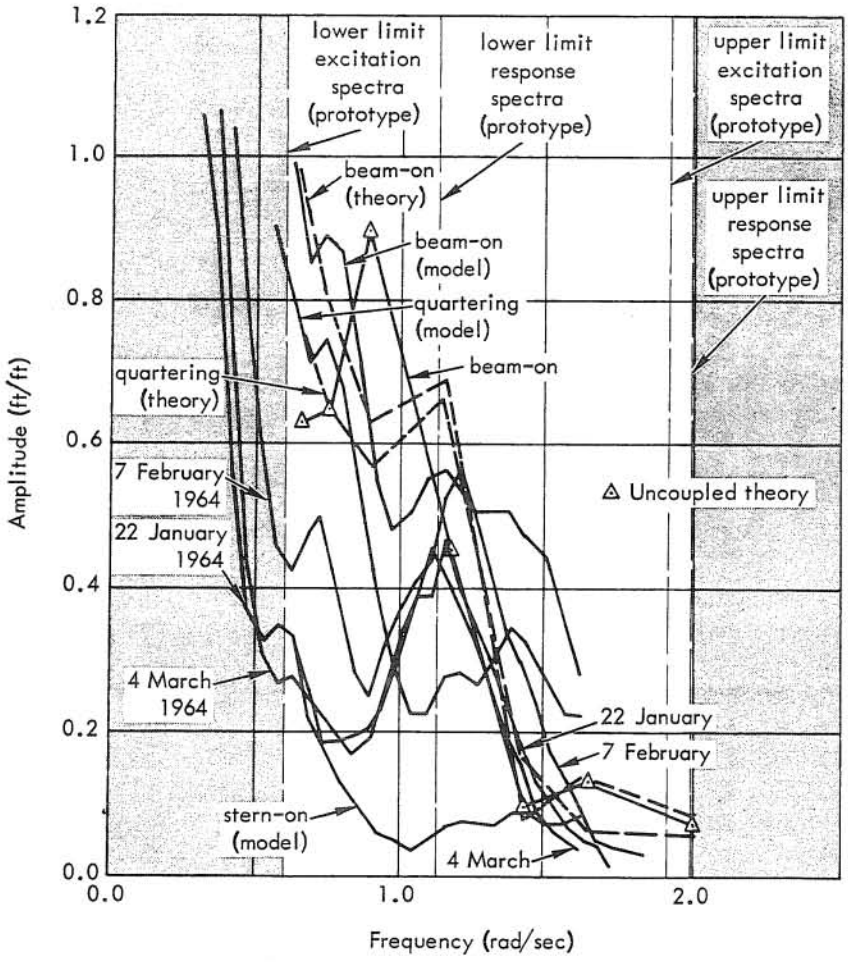

Figure 32. Comparison of sway amplitude response operators as obtained from model and prototype measurements and theory.

The model results clearly show that the response amplitude is greatest for beam-on waves and least for stern-on waves, as expected. It is recalled that the response in sway as obtained from the model tests is greatest at the characteristic period of oscillation (i.e., approximately equal to 36 seconds) of the moored barge system where the excitation was practically nil. Amplitude response operators obtained from the excitation and response spectra in this period range have little meaning because of the nonlinear behavior of the oscillating barge. Hence, no results are shown for this frequency band.

Again, as in the case for the longitudinal motions, the effects of coupling were studied. The uncoupled equation for the sway response operator, consistent with the notation employed in Appendix A, is

$$a_y = \frac{\sqrt{\left(A_y{}^w\right)^2 + \left(B_y{}^w\right)^2}}{\sqrt{\left[k_y - \left(m + \int A_{22}'d\xi\right)\omega^2\right]^2 + \left(\omega C_y N_y\right)^2}} \tag{4}$$

where $\sqrt{\left(A_y{}^w\right)^2 + \left(B_y{}^w\right)^2}$ for beam-on waves is given by

$$\frac{\sin\frac{\pi B}{\lambda}}{\frac{\pi B}{\lambda}} \; e^{\frac{-2\pi h}{\lambda}} \sqrt{\left[\left(m + \int A_{22}'d\xi\right)\omega^2 + \omega^2 \frac{2\pi}{\lambda}\int A_{42}'d\xi\right]^2 + \left(\omega C_y N_y\right)^2}$$

Except for the very short waves, the quantity

$$\frac{\sin\frac{\pi B}{\lambda}}{\frac{\pi B}{\lambda}} \; e^{\frac{-2\pi h}{\lambda}}$$

has a value close to unity. Thus, from the "uncoupled" equation, the magnitude of the sway amplitude response operator is dependent upon the relative contributions of the sway restoring force term, k_y, and the added mass coefficient in sway due to motion in roll, A_{42}'. The restoring force, k_y, is not a function of frequency. This is in contrast to the frequency-dependent off-diagonal tensor, A_{42}', which incidentally is a negative quantity.

In summary, the sway amplitude response operators as obtained from theory, prototype, and model results are in substantial agreement within the frequency ranges where the results are applicable. Outside of these ranges, the trends are compatible.

Yaw. The amplitude response operators for yaw are shown in Figure 33. Comparison is poor. In the case of the model results, the response in yaw over the indicated frequency range was entirely within the noise level of the recording system. Hence, the model results are not considered reliable. The assumption of a slender body theory and its application to the barge in question, with the attendant approximations which were required for the computations, is not justified - at least in the case of yaw. Nevertheless, it is to be observed that the model, theory, and prototype results show some yaw for beam-on and stern-on waves. This is to be expected since the barge is nonsymmetrical both fore and aft and port and starboard.

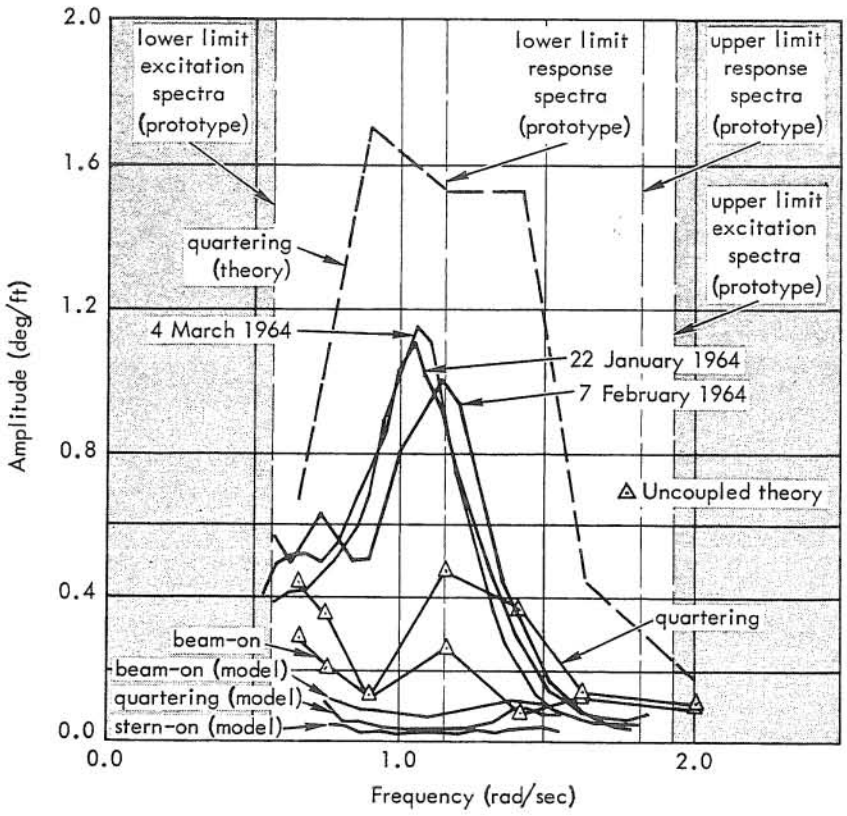

Figure 33. Comparison of yaw amplitude response operators as obtained from model and prototype measurements and theory.

The uncoupled equation for the yaw amplitude response operator is

$$a_{\psi} = \frac{\sqrt{\left(A_{\psi}^{w}\right)^2 + \left(B_{\psi}^{w}\right)^2}}{\sqrt{\left[k_{\psi} - \left(I_z + \int A_{22}' \xi^2 d\xi\right)\omega^2\right]^2 + \left(\omega C_{\psi} N_{\psi}\right)^2}} \tag{5}$$

where A_{ψ}^{w} and B_{ψ}^{w} are as given in Appendix A. Values of the yaw amplitude response operator for quartering and beam-on seas were computed and are indicated by the small triangles in Figure 33. It appears that in contrast to the other motions discussed to this point, the yaw amplitude operator is highly dependent upon the coupling effects. In addition to the frequency-dependent coefficients, A_{22}' and N_{ψ}, appearing in Equation 5, the omitted coupling terms also include the added mass coefficient in sway due to motion in roll, A_{42}'.

In summary, the poor comparison of the yaw response operators as obtained from theory and prototype results is believed to be caused by values of the coefficients appearing in the coupling terms used in the theory.

The poor comparison between the operators as obtained from model and prototype data is believed to be due to the relatively high "noise" level in the model yaw response at frequencies corresponding to the prototype yaw response.

Roll. The amplitude response operators for roll are shown in Figure 34. Comparison is excellent. Peak period of the response operators is 6.3 seconds, which corresponds to the natural period in roll of 6.1 seconds. Comments made in the case of the pitch response operators apply also to the roll response operators. The small response for stern-on waves is explained by Pierson (1957) as:

> ... the oncoming apparent wave will at one time be high on the port side and at another time be high on the starboard side causing the vessel to roll first one way and then the other for the same apparent wave form...

It may also be explained on the basis that nonsymmetries in the vessel permit yawing motion and that once the vessel yaws, however slightly, the incident wave is no longer directly stern-on but has a beam-on component which induces roll.

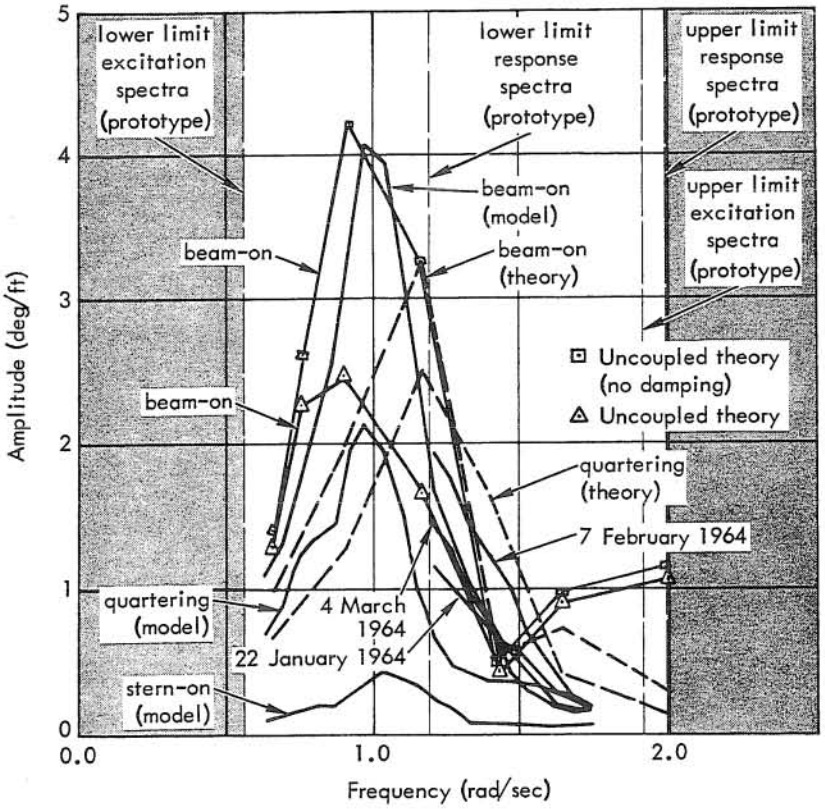

Figure 34. Comparison of roll amplitude response operators as obtained from model and prototype measurements and theory.

The uncoupled equation for the roll amplitude response operator is

$$a_\phi = \frac{\sqrt{\left(A_\phi{}^W\right)^2 + \left(B_\phi{}^W\right)^2}}{\sqrt{\left(W|GM| - I_{xt}\omega^2\right)^2 + \left(\omega N_\phi\right)^2}} \tag{6}$$

where $A_\phi{}^W$ and $B_\phi{}^W$ are as given in Appendix A. Values of a_ϕ were computed according to Equation 6 and are indicated by the small triangles in Figure 34. The effect of the coupling terms is to shift the peak period of the response amplitude operator from 5.4 to 7.0 seconds with an attendant slight decrease in the amplitude ordinate.

In summary, there is excellent agreement between the theory, prototype, and model results for the roll amplitude response operator.

Chain Tension Operators. The amplitude response operators for chain tension in kips/foot versus frequency as obtained from the model and prototype tests are given in Figures 35 through 38. For completeness, values of the ordinates are given for the entire frequency range in the case of the prototype even though spurious signal "noise" constituted a large percentage of the energy spectra of excitation and response at a number of frequencies. Notice that one ordinate scale is employed for all model results (Figure 38) and a different one for all prototype results. The prototype and model results are not directly comparable since the prototype included total tension, whereas only the horizontal component of tension was simulated and measured in the model.

In the case of the prototype, all response operators are characterized by low-frequency and high-frequency peaks. The low-frequency peak corresponds to the free period of oscillation of the mooring chains in the horizontal plane (i.e., sway, surge, and yaw), while the high-frequency peak corresponds to free oscillations in the vertical plane (i.e., roll, pitch, and heave). The mooring is decidedly unbalanced for certain incident wave directions, notably a combined quartering-beam-on sea such as occurred on January 22, 1964.

In this instance, the starboard stern chain (No. 14) was subjected to the greatest loads. With the center well gage used as a reference, the loading was approximately 14.3 kips/foot of wave amplitude. This compares with a wave loading of 2.2, 4.3, and 4.9 kips/foot for the port bow, starboard bow, and port stern chains, respectively. With the port stern gage used as a reference, Figure 35 indicates that unit amplitude waves may induce loads up to 21.0 kips.

The response operators obtained from the model tests are not shown in the low-frequency range since the corresponding excitation was virtually zero.

The theoretical amplitude response operators for chain tension were not calculated. In principle, they can be determined from the complex (i.e., phase and amplitude) response operators and the geometry of the moorings.

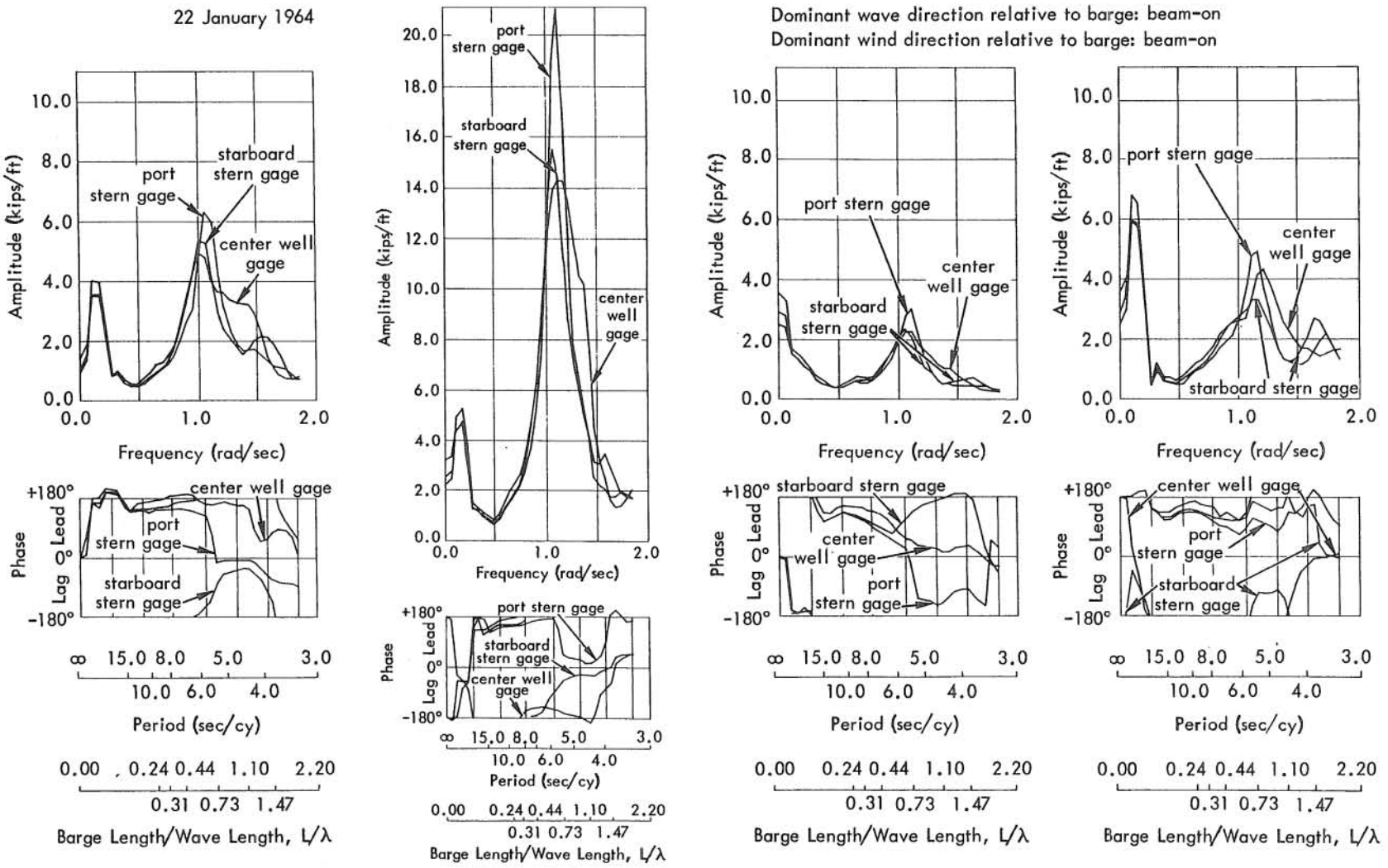

Figure 35. Prototype chain tension response operators from 22 January 1964 measurements.

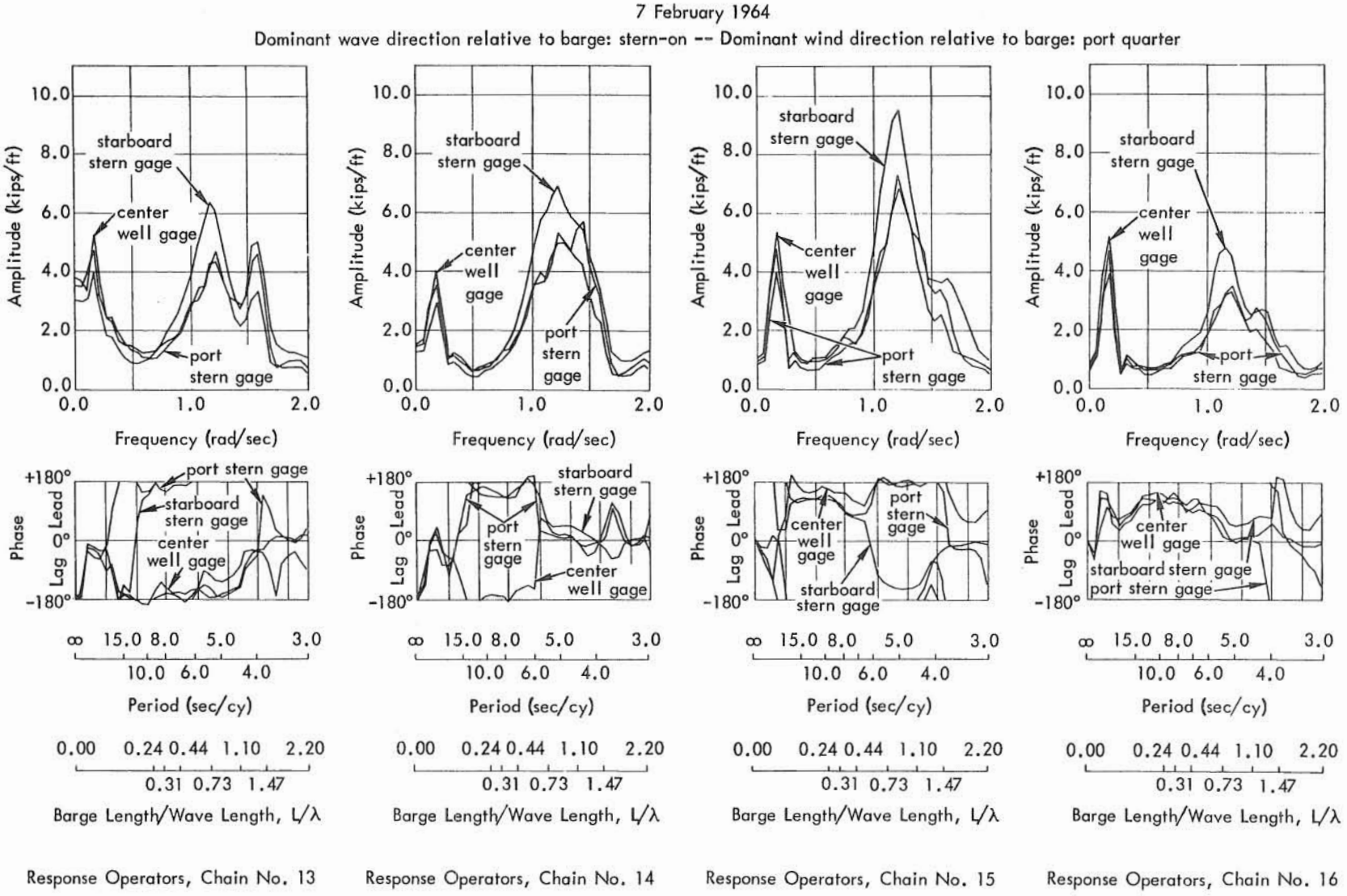

Figure 36. Prototype chain tension response operators from 7 February 1964 measurements.

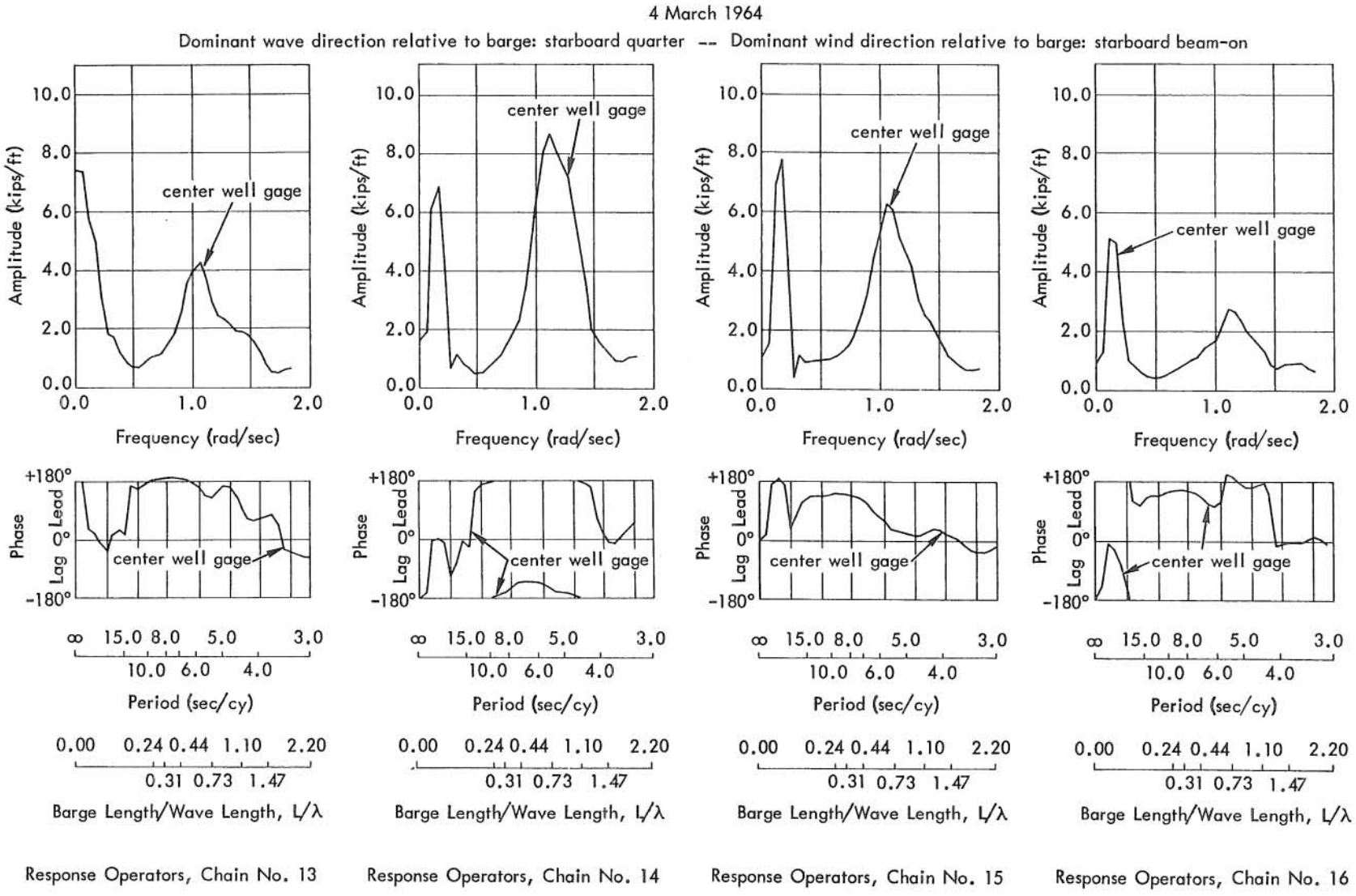

Figure 37. Prototype chain tension response operators from 4 March 1964 measurements.

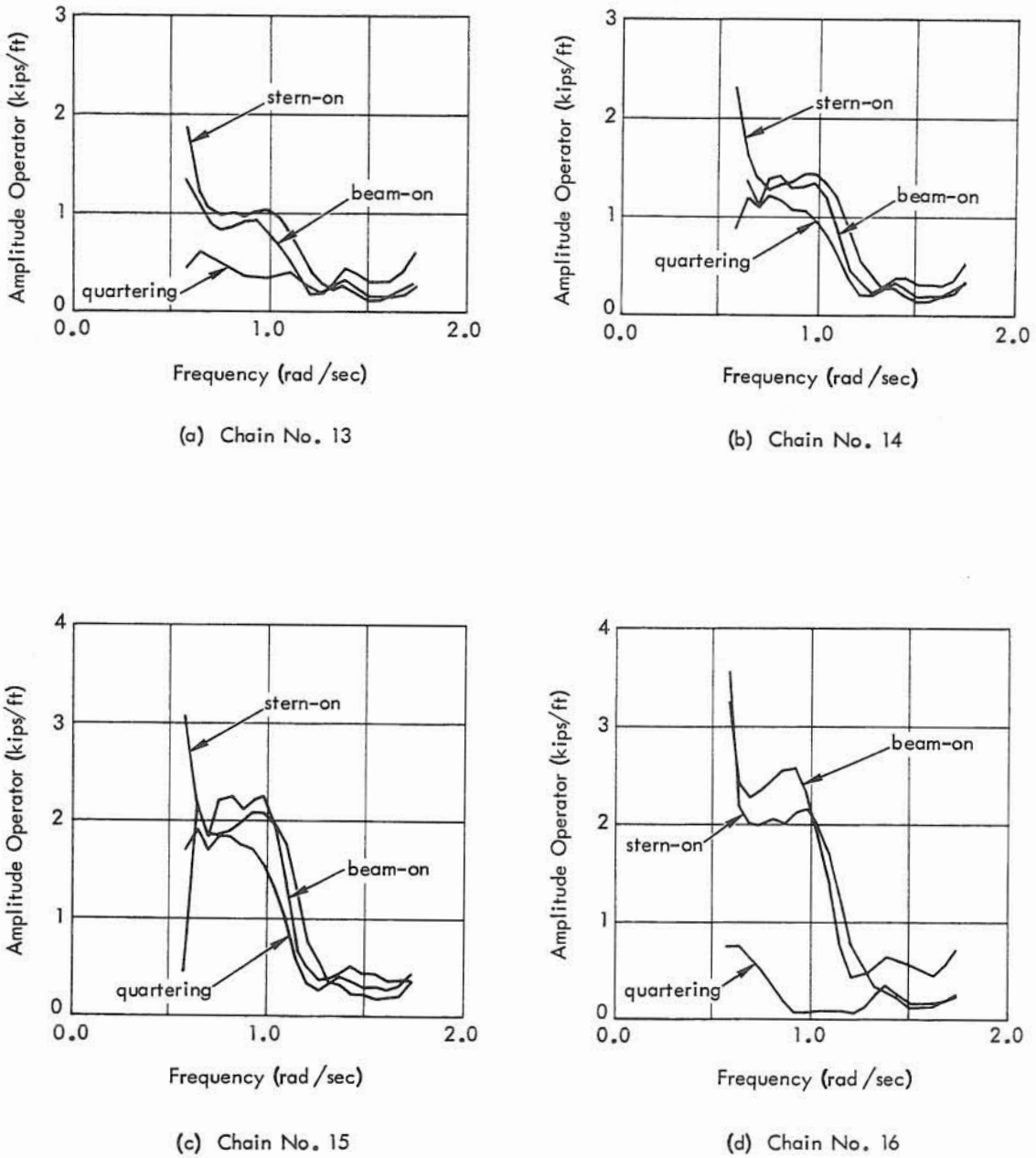

(a) Chain No. 13

(b) Chain No. 14

(c) Chain No. 15

(d) Chain No. 16

Figure 38. Linear amplitude response operators from model measurements corresponding to frequency band of exciting waves.

Phase and Coherence

The phase and coherence graphs for the prototype measurements are shown in Figures 39 through 41. Those for the model measurements are shown in Figures 42 through 44. The values for phase indicate the amount in degrees by which the peak amplitude of the output function lags the peak amplitude of the driving function. Thus, a value of 0 degrees or 360 degrees indicates that the two time history records are in phase, whereas a value of 180 degrees indicates that the functions are out of phase. Only values of coherence above 0.50 are shown in the figures. Canham et al. (1962) define coherency as the "ratio of the actual related energy between two records as computed by cross-correlation to the assumed related energy computed by auto-correlation." Canham et al. further state that if the "records are linearly related and there are no other errors of any kind, computational or otherwise, the result computed by cross-correlation will be the same as the result computed by auto-correlation, and consequently a value of unity will be obtained. Since in practice there are always sampling errors and possibly computational errors, low coherency does not necessarily indicate a nonlinear relationship between two records, but high coherency provides reliable confirmation of the accuracy of the data, the accuracy of the computation, and the linearity of the relationship between the two sets of data." Pierson (1957) notes that in the case of ship motion, short-crestedness of the wave system will also tend to lower coherencies between the ship motions and the exciting waves.

Referring to Figures 39 through 41, all possible combinations were compared for the prototype. However, not all model measurements were recorded to precisely the same time base. Treatment of a portion of the model data, to enlarge the number of combinations which could be computed, revealed that the effort would be excessive from both time and budgetary standpoints. Hence, only those combinations which could be readily computed from the original model data were attempted.

All expected trends are apparent in the figures. For example, the subsurface pressure gages were in phase with their corresponding wire wave gages and exhibited marked high coherencies. Chain tensions in the prototype generally were coherent with each other in spite of variable incident wave direction. The stern chains (No. 13 and 14) tended to be in phase with each other and out of phase with the pair of bow chains (No. 15 and 16). The dependency of the phase relationships on the incident wave direction is readily apparent in the case of the model results. When the waves were stern-on, the stern chains were in phase with each other and out of phase with the pair of bow chains. On the other hand, when the waves were beam-on, the pair of port chains were in phase with each other over a significant portion of the frequency band and out of phase with the pair of starboard chains. The high degree of coherency between the wave measurement and the chain tensions and appropriate motions in the case of the model confirms a fact already noted - that the model behavior was significantly linear over the dominant portion of the exciting wave spectrum.

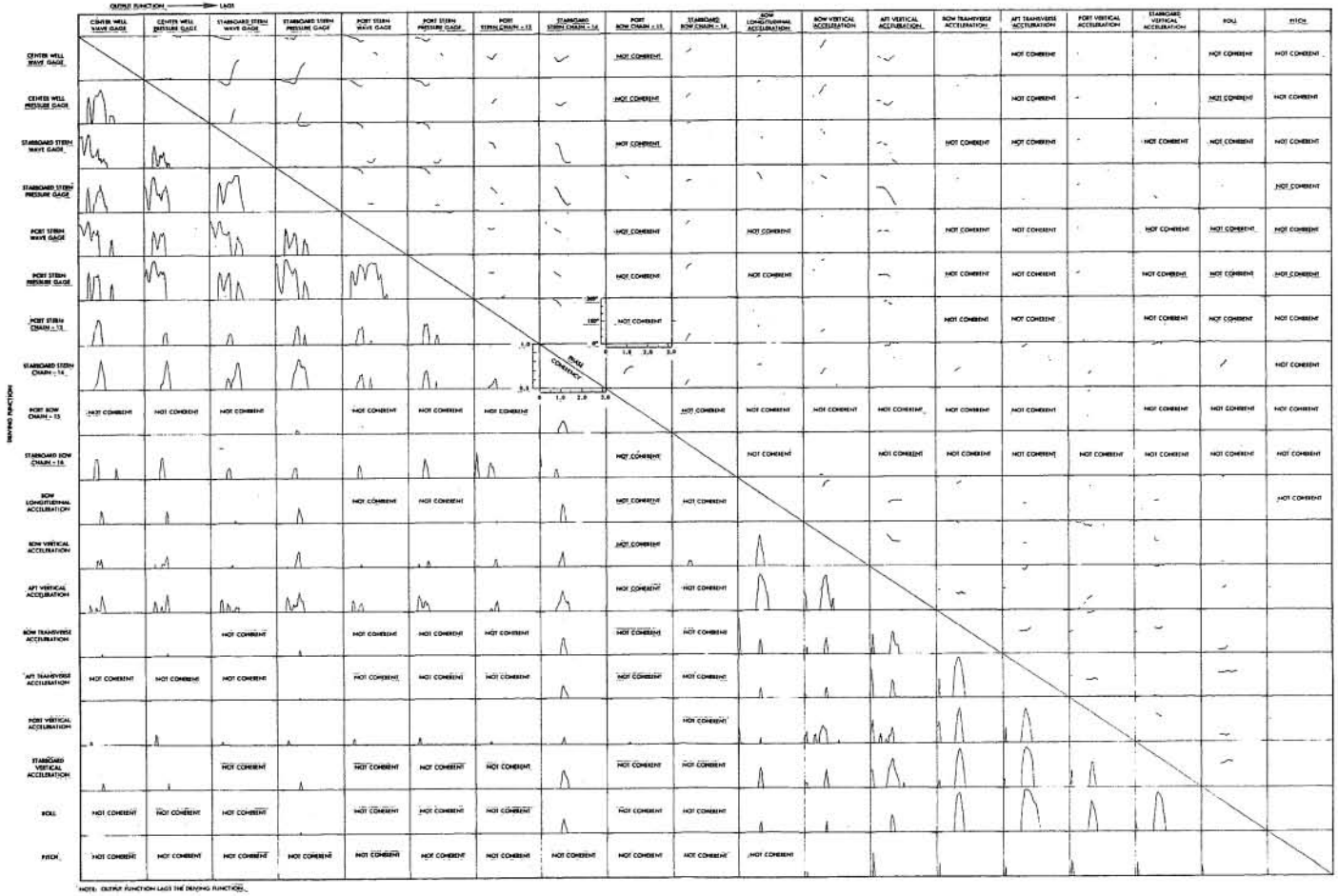

Figure 39. Phase and coherency graph, 22 January 1964 - prototype.

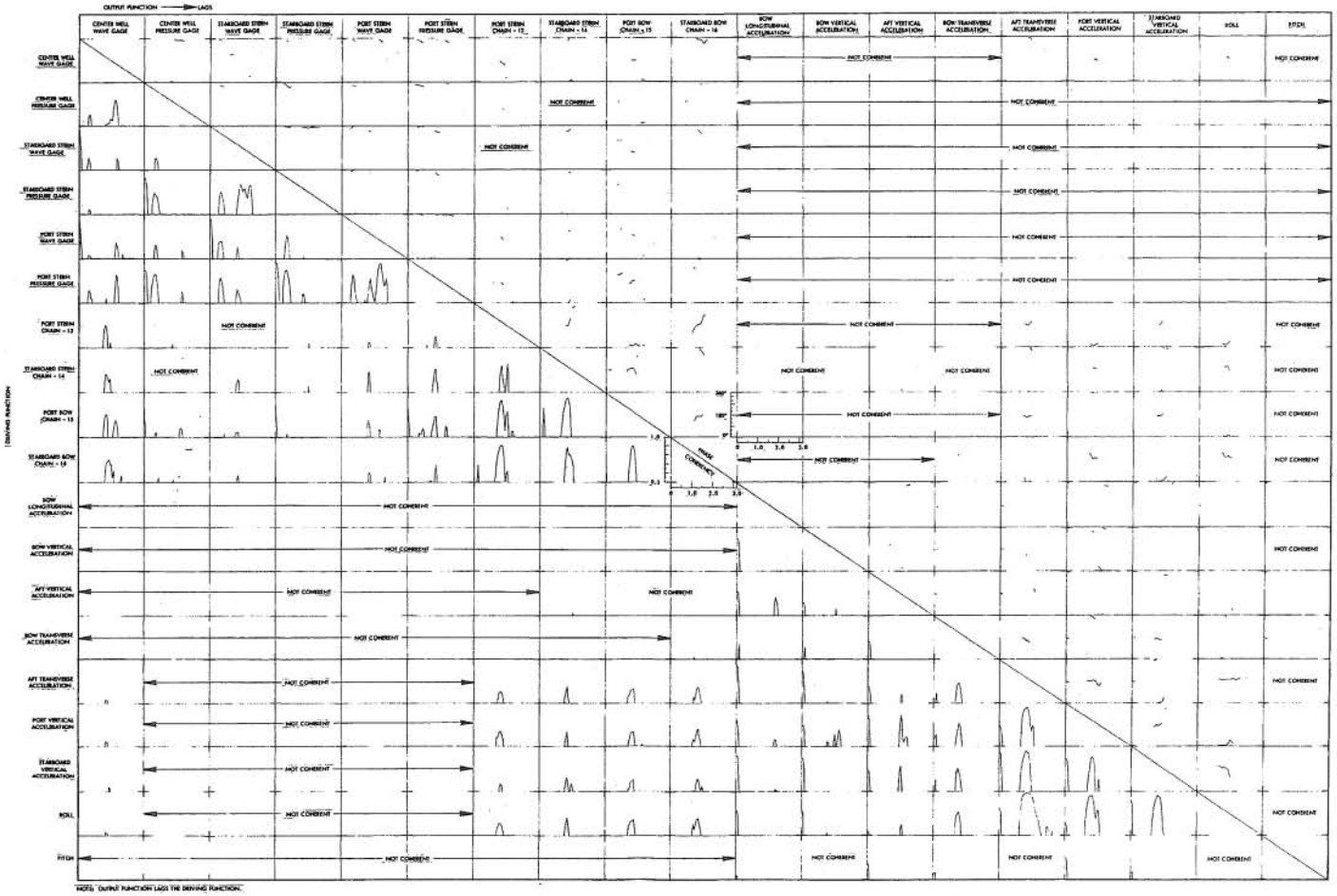

Figure 40. Phase and coherency graph, 7 February 1964 - prototype.

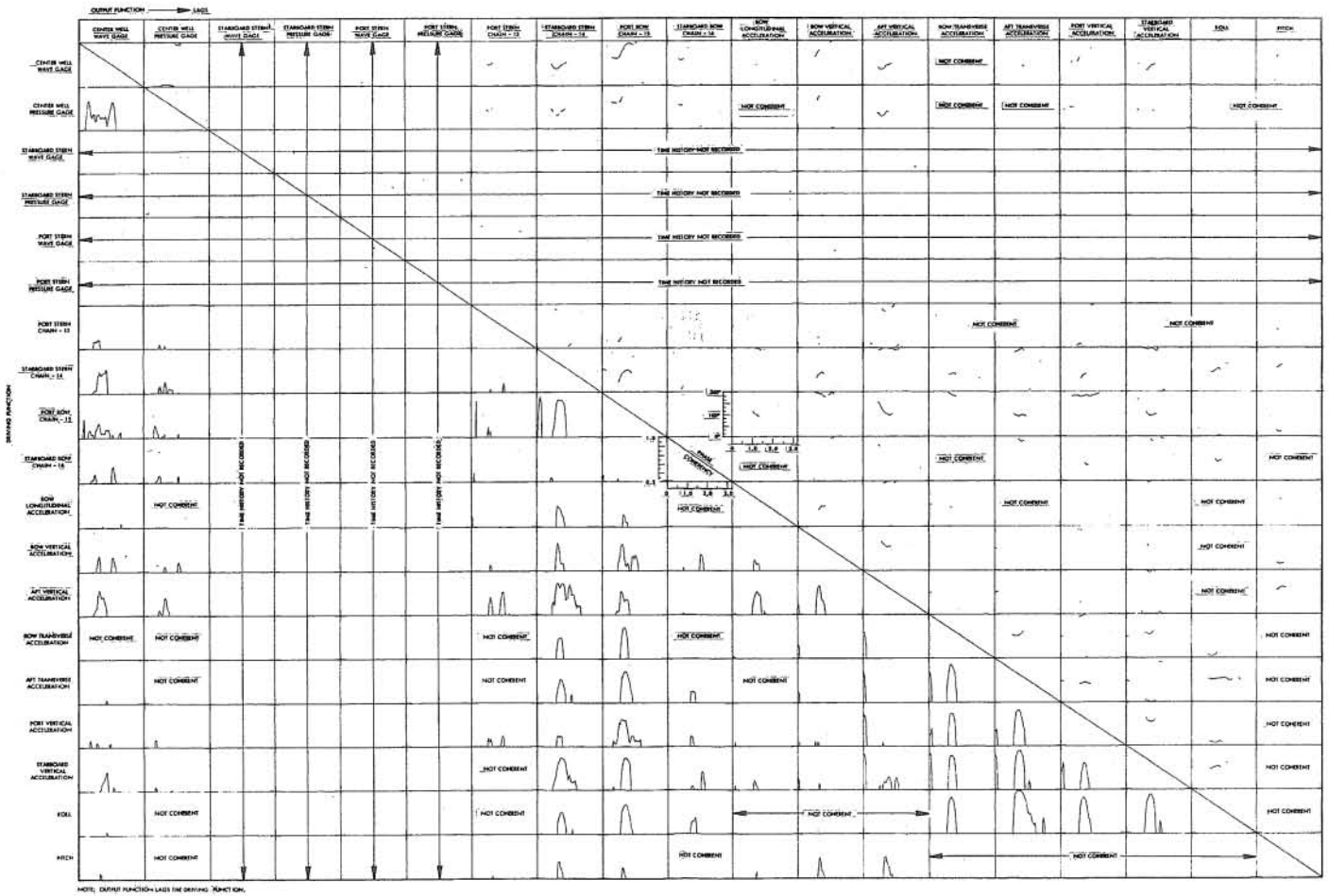

Figure 41. Phase and coherency graph, 4 March 1964 - prototype.

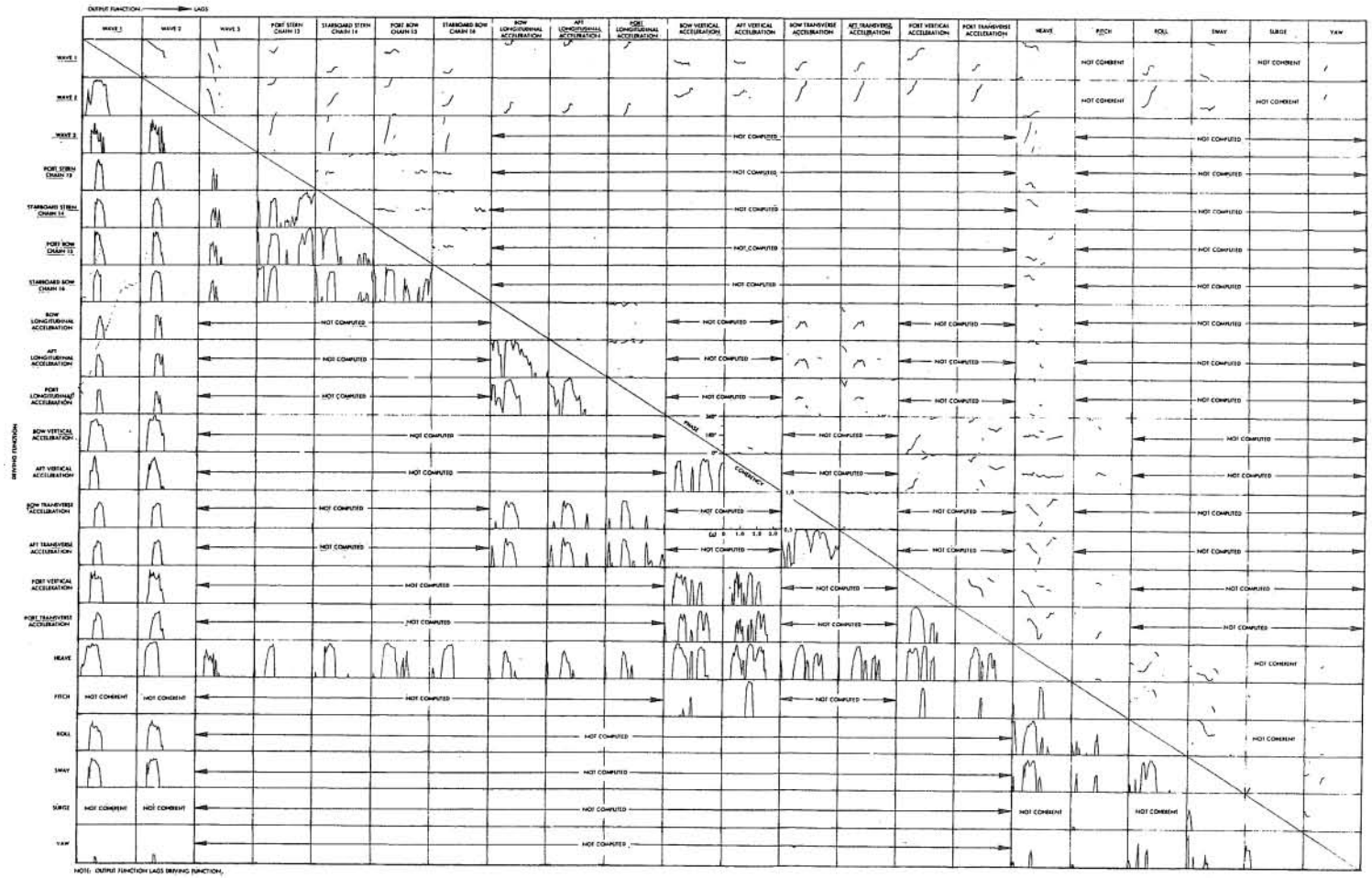

Figure 42. Phase and coherency graph, beam-on - model.

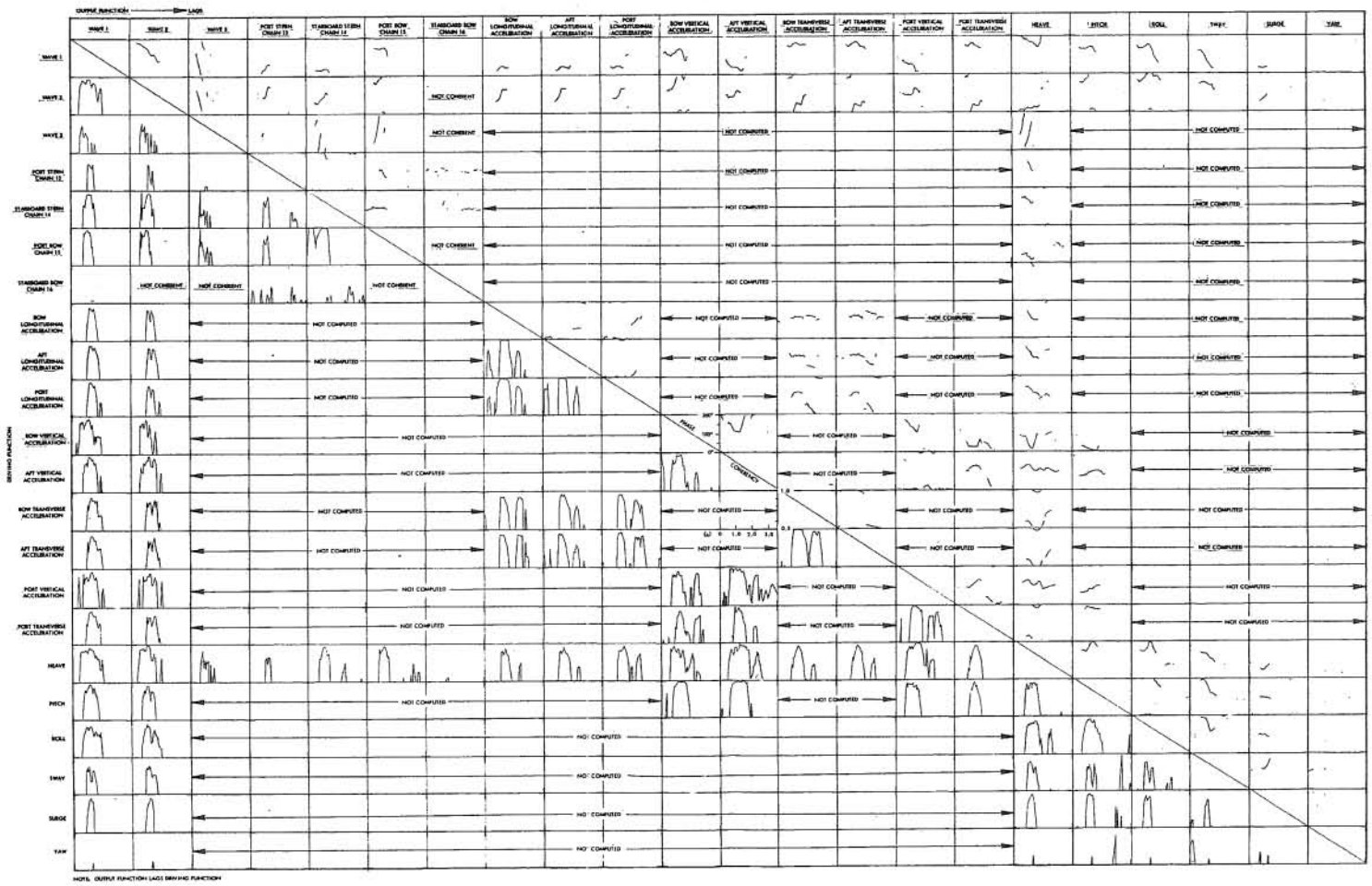

Figure 43. Phase and coherency graph, quartering - model.

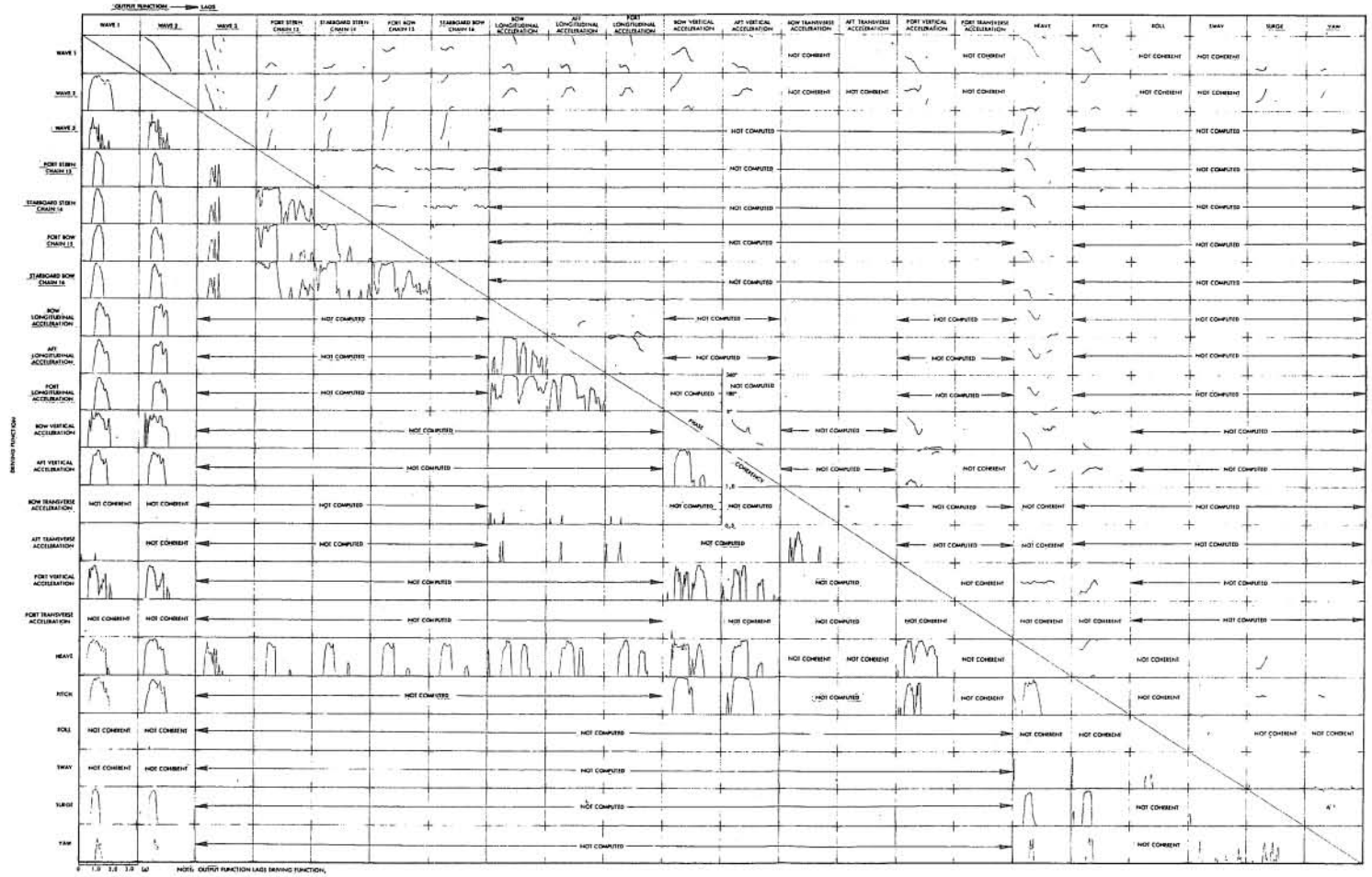

Figure 44. Phase and coherency graph, stern-on - model.

Only a limited number of the important observations concerning Figures 39 through 41 are presented here. In the case of the prototype, the roll motion was highly coherent with the bow and stern transverse acceleration and with the port and starboard vertical acceleration. Only starboard stern chain No. 14 appears to be coherent with all of the acceleration and the roll motion measurements for January 22. Coherency between the chain tension measurements and certain of the acceleration measurements was very similar for February 7. Chains No. 14 and 15 had approximately the same coherency with the acceleration measurements on March 4 when the waves approached generally from a direction coincident with the vertical plane containing chains No. 14 and 15.

In the case of the model, roll and sway were not coherent with the wave measurements for stern-on waves, while pitch and surge were not coherent with the beam-on wave measurements. When the waves were from a quartering direction, all motions had some degree of coherency with each other and with the forcing waves.

In summary, a study of the phase and coherency relationships for the prototype (Figures 39 through 41) and for the model (Figures 42 through 44) reveal no anomalies and confirm many of the expected trends. A detailed review of the wealth of information contained in these figures potentially constitutes a complete study in itself.

APPLICATION OF RESULTS. (Effects of the Historical Weather Environment)

Statistics of the wind and wave environment for San Clemente Island have been reported by Porter, Urquhart, McCreary, and O'Brien (1956). Those statistics pertinent to the Wilson Cove area are summarized herein. The general location of San Clemente Island and Wilson Cove is shown in Figure 1.

Probable Wind Environment

The then-existing air facility (elevation 900 feet) located 5 miles south of Wilson Cove recorded wind direction and intensity for the two periods of August 1940 through January 1941 and November 1943 through March 1954. From these observations, Porter et al. tabulated the data below:

	Percentage of Frequency		
Direction	4-11 Knots	11-22 Knots	>22 Knots
N	3.6	0.7	0
NE	3.2	1.3	0.1
E	4.7	1.3	0.1
SE	0.8	0.2	0.2
S	2.9	1.3	0.4
SW	17.0	3.4	0.2
W	22.0	12.8	0.8
NW	4.7	3.1	0.5
Totals	60.0	24.0	2.0

Calms (0-4 knots) - 14 percent

Porter et al. state that the westerly and northwesterly winds sometimes cause annoying and troublesome gusts in the area of Wilson Cove. The strongest observed gusts at Wilson Cove have been estimated to attain a speed of from 40 to 60 knots and to occur from four to six times each year, especially in winter and spring months (December through May). No data is available on the periodicity of these gusts. The surging period of small craft moored at the Wilson Cove Pier during mild gusts has been observed to be between 20 and 25 seconds. Sizable open-water waves are generated by winds from the northerly directions in the winter and spring, and from the easterly directions in the spring and fall. The latter are colloquially known as "Santa Ana" winds. Along the mainland there are usually four to five occurrences of significance each year; however, their strength attenuates rapidly outward from the mainland and they rarely reach the island with as much as 17 to 20 knots' velocity (Sergius, L. A., 1952). Nevertheless, they are responsible for generating restricted fetch waves which attain considerable height.

In summary, westerly and northwesterly winds with mean speeds of 22 knots and with attendant gusts up to 60 knots are estimated to occur at Wilson Cove from four to six times per year. This conclusion is compatible with the statistics on the distribution of extreme winds in the United States compiled and reported by Thom (1954, 1960).

Probable Wave Environment

Characteristics of the larger waves generated outside the coastal islands which enter Southern California waters are presented in Figure 45. San Clemente Island is not exposed to all the waves indicated there, being sheltered from the medium- and long-period waves from directions greater than 302 degrees by the Santa Barbara Channel Islands and Point Conception. For those directions sheltered from the open ocean, short-period restricted fetch waves generated by the offshore winds are dominant. Characteristics of the larger of these waves are given in Figure 46. The exposure of Wilson Cove to variously caused waves is illustrated in Figure 47.

In connection with previous studies, estimates of the frequency of occurrence of waves having various heights and directions were made by Marine Advisers, Inc., of La Jolla, California. Original source information for such waves is given below.

Wave Origin	Source
I. Waves approaching from outside the coastal islands	Horrer, P. L., and Associates, 1954. "Waves Outside Southern California Islands, their Sources and Dimensions. Reference 54-1." Prepared for Standard Oil Company. Developed using: (a) Hindcasts of waves from six of the most severe storms that entered Southern California between 1899 and 1953.

Wave Origin	Source
I. Waves approaching from outside the coastal islands (cont)	(b) Hindcasts (2 years) of swell from southern hemisphere storms utilizing weather maps and wave records from El Segundo and Huntington Beach. (c) Visual observations of waves (4 years) by Scripps Institution of Oceanography research vessels. (d) Wave hindcasts (3 years) from Scripps Institution of Oceanography Wave Report No. 68.
II. Waves approaching from mainland and other coastal islands	Marine Advisers, Inc., in report to Porter, Urquhart, McCreary, and O'Brien: "Feasibility Study for Harbor Development of San Clemente Island," December 1956, using: (a) Hindcasts of wind-generated waves from (1) San Nicholas Island wind data 1945-1953, and (2) daily synoptic weather maps, northeastern Pacific and U. S. West Coast, 1950 and 1952.

A summary of the data compiled from these studies as given by Porter et al. is shown in Table 7. The frequency of occurrence in hours per year is presented for various significant wave heights and directions. These estimates do not take into account the attenuation of wave height due to shoaling and refraction. However, since the barge is located approximately 1/2 mile from the shore in 165 feet of water, waves having a period less than approximately 10 seconds are not affected by shoaling. The restricted fetch waves are not modified severely by refraction. Thus, estimates for the significant heights of restricted fetch waves, given in Table 7, may be regarded as approximately those existing at the barge location. The attenuation of the heights of waves approaching from outside the islands can only be determined by preparation of detailed refraction diagrams. Such information has not been developed. Nevertheless, it may be stated that from studies (Porter et al., 1956) undertaken at an adjacent location (in 24 feet of water), the refraction effect greatly reduces the heights of waves approaching from outside the islands.

In a somewhat more exhaustive study, National Marine Consultants (1960) compiled deep-water wave statistics based upon meteorological records and charts for the years 1956, 1957, and 1958. The general area of study covered the entire coast of California as represented by seven carefully selected deep water stations.

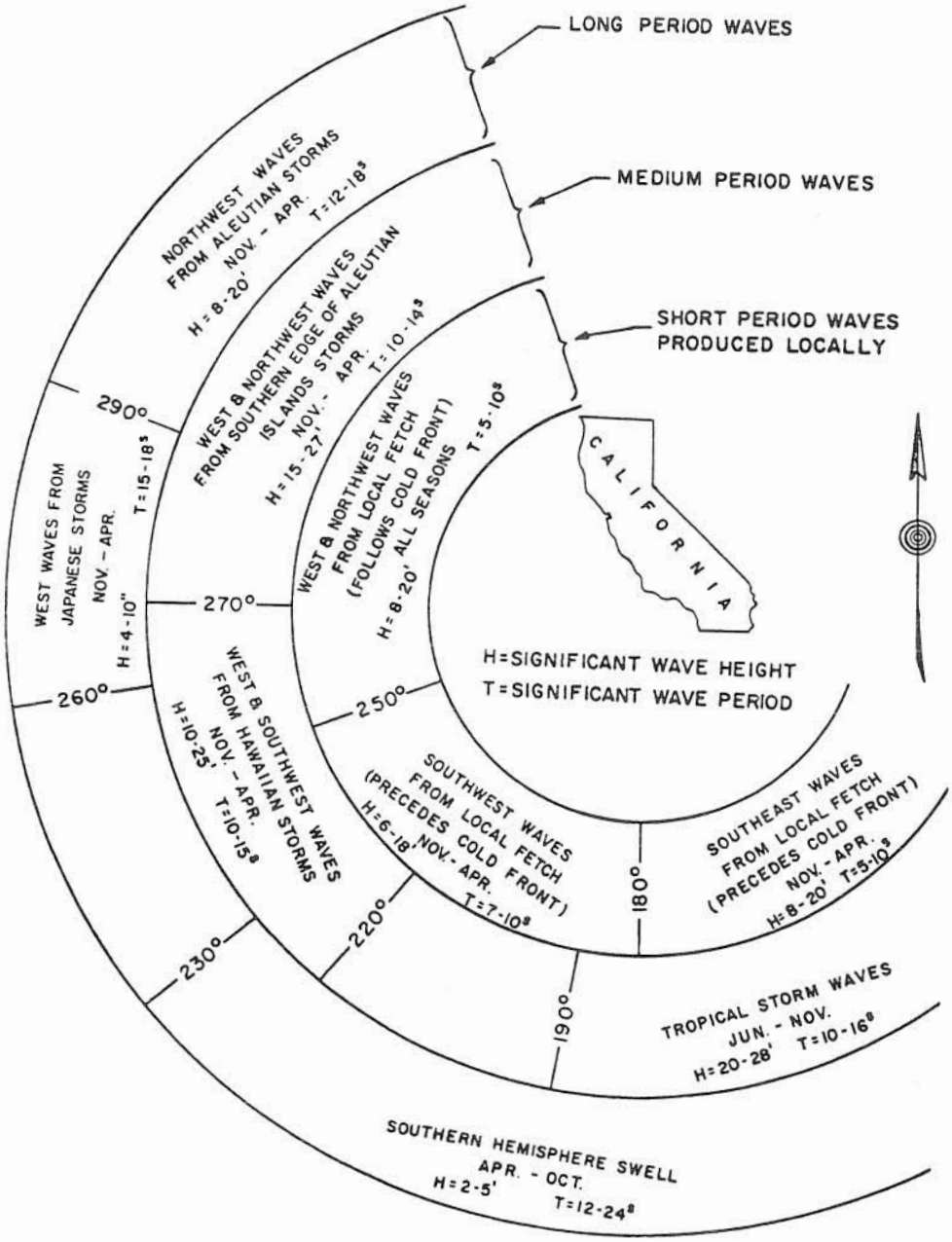

Figure 45. Characteristics of the larger waves generated outside the coastal islands which enter Southern California waters. (From Porter et al., 1956, prepared by Marine Advisers, La Jolla, California.)

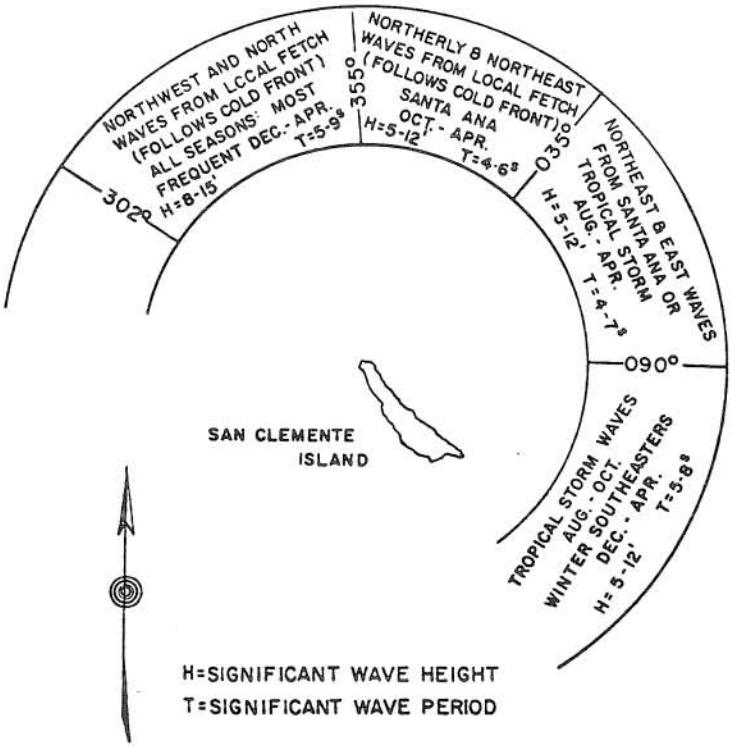

Figure 46. Characteristics of the larger waves that reach San Clemente Island from direction of the mainland and other coastal islands. (From Porter et al., 1956, prepared by Marine Advisers, La Jolla, California.)

Deep water station No. 7 is located approximately 65 miles from Wilson Cove at coordinates latitude 33.5°N, longitude 119.5°W. (See Figure 1, General Location Plan.) The annual summary of statistics compiled for deep water station No. 7 are presented in Table 8.

The statistics compiled for both sea and swell are wave-height, -period, -direction frequency distributions. The wave height is in terms of significant height in feet ($H_{1/3}$) or that height representing the average of the highest one-third of all waves; the wave period in seconds is that average period associated with the significant height. The wave directions are the directions from which the waves approach. Frequencies are given in annual percent terms and are rounded to the nearest one hundredth of 1 percent.

The total number of hours of swell is given in the upper left-hand corner of the table. Some of the important details are not revealed by this annual summary. For example, the total number of swell hours could be greater than the total number of hours in any given time period, since the number of swell trains arriving simultaneously at a station is variable (i.e., not necessarily limited to one). On the other hand, the total percentage of sea will equal 100 when the category of calm is included. In addition, maximum swell occurs during the spring, whereas maximum sea occurs during fall and winter months.

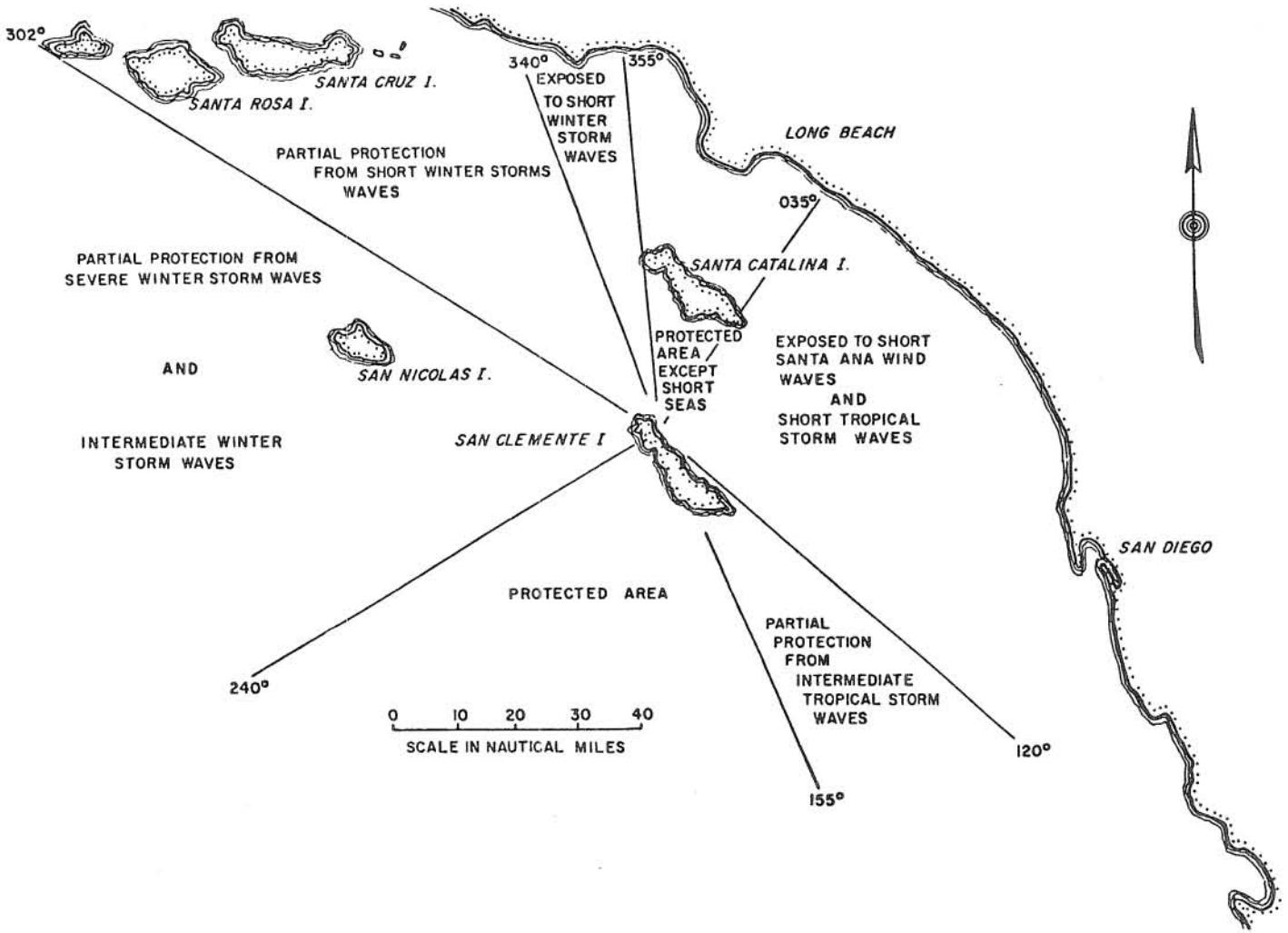

Figure 47. Wave exposure of Wilson Cove. (From Porter et al., 1956, prepared by Marine Advisers, La Jolla, California.)

Table 7. Frequency of Waves Reaching San Clemente Island That Have Specified Deep Water Directions and Significant Heights, in Hours per Year. (From Porter et al., 1956.)

Restricted Fetch Waves								
Direction (deg)	Height (ft)							
	3-4	4-5	5-6	6-8	8-10	10-12	12-15	15-20
302-314	399.0	40.0	250.0	373.0	117.0	272.0	1.6	18.3
315-324	400.0	41.0	250.0	373.0	117.0	277.0	1.6	18.7
325-334	81.0	8.3	29.0	41.0	9.0	19.8		0.7
335-344	82.0	8.4	29.0	41.2	10.0	20.0	0.6	
345-354	28.0	2.8	4.0	5.5	2.5	1.7	0.6	
355-004	30.9		7.6	4.7	1.7	1.9	0.2	
005-014	32.0		7.6	4.7	1.8	1.9	0.1	
015-024	6.6		1.6	0.8				
025-034	6.9	1.5		0.8				
035-044	10.8		3.4	0.8				
045-054	10.9		2.3	2.0	0.4			
055-064	5.6		0.8	0.5				
065-074	5.7		0.9	0.4				
075-084	5.8	0.6	0.8	0.7	0.3	0.1		
085-094	6.8	0.7	0.9	0.7	0.3	0.4		
095-104	6.9	0.7	0.9	0.7	0.3	0.2		
105-114	6.0		0.2	0.1		0.1		
115-124	6.0		0.3	0.1				
125-134	7.5		7.5	9.0	0.1			
135-144	7.5		7.5	9.0				
145-154	12.0		4.5	4.5		3.1		

Other Except Southern Hemisphere Swell								
Direction (deg)	Height (ft)							
	2-4	4-6	6-8	8-10	10-15	15-20	20-25	25-30
155-164	2.7	0.4						0.1
165-174								
175-184	4.0	1.7	0.3	0.2				0.1
185-194	8.2	4.9	1.3	0.6	0.2			
195-204	11.2	6.1	2.9	1.5	0.5			
205-214	8.9	6.5	2.4	1.1	0.3			
215-224	11.7	8.3	3.5	1.2				
225-234	23.2	14.0	6.1	2.3				
235-244	31.1	21.1	10.5	4.3	0.7			
245-254	55.0	38.5	19.9	9.5	2.6	0.5	0.2	0.2
255-264	91.1	67.1	35.4	16.7	6.1	2.1	0.6	0.3
265-274	132.1	107.7	61.8	27.9	9.6	2.6	1.3	0.4
275-284	192.8	148.3	83.3	38.5	11.1	3.6	1.2	0.6
285-294	285.9	221.1	126.6	58.6	21.9	5.5	1.4	0.5
295-302	364.2	275.0	158.5	87.5	32.5	8.6	1.4	0.4

Southern Hemisphere Swell			
Direction (deg)	Height (ft)		
	1-2	2-3	3-4
155-164	697.8	267.7	48.9
165-174	483.0	74.9	9.1
175-184	290.5	50.1	2.9
185-194	70.2	6.9	
195-204	206.8	125.2	47.6
205-214	505.2	96.5	44.6
215-224	394.2	422.2	133.0
225-234	523.4	301.2	80.5

Table 8. Average Annual Height-Period-Direction Frequency Distribution in Percent Based on 365-1/3-Day Year. (From "Wave Statistics for Seven Deep Water Stations Along the California Coast," National Marine Consultants, 1960)

STATION 7 (1956, 1957, 1958)

SWELL AVERAGE TOTAL HOURS 8,150.64

DIR.	NNW							NW							WNW							W							WSW							SW							SSW							S							SSE							Σ
T_s	6	8	10	12	14	16	18	6	8	10	12	14	16	18	6	8	10	12	14	16	18	6	8	10	12	14	16	18	6	8	10	12	14	16	18	6	8	10	12	14	16	18	6	8	10	12	14	16	18	6	8	10	12	14	16	18	6	8	10	12	14	16	18	
H_s	8	10	12	14	16	18	+	8	10	12	14	16	18	+	8	10	12	14	16	18	+	8	10	12	14	16	18	+	8	10	12	14	16	18	+	8	10	12	14	16	18	+	8	10	12	14	16	18	+	8	10	12	14	16	18	+	8	10	12	14	16	18	+	
1-1.9															23	24	9	3	1	6	0	5	7	.2	.1	.0				.2	2																													.0	2						.0	2	.0	2				25.04
2-2.9															23	8	10	6	8	1	5	5	1	7	4	1	6		8	8	20	7	10	6	6	2	3	5	1	1	.0	2	2	0	1	2	.0	2																		.0	2			.0	5	.0	5		.0	3	29.12
3-3.9															10	1	6	8	6	2	7	1	4	5	.7	2	.5	8	.1	4	2	.8	7	.5	0	.3	5	.0	2	.0	9	.0	2	1	6	.0	9	.0	2																.0	2	.0	2				.0	2					16.13
4-4.9															.1	2	.7	8	2	.1	9	.5	1	.3	9	.7	9	.3	0	.0	5	.1	6	.4	8	.2	3	.0	9	.1	2	.0	2			.0	7	.0	9		.0	2															.0	2		.0	2		.0	2	.0	2	.0	2		8.82
5-5.9															.0	2	2	.1	1	.4	7	.7	7	.1	9	.0	9			.1	2	.2	8	.3	2	.1	4	.1	0			.0	2	.0	9	.0	9																															5.87
6-6.9																	6	7	1	2	7	.4	2	.2	6	.0	7				.3	1	.3	2	.1	2	.0	7	.0	5			.0	7																																	3.63
7-8.9																	.2	1	.8	7	.5	6	.1	7	.0	2					.2	2	.3	2	.2	0	.0	2					.0	2	1	3	.0	5	.0	2																											2.81
9-10.9																	.0	2	.2	1	.1	7	.0	7							.0	2	.2	3	.1	6	.1	0							.0	4																															1.02
11-12.9																	.0	2			.0	2											.1	7	.0	2	.0	7	.0	2																																							.32
13-14.9																			.0	2	.0	2											.0	5	.0	9																																										.18
15-16.9																						.0	2																																																												.02
17-18.9																																																																																								
19 +																																																																																								
Σ															.3	7	6	1	5	3	3	2	4	6	8	1	7	3	4	3	1	6	0	4	7	3	3	4	3	1	6	0	.9	0	.2	9	.0	4	.1	5	.7	0	.3	9	.0	9	.0	2				.0	7					.0	2	.0	4	.0	4	.0	2		.0	6	.0	4	.0	7	.0	7	.0	2	.0	5	92.96

SEA

DIR.	N					NNW					NW					WNW					W					WSW					SW					SSW					S					SSE					SE					NE					CALM (0-0.9)	Σ
T_s	4	6	8	10	12	4	6	8	10	12	4	6	8	10	12	4	6	8	10	12	4	6	8	10	12	4	6	8	10	12	4	6	8	10	12	4	6	8	10	12	4	6	8	10	12	4	6	8	10	12	4	6	8	10	12	4	6	8	10	12		
H_s	6	8	10	12	+	6	8	10	12	+	6	8	10	12	+	6	8	10	12	+	6	8	10	12	+	6	8	10	12	+	6	8	10	12	+	6	8	10	12	+	6	8	10	12	+	6	8	10	12	+	6	8	10	12	+	6	8	10	12	+		
1-1.9	.3	4				.5	9				.1	4	8			.2	5				.4	2				.1	0				.3	2				.3	7				.0	8				.1	6				.0	7	.0	2					8.15
2-2.9	.5	9				.8	8	.0	5		.8	2	1	.4	6	.4	7	.0	2		.7	4	.0	7		.2	9	.0	5		.5	8	.0	1		.0	9	.0	2		.6	0				.1	9				.2	6				.2	1	.8	3			14.68
3-3.9	.0	5	.0	4		.2	7	.1	9		.7	6	7	.4	0	3	.2	5		.0	4	.1	7	.0	7		.0	7	.0	7		.1	4	.1	6		.0	5	.0	2		.1	4	.1	1		.0	7	.0	2		.0	7	.0	7		.1	1	.1	0	4		10.32
4-4.9			.2	4			.4	0				.0	2	.7	8	4	.2	1				.5	8	.0	5	.0	2				.3	1				.1	5				.0	2				.2	3				.1	2				.1	2	.5	9			11.12
5-5.9			.0	2			.2	3				.4	4	.0	9		.1	2	.0	2	.0	2					.0	2				.0	2				.0	2				.0	2				.0	2				.0	7				.2	0				5.35
6-6.9			.0	5	.0	2			.2	1			.1	7	1	.1	5	3			.0	7	.0	5		.0	9				.0	2				.0	2				.0	1				.0	2				.0	5				.0	7				4.00
7-8.9													.3	7	.6	9	6						.0	7							.0	5				.1	2				.2	5			.0	2				.0	5				.0	2				8.11
9-10.9															1	.8	2	.1	0					.1	6	.0	7									.0	2				.0	7									.0	5								2.79
11-12.9														.2	1	.6	4																																					.0	5	.0	2					.87
13-14.9														.0	4	.2	2																																														.26
15-16.9																.0	2																																												.02
17-18.9																																																																																							
19 +																																																																																								
Σ	.9	8	.4	0	.0	2	1	.6	9	.1	0	6	.4	5	8	.4	8	.0	3	.0	1	.9	7	.1	0	4	.6	1	.1	5	.1	3	3	.5	8	.0	7	.4	6	.3	9	.1	0	4	.1	4	.0	5	.1	4	.1	5	.1	4	.1	1	.4	3	.1	9	.3	4	.1	8	.0	2	.4	9	.3	1	.1	2	.4	1	2	.7	1	.1	3	4.33	34.33	100.00

These statistics are presented in Figures 48 and 49 which illustrate the average annual swell and sea roses, respectively, with appropriate histograms for station No. 7.

Putting all these facts together, waves of up to 20 feet in significant height may be expected to approach the site of the moored barge from a westerly to northwesterly direction (302 to 334 degrees azimuth) on an average of from four to six times per year. The duration of wave intensity at this level is from 6 to 9 hours. This information may be used in conjunction with Figure 50 to determine the maximum probable wave (under certain assumptions) which occurs at the site during times of fully developed seas. These seas are generated by the severe local northwesterly winds on an average of from four to six times per year.

Figure 50, based on the statistical results developed by Longuet-Higgins (1952), is a plot of the ratio of the expected value of the maximum amplitude to the root mean square amplitude versus the number of consecutive oscillations in a time history record. Assuming an average wave period of 15 seconds, at least 1400 oscillations in the time history may be expected to occur in a 6-hour record. From Figure 50, the ratio, $E(A_{max})/\sqrt{E}$ (where $E(A_{max})$ is the expected value of the maximum wave and $\sqrt{E}$ is the root mean square value of the time history), is found to be approximately 2.8. Assuming further that instantaneous ordinates to the envelope of the wave time history record have a Rayleigh distribution (narrow-band spectra), then $A_{1/3} = 1/2(20) = 1.414\sqrt{E}$, where 20 feet is the significant wave or the average height of the highest one-third waves in the record.

From the above, the root mean square, $\sqrt{E}$, is found to be 7.1 feet, and A_{max} is 19.8 feet. Thus, the maximum probable wave height is estimated to be approximately 39.6 feet. A 39.6-foot wave is physically possible since the breaking wave height in 165 feet of water is 115 feet. It is implied that the fetch is sufficiently long in the northwesterly direction to permit seas to be fully developed. From Hydrographic Office Publication No. 603, it is found that the minimum fetch and minimum duration of winds of 29 knots required to generate such a sea are 250 nautical miles and 22 hours, respectively. Neither of these criteria is satisfied completely. A fetch of 250 nautical miles in the westerly to northwesterly direction requires a slight refraction of the waves incident on Wilson Cove. The meager statistics of wind observations do not support the required wind speed of 29 knots for a duration of 22 hours. Nevertheless, the statistics of the wind-generated wave observations require an equivalent energy transfer.

Thus, consistent with the wave observations, let it be assumed that a fully arisen sea with a significant wave height of 20 feet can be generated and directed in the vicinity of Wilson Cove. The spectral nature of such a sea is indicated by Figure 51.

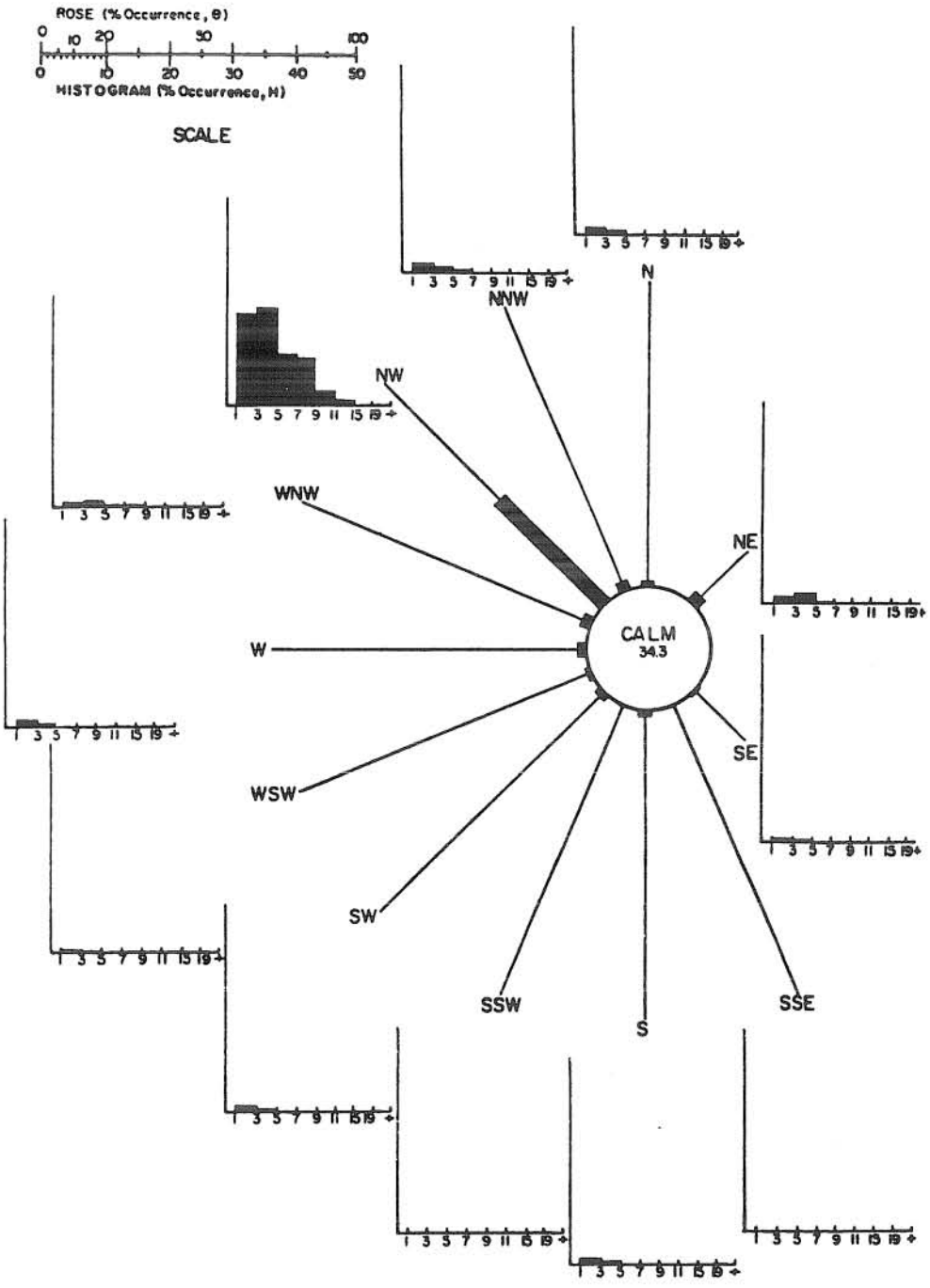

Figure 48. Average annual sea rose for station No. 7 - latitude 33.5°N, longitude 119.5°W. (From "Wave Statistics for Seven Deep Water Stations Along the California Coast," National Marine Consultants, 1960.)

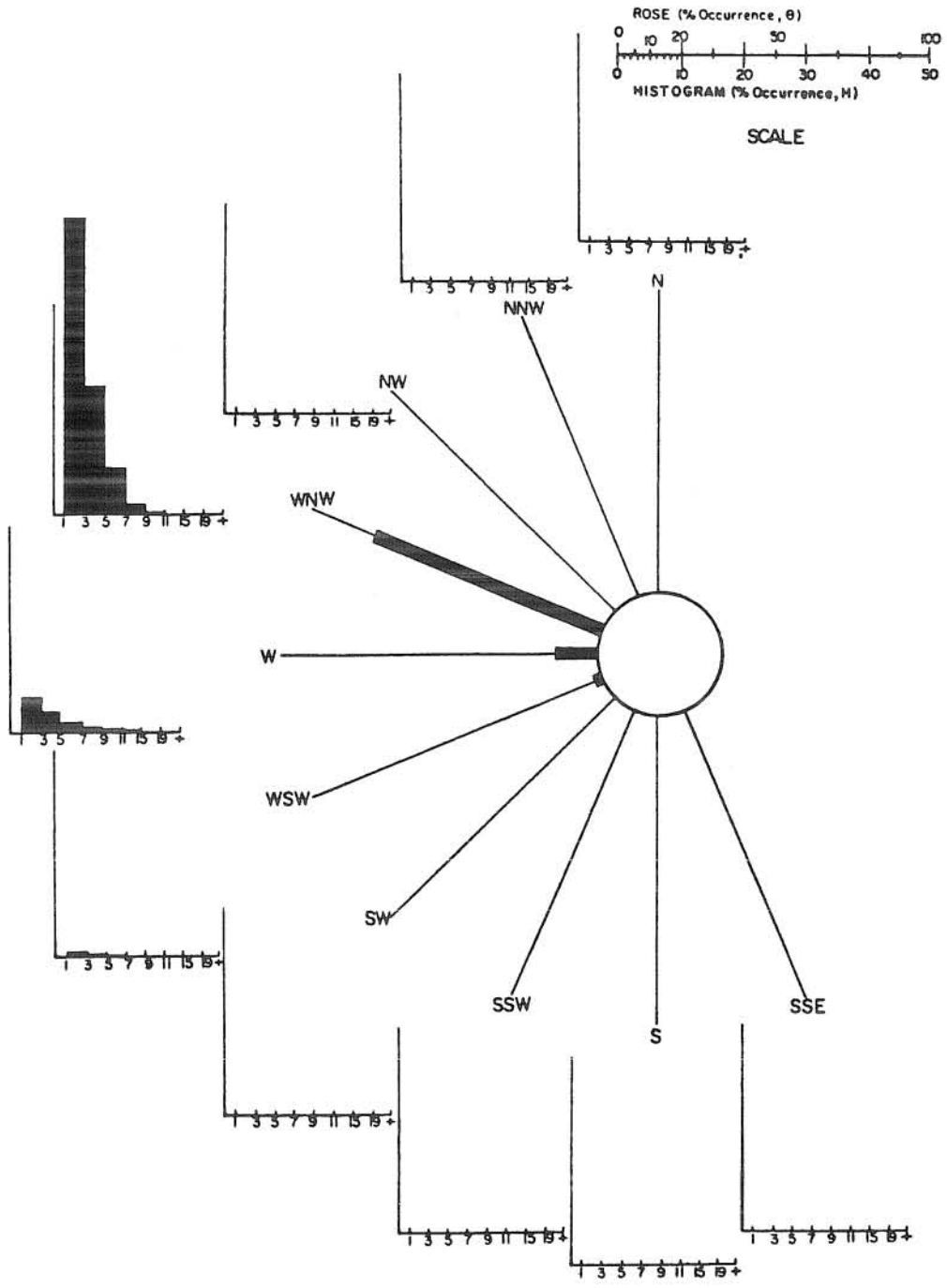

Figure 49. Average annual swell rose for station No. 7 - latitude 33.5°N, longitude 119.5°W. (From "Wave Statistics for Seven Deep Water Stations Along the California Coast," National Marine Consultants, 1960.)

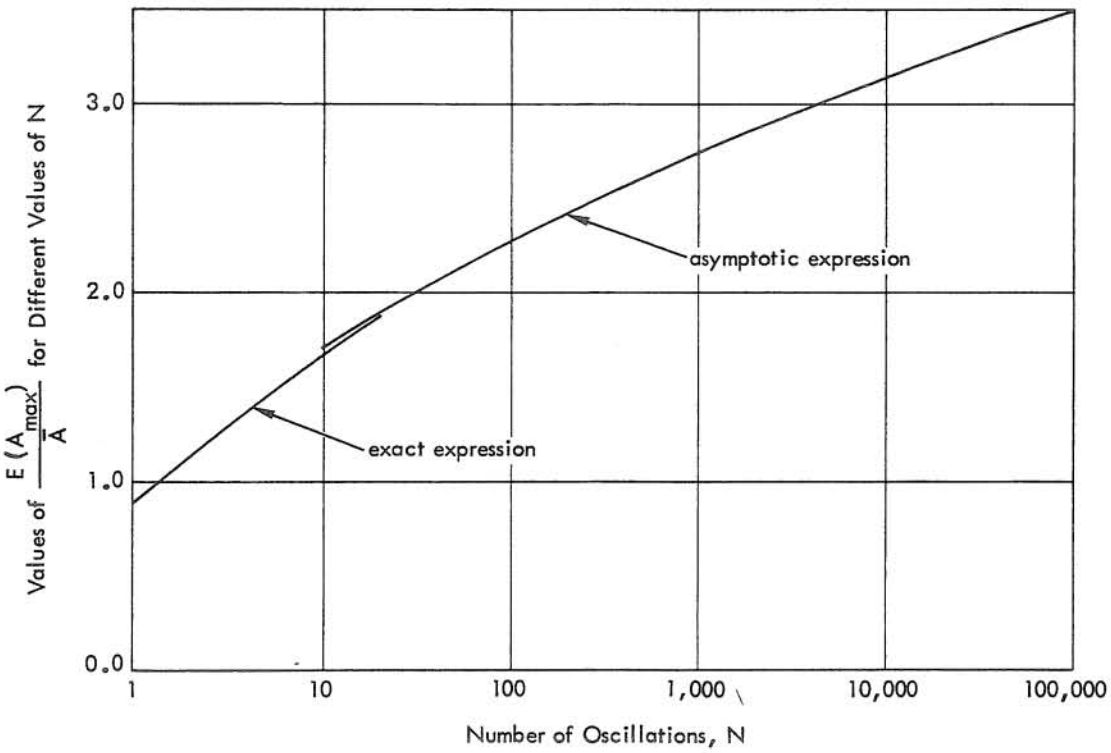

Figure 50. Expected relative value of maximum wave amplitude for various numbers of waves.

The pertinent characteristics are:

Average wave height	12.6 ft
Significant wave height	20.0 ft
Average height of one-tenth highest waves	25.8 ft
Range of dominating periods	4-17 sec
Average "period" and approximately most frequent "period"	8 sec
Period of energy maximum in wave spectrum	11.3 sec
Average "wave length"	240.0 ft

From the maximum annual wave spectra shown in Figure 51, the spectra of chain tensions may be derived by linear multiplication of the prototype response operators as given in the preceding section. The results for chain No. 14 as obtained from the stern wave gages are given in Figure 52. Integrating the area under the spectra provides the variance, E, which amounts to approximately 700 kips^2. Taking its square root and applying the statistics developed by Longuet-Higgins for a "narrow-band" gaussian process, the following statistics may be obtained:

Most frequent value	$= 1.41 \times \sqrt{E}/\sqrt{2} = 26.5$ kips
Average value	$= 1.77 \times \sqrt{E}/\sqrt{2} = 33.2$ kips
Average of the highest one-third	$= 2.83 \times \sqrt{E}/\sqrt{2} = 53.0$ kips
Average of the highest one-tenth	$= 3.60 \times \sqrt{E}/\sqrt{2} = 67.5$ kips
Most probable value of the maximum for N = 1,400 oscillations	$= 3.80 \times \sqrt{E}/\sqrt{2} = 70.5$ kips

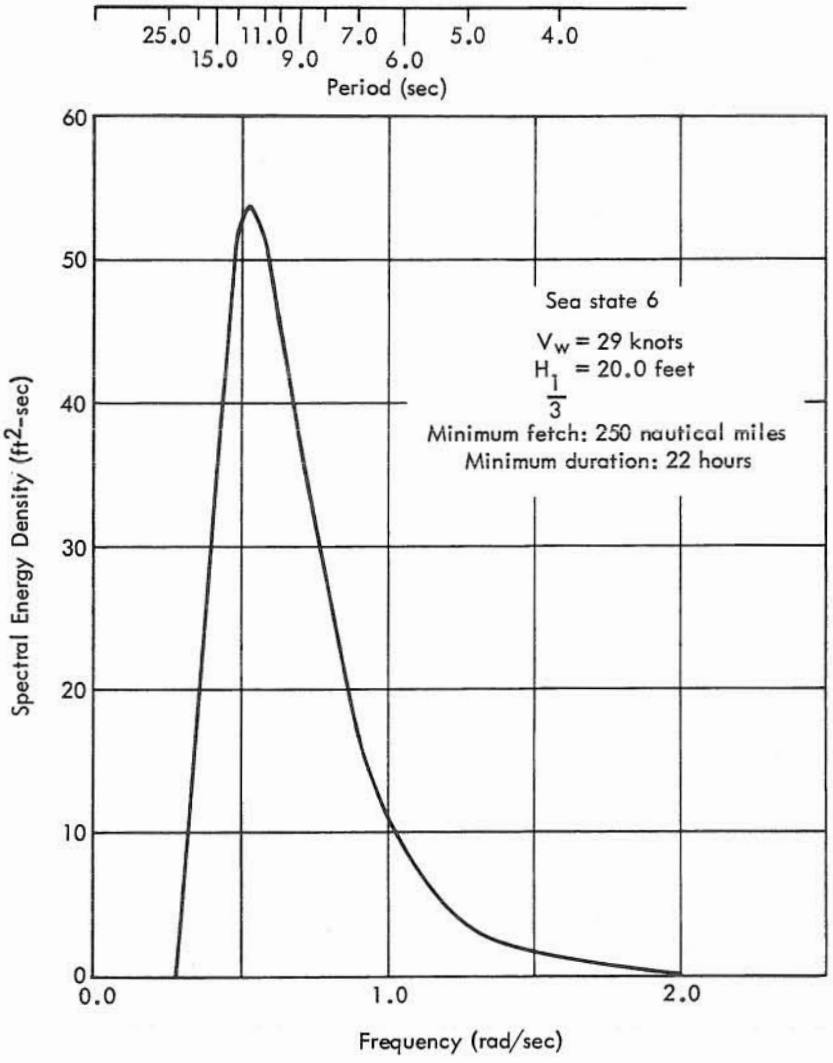

Figure 51. Spectral energy density for surface elevations. (Neumann model for wind velocity indicated.)

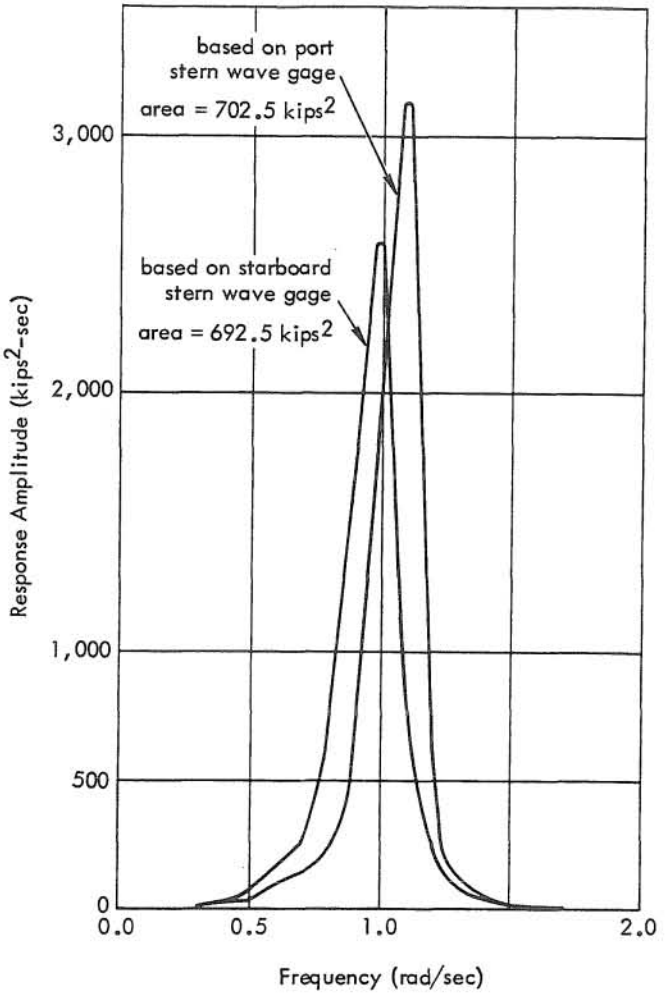

Figure 52. Response spectra for tension, chain No. 14.

When the most probable value of the maximum amplitude is added to the initial tensions of between 30 and 50 kips, the most probable value of the maximum peak in the time history record is found to be between 100 and 120 kips. For comparative purposes, "Table 7-7, Table of Proof Loads and Breaking Strengths of Stud-Link Chain," and "Table 7-8, Table of Proof Loads and Breaking Strengths of Die-Lock Chain," from the Bureau of Yards and Docks' Design Manual (NAVDOCKS DM-26, 1962), are reproduced in Figure 53. These tables contain values applicable to new chains; hence, no allowance is made for deterioration, whether from the corrosive effects of the salt water environment or from continual in-service use. In addition, the tabulated breaking strengths contain an unknown statistical variability. Thus, these values are presented for use herein to indicate orders of magnitude only.

TABLE 7-7
Table of Proof Loads and Breaking Strength of Stud-Link Chain

Size (inches)	Cast steel		Weight for cast and W.I. chains (pounds per 15 fathoms)	Wrought iron	
	Proof load (pounds)	Breaking strength (pounds)		Proof load (pounds)	Breaking strength (pounds)
3/4[1]	34,680	48,550	500	22,680	33,880
7/8	46,630	65,280	700	30,800	46,200
1[1]	60,360	84,500	850	40,320	60,480
1-1/8	75,770	106,080	1,100	50,960	76,440
1-1/4[1]	92,910	130,070	1,350	63,000	94,360
1-3/8	111,660	156,330	1,600	76,120	114,240
1-1/2[1]	132,190	185,060	1,900	90,720	131,488
1-5/8	154,310	216,030	2,200	106,400	148,960
1-3/4[1]	178,000	249,210	2,550	123,480	172,760
1-7/8	203,250	284,540	2,950	141,680	198,240
2[1]	230,000	322,000	3,300	161,280	225,792
2-1/8	258,240	361,530	3,700	182,000	254,800
2-1/4[1]	287,930	403,100	4,200	204,120	285,600
2-3/8	319,050	446,660	4,650	227,360	318,304
2-1/2[1]	351,560	492,190	5,200	252,000	352,800
2-5/8	385,440	539,620	5,700	270,816	379,120
2-3/4[1]	420,660	588,930	6,300	289,632	405,440
2-7/8	457,190	640,070	6,900	308,224	431,480
3[1]	495,000	693,000	7,500	326,592	457,184
3-1/8	534,060	747,680	8,200	344,400	482,160
3-1/4	574,340	804,070	8,850	361,984	506,688
3-3/8	615,800	862,130	9,550	378,840	530,320
3-1/2[1]	658,440	921,810	10,300	395,136	553,056
3-5/8	702,200	983,080	11,050	.....	.....
3-3/4	747,070	1,045,900	11,800	.....	.....
3-7/8	793,010	1,110,210	12,600	.....	.....
4[1]	840,000	1,176,000	13,400	.....	.....
4-1/8	888,000	1,243,200	14,300	.....	.....
4-1/4	936,990	1,311,790	15,300	.....	.....
4-3/8	986,000	1,381,330	16,550	.....	.....
4-1/2	1,037,800	1,452,930	17,850	.....	.....

[1]Standard sizes of cast-steel chain.

TABLE 7-8
Table of Proof Loads and Breaking Strength of Die-Lock Chain

Size (inches)	Proof load (pounds)	Breaking load (pounds)	Weights (pounds per 15 fathoms)
3/4	48,000	75,000	490
7/8	64,000	98,000	680
1	84,000	129,000	890
1-1/8	106,000	161,000	1,130
1-1/4	130,000	198,000	1,400
1-3/8	157,000	235,000	1,690
1-1/2	185,000	280,000	2,010
1-5/8	216,000	325,000	2,325
1-3/4	249,000	380,000	2,695
1-7/8	285,000	432,000	3,095
2	322,000	488,000	3,490
2-1/8	362,000	548,000	3,935
2-1/4	403,000	610,000	4,415
2-3/8	447,000	675,000	4,915
2-1/2	492,000	744,000	5,475
2-5/8	540,000	813,000	6,050
2-3/4 std.	590,000	885,000	6,660
2-3/4 hd.	649,000	981,000	7,000
2-7/8	640,000	965,000	7,295
3 std	693,000	1,045,000	7,955
3 hd	762,000	1,150,000	8,100
3-1/8	748,000	1,128,000	.....
3-1/4	804,100	1,210,000	9,410
3-3/8	862,200	1,296,000	10,112
3-1/2 std.	922,000	1,383,100	.....
3-1/2 hd.	1,080,000	1,700,000	12,000
3-3/4	1,120,000	1,750,000	12,500

Figure 53. Proof loads and breaking strengths. (From "Design Manual - Harbor and Coastal Facilities," NAVDOCKS DM-26, Bureau of Yards and Docks, Department of the Navy, 1962.)

From the data in Figure 53, it is found that the proof load of the 1-1/2-inch stud-link chain is approximately 132 kips for cast steel and 91 kips for wrought iron. Both these values are either exceeded or dangerously close to the maximum probable value of the peak in the time history record. Hence, the 1-1/2-inch stud-link chain may be considered unsafe for mooring the Fishhook barge at the Wilson Cove site.

On the other hand, the 2-1/2-inch die-lock chain has a proof load of 492 kips, which is almost four times the most probable value of the peak tension of the time history record. This suggests that the 1-3/4-inch or 2-inch die-lock chains would afford a sufficient degree of safety. It must be considered, however, that the chain tension response operators were obtained during very low excitation levels when the chain force-displacement relationships could be considered approximately linear. During high excitation levels, the nonlinear behavior of the moorings should not be minimized. Previous studies (O'Brien and Muga, 1963, 1964) have indicated that the moorings are relatively ineffective in restraining the barge, yet these relatively unrestrained movements are responsible for inducing large tensile forces in the mooring chains.

In summary, the spectral distribution of the most intense storm occurring at the Wilson Cove site on the average of once a year is indicated by Figure 51. This storm is generated by winds with a mean wind speed of 29 knots blowing continuously over a fetch of 250 nautical miles for 22 hours. The duration of the water level variations having a significant height of 20.0 feet is from 6 to 9 hours. The surface water level variations induce the chain tension spectra (for chain No. 14) shown in Figure 52. The most probable value of the maximum force induced in chain No. 14 is from 100 to 120 kips, depending on the value of the initial tension.

FINDINGS

The important findings of this study are:

1. During the prototype tests, the wave excitation was relatively low, corresponding to a sea state 2 or 3 as defined, for example, by Marks (Kaplan and Putz, 1962).

2. The wave excitation corresponded to a sea state 4 during the model tests.

3. The mooring chains of the prototype barge responded in tension primarily to wind-generated exciting waves in a linear fashion. The response at long periods is attributed to (1) long-period surface gravity waves characteristic of the offshore basin, (2) wind gusts, and (3) subharmonic response to wind-generated surface gravity waves.

4. The simulated moorings of the model barge responded in tension primarily at the characteristic period of the moorings rather than the period of the exciting waves.

5. The heave, pitch, and roll motions induced the largest forces in the mooring chains in the prototype, whereas surge, sway, and yaw induced the greatest forces in the model restoring springs.

6. Within the frequency range of the exciting waves, the linear theory predicted the motion response operators to a satisfactory degree with the one exception of the yaw mode.

7. Waves which are important for sites located off the Southern California coast but protected by the Channel Islands are generated by the northwesterly winds and not the offshore winds colloquially known as "Santa Anas."

8. The most probable value of maximum tension induced in any of the mooring chains on an average of once per year is determined to be 120 kips. This is considered sufficient to break slightly weakened 1-1/2-inch stud-link chain of cast steel.

Other findings of this study are:

a. The method used for obtaining the heave and pitch spectra and/or the heave and roll spectra or any other similar combination from the records of strategically placed pair of accelerometers is correct.

b. The natural period of the moored-craft system is relatively long, being approximately 30 seconds.

CONCLUSIONS

1. In sea states up to 3, motions of moored-ship systems of the type studied can be suitably predicted by the linear theory of ship motion as modified herein to include effects of the moorings. Above a sea state 3, the nonlinear effects invalidate the linear assumption.

2. The linear theory used requires a vast amount of information relevant to added mass, damping (drag-related), and restoring coefficients. To a large extent, such information has not been developed systematically. Only engineering estimates of such coefficients are available in the case of construction-type platforms having large beam-draft ratios or other essentially nonstreamlined ship forms.

3. A generalized nonlinear theory to predict motions and forces induced on moored craft by random irregular surface gravity waves has not been developed.

4. The analysis method used offers a suitable basis for correlating prototype and model behavior. Within the limits of the linear theory, the model and prototype results agree qualitatively.

5. The most probable value of the annual maximum force induced on any chain of the moorings is 120 kips.

6. The present mooring configuration of 2-1/2-inch die-lock chain, although slightly unbalanced for certain incident wave directions, possesses sufficient reserve strength to preclude failure of the moorings resulting from wave-induced motions.

7. The detail motions of the mooring chain were not studied herein. It is suggested that the overall motion of the chain rather than simply that of the upper attachment point (ie. the moored barge) may be important factors affecting the service life of mooring chains and especially in assessing failures.

8. The barge studied herein is very stable despite its unusual naval architectural characteristics. Thus, it is relatively unresponsive to incident waves.

9. The catamaran shape is an ideally shaped platform from which construction operations at sea may be conducted.

10. Finally, the behavioral response of non-linear systems to random vibrations is incompletely understood. Analyses of such systems invariably fail to account for the "transient" responses which are continually and continuously generated. In this sense, the work "transient" is a misnomer since such responses are permanent features of the time series record.

NOMENCLATURE

General Note:

Superscripts	
i	inertial
d	damping
m	mooring restoring
h	hydrostatic restoring
w	wave-induced

Subscripts	
bm	Due to body motions (inertial effects)
d	Due to damping
h	Due to hydrostatic effects
m	Due to moorings
w	Due to waves
o	Relative to waterline reference position
β	Relating to a particular relative heading to the waves
ω	Relating to a particular angular frequency

A_{ij}'	Component of added mass tensor
a_{ij}	Matrix element for longitudinal plane motions
Arg	The argument or phase of a complex quantity in an Argand representation
$\overline{A}_y$	Ratio of wave amplitude to sway amplitude for lateral motion-induced wave
$\overline{A}_z$	Ratio of wave amplitude to heave amplitude for vertical motion-induced wave
a_i	Response amplitude operator
B*	Local beam of barge section
BG	Vertical distance between CB and CG
BM	Vertical distance between CB and the metacenter (metacentric radius)
b_{ij}	Matrix element for lateral plane motions
c	Propagation speed of surface wave
C_s	Section coefficient (ratio of section area to product of section beam and draft)
C_y	Three-dimensional damping factor for sway motion
C_z	Three-dimensional damping factor for heave motion
CB	Center of buoyancy
CG	Center of gravity
C_θ	Three-dimensional damping factor for pitch motion
C_ψ	Three-dimensional damping factor for yaw motion
E	Total energy (integrated area) under spectral curve
F	Force
$F_{1, 2, \cdots}$	Mooring chain forces (with numbering subscripts)

g	Acceleration due to gravity
GM	Perpendicular distance from CG to keel
H	Local section draft
$\bar{h}$	Average half-draft
$H_{1/3}$	Significant wave height (mean of highest third)
I	Moment of inertia
IT.	Initial tension
Im	The imaginary part of a complex quantity
K	Roll moment, positive about the x-axis
KG	Vertical distance from keel to CG
k_x	Mooring spring constant for surge motion
k_y	Mooring spring constant for sway motion
k_z'	Added mass factor for lateral motion (zero frequency)
k_4'	Frequency dependent term in lateral added mass factor
k_ψ	Mooring spring constant for yawing motion
L	Length of barge
M	Pitch moment, positive about the y-axis
Mod	Modulus or magnitude
MWL	Mean water level
m	Mass
N	Yawing moment, positive about the x-axis
N_y	Sway damping coefficient
N_{yy}'	Local sway damping coefficient
$N_{y\psi}$	Sway-yaw coupling coefficient
N_z	Heave damping coefficient
N_{zz}'	Local heave damping coefficient
$N_{z\theta}$	Heave-pitch coupling coefficient
N_θ	Pitch damping coefficient
N_ϕ	Roll damping coefficient
N_ψ	Yaw damping coefficient
OB	Vertical distance from CB to free surface
OG	Perpendicular distance from the free surface to the CG
q_i	Effective body velocity
$\Re e$	The real part of a complex quantity
S	Cross-sectional area and arc length of cable catenary
T	Mooring chain
v_w	Wind speed
W	Displacement of barge
X, Y, Z	Forces acting (positively along the x-, y-, and z-axes, respectively)
$\bar{z}_{cb}$	Local center of buoyancy of section

x, y, z	Orthogonal axis systems; x-axis horizontal, positive toward the bow; y-axis horizontal, positive to port; z-axis vertical, positive upward. Also used to represent translational ship motions surge, sway, and heave, respectively, relative to a state of rest
α	Angle made by the mooring lines from the longitudinal axis horizontally
β	Heading angle of waves relative to the heading of the barge ($\beta = \beta_W - \beta_B$)
β_B	Heading angle of barge relative to the wind
β_W	Heading angle of an individual wave relative to the wind
η	Elevation of the free surface
θ	Angular displacement (pitch) positive for rotation about the y-axis
λ	Wave length
ξ	A dummy variable coincident with x
ρ	Mass density of the fluid
ϕ	Angular displacement (roll) positive for rotation about the x-axis
ψ	Angular displacement (yaw) positive for rotation about the z-axis
ω	Angular frequency

Appendix A

LINEAR THEORY OF SHIP MOTION USING SLENDER BODY APPROACH

DERIVATION OF THE EQUATIONS OF MOTION

The derivation of the equations of motion of the moored barge follows, in general, the form given by St. Denis and Pierson (1953) and Kaplan and Putz (1962). Two important differences are noted. The first is that no assumption is made concerning the depth of water in which the barge is moored. Thus, the expressions for the exciting forces and moments are equally valid in deep or shallow water, subject only to the limitation that the linear theory of ship motion remains valid. St. Denis and Pierson considered the free ship in deep water and Kaplan and Putz considered the moored ship, but again only in deep water. The present analysis treats the moored ship in water of any depth.

Even for the idealistic deep water case, the behavior of real physical moorings is complicated. Kaplan and Putz proposed a considerable simplification by relating expressions for mooring restoring forces for the deep water case to the elastic effects in the mooring cables. However, the mooring restoring forces of the present problem arise from displacements of the catenary, and a similar simplification, although possible, is not realistic. Thus it is necessary to derive general expressions for the mooring line with sinker which may then be linearized for small displacements about the point of equilibrium.

The second difference noted concerns the geometric shape of the platform under study. This differs from normal ship forms in that the breadth-to-draft ratio is extremely large, and in the course of the analysis the modifications necessary to apply certain coefficients, most of which were derived for normal ship forms, will be indicated.

Coordinate System

Following Korvin-Kroukovsky (1961), in analyzing ship motions in waves, it is generally necessary to stipulate two systems of axes, one fixed in the body and one fixed in space.

The system fixed in the body is a translating right-hand Cartesian system with the origin at the center of gravity of the body. The axes have a fixed orientation in that the origin translates with the center of gravity of the body but the axes cannot rotate. Thus the axes may be considered to occupy the mean position of small angular oscillations. For this reason some authors refer to them as "mean body" axes. With respect to the orientation of the barge (or ship), the x-axis is chosen positive toward the bow, the y-axis is positive to port, and the z-axis is positive upward. The dynamic variables are the linear displacements, surge (x), sway (y), and heave (z), along the respective axes, and the angular displacements, roll (ϕ), pitch (θ), and yaw (ψ), which are defined as positive in a direction of positive rotation about the x-, y-, and z-axes, respectively (i. e., port-upward, bow-downward, bow-portward). The positive direction of the forces and moments is similarly defined. The foregoing system of axes is sufficient to describe most of the motions of the barge in still water.

In order to describe the excitation effects, that is, the motion of the barge induced by the wave system, it has been found useful to introduce another system of coordinate axes which is fixed in space. This is a nontranslating and nonrotating system and has its origin at the free surface directly above mean position of the center of gravity. It is also a right-hand coordinate system. The axes are shown in the sketch below.

Formulation of Equations of Motion

The equations of motion are formulated by equating to the motions the sum of the forces (and moments) acting on the body. The total force (or moment) acting on the body is the sum of the forces arising from dynamic body motions, F_{bm}, damping, F_d, hydrostatic restoring, F_h, mooring restoring, F_m, and excitation, F_w.

The force exerted by the body in accelerating the surrounding water gives rise to equal and opposite forces by the water on the ship. These forces (and moments) arise from the dynamic body motions; they are of an inertial nature, and being proportional to acceleration are usually expressed in terms of a fictitious added mass, which in combination with the body's intrinsic mass yields the commonly known "virtual mass." The total inertial force (moment) has components in all the translation (rotation) directions.

The damping forces involve the dissipation of energy and result from wave generation, viscosity, and eddy-making. Except for the roll motion, only damping due to wave generation is considered in the present study. The total damping force (moment) has components in all the translation (rotation) directions.

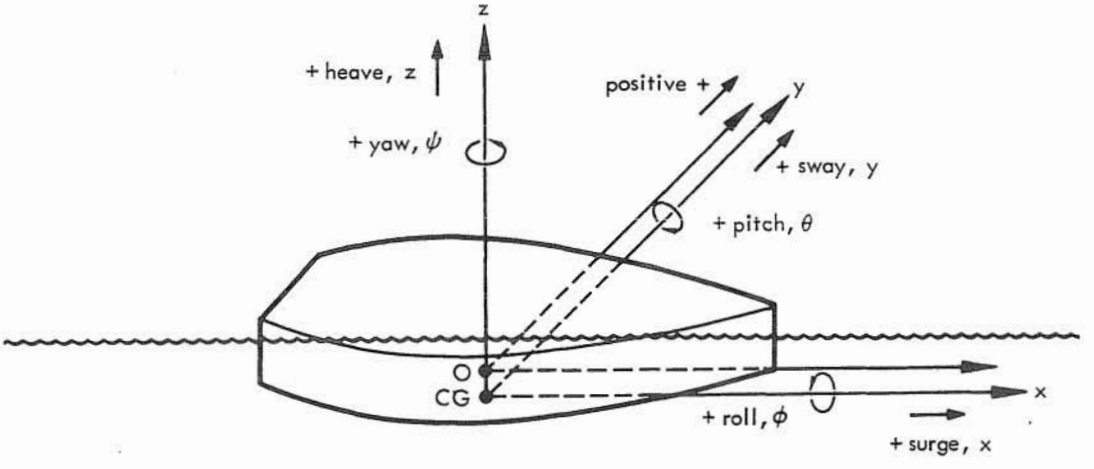

CG = origin of "mean body" axes (i.e., that system fixed in body)

O = origin of axes fixed in space

OG = distance between CG and mean water level

The hydrostatic restoring forces (moments) arise from buoyancy effects induced by static displacement. The total hydrostatic restoring force has a component only in the vertical (z) direction, while the hydrostatic restoring moment has components in the roll (ϕ) and pitch (θ) directions.

The mooring restoring forces result from displacement of the body from the equilibrium mooring position. These forces are assumed to be linear functions of displacement, an assumption justified for small displacements. For large displacements, however, the forces are known (from other experiments) to be nonlinear. Furthermore, the total mooring force is assumed to have components only in the surge (x) and sway (y) directions, while the total mooring moment is assumed to have a component only in the yaw (ψ) direction.

Finally, the excitation forces (moments) are assumed to be due only to the waves. The effects of winds and currents are not considered. The wave forces (moments) have components in all the translation (rotation) directions. In view of the foregoing, the six equations of motion corresponding to the 6 degrees of physical freedom in which the body is permitted to move, may be written as follows:

Surge (x)

$$m\ddot{x} = X_i + X_d + X_m + X_w \tag{A-1}$$

Sway (y)

$$m\ddot{y} = Y_i + Y_d + Y_m + Y_w \tag{A-2}$$

Heave (z)

$$m\ddot{z} = Z_i + Z_d + Z_h + Z_w \tag{A-3}$$

Roll (ϕ)

$$I_x\ddot{\phi} = K_i + K_d + K_h + K_w \tag{A-4}$$

Pitch (θ)

$$I_y\ddot{\theta} = N_i + N_d + N_h + N_w \tag{A-5}$$

Yaw (ψ)

$$I_z\ddot{\psi} = M_i + M_d + M_m + M_w \tag{A-6}$$

where m = mass of body

I_r = moment of inertia of ship about the r-axis

X, Y, Z = force in surge, sway, and heave, respectively

K, N, M = moment in roll, pitch, and yaw, respectively

with subscripts on the forces and moments indicating the type of force or moment, according to the following notation:

i = inertial

d = damping

h = hydrostatic restoring

m = mooring restoring

w = wave excitation

The fundamental assumption of the present approach is that of linearity. Specifically, it is assumed that if the excitation terms in Equations A-1 through A-6 are neglected, the resulting equations are second-order linear differential equations with time, t, as the independent variable. The excitation terms merely add to the "right-hand side" a term of sinusoidal nature. In accordance with the linear theory, there is no coupling between the variables in the two planes of motion, the longitudinal-vertical (surge, heave, and pitch) and the horizontal (sway, roll, and yaw). However, the longitudinal motions in the vertical plane are coupled to each other, and similarly the lateral equations in the horizontal and transverse vertical planes are coupled to each other.

To find analytical expressions for force and moment terms appearing in Equations A-1 through A-6, an approximate method is employed which has been successfully applied to many studies of ship motion in waves. The method is the well-known slender body theory. Essentially, this theory makes the assumption that, for an elongated body where a transverse dimension is small compared to its length, the flow at any cross section is independent of the flow at any other section and, hence, the flow problem is reduced to a two-dimensional problem in the transverse plane. The forces at each section are found by this method, and the total force is found by carrying out an integration over the body length. Although the barge dimension in the y-direction (breadth) is not small relative to that in the x-direction (length), the technique has also been successfully applied to wing sections with low aspect ratios (approximately equal to 1). Kotik and Thomsen (1963) have shown that the expressions given by Hogner (1932) for calculating wave resistance for shallow ships (i.e., large beam-draft ratios) agree with the Michell slender ship theory when the beam is made small. Hence there is sufficient precedent for use of the slender body approach in the present case. Nevertheless, the large beam-draft ratios require that certain modifications to the approach be employed. Such modifications will be indicated in the course of the analysis.

The following five sections (indicated by headings in capital letters) are devoted to a detailed derivation of the different force and moment components appearing in Equations A-1 through A-6. Particular attention is placed on the evaluation of these components as they are related to the unique barge being studied.

DYNAMIC FORCES AND MOMENTS DUE TO BODY MOTIONS

The hydrodynamic forces and moments of an inertial nature arise from the action of the forces and moments of the surrounding water on the barge, and are caused by the temporal displacement of the barge. The simplified result of slender body theory calculation is that the local force at any section is equal to the negative time rate of change of fluid momentum. The equations for the forces at each section then have the general form

$$\frac{dF_{bm}}{d\xi} = -\frac{D}{Dt}\left(\sum A_{ij}' \, \bar{q}_j\right) \tag{A-7}$$

where the A_{ij}' denotes the sectional added mass along the ith direction due to motion in the jth direction; $\bar{q}_j$ is the effective average velocity in the jth direction, and D/Dt denotes the substansive or material derivative. Since the analysis is for zero speed, then D/Dt becomes simply $\partial/\partial t$.

The added mass terms, A_{ij}', are frequency-dependent and thus take into account the effects of the free surface. The sum of the products $A_{ij}' \, \bar{q}_j$ insures that all couplings are included in the analysis subject to the limitation previously indicated (i. e., there are no couplings of any of the longitudinal motions with any of the lateral motions).

Surge, X_i

Since pitch is the only motion other than surge having a component in the surge direction, the summation indicated by equation A-7 is $A_{11} \dot{x} + A_{15} \dot{\theta}$. Thus the sectional surging force is

$$\frac{dX_i}{d\xi} = -\left(A_{11}' \ddot{x} + A_{15}' \ddot{\theta}\right) \tag{A-8}$$

There is no simple means for estimating the added mass component A_{11}', but it is known to be quite small for slender bodies and hence the first term in Equation A-8 is neglected. Rewriting Equation A-8,

$$X_i = -\ddot{\theta} \int A_{15}' \, d\xi \tag{A-9}$$

The symmetrical nature of the added mass tensor, A_{ij}, may be utilized to evaluate the integral appearing in Equation A-9. It is noted that surging induces a pitching moment of magnitude $m \left| \overline{BG} \right| \ddot{x}$, where m is the barge mass, $\overline{BG}$ the vertical distance from the center of buoyancy to the center of gravity, and $\ddot{x}$ is the acceleration in the longitudinal direction (surge). Thus, the added mass in pitch due to motion in surge, A_{51}, is equal to the coefficient of the pitching moment, or $A_{51} = m \left| \overline{BG} \right|$. But from symmetry, $A_{15} = -A_{51}$. Thus, Equation A-9 becomes

$$X_i = m \left| \overline{BG} \right| \ddot{\theta} \tag{A-10}$$

It is clear that the integral of the sectional added mass coefficients, A_{15}', may be replaced by its composite A_{15}. The unprimed notation is employed to indicate that a summation has been carried out over the body length.

Sway, Y_i

The sectional damping force for lateral motion is formulated by reference to the coordinate axis fixed in space (i. e., at the mean free-water surface level). This axis is chosen because the roll axis coincides with the longitudinal axis passing through the CG of the barge and the necessity for determining individual CG's of each sectional element may be eliminated.

Thus,

$$\frac{dY_{i_o}}{d\xi} = -\left(A_{22}' \ddot{y} + A_{26}' \ddot{\psi} - A_{24}' \ddot{\phi} \right) \tag{A-11}$$

where the subscript "o" refers to the mean water surface level. The difficulty of evaluating A_{26}' demands an appropriate substitution. Kaplan and Putz (1962) suggest that since the quantity $\xi \ddot{\psi}$ represents the linear acceleration of the CG of a sectional element in the sway direction due to motion in yaw, the use of $A_{22}' \xi$ in place of A_{26}' is justified. Further, since $A_{24}' = -A_{42}'$, Equation A-11 becomes, upon substitution,

$$\frac{dY_{i_o}}{d\xi} = -A_{22}' \ddot{y} - A_{22}' \xi \ddot{\psi} - A_{42}' \ddot{\phi} \tag{A-12}$$

The last term in Equation A-12 represents rolling motion about the free surface level. Rolling motion about the composite center of gravity may be geometrically decomposed into an equivalent linear velocity and a roll motion about the free surface level. Thus, in referring the sway force to the origin at the center of gravity of the body, it is necessary to add an equivalent linear velocity term. Kaplan and Putz give the following equation for the sway force:

$$Y_i = -\ddot{y}\int_{\xi_s}^{\xi_b} A_{22}'\, d\xi - \ddot{\psi}\int_{\xi_s}^{\xi_b} A_{22}'\, \xi\, d\xi - \ddot{\phi}\int_{\xi_s}^{\xi_b} \left(A_{42}' + \overline{OG}\, A_{22}'\right) d\xi \qquad \text{(A-13)}$$

where $\overline{OG}$ is the distance from the center of gravity to the free surface level.

Heave, Z_i

In the case of the vertical force, the displacement of the center of gravity of a sectional element is the resultant of pure heave and pitch motions. The sectional vertical force is

$$\frac{dZ_i}{d\xi} = -\frac{D}{Dt}\left(A_{33}'\, \dot{z} - A_{35}'\, \dot{\theta}\right) \qquad \text{(A-14)}$$

or

$$Z_i = -\ddot{z}\int_{\xi_s}^{\xi_b} A_{33}'\, d\xi + \ddot{\theta}\int_{\xi_s}^{\xi_b} A_{35}'\, d\xi \qquad \text{(A-15)}$$

The last term represents the heave contribution from pitching about the body center of gravity. The quantity $\xi\ddot{\theta}$, however, represents the linear acceleration of the CG of a sectional element in the heave direction due to motion in pitch. Thus, $A_{33}'\xi$ may be employed in place of A_{35}', and Equation A-15 becomes

$$Z_i = -\ddot{z}\int_{\xi_s}^{\xi_b} A_{33}'\, d\xi + \ddot{\theta}\int_{\xi_s}^{\xi_b} A_{33}'\xi\, d\xi \qquad \text{(A-16)}$$

Pitch Moment, M_i

The values of the moments are easily obtained from the forces. Thus the sectional pitch moment is

$$\frac{dM_i}{d\xi} = -\xi\frac{dZ_i}{d\xi} + \zeta\frac{dX_i}{d\xi} \qquad \text{(A-17)}$$

where ζ is a dummy variable along the z-axis.

$$M_i = \int_{\xi_s}^{\xi_b} \xi\, \frac{dZ_i}{d\xi}\, d\xi + \int_{\xi_s}^{\xi_b} \zeta\, \frac{dX_i}{d\xi}\, d\xi \qquad \text{(A-18)}$$

The last expression in Equation A-18 represents the contribution to pitch moment resulting from surging motion. Since the surging force acts through the center of buoyancy (distance $|BG|$ below the center of gravity), this term can be evaluated separately and the need for determining an average ζ can be eliminated. Thus,

$$\int_{\xi_s}^{\xi_b} \zeta \frac{dX_i}{d\xi} d\xi = m |BG| \ddot{x} \tag{A-19}$$

The pitch moment thus becomes

$$M_i = \ddot{z} \int_{\xi_s}^{\xi_b} A_{33}' \xi \, d\xi - \ddot{\theta} \int_{\xi_s}^{\xi_b} A_{33}' \xi^2 \, d\xi + m |BG| \ddot{x} \tag{A-20}$$

Yaw, N_i

The yaw moment is likewise obtained from the forces. The sectional yaw moment is

$$\frac{dN_i}{d\xi} = \xi \frac{dY_i}{d\xi} \tag{A-21}$$

Substitution of Equation A-13 into Equation A-21, and integrating, yields the total yaw moment

$$N_i = -\ddot{y} \int_{\xi_s}^{\xi_b} A_{22}' \xi \, d\xi - \ddot{\psi} \int_{\xi_s}^{\xi_b} A_{22}' \xi^2 \, d\xi$$

$$- \ddot{\phi} \int_{\xi_s}^{\xi_b} \left(A_{42}' + |\overline{OG}| A_{22}' \right) \xi \, d\xi \tag{A-22}$$

Roll, K_i

The roll moment relative to the mean free surface level is formulated according to Equation A-7 as

$$\frac{dK_{i_o}}{d\xi} = -\frac{D}{Dt} \left(A_{42}' \dot{y} + A_{44}' \dot{\phi} + A_{46}' \dot{\psi} \right) \tag{A-23}$$

Reference to the coordinate axis whose origin is fixed in space eliminates the need for determining location of the sectional CG's. As in the case of sway, since the quantity $\xi \ddot{\psi}$ represents the linear acceleration in sway due to motion in yaw, Kaplan and Putz (1962) suggest substituting $A_{42}' \xi$ for A_{46}'. Equation A-23 then becomes

$$K_{i_o} = \ddot{y} \int A_{42}' \, d\xi - \ddot{\psi} \int A_{42}' \, \xi \, d\xi - \ddot{\phi} \int A_{44}' \, d\xi \tag{A-24}$$

The last integral in Equation A-24 when combined with the body roll moment of inertia yields the total effective roll moment of inertia. The value of the latter quantity is obtained from prototype measurements of the natural roll period and metacentric heights. The roll moment may now be referred to the center of gravity of the barge by including the product of the lateral forces referred to the free surface level and an appropriate moment arm. Thus,

$$K_i = K_{i_o} + \left| \overline{OG} \right| Y_{i_o} \tag{A-25}$$

Substituting Equations A-24 and A-12 into Equation A-25, the roll moment representation becomes

$$K_i = -\ddot{y} \int_{\xi_s}^{\xi_b} \left(A_{42}' + \left| \overline{OG} \right| A_{22}' \right) d\xi - \ddot{\psi} \int_{\xi_s}^{\xi_b} \left(A_{42}' + \left| \overline{OG} \right| A_{22}' \right) \xi \, d\xi$$

$$- \ddot{\phi} \int_{\xi_s}^{\xi_b} \left(A_{44}' - \left| \overline{OG} \right| A_{42}' \right) d\xi \tag{A-26}$$

where the integral appearing in the final term represents the total added moment of inertia in roll.

The representations for the forces and moments of an inertial nature presented in this section are seen to consist of linear combinations of terms proportional to acceleration.

DAMPING FORCES AND MOMENTS

The damping forces and moments arise from wave generation and viscous effects. Except for the roll motion, only damping due to wave generation has been treated in the literature. The damping forces and moments are assumed to be proportional to the body velocity and hence the problem reduces to a determination of the coefficients of velocity in the equations of motion. In accordance with the generalized formulations presented herein, the sectional damping terms appear as

$$\frac{dF_d}{d\xi} = \sum (CN')_{ij} \, \bar{q}_j \tag{A-27}$$

where $\bar{q}_j$ is the velocity component in the jth direction; $(CN')_{ij}$ is the sectional force per unit velocity along the jth direction due to motion in the ith direction and takes into account the three-dimensional effect on the damping force calculated from two-dimensional sections.

Simply stated, the correction factor, C, is the ratio of three-dimensional to two-dimensional damping in the jth direction when the motion is in the ith direction. They are termed "pure" damping factors and, with the exception of roll motion, are applied only when j = i. Otherwise, C = 1.

In the literature on ship motion studies, the treatment of damping forces and moments has followed in general an empirical rather than a theoretical approach. As a result, in order to evaluate the effect of these forces and moments on the body of interest, a detailed and voluminous background of information would be required. Therefore, only the final results with appropriate references are presented in this section.

Surge, X_d

The surge damping force has the form

$$\frac{dX_d}{d\xi} = C_{xx} N_{xx}' \dot{x} \tag{A-28}$$

$$X_d = C_{xx} \dot{x} \int_{\xi_s}^{\xi_b} N_{xx}' \, d\xi \tag{A-29}$$

For normal ship forms, the surge damping is known to be quite small since the surge motions do not produce appreciable waves. Viscous effects are also small. Newman (1961) points out that for three-dimensional damping of submerged ellipsoids at zero forward speed, the general behavior of surge and heave damping functions of frequency is similar. Substituting the unit total damping force (unprimed) for the summation of the sectional damping forces, Equation A-28 becomes

$$X_d = C_{xx} N_{xx} \dot{x}$$

Equating the surge damping coefficient to the heave damping coefficient and introducing the fractional product factors, $f(\omega)$, obtained from the results of Newman, the surge damping force becomes

$$X_d = f C_z N_z \dot{x} \tag{A-30}$$

where C_z is the three-dimensional damping factor for pure heave and N_z is the total unit damping force in heave. The double-index subscript has been dropped in this notation. N_z is given by the relationship

$$N_z = \frac{\rho g^2}{\omega^3} \int_{\xi_s}^{\xi_b} \left(\bar{A}_z\right)^2 \, d\xi$$

where $\bar{A}_z$ is the ratio of amplitude of the heave-generated wave to the amplitude of heaving motion of the elementary section.

Sway, Y_d

For the case of lateral motion, the sway damping force at each section has the form

$$\frac{dY_d}{d\xi} = -C_{yy} N_{yy}' \dot{y} + C_{y\phi} N_{y\phi}' \dot{\phi} - C_{y\psi} N_{y\psi}' \dot{\psi} \qquad \text{(A-31)}$$

where N_{yy}' is the unit swaying force per unit lateral velocity. Equation A-31 can be written

$$Y_d = -C_{yy} \dot{y} \int N_{yy}' \, d\xi + C_{y\phi} \dot{\phi} \int N_{y\phi} \, d\xi - C_{y\psi} \dot{\psi} \int N_{y\psi}' \, d\xi \qquad \text{(A-32)}$$

Noting that $N_{y\phi}'$ is the unit swaying force per unit angular velocity due to roll and that rolling about the longitudinal axis induces a swaying force acting at the center of pressure (i.e., at a distance $|BG|$ from the CG), the quantity "$-|BG| N_{yy}'$" may be substituted for the term $N_{y\phi}'$. Kaplan and Putz (1962) state that the sway damping factor can also be applied to the lateral damping contribution from rolling motion. On that basis, and with $C_{y\psi} = 1$, the final form of the total sway damping force becomes

$$Y_d = -C_{yy} N_y \dot{y} - N_{y\psi} \dot{\psi} - C_{yy} |BG| N_y \dot{\phi} \qquad \text{(A-33)}$$

where N_{yy}' is given by the expression

$$N_{yy}' = \frac{\rho g^2}{\omega^3} \bar{A}_y^2 \qquad \text{(A-34)}$$

The quantity $\bar{A}_y$ is the ratio of the amplitude of the sway-generated wave to the amplitude of swaying motion of the elementary section. Vossers (1960) provides a means of evaluating $\bar{A}_y$ from the relationship

$$\bar{A}_y = d_y \left(\frac{\omega^2 B^*}{2g}\right)^2 \qquad \text{(A-35)}$$

Substituting $\bar{A}_y$ into Equation A-34, the lateral damping force per unit vertical velocity of the section is

$$N_{yy}' = \frac{\rho g^2}{\omega^3} \left(d_y\right)^2 \left(\frac{\omega^2 B^*}{2g}\right)^4$$

or

$$N_{yy}' = \frac{\rho g^2}{\omega^3} \left(d_y\right)^2 \left[\frac{\omega^8 \left(B^*\right)^4}{16 g^4}\right] = \frac{\rho \omega^5}{16 g^2} \left(B^*\right)^4 \left(d_y\right)^2 \tag{A-36}$$

Thus,

$$N_y = \int_{\xi_s}^{\xi_b} N_{yy}' \, d\xi = \frac{\rho \omega^2}{16 g^2} \int_{\xi_s}^{\xi_b} (B^*)^4 \left(d_y\right)^2 d\xi \tag{A-37}$$

and

$$N_{y\psi} = \int_{\xi_s}^{\xi_b} \xi N_{yy}' \, d\xi = \frac{\rho \omega^5}{16 g^2} \int_{\xi_s}^{\xi_b} (B^*)^4 \left(d_y\right)^2 \xi \, d\xi \tag{A-38}$$

Heave, Z_d

The vertical damping force at each section has the form

$$\frac{dZ_d}{d\xi} = -C_{zz} N_{zz}' \dot{z} + C_{z\theta} N_{z\theta}' \dot{\theta} \tag{A-39}$$

or

$$Z_d = -C_{zz} \dot{z} \int_{\xi_s}^{\xi_b} N_{zz}' \, d\xi + C_{z\theta} \dot{\theta} \int_{\xi_s}^{\xi_b} N_{z\theta}' \, d\xi \tag{A-40}$$

where

$$N_{zz}' = \frac{\rho g^2 \left(\overline{A}_z\right)^2}{\omega^3} \tag{A-41}$$

and

$$N_{z\theta} = \xi N_{zz}' \tag{A-42}$$

Thus, since $C_{z\theta} = 1$, Equation A-40 becomes

$$Z_d = C_{zz} N_z \dot{z} + N_{z\theta} \dot{\theta} \tag{A-43}$$

where

$$N_z = \int_{\xi_s}^{\xi_b} N_{zz}' \, d\xi \quad \text{and} \quad N_{z\theta} = \int_{\xi_s}^{\xi_b} N_{zz}' \, \xi \, d\xi$$

Pitch, M_d

The moments pitch, yaw, and roll are easily derived from the forces. The form of the sectional pitch damping moment is

$$\frac{dM_d}{d\xi} = -\xi \frac{dZ_d}{d\xi} = C_{\theta z} N_{zz}' \xi \dot{z} - C_{\theta\theta} N_{zz}' \xi^2 \dot{\theta} \tag{A-44}$$

or

$$M_d = C_{\theta z} \dot{z} \int_{\xi_s}^{\xi_b} N_{zz} \xi \, d\xi - C_{\theta\theta} \dot{\theta} \int_{\xi_s}^{\xi_b} N_{zz}' \xi^2 \, d\xi \tag{A-45}$$

Making the substitution that $N_\theta = \int_{\xi_s}^{\xi_b} N_{zz}' \xi^2 \, d\xi$, and setting $C_{\theta z} = 1$, and $C_{\theta\theta} = C_{zz}$, the final form of the pitch moment becomes

$$M_d = N_{z\theta} \dot{z} - C_{zz} N_\theta \dot{\theta} \tag{A-46}$$

Yaw, N_d

The sectional yaw damping moment is

$$\frac{dN_d}{d\xi} = \xi \frac{dY_d}{d\xi} = -C_{\psi y} N_{yy}' \xi \dot{y} - C_{\psi\psi} N_{yy}' \xi^2 \dot{\psi} - C_{\psi\phi} \left| BG \right| N_{yy}' \xi \dot{\phi} \tag{A-47}$$

but $C_{\psi y} = C_{\psi\phi} = 1$, and Equation A-47 becomes

$$N_d = -\dot{y}\int_{\xi_s}^{\xi_b} N_{yy}'\,\xi\,d\xi - C_{\psi\psi}\,\dot{\psi}\int_{\xi_s}^{\xi_b} N_{yy}'\,\xi^2\,d\xi - |BG|\,\dot{\phi}\int_{\xi_s}^{\xi_b} N_{yy}'\,\xi\,d\xi \qquad (A-48)$$

Setting

$$N_\psi = \int_{\xi_s}^{\xi_b} N_{yy}'\,\xi^2\,d\xi = \frac{\rho\omega^5}{16\,g^2}\int_{\xi_s}^{\xi_b} (B^*)^4\left(d_y\right)^2\,\xi^2\,d\xi$$

the final representation of the pitch moment is

$$N_d = -N_{y\psi}\,\dot{y} - C_{\psi\psi}\,N_\psi\,\dot{\psi}\,|BG|\,N_{y\psi}\,\dot{\phi} \qquad (A-49)$$

Roll, K_d

The roll damping term due to lateral motions is approximated by the relation

$$K_d = |BG|\,Y_d \qquad (A-50)$$

where it is assumed that the center of action of the lateral force is at the center of buoyancy; thus the total force due to roll damping is

$$K_d = -C_{yy}\,|BG|\,N_y\,\dot{y} - |BG|\,N_{y\psi}\,\dot{\psi} - C_{yy}\left(|BG|\right)^2 N_y\,\dot{\phi} \qquad (A-51)$$

Kaplan and Putz (1962) state that the quantity $C_{yy}\left(|BG|\right)^2 N_y$ should be replaced by a pure roll damping term N_ϕ which may be obtained from experimental data. Specifically, N_ϕ is obtained from an examination of the roll decay curve. However, roll is a highly tuned motion and the damping value is only important near the natural roll period. Thus, Kaplan and Putz suggest that the damping coefficient N_ϕ be calculated from the total roll moment of inertia, natural roll frequency, and the extinction characteristics of the roll decay curve. Thus, N_ϕ may be calculated from the following relationship:

$$N_\phi = 2\mu\,I_{xt}\,\frac{2\pi}{T_\phi} \qquad (A-52)$$

where I_{xt} is the total roll moment of inertia, T_ϕ is the natural roll period, and μ is the dimensionless coefficient of decay, which is usually obtained from experimental data.

HYDROSTATIC RESTORING FORCES AND MOMENTS

The hydrostatic reactions are those caused by displacements of the barge from the equilibrium position in still water. These restoring effects, which exist only for the heave, pitch, and roll motions, are well known, being derived in detail in a number of important references (e.g., St. Denis and Pierson, 1953), and therefore only the simplified results are presented herein.

Assuming that the angular displacements in roll are small and that the effective buoyancy change is due to total immersion of the local cross-sectional element (whose sides are assumed to be almost parallel near the intersection with the free surface), the sectional vertical force due to net vertical displacements is

$$\frac{dZ_h}{d\xi} = -\rho g B^* (z - \xi\theta) \tag{A-53}$$

Similarly, the hydrostatic restoring pitch moment is

$$\frac{dM_h}{d\xi} = -\xi \frac{dZ_h}{d\theta} \tag{A-54}$$

From Equations A-53 and A-54, the final forms of the hydrostatic restoring heave force and pitch moment are respectively

$$Z_h = -\rho g z \int_{\xi_s}^{\xi_b} B^* \, d\xi + \rho g \theta \int_{\xi_s}^{\xi_b} B^* \xi \, d\xi \tag{A-55}$$

and

$$M_h = \rho g z \int_{\xi_s}^{\xi_b} B^* \xi \, d\xi - \rho g \theta \int_{\xi_s}^{\xi_b} B^* \xi^2 \, d\xi \tag{A-56}$$

The righting moment for roll motion is the well-known expression

$$K_h = -\rho g \nabla |GM| \phi = -W |GM| \phi \tag{A-57}$$

where ∇ is the displaced volume; $|GM|$ is the transverse metacentric height, which is the distance between the center of gravity and the metacenter (a point on the vertical axis of symmetry intersected by the resultant of the displaced center of buoyancy caused by small roll motions); and W is the total barge displacement.

MOORING FORCES AND MOMENTS

The barge is spread moored by an unusual chain and stake pile system, with both bow and stern moorings. Figure 4 presents a schematic representation of the mooring configuration and the catenary profile which the chain and stake pile system assumes when the sinker is attached. Thus, any changes in the mooring forces on the barge (and therefore also in the chain) occur as a result of changes in the catenary profile (i.e., changes in energy state) resulting from barge displacement. Hence, it is necessary to determine relationships between the displacement of the barge and forces in the chains.

Simple Catenary Equation

The general mooring line equations for a chain of constant linear density with an attached sinker are derivable from the simple catenary equations, which are well known. The following relationships, referring to the definition sketch shown below, have been found useful in describing the catenary profile and the tensile forces:

$$T_v = ws \qquad L^2 - B^2 = 2c \sinh \frac{k}{2c}$$

$$T_h = wc \qquad \frac{B}{L} = \tanh \frac{x_m}{c}$$

$$T = wy \qquad x_m = x_a + \frac{k}{2}$$

$$y^2 = s^2 + c^2 \qquad x = x_m + \frac{k}{2}$$

$$s = c \sinh \frac{x}{c}$$

where T_v = vertical force at point (x, y)

T_h = horizontal force at point (x, y)

T = axial tension at point (x, y)

s = length of curve from point (0, c) to point (x, y)

w = weight of chord per unit length

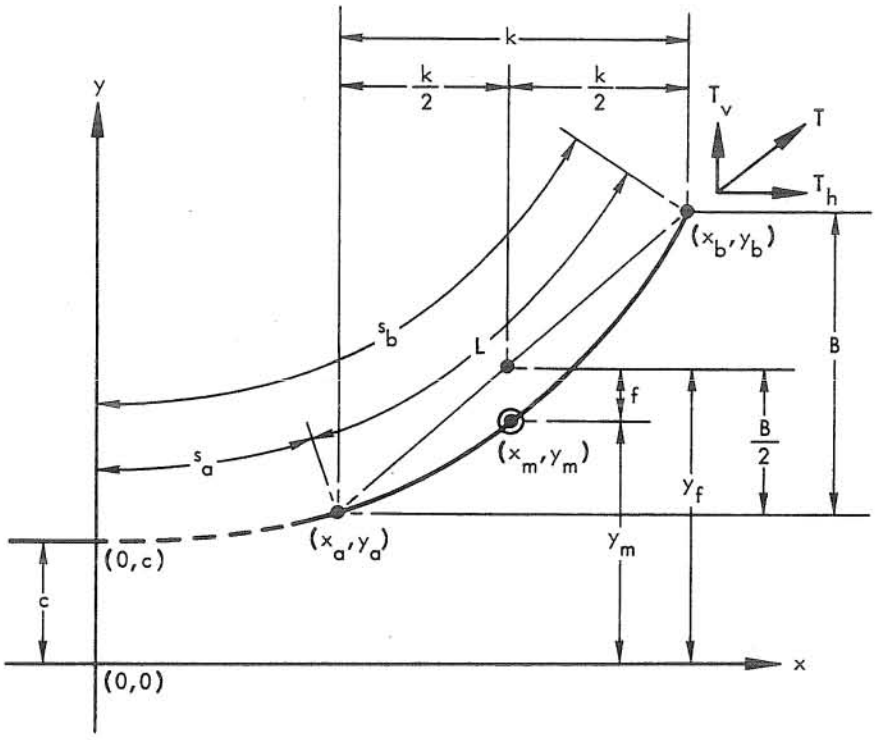

When a sinker of weight W is added, the chain axis follows the curves of two catenaries as shown by the following sketch.

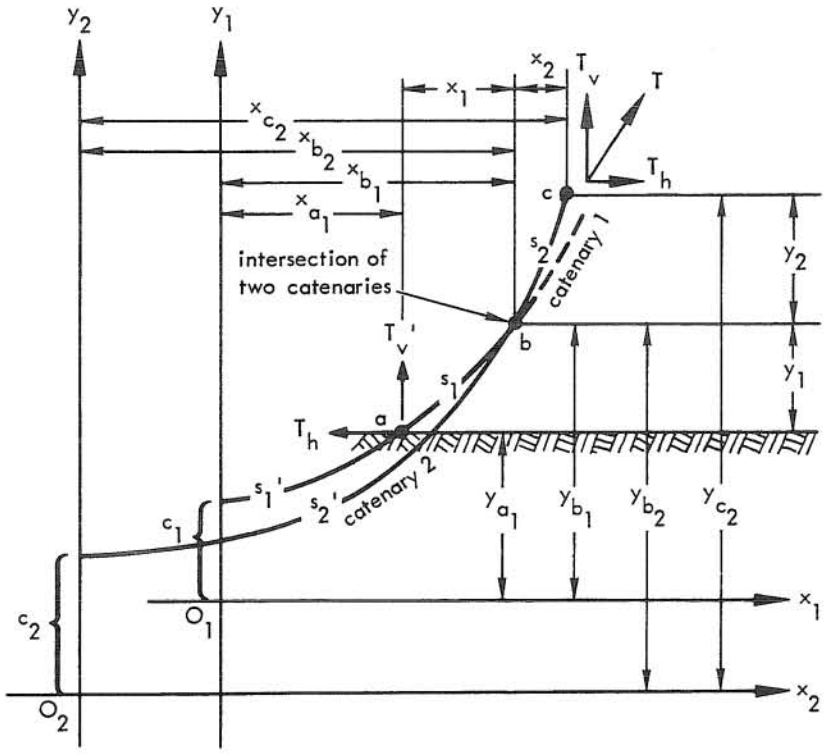

Through appropriate algebraic manipulation, it is possible to derive expressions relating the ordinates labeled y_1, y_2, x_1, and x_2 and the parameters w, T_h, T_v', s_2, s_1, and W. These expressions are:

$$y_1 = \frac{1}{w}\left\{\left[T_h^{\,2} + \left(T_v' + ws_1\right)^2\right]^{\frac{1}{2}} - \left(T_h^{\,2} + T_v'^{\,2}\right)^{\frac{1}{2}}\right\} \tag{A-58}$$

$$y_2 = \frac{1}{w}\left\{\left[T_h^{\,2} + \left(T_v' + ws_2 + W + ws_1\right)^2\right]^{\frac{1}{2}} - \left[T_h^{\,2} + \left(T_v' + ws_2 + W\right)^2\right]^{\frac{1}{2}}\right\} \tag{A-59}$$

$$x_1 = \frac{T_h}{w}\log\frac{1}{2}\left\{\left[\frac{w^2}{T_h^{\,2}}\left(s_1^{\,2} - y_1^{\,2}\right) + 2\right] + \left(\left[\frac{w^2}{T_h^{\,2}}\left(s_1^{\,2} - y_1^{\,2}\right) - 2\right]^2 - 4\right)^{\frac{1}{2}}\right\} \tag{A-60}$$

$$x_2 = \frac{T_h}{w}\log\frac{1}{2}\left\{\left[\frac{w^2}{T_h^{\,2}}\left(s_2^{\,2} - y_2^{\,2}\right) + 2\right] + \left(\left[\frac{w^2}{T_h^{\,2}}\left(s_2^{\,2} - y_2^{\,2}\right) + 2\right]^2 - 4\right)^{\frac{1}{2}}\right\} \tag{A-61}$$

For the usual problem, W, w, s_1, s_2 and $(y_1 + y_2)$ and $(x_1 + x_2)$ are known and it is desired to find T_h and T_v. Thus, we have the equivalent of two equations in two unknowns which are easily (though laboriously) obtained.

A special case exists, however, when s_2 and $(x_1 + x_2)$ are also unknown. This happens when a portion of the chain is lying on the ocean bottom. In order to overcome this difficulty, total initial tensions were measured on the barge and checked with the values obtained from Equations A-58 through A-61. Adjustments in s_2 and $(x_1 + x_2)$ were then made to effect agreement between the calculated and measured values. The results for each of the four chains are shown in Figures A-1 and A-2, where the restoring force relationships are indicated. The resultant of the four horizontal tension components must also be zero, which serves as an additional check on the equilibrium position of the barge.

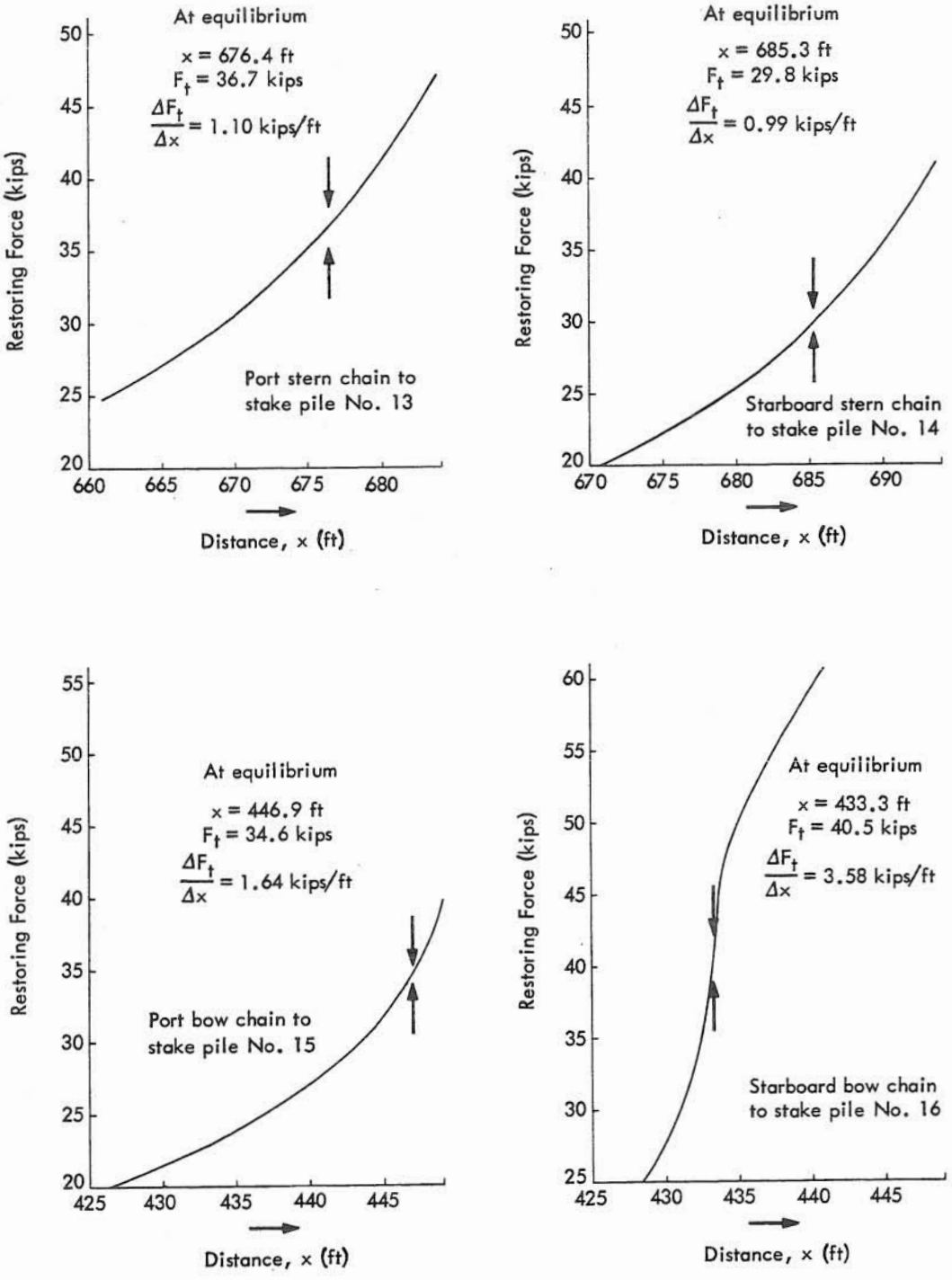

Figure A-1. Restoring force relationships: total tension.

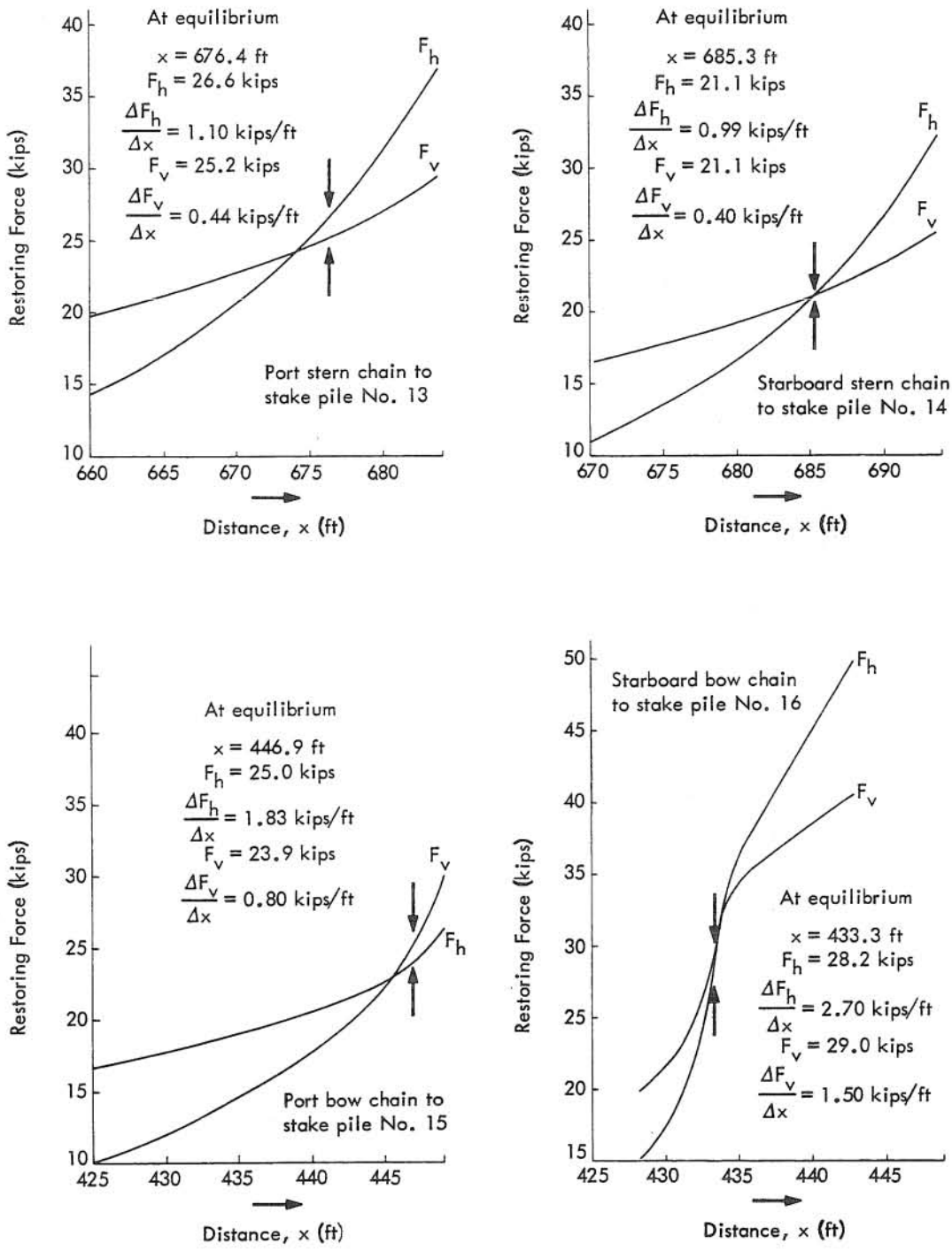

Figure A-2. Restoring force relationships: horizontal and vertical force components.

Barge Displacement

At the equilibrium position, the restoring effects may be considered linear since the displacements are small relative to the chain lengths. Thus, with the barge moored as shown in the following sketch,

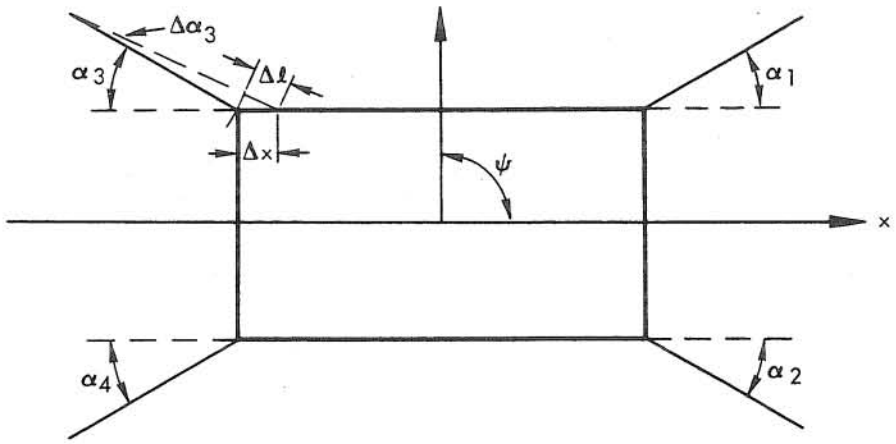

the displacement of a single cable such as No. 3, caused by motion of the cable in surge, x, is $\Delta\ell = \Delta x \cos\left(\alpha_3 + \Delta\alpha_3\right)$. Since $\Delta\alpha_3$ is small, then $\Delta\ell = \Delta x \cos\left(\alpha_3\right)$. The restoring force in the x direction due to motion in the x direction in the cable is

$$C_3 \Delta x \cos\alpha_3 \cos\alpha_3 = C_3 \Delta x \cos^2\alpha_3$$

where C_3 is the effective spring constant (the slope of the displacement-force curve). The total longitudinal force on the barge induced by the moorings is

$$X_m = -x \sum_{i=1}^{4} C_i \cos^2\alpha_i = -x \sum_{i=x}^{i=4} \left(k_x\right)_i$$

where

$$\left(k_x\right)_i = C_i \cos^2\alpha_i$$

For sway motion, the effective displacement along the cable is $\Delta y \sin\left(\alpha_3 + \Delta\alpha_3\right)$. Again, combining the components from all the cables, the total lateral force is given by

$$Y_m = -y \sum_{i=1}^{i=4} C_i \sin^2 \alpha_i = -y \sum_{i=1}^{i=4} \left(k_y\right)_i$$

For yaw motion, the lateral displacement at one end of the barge is $(L/2)\,\psi$, where L is the barge length. The net lateral force at one end of the barge is then

$$Y_m\Big|_{y=\frac{L}{2}} = \left(C_1 \sin^2 \alpha_1\right) \frac{L}{2}\psi + \left(C_2 \sin^2 \alpha_2\right) \frac{L}{2}\psi$$

$$= \frac{L}{2}\psi \sum_{i=1}^{2} C_i \sin^2 \alpha_i$$

The moment arm is $L/2$ and the contribution to the yaw moment (at each end) is

$$\frac{1}{2} N_m = \frac{L^2}{4}\psi \sum_{i=1}^{2} C_i \sin^2 \alpha_i$$

Now that the forces at each end are opposite and approximately equal (since the yaw axis origin is at the center of gravity and not midway between the points of action of the mooring forces), the net contribution to the yaw moment acting on the barge is given by

$$N_m = -\frac{L^2}{4}\psi \sum_{i=1}^{i=4} C_i \sin^2 \alpha_i = -\frac{L^2}{4}\psi \sum_{i=1}^{i=4} \left(k_\psi\right)_i$$

Alternatively, the variations in the force in the mooring chains due to motions of the barge can be easily found. The longitudinal displacement, x, and the net lateral displacements $\left[y = (L/2)\,\psi\right]$ at the bow and $\left[y - (L/2)\,\psi\right]$ at the stern, can be combined to determine the net variation in elongation of each mooring chain. In the case of the stern port chain, the displacement from surging motion of the barge is $x \cos \alpha_3$, while the chain displacement due to motions of sway and yaw is $\left[y - (L/2)\,\psi\right] \sin \alpha_3$.

Lateral motions create different effects in chain displacement direction at either bow or stern, whereas longitudinal motion (surge) causes the same displacement direction, at either bow or stern. The general expression for the fluctuating mooring force in the chains is

$$F_c = C\left[x\cos\alpha \pm \left(y \pm \frac{L}{2}\psi\right)\sin\alpha\right]$$

The expressions for the individual chain forces are:

Bow -

$$F_1 = -C_1\left[x\cos\alpha_1 + \left(y + \frac{L}{2}\psi_1\right)\sin\alpha_1\right] \qquad \text{port}$$

$$F_2 = -C_2\left[x\cos\alpha_2 - \left(y + \frac{L}{2}\psi_2\right)\sin\alpha_2\right] \qquad \text{starboard}$$

Stern -

$$F_3 = C_3\left[x\cos\alpha_3 - \left(y - \frac{L}{2}\psi_3\right)\sin\alpha_3\right] \qquad \text{port}$$

$$F_4 = C_4\left[x\cos\alpha_4 + \left(y - \frac{L}{2}\psi_4\right)\sin\alpha_4\right] \qquad \text{starboard}$$

For the present study, Figures A-1 and A-2 and Table A-1 summarize the results obtained from the mooring calculations. The values of k_x, k_y, and k_ψ may be considered the effective spring constants for surge, sway, and yaw. As a result, natural periods for these motions exist in the case of moored ships which do not exist or are effectively zero in the case of free ships. The introduction of the existence of these natural periods is the main feature which distinguishes the resulting motions of moored ships from those of free ships. The other natural periods of heave, pitch, and roll still exist for moored ships as they do for free ships. Since the natural periods in heave, pitch, and roll are related to the hydrostatic restoring forces and moments, a measure of the influence of the moorings can be obtained by comparing the relative magnitudes of hydrostatic and mooring restoring forces. Previous work on normal ship forms has indicated that the mooring restoring forces are small relative to the hydrostatic restoring forces. Thus, there is some justification for concluding that the natural periods of heave, pitch, and roll are relatively unaffected by the presence of the moorings.

Table A-1. Mooring Spring Constants

Stake Pile No.	Connects to	C* (kip/ft)	α (deg)	k_x (kip/ft)	k_y (kip/ft)	k_ψ (kip-ft/rad)
13	Stern port	1.10	36.5	0.712	0.389	--
14	Stern starboard	0.99	44.0	0.516	0.477	--
15	Bow port	1.83	49.5	0.775	1.060	--
16	Bow starboard	2.70	51.5	1.070	1.650	--
				3.073	3.576	8940

EVALUATION OF WAVE-EXCITING FORCES AND MOMENTS

The hydrodynamic forces and moments induced by waves are obtained by application of slender body theory. Kaplan (1957) states that:

> A consequence of the use of slender body theory is that the crossflow in each cross section is independent of the flow at other sections, and the connection of this two-dimensional flow with the actual three-dimensional problem is through the boundary condition, which contains the longitudinal coordinate ξ as a parameter. At each section the boundary condition is a function of x, since it is dependent on the body geometry. The total force acting on the body is found by integrating the elemental forces at each section over the length of the body.

In a general survey of the application of strip theory to wave-induced effects for slender bodies, Korvin-Kroukovsky (1961) states that the wave-induced force acting on an individual ship section of the length, $d\xi$, is composed of inertial, damping, and displacement components. The inertial component is proportional to acceleration; the damping component is proportional to velocity, and the displacement component is of course proportional to a displacement term.

Thus, the total wave-induced force acting on an elemental section is

$$\frac{dF_w}{d\xi} = \frac{dF_w^{(1)}}{d\xi} + \frac{dF_w^{(2)}}{d\xi} + \frac{dF_w^{(3)}}{d\xi} \qquad \text{(A-62)}$$

where 1 indicates an inertial contribution, 2 indicates a damping contribution, and 3 indicates a displacement contribution.

Inertial Terms

Kaplan and Putz (1962) state that the wave forces on a surface ship can be represented in the same manner as for a submerged body, but with the frequency dependence of the added mass terms included in the final representation. On this basis, the inertial contribution to the wave-exciting forces for the present case of zero speed is represented by

$$\frac{dF_w^{(1)}}{d\xi} = \left(\rho S + \sum A_{ij}\right) \frac{D\bar{q}_{oi}}{Dt} \tag{A-63}$$

where $dF_w^{(1)}$ is the inertial wave force acting on the elemental section, $d\xi$; ρ is the mass density of sea water; S is the cross-sectional area; A_{ij} is the sectional added mass coefficient along the i direction due to its motion in the j direction; D/Dt is an operator denoting the substansive or material derivative; and $\bar{q}_{oi}$ is a component of the orbital velocity evaluated at some reference point on the barge hull. The reference point chosen for this analysis is the intersection of the vertical plane containing the longitudinal centerline (due to symmetry) and the horizontal plane representing the mean half draft of the barge. The latter is an approximation to allow for the influence of the exponential decay of wave particle velocity. The wave particle velocity, $\bar{q}_{oi}$, is obtained from the velocity potential given by Lamb (1945) and compatible with the adopted coordinate system. This wave potential is

$$\phi_w = a c e^{\frac{2\pi z}{\lambda}} \cos \frac{2\pi}{\lambda} (x \cos\beta + y \sin\beta - ct) \tag{A-64}$$

where a is the wave amplitude; c is the propagation velocity, $\left[C^2 = (g\lambda/2\pi) \tanh (2\pi d/\lambda)\right]$; λ is the wave length; z is the vertical coordinate denoting the point at which the velocity will be evaluated and will be set equal to the mean half draft of the barge, $-\bar{h}$; β is the angle lying between the x-axis and the normal to the wave crests and lying in the range $-\pi \leq \beta \leq \pi$; and d is the mean water depth. Note that the terms $x \cos\beta$ and $y \sin\beta$ are merely the projections of $\sqrt{x^2 + y^2}$ on the lines $\cos\beta$ and $\sin\beta$, respectively. The surface wave elevation, η, is

$$\eta = \frac{1}{g} \left.\frac{\partial \phi_w}{\partial t}\right|_{z=0}$$

$$\eta = \frac{1}{g} a c^2 \frac{2\pi}{\lambda} \sin \frac{2\pi}{\lambda} (x \cos\beta + y \sin\beta - ct) \tag{A-65}$$

or, substituting,

$$\eta = a \tanh \frac{2\pi d}{\lambda} \sin \frac{2\pi}{\lambda} (x \cos \beta + y \sin \beta - ct) \tag{A-66}$$

For deep water $\tanh 2\pi d/\lambda \approx 1$, and Equation A-66 becomes

$$\eta = a \sin \frac{2\pi}{\lambda} (x \cos \beta + y \sin \beta - ct) \tag{A-67}$$

Damping Terms

Damping forces arising from wave action are due to the difference between the body velocities and the wave orbital velocities. These forces should not be confused with damping due to motion of the body in otherwise still water, discussed elsewhere. Kaplan and Putz (1962) state that the "basis for including such a representation in the wave-induced effects for slender bodies is in the recent thesis by Vossers (1962), while it has been used in other studies purely on the basis of empirical reasoning." Thus, formulating an expression for the damping forces, we have

$$\frac{dF_w^{(2)}}{d\xi} = C_i N_{ij} \bar{q}_{oi} \tag{A-68}$$

where $\bar{q}_{oi}$ is as defined previously, C_i is a three-dimensional damping factor, and N_{ij} is the sectional (elemental) damping coefficient.

Displacement Terms

The displacement terms are due to the buoyant effect of the waves as they pass the barge hull. Thus, the displacement terms are included only in the vertical force and may be represented by

$$\frac{dF_w^{(3)}}{d\xi} = \rho g \beta^* \eta(\xi, t) \tag{A-69}$$

where β^* is the local section beam. The wave force expressions for surge, X_w; sway, Y_w; heave, Z_w; pitch, M_w; yaw, N_w; and roll, K_w, may now be derived in accordance with Equations A-62, A-63, A-68, and A-69.

Surge, X_w

Evaluating the wave orbital velocity, q_{ox}, from the wave potential, Equation A-64, gives

$$q_{ox} = u = -\frac{\partial \phi_w}{\partial x} = -ac\frac{2\pi}{\lambda} e^{+\frac{2\pi z}{\lambda}} \cos\beta \left[\sin\frac{2\pi}{\lambda}(x\cos\beta + y\sin\beta - ct)\right] \quad \text{(A-70)}$$

The substansive derivative,

$$\frac{D(u)}{Dt} = \frac{\partial(u)}{\partial t} + (u)\frac{\partial(u)}{\partial x} + (v)\frac{\partial(u)}{\partial y} + w\frac{\partial(u)}{\partial z} \quad \text{(A-71)}$$

where the first term on the right-hand side represents the temporal acceleration and the last three terms represent the convective acceleration due to convergence of the flow. Since one of the basic assumptions of slender body theory as used herein is that the convergence of the wave motion flow pattern resulting from presence of the body is negligible, the convective terms may be set equal to zero. Thus,

$$u\frac{\partial u}{\partial x} + v\frac{\partial u}{\partial y} + w\frac{\partial u}{\partial z} = 0 \quad \text{(A-72)}$$

and

$$\frac{Du}{Dt} = \frac{\partial u}{\partial t}$$

So,

$$\frac{\partial u}{\partial t} = -ac^2\left(\frac{2\pi}{\lambda}\right)^2 e^{+\frac{2\pi z}{\lambda}} \cos\beta \left[\cos\frac{2\pi}{\lambda}(x\cos\beta + y\sin\beta - ct)\right] \quad \text{(A-73)}$$

Recall that

$$\cos(A - B) = \cos A\cos B + \sin A\sin B \quad \text{(A-74)}$$

and

$$\frac{Du}{Dt} = \frac{\partial u}{\partial t} = -a\,c^2 \left(\frac{2\pi}{\lambda}\right)^2 e^{+\frac{2\pi z}{\lambda}} \cos\beta \left\{ \left[\cos \frac{2\pi}{\lambda} (x \cos\beta + y \sin\beta)\right] \cos \frac{2\pi c t}{\lambda} \right.$$

$$\left. + \left[\sin \frac{2\pi}{\lambda} (x \cos\beta + y \sin\beta)\right] \sin \frac{2\pi c t}{\lambda} \right\} \qquad \text{(A-75)}$$

From Equation A-63,

$$X_w^{(1)} = \int_{\xi_s}^{\xi_b} \left(\rho S + \sum A_{ij}'\right) \frac{Du}{Dt}\, d\xi$$

Since $\sum A_{ij}$ is the sum of the added masses in surge and is approximately equal to zero for a slender body, then

$$X_w^{(1)} = -\rho a\,c^2 \left(\frac{2\pi}{\lambda}\right)^2 e^{+\frac{2\pi z}{\lambda}} \cos\beta \left[\cos \omega t \int_{\xi_s}^{\xi_b} S \cos \frac{2\pi}{\lambda} (x \cos\beta + y \sin\beta)\, d\xi \right.$$

$$\left. + \sin \omega t \int_{\xi_s}^{\xi_b} S \sin \frac{2\pi}{\lambda} (x \cos\beta + y \sin\beta)\, d\xi \right] \qquad \text{(A-76)}$$

where $S = f(\xi)$, and $c = \lambda/T = \lambda\omega/2\pi$ by definition.

In order to compute $X_w^{(1)}$, the right-hand side must be evaluated at some reference point z, y. The reference point chosen in this analysis is $z = -\bar{h}$, $y = 0$. The mean half draft, $\bar{h}$, is chosen to approximate the influence of the exponential decay of wave particle velocity. The vertical centerline is chosen because of symmetry. However, since the barge is not really slender, and since the beam of the barge is not small relative to some of the wave lengths, an additional correction must be introduced. Kaplan and Putz (1962) state that:

"Since the various integrals are really of the form

$$\int_{\xi_s}^{\xi_b} f(\xi) \begin{matrix}\cos \\ \sin\end{matrix} \left(\frac{2\pi x}{\lambda} \cos\beta + \frac{2\pi y}{\lambda} \sin\beta\right) d\xi$$

a proper move would be to represent the influence of this additional term by finding the mean value of the beam. Using maximum beam, B, as a base, since the barge is close to a full planform shape, the quantity of interest is

$$\frac{1}{B}\int_{-\frac{B}{2}}^{\frac{B}{2}} dy \int_{\xi_s}^{\xi_b} f(\xi) \begin{matrix}\cos\\ \sin\end{matrix}\left(\frac{2\pi x}{\lambda}\cos\beta + \frac{2\pi y}{\lambda}\sin\beta\right) d\xi$$

which is equal to

$$\frac{\sin\left(\frac{\pi B}{\lambda}\sin\beta\right)}{\frac{\pi B}{\lambda}} \int_{\xi_s}^{\xi_b} f(\xi) \begin{matrix}\cos\\ \sin\end{matrix}\left(\frac{2\pi x}{\lambda}\cos\beta\right) d\xi$$

which accounts for the influence of the beam-wave length ratio in a more rational manner (although not the most precise method) than simply setting $y = 0$."

Therefore, setting $z = -\bar{h}$, $y = 0$ and introducing the product factor

$$\frac{\sin\left(\frac{\pi B}{\lambda}\sin\beta\right)}{\frac{\pi B}{\lambda}\sin\beta}$$

the expression for the surging force $X_w^{(1)}$ becomes

$$X_w^{(1)} = -\rho a c^2 \left(\frac{2\pi}{\lambda}\right)^2 e^{-\frac{2\pi\bar{h}}{\lambda}} \left[\frac{\sin\left(\frac{\pi B}{\lambda}\sin\beta\right)}{\frac{\pi B}{\lambda}\sin\beta}\right] \cos\beta \left[\cos\omega t \int_{\xi_s}^{\xi_b} S\cos\frac{2\pi}{\lambda}(x\cos\beta)\, d\xi + \sin\omega t \int_{\xi_s}^{\xi_b} S\sin\frac{2\pi}{\lambda}(x\cos\beta)\, d\xi\right] \quad \text{(A-77)}$$

where $c^2 = (g\lambda/2\pi)\tanh(2\pi d/\lambda)$.

Surge damping due to wave generation is generally quite small, and in the absence of more detailed information is neglected. Thus,

$$X_w^{(2)} = 0 \quad \text{(A-78)}$$

Adding Equations A-77 and A-78 gives the general expression for evaluating the surging force in deep or shallow water. In terms of ω and λ, it may be written as

$$X_w = -\rho a \omega^2 \, e^{-\frac{2\pi\bar{h}}{\lambda}} \left[\frac{\sin\left(\frac{\pi B}{\lambda} \sin\beta\right)}{\frac{\pi B}{\lambda} \sin\beta} \right] \cos\beta \left[\cos\omega t \int_{\xi_s}^{\xi_b} S \cos\frac{2\pi}{\lambda}(x\cos\beta)\, d\xi \right.$$

$$\left. + \sin\omega t \int_{\xi_s}^{\xi_b} S \sin\frac{2\pi}{\lambda}(x\cos\beta)\, d\xi \right] \qquad \text{(A-79)}$$

where the only variable is ω, since λ may be found from the relationship

$$\omega^2 = \left(\frac{2\pi}{\lambda}\right) g \tanh\frac{2\pi d}{\lambda} \, .$$

For head-on waves, $\beta = +\pi$, $\cos\beta = -1$, $\sin\beta = 0$, and Equation A-79 becomes

$$X_w = +\rho a \omega^2 \, e^{-\frac{2\pi\bar{h}}{\lambda}} \left[\cos\omega t \int_{\xi_s}^{\xi_b} S \cos\left(-\frac{2\pi x}{\lambda}\right) d\xi \right.$$

$$\left. + \sin\omega t \int_{\xi_s}^{\xi_b} S \sin\left(-\frac{2\pi x}{\lambda}\right) d\xi \right] \qquad \text{(A-80)}$$

Making use of the trigonometric properties,

$$X_w = \rho a \omega^2 \, e^{-\frac{2\pi\bar{h}}{\lambda}} \left[\cos\omega t \int_{\xi_s}^{\xi_b} S \cos\left(\frac{2\pi x}{\lambda}\right) d\xi \right.$$

$$\left. - \sin\omega t \int_{\xi_s}^{\xi_b} S \sin\left(\frac{2\pi x}{\lambda}\right) d\xi \right] \qquad \text{(A-81)}$$

For deep water, $2\pi/\lambda = \omega^2/g = g/c^2$ and Equation A-81 may be written

$$X_w = a\rho\omega^2 \, e^{-\frac{\omega^2}{g}\bar{h}} \left[\cos\omega t \int_{\xi_s}^{\xi_b} S \cos\left(\frac{\omega^2}{g} x\right) d\xi - \sin\omega t \int_{\xi_s}^{\xi_b} S \sin\frac{\omega^2}{g} x \, d\xi \right] \qquad \text{(A-82)}$$

For beam-on waves, $B = \pi/2$, $\cos\beta = 0$, and $\sin\beta = 1$, and Equation A-79 becomes

$$X_w = 0 \tag{A-83}$$

which is the result in all depths of water.

Sway Y_w

Evaluating the wave orbital velocity, q_{oy}, from the wave potential, Equation A-64 gives

$$q_{oy} = v = -\frac{\partial \phi_w}{\partial y} = ac\left(\frac{2\pi}{\lambda}\right) e^{\frac{2\pi z}{\lambda}} \sin\beta \left[\sin\frac{2\pi}{\lambda}(x\cos\beta + y\sin\beta - ct)\right] \tag{A-84}$$

Again, the convective acceleration terms are set equal to zero, and

$$\frac{Dv}{Dt} = \frac{\partial v}{\partial t} = -ac^2\left(\frac{2\pi}{\lambda}\right)^2 e^{\frac{2\pi z}{\lambda}} \sin\beta \left[\cos\frac{2\pi}{\lambda}(x\cos\beta + y\sin\beta - ct)\right] \tag{A-85}$$

or

$$\frac{\partial v}{\partial t} = -a\omega^2 e^{\frac{2\pi z}{\lambda}} \sin\beta \left\{(\cos\omega t)\left[\cos\frac{2\pi}{\lambda}(x\cos\beta + y\sin\beta)\right] + (\sin\omega t)\sin\frac{2\pi}{\lambda}(x\cos\beta + y\sin\beta)\right\} \tag{A-86}$$

From Equation A-63,

$$Y_w^{(1)} = \int_{\xi_s}^{\xi_b} \left(\rho S + \sum A_{ij}'\right) \frac{Dv}{Dt}\, d\xi$$

but, $\sum A_{ij} = A_{22}' - A_{42}'\,(2\pi/\lambda)$ for sway motions, where A_{22}' is the sectional added mass in sway due to motion in sway and A_{42}' is the sectional added mass in roll due to motion in sway. Justification for including the latter term, although not germane to the immediate problem, is to take account of the possible effect of relative dimension of draft to wave length. Since the orbital velocities in deep water waves decay with depth exponentially, and since the velocities are evaluated at the mean half draft, it can be shown that there is in addition a "roll moment," which is substantially accounted for by including the next highest order inertial term in powers of wave number $(2\pi/\lambda)$.

The sway force, $Y_w^{(1)}$, then becomes

$$Y_w^{(1)} = -\rho\omega^2 a e^{\frac{2\pi z}{\lambda}} \sin\beta \left\{ \cos\omega t \int_{\xi_s}^{\xi_b} \left(S + \frac{A_{22}'}{\rho} + \frac{2\pi A_{42}'}{\lambda\rho} \right) \cos\left[\left(\frac{2\pi}{\lambda}\right) (x\cos\beta + y\sin\beta) \right] d\xi + \sin\omega t \int_{\xi_s}^{\xi_b} \left(S + \frac{A_{22}'}{\rho} + \frac{2\pi A_{42}'}{\lambda\rho} \right) \sin\left[\left(\frac{2\pi}{\lambda}\right) (x\cos\beta + y\sin\beta) \right] d\xi \right\} \quad \text{(A-87)}$$

Evaluating the force at the mean half draft, -h, and at the centerline reference position, y = 0, and introducing the correction for the relative dimensions of the barge beam and wave lengths results in

$$Y_w^{(1)} = -\rho\omega^2 a e^{-\frac{2\pi h}{\lambda}} \frac{\sin\frac{\pi B}{\lambda}\sin\beta}{\frac{\pi B}{\lambda}\sin\beta} \sin\beta \left\{ \cos\omega t \int_{\xi_s}^{\xi_b} \left(S + \frac{A_{22}'}{\rho} + \frac{2\pi A_{42}'}{\lambda\rho} \right) \cos\left[\left(\frac{2\pi}{\lambda}\right) (x\cos\beta) \right] d\xi + \sin\omega t \int_{\xi_s}^{\xi_b} \left(S + \frac{A_{22}'}{\rho} + \frac{2\pi A_{42}'}{\lambda\rho} \right) \sin\left[\frac{2\pi}{\lambda} (x\cos\beta) \right] d\xi \right\} \quad \text{(A-88)}$$

The damping force, $Y_w^{(2)}$, from Equation A-68, is

$$Y_w^{(2)} = \int_{\xi_s}^{\xi_b} C_y N_{iy}' q_{oy}\, d\xi = C_y \int_{\xi_s}^{\xi_b} N_{yy}' v\, d\xi \quad \text{(A-89)}$$

or

$$Y_w^{(2)} = C_y\, a\, \omega\, e^{\frac{2\pi z}{\lambda}} \sin\beta \left[\cos\omega t \int_{\xi_s}^{\xi_b} N_{yy}' \sin\frac{2\pi}{\lambda}(x\cos\beta + y\sin\beta)\, d\xi \right.$$

$$\left. - \sin\omega t \int_{\xi_s}^{\xi_b} N_{yy}' \cos\frac{2\pi}{\lambda}(x\cos\beta + y\sin\beta)\, d\xi \right] \qquad \text{(A-90)}$$

Again evaluating at the mean half draft, $-\bar{h}$, and at the centerline reference, $y = 0$, yields

$$Y_w^{(2)} = C_y\, a\, \omega\, e^{-\frac{2\pi\bar{h}}{\lambda}} \frac{\sin\frac{\pi B}{\lambda}\sin\beta}{\frac{\pi B}{\lambda}\sin\beta} \sin\beta \left[\cos\omega t \int_{\xi_s}^{\xi_b} N_{yy}' \sin\left(\frac{2\pi}{\lambda} x\cos\beta\right) d\xi \right.$$

$$\left. - \sin\omega t \int_{\xi_s}^{\xi_b} N_{yy}' \cos\left(\frac{2\pi}{\lambda} x\cos\beta\right) d\xi \right] \qquad \text{(A-91)}$$

The swaying force, Y_w, is equal to the sum of $Y_w^{(1)}$ and $Y_w^{(2)}$.

$$Y_w = -\rho\omega^2 a\, e^{-\frac{2\pi\bar{h}}{\lambda}} \frac{\sin\frac{\pi B}{\lambda}\sin\beta}{\frac{\pi B}{\lambda}\sin\beta} \sin\beta \left[\cos\omega t \int_{\xi_s}^{\xi_b} \left(S + \frac{A_{22}'}{\rho} \right.\right.$$

$$\left.\left. + \frac{2\pi A_{42}'}{\lambda\rho} \right) \cos\left(\frac{2\pi}{\lambda} x\cos\beta\right) + \sin\omega t \int_{\xi_s}^{\xi_b} \left(S + \frac{A_{22}'}{\rho} \right.\right.$$

$$\left.\left. + \frac{2\pi A_{42}'}{\lambda\rho} \right) \sin\left(\frac{2\pi}{\lambda} x\cos\beta\right) d\xi \right] + C_y\, a\, \omega\, e^{-\frac{2\pi\bar{h}}{\lambda}}$$

$$\cdot \frac{\sin\frac{\pi B}{\lambda}\sin\beta}{\frac{\pi B}{\lambda}\sin\beta} \sin\beta \left[\cos\omega t \int_{\xi_s}^{\xi_b} N_{yy}' \sin\left(\frac{2\pi}{\lambda} x\cos\beta\right) d\xi \right.$$

$$\left. - \sin\omega t \int_{\xi_s}^{\xi_b} N_{yy}' \cos\left(\frac{2\pi}{\lambda} x\cos\beta\right) d\xi \right] \qquad \text{(A-92)}$$

which is the general expression for evaluating the swaying force.

For head-on waves, $\beta = \pi$, $\cos\beta = -1$, $\sin\beta = 0$, and Equation A-92 reduces to

$$Y_w = 0 \tag{A-93}$$

which is the result for both deep and shallow water waves.

For beam-on waves, $\beta = \pi/2$, $\cos\beta = 0$, $\sin\beta = 1$, and Equation A-92 reduces to

$$Y_w = -\rho\omega^2 a\, e^{-\frac{2\pi\bar{h}}{\lambda}} \frac{\sin\frac{\pi B}{\lambda}}{\frac{\pi B}{\lambda}} \left[\cos\omega t \int_{\xi_s}^{\xi_b} \left(S + \frac{A_{22}'}{\rho} + \frac{2\pi A_{42}'}{\lambda\rho}\right) d\xi\right]$$

$$- C_y a\omega\, e^{-\frac{2\pi\bar{h}}{\lambda}} \frac{\sin\frac{\pi B}{\lambda}}{\frac{\pi B}{\lambda}} \left(\sin\omega t \int_{\xi_s}^{\xi_b} N_{yy}'\, d\xi\right) \tag{A-94}$$

which is a valid expression for both deep and shallow water waves.

Heave, Z_w

Evaluating the wave orbital velocity, q_{oz}, from the wave potential, Equation A-64, gives

$$q_{oz} = w = -\frac{\partial\phi_w}{\partial z} = -ac\,\frac{2\pi}{\lambda}\, e^{\frac{2\pi z}{\lambda}} \cos\frac{2\pi}{\lambda}(x\cos\beta + y\sin\beta - ct) \tag{A-95}$$

Again, the convective acceleration terms are set equal to zero, and

$$\frac{Dw}{Dt} = \frac{\partial w}{\partial t} = -ac^2\left(\frac{2\pi}{\lambda}\right)^2 e^{\frac{2\pi z}{\lambda}} \sin\frac{2\pi}{\lambda}(x\cos\beta + y\sin\beta - ct) \tag{A-96}$$

Making use of the trigonometric identities

$$\frac{\partial w}{\partial t} = -ac^2\left(\frac{2\pi}{\lambda}\right)^2 e^{\frac{2\pi z}{\lambda}} \left[\cos\omega t \sin\frac{2\pi}{\lambda}(x\cos\beta + y\sin\beta)\right.$$

$$\left. - \sin\omega t \cos\frac{2\pi}{\lambda}(x\cos\beta + y\sin\beta)\right] \tag{A-97}$$

From Equation A-63,

$$Z_w^{(1)} = \int_{\xi_S}^{\xi_b} \left(\rho S + \sum A_{ij}' \right) \frac{Dw}{Dt} \, d\xi \tag{A-98}$$

and the only added mass tensor of interest is A_{33}', which is the sectional added mass coefficient in heave due to motion in heave.

Therefore, $\sum A_{ij}' = A_{33}'$, and

$$Z_w^{(1)} = \int_{\xi_S}^{\xi_b} \left(\rho S + A_{33}' \right) \frac{Dw}{Dt} \, d\xi \tag{A-99}$$

so that

$$Z_w^{(1)} = -\rho a \omega^2 e^{\frac{2\pi z}{\lambda}} \left[\cos \omega t \int_{\xi_S}^{\xi_b} \left(S + \frac{A_{33}'}{\rho} \right) \sin \frac{2\pi}{\lambda} (\cos \beta + y \sin \beta) \, d\xi \right.$$

$$\left. - \sin \omega t \int_{\xi_S}^{\xi_b} \left(S + \frac{A_{33}'}{\rho} \right) \cos \frac{2\pi}{\lambda} (x \cos \beta + y \sin \beta) \, d\xi \right] \tag{A-100}$$

Evaluating the force at the mean half draft, $-\bar{h}$, and at the centerline, $y = 0$, after introducing the proper corrective term, results in

$$Z_w^{(1)} = -\rho a \omega^2 e^{-\frac{2\pi \bar{h}}{\lambda}} \frac{\sin \frac{\pi B}{\lambda} \sin \beta}{\frac{\pi B}{\lambda} \sin \beta} \left[\cos \omega t \int_{\xi_S}^{\xi_b} \left(S + \frac{A_{33}'}{\rho} \right) \sin \left(\frac{2\pi}{\lambda} x \cos \beta \right) d\xi \right.$$

$$\left. - \sin \omega t \int_{\xi_S}^{\xi_b} \left(S + \frac{A_{33}'}{\rho} \right) \cos \left(\frac{2\pi}{\lambda} x \cos \beta \right) d\xi \right] \tag{A-101}$$

The damping force, $A_w^{(2)}$, from Equation A-68, is

$$Z_w^{(2)} = \int_{\xi_S}^{\xi_b} C_z N_{iz}' q_{oz} \, d\xi = C_z \int_{\xi_S}^{\xi_b} N_{zz}' w \, d\xi \tag{A-102}$$

or

$$Z_w^{(2)} = -C_z\, a\omega e^{\frac{2\pi z}{\lambda}} \left[\cos \omega t \int_s^b N_{zz}' \cos \frac{2\pi}{\lambda} (x \cos \beta + y \sin \beta)\, d\xi \right.$$

$$\left. + \sin \omega t \int_{\xi_s}^{\xi_b} N_{zz}' \sin \frac{2\pi}{\lambda} (x \cos \beta + y \sin \beta)\, d\xi \right] \qquad \text{(A-103)}$$

which becomes upon evaluation

$$\dot{Z}_w^{(2)} = -C_z\, a\omega e^{-\frac{2\pi \bar{h}}{\lambda}} \frac{\sin \frac{\pi B}{\lambda} \sin \beta}{\frac{\pi B}{\lambda} \sin \beta} \left[\cos \omega t \int_{\xi_s}^{\xi_b} N_{zz}' \cos \left(\frac{2\pi}{\lambda} x \cos \beta \right) d\xi \right.$$

$$\left. + \sin \omega t \int_{\xi_s}^{\xi_b} N_{zz}' \sin \left(\frac{2\pi}{\lambda} x \cos \beta \right) d\xi \right] \qquad \text{(A-104)}$$

The displacement force, $Z_w^{(3)}$, is due to the periodic buoyancy alterations of the barge as the wave passes along the hull, and is therefore proportional to the displacement of the water surface. Thus,

$$Z_w^{(3)} = \int_{\xi_s}^{\xi_b} \rho g B^* \eta (\xi, t)\, d\xi \qquad \text{(A-105)}$$

where B^* is the local section beam and $\eta (\xi, t)$ is the water surface elevation.

Since $\eta = a \left[\tanh (2\pi d/\lambda) \right] \sin (2\pi/\lambda) (x \cos \beta + y \sin \beta - c t)$

then

$$Z_w^{(3)} = \rho g a \left(\tanh \frac{2\pi d}{\lambda} \right) \left[\cos \omega t \int_{\xi_s}^{\xi_b} B^* \sin \frac{2\pi}{\lambda} (x \cos \beta + y \sin \beta)\, d\xi \right.$$

$$\left. - \sin \omega t \int_{\xi_s}^{\xi_b} B^* \cos \frac{2\pi}{\lambda} (x \cos \beta + y \sin \beta)\, d\xi \right] \qquad \text{(A-106)}$$

or after evaluation

$$Z_w^{(3)} = \rho g a \left(\tanh \frac{2\pi d}{\lambda}\right) \frac{\sin \frac{\pi B}{\lambda} \sin \beta}{\frac{\pi B}{\lambda} \sin \beta} \left[\cos \omega t \int_{\xi_s}^{\xi_b} B^* \sin \left(\frac{2\pi}{\lambda} x \cos \beta\right) d\xi \right.$$

$$\left. - \sin \omega t \int_{\xi_s}^{\xi_b} B^* \cos \left(\frac{2\pi}{\lambda} x \cos \beta\right) d\xi \right] \qquad \text{(A-107)}$$

The total heaving force, Z_w, is equal to the sum of $Z_w^{(1)}$, $Z_w^{(2)}$, and $Z_w^{(3)}$, or

$$Z_w = -\rho a \omega^2 e^{-\frac{2\pi \bar{h}}{\lambda}} \frac{\sin \frac{\pi B}{\lambda} \sin \beta}{\frac{\pi B}{\lambda} \sin \beta} \left[\cos \omega t \int_{\xi_s}^{\xi_b} \left(S + \frac{A_{33}'}{\rho}\right) \sin \left(\frac{2\pi}{\lambda} x \cos \beta\right) d\xi \right.$$

$$\left. - \sin \omega t \int_{\xi_s}^{\xi_b} \left(S + \frac{A_{33}'}{\rho}\right) \cos \left(\frac{2\pi}{\lambda} x \cos \beta\right) d\xi \right]$$

$$- C_z a \omega e^{-\frac{2\pi \bar{h}}{\lambda}} \frac{\sin \frac{\pi B}{\lambda} \sin \beta}{\frac{\pi B}{\lambda} \sin \beta} \left[\cos \omega t \int_{\xi_s}^{\xi_b} N_{zz}' \cos \left(\frac{2\pi}{\lambda} x \cos \beta\right) d\xi \right.$$

$$\left. + \sin \omega t \int_{\xi_s}^{\xi_b} N_{zz}' \sin \left(\frac{2\pi}{\lambda} x \cos \beta\right) d\xi \right]$$

$$+ \rho g a \tanh \frac{2\pi d}{\lambda} \frac{\sin \frac{\pi B}{\lambda} \sin \beta}{\frac{\pi B}{\lambda} \sin \beta} \left[\cos \omega t \int_{\xi_s}^{\xi_b} B^* \sin \left(\frac{2\pi}{\lambda} x \cos \beta\right) d\xi \right.$$

$$\left. - \sin \omega t \int_{\xi_s}^{\xi_b} B^* \cos \left(\frac{2\pi}{\lambda} x \cos \beta\right) d\xi \right] \qquad \text{(A-108)}$$

For head-on waves, $\beta = \pi$, $\cos\beta = -1$, $\sin\beta = 0$, and Equation A-108 becomes

$$Z_w = +\rho a \omega^2 e^{-\frac{2\pi\bar{h}}{\lambda}} \left[\cos\omega t \int_{\xi_s}^{\xi_b} \left(S + \frac{A_{33}'}{\rho} \right) \sin\left(\frac{2\pi}{\lambda} x\right) d\xi \right.$$

$$\left. + \sin\omega t \int_{\xi_s}^{\xi_b} \left(S + \frac{A_{33}'}{\rho} \right) \cos\left(\frac{2\pi}{\lambda} x\right) d\xi \right]$$

$$- C_z a \omega e^{-\frac{2\pi\bar{h}}{\lambda}} \left[\cos\omega t \int_{\xi_s}^{\xi_b} N_{zz}' \cos\left(\frac{2\pi}{\lambda} x\right) d\xi \right.$$

$$\left. - \sin\omega t \int_{\xi_s}^{\xi_b} N_{zz}' \sin\left(\frac{2\pi}{\lambda} x\right) d\xi \right]$$

$$- \rho g a \tanh\left(\frac{2\pi d}{\lambda}\right) \left[\cos\omega t \int_{\xi_s}^{\xi_b} B^* \sin\left(\frac{2\pi}{\lambda} x\right) d\xi \right.$$

$$\left. + \sin\omega t \int_{\xi_s}^{\xi_b} B^* \cos\left(\frac{2\pi}{\lambda} x\right) d\xi \right] \qquad \text{(A-109)}$$

For beam-on waves, $\beta = \pi/2$, $\cos\beta = 0$, $\sin\beta = 1$, and

$$Z_w = \rho a \omega^2 e^{-\frac{2\pi\bar{h}}{\lambda}} \frac{\sin\frac{\pi B}{\lambda}}{\frac{\pi B}{\lambda}} \sin\omega t \int_{\xi_s}^{\xi_b} \left(S + \frac{A_{33}'}{\rho} \right) d\xi$$

$$- C_z a \omega e^{-\frac{2\pi\bar{h}}{\lambda}} \frac{\sin\frac{\pi B}{\lambda}}{\frac{\pi B}{\lambda}} \cos\omega t \int_{\xi_s}^{\xi_b} N_{zz}' \, d\xi$$

$$- \rho g a \tanh\left(\frac{2\pi d}{\lambda}\right) \frac{\sin\frac{\pi B}{\lambda}}{\frac{\pi B}{\lambda}} \sin\omega t \int_{\xi_s}^{\xi_b} B^* \, d\xi \qquad \text{(A-110)}$$

Equations A-109 and A-110 are valid for both deep and shallow water waves.

Yaw, N_w

The wave-induced yaw moment, N_w, is readily obtained from the swaying force, Y_w, since

$$N_w = \int_{\xi_s}^{\xi_b} \xi \, dY_w \, d\xi \tag{A-111}$$

where ξ is the moment arm measured from the center of gravity. Thus, the general expression for the yaw moment, N_w, is

$$N_w = -\rho \omega^2 a e^{-\frac{2\pi\bar{h}}{\lambda}} \frac{\sin\frac{\pi B}{\lambda}\sin\beta}{\frac{\pi B}{\lambda}\sin\beta} \sin\beta \left[\cos\omega t \int_{\xi_s}^{\xi_b} \left(S + \frac{A_{22}'}{\rho} + \frac{2\pi A_{42}'}{\lambda\rho}\right)(\xi)\cos\left(\frac{2\pi}{\lambda} x \cos\beta\right) d\xi + \sin\omega t \int_{\xi_s}^{\xi_b} \left(S + \frac{A_{22}'}{\rho} + \frac{2\pi A_{42}'}{\lambda\rho}\right)(\xi)\sin\left(\frac{2\pi}{\lambda} x \cos\beta\right) d\xi\right] + C_y a \omega e^{-\frac{2\pi\bar{h}}{\lambda}} \cdot \frac{\sin\frac{\pi B}{\lambda}\sin\beta}{\frac{\pi B}{\lambda}\sin\beta} \sin\beta \left[\cos\omega t \int_{\xi_s}^{\xi_b} N_{yy}'(\xi)\cos\left(\frac{2\pi}{\lambda} x \cos\beta\right) d\xi - \sin\omega t \int_{\xi_s}^{\xi_b} N_{yy}'(\xi)\sin\left(\frac{2\pi}{\lambda} x \cos\beta\right) d\xi\right] \tag{A-112}$$

In the case of head-on waves, $\beta = \pi$, $\sin\beta = 0$, and Equation A-112 becomes

$$N_w = 0 . \tag{A-113}$$

In the case of beam-on waves, $\beta = \pi/2$, $\sin\beta = 1$, $\cos\beta = 0$, and Equation A-112 becomes

$$N_w = -\rho\omega^2 a e^{-\frac{2\pi\bar{h}}{\lambda}} \frac{\sin\frac{\pi B}{\lambda}}{\frac{\pi B}{\lambda}} \left[\cos\omega t \int_{\xi_s}^{\xi_b} \left(S + \frac{A_{22}'}{\rho} + \frac{2\pi A_{42}'}{\lambda\rho}\right)(\xi) \cos\left(\frac{2\pi}{\lambda} x\right) d\xi\right]$$

$$- C_y a\omega e^{-\frac{2\pi\bar{h}}{\lambda}} \frac{\sin\frac{\pi B}{\lambda}}{\frac{\pi B}{\lambda}} \left[\cos\omega t \int_{\xi_s}^{\xi_b} N_{yy}'(\xi)\, d\xi\right] \qquad \text{(A-114)}$$

Equations A-113 and A-114 are valid for both deep and shallow water.

Pitch, M_w

The wave-induced pitch moment, M_w, is readily obtained from the heaving force, Z_w, since

$$M_w = -\int_{\xi_s}^{\xi_b} \xi \cdot dZ_w\, d\xi \qquad \text{(A-115)}$$

where ξ is the moment arm measured from the center of gravity and the minus sign is necessary to preserve the right-hand notation. Thus, the general expression for the pitch moment is

$$M_w = +\rho a \omega^2 e^{-\frac{2\pi\bar{h}}{\lambda}} \frac{\sin\frac{\pi B}{\lambda}\sin\beta}{\frac{\pi B}{\lambda}\sin\beta} \left[\cos\omega t \int_{\xi_s}^{\xi_b} \left(S + \frac{A_{33}'}{\rho}\right)(\xi) \sin\left(\frac{2\pi}{\lambda} x \cos\beta\right) d\xi \right.$$

$$\left. - \sin\omega t \int_{\xi_s}^{\xi_b} \left(S + \frac{A_{33}'}{\rho}\right)(\xi) \cos\left(\frac{2\pi}{\lambda} x \cos\beta\right) d\xi \right]$$

$$+ C_z a \omega e^{-\frac{2\pi\bar{h}}{\lambda}} \frac{\sin\frac{\pi B}{\lambda}\sin\beta}{\frac{\pi B}{\lambda}\sin\beta} \left[\cos\omega t \int_{\xi_s}^{\xi_b} N_{zz}'(\xi) \cos\left(\frac{2\pi}{\lambda} x \cos\beta\right) d\xi \right.$$

$$\left. + \sin\omega t \int_{\xi_s}^{\xi_b} N_{zz}'(\xi) \sin\left(\frac{2\pi}{\lambda} x \cos\beta\right) d\xi \right]$$

$$- \rho g a \tanh\frac{2\pi d}{\lambda} \frac{\sin\frac{\pi B}{\lambda}\sin\beta}{\frac{\pi B}{\lambda}\sin\beta} \left[\cos\omega t \int_{\xi_s}^{\xi_b} B^*(\xi) \sin\left(\frac{2\pi}{\lambda} x \cos\beta\right) d\xi \right.$$

$$\left. - \sin\omega t \int_{\xi_s}^{\xi_b} B^*(\xi) \cos\left(\frac{2\pi}{\lambda} x \cos\beta\right) d\xi \right] \qquad \text{(A-116)}$$

For head-on waves, $\beta = \pi$, $\cos\beta = 1$, $\sin\beta = 0$, and the appropriate expression for the wave-induced pitch moment becomes

$$M_w = -\rho a \omega^2 e^{-\frac{2\pi\bar{h}}{\lambda}} \left[\cos\omega t \int_{\xi_s}^{\xi_b} \left(S + \frac{A_{33}'}{\rho} \right) (\xi) \sin\left(\frac{2\pi}{\lambda} x\right) d\xi \right.$$

$$\left. + \sin\omega t \int_{\xi_s}^{\xi_b} \left(S + \frac{A_{33}'}{\rho} \right) (\xi) \cos\left(\frac{2\pi}{\lambda} x\right) d\xi \right]$$

$$+ C_z a \omega e^{-\frac{2\pi\bar{h}}{\lambda}} \left[\cos\omega t \int_{\xi_s}^{\xi_b} N_{zz}'(\xi) \cos\left(\frac{2\pi x}{\lambda}\right) d\xi \right.$$

$$\left. - \sin\omega t \int_{\xi_s}^{\xi_b} N_{zz}'(\xi) \sin\left(\frac{2\pi x}{\lambda}\right) d\xi \right]$$

$$+ \rho g a \tanh\frac{2\pi d}{\lambda} \left[\cos\omega t \int_{\xi_s}^{\xi_b} B^*(\xi) \sin\left(\frac{2\pi}{\lambda} x\right) d\xi \right.$$

$$\left. + \sin\omega t \int_{\xi_s}^{\xi_b} B^*(\xi) \cos\left(\frac{2\pi}{\lambda} x\right) d\xi \right] \qquad \text{(A-117)}$$

For beam-on waves, $\beta = \pi/2$, $\cos\beta = 0$, and $\sin\beta = 1$, and Equation A-117 becomes

$$M_w = -\rho g a \omega^2 e^{-\frac{2\pi\bar{h}}{\lambda}} \frac{\sin\frac{\pi B}{\lambda}}{\frac{\pi B}{\lambda}} \left[\sin\omega t \int_{\xi_s}^{\xi_b} \left(S + \frac{A_{33}'}{\rho} \right) (\xi) d\xi \right]$$

$$+ C_z a \omega e^{-\frac{2\pi\bar{h}}{\lambda}} \frac{\sin\frac{\pi B}{\lambda}}{\frac{\pi B}{\lambda}} \left[\cos\omega t \int_{\xi_s}^{\xi_b} N_{zz}'(\xi) d\xi \right]$$

$$+ \rho g a \tanh\frac{2\pi d}{\lambda} \frac{\sin\frac{\pi B}{\lambda}}{\frac{\pi B}{\lambda}} \left[\sin\omega t \int_{\xi_s}^{\xi_b} B^*(\xi) d\xi \right] \qquad \text{(A-118)}$$

Equations A-116, A-117, and A-118 are valid in both deep and shallow water.

Roll, K_w

The roll moment, $K_o^{(1)}$, referring to the free surface level, is given by Hu (1961) and Kaplan and Putz (1962) as

$$K_{ow}^{(1)} = \int_{\xi_s}^{\xi_b} \left(-\rho S \bar{z}_{cb} + A_{42}' + A_{44}' \frac{2\pi}{\lambda}\right) \frac{D\bar{q}_{oy}}{Dt} d\xi \qquad \text{(A-119)}$$

where $\bar{z}_{cb}$ is the location of the center of buoyancy of each section ($\bar{z}_{cb} < 0$), and is measured from the free surface level; A_{42}' is the sectional added moment of inertia in roll due to motion in sway; A_{44}' is the sectional added moment of inertia in roll due to motion in roll.

Since damping in roll is known to be quite small, then $K_o^{(2)} = 0$. Hu also gives the roll moment, $K_o^{(3)}$, as

$$K_{ow}^{(3)} = \int_{\xi_s}^{\xi_b} \left[-\frac{\rho}{12} (B^*)^3 \frac{D\bar{q}_{oy}}{Dt}\right] d\xi \qquad \text{(A-120)}$$

Adding Equations A-119 and A-120 gives

$$K_{ow} = \int_{\xi_s}^{\xi_b} \left[-\rho S \bar{z}_{cb} - \frac{\rho}{12} (B^*)^3 + A_{42}' + \frac{2\pi}{\lambda} A_{44}'\right] \frac{D\bar{q}_{oy}}{Dt} d\xi \qquad \text{(A-121)}$$

Since Kaplan and Putz state that "the added moment of inertia in roll, A_{44}', is quite difficult to compute, and with little faith in the validity of such a result for motions of this type," an approximation is necessary to assist in the evaluation of the additional roll moment. Therefore, disregarding the term $(2\pi/\lambda)\, A_{44}'$ for the moment, the remaining terms are evaluated as

$$K_{ow}' = \int_{\xi_s}^{\xi_b} \left[A_{42}' - \rho\, S\, \bar{z}_{cb} - \frac{\rho}{12} (B^*)^3 \right] \frac{Dv}{Dt}\, d\xi$$

$$K_{ow}' = -a\,\omega^2\, e^{-\frac{2\pi\bar{h}}{\lambda}} \left(\frac{\sin \frac{\pi B}{\lambda} \sin\beta}{\frac{\pi B}{\lambda} \sin\beta} \right) \sin\beta \left\{ \cos\omega t \int_{\xi_s}^{\xi_b} \left[A_{42}' \right.\right.$$

$$\left. - \rho\, S\, \bar{z}_{cb} - \frac{\rho}{12} (B^*)^3 \right] \cos\left(\frac{2\pi}{\lambda} x \cos\beta \right) d\xi + \sin\omega t \int_{\xi_s}^{\xi_b} \left[A_{42}' \right.$$

$$\left. \left. - \rho\, S\, \bar{z}_{cb} - \frac{\rho}{12} (B^*)^3 \right] \sin\left(\frac{2\pi}{\lambda} x \cos\beta \right) d\xi \right\} \qquad \text{(A-122)}$$

Kaplan and Putz point out that the added moment of inertia, A_{44}', is actually that of the submerged part of the barge rolling about a point either at the free surface or at the mean half depth. They give an effective total added roll inertia of the form

$$K_{ow}'' = -\frac{A_{44}}{L}\, a\omega^2 \left(\frac{2\pi}{\lambda} \right) e^{-\frac{2\pi\bar{h}}{\lambda}} \frac{\sin\left(\frac{\pi B}{\lambda} \sin\beta \right)}{\frac{\pi B}{\lambda} \sin\beta} \sin\beta \left[\cos\omega t \int_{\xi_s}^{\xi_b} \cos\left(\frac{2\pi}{\lambda} x \cos\beta \right) d\xi \right.$$

$$\left. + \sin\omega t \int_{\xi_s}^{\xi_b} \sin\left(\frac{2\pi}{\lambda} x \cos\beta \right) d\xi \right] \qquad \text{(A-123)}$$

where L is the length of the barge and A_{44} is the added moment of inertia of the barge due to rotation about the center of gravity. If the waterline length ($|\xi_b| + |\xi_s|$) and barge length, L, are approximately equal, then Equation A-123 can be simplified to

$$K_{ow}'' = -A_{44}\, a\, \omega^2 \left(\frac{2\pi}{\lambda}\right) e^{-\frac{2\pi\bar{h}}{\lambda}} \frac{\sin\left(\frac{\pi B}{\lambda}\sin\beta\right)}{\frac{\pi B}{\lambda}\sin\beta} \sin\beta \cos\omega t \frac{\sin\left(\frac{\pi L}{\lambda}\cos\beta\right)}{\frac{\pi L}{\lambda}\cos\beta} \quad \text{(A-124)}$$

The total roll moment, K_{ow}, about the free surface is, therefore,

$$K_{ow} = K_{ow}' + K_{ow}'' \quad \text{(A-125)}$$

Referring the roll moment to the center of gravity results in

$$K_w = K_{ow} + \overline{OG}\, Y_w = K_{ow}' + K_{ow}'' + \overline{OG}\, Y_w \quad \text{(A-126)}$$

where $\overline{OG}$ is the moment arm from the center of gravity to the free surface. The general expression for the roll moment thus becomes

$$K_w = -\rho\, a\, \omega^2\, e^{-\frac{2\pi\bar{h}}{\lambda}} \left(\frac{\sin\frac{\pi B}{\lambda}\sin\beta}{\frac{\pi B}{\lambda}\sin\beta}\right) \sin\beta \left\{ \cos\omega t \int_{\xi_s}^{\xi_b} \left[\frac{A_{42}'}{\rho} - S\,\bar{z}_{cb} - \frac{(B^*)^3}{12}\right] \cos\left(\frac{2\pi}{\lambda} x \cos\beta\right) d\xi + \sin\omega t \int_{\xi_s}^{\xi_b} \left[\frac{A_{42}'}{\rho} - S\,\bar{z}_{cb} - \frac{(B^*)^3}{12}\right] \sin\left(\frac{2\pi}{\lambda} x \cos\beta\right) d\xi \right\} - \frac{A_{44}}{L}\, a\, \omega^2 \left(\frac{2\pi}{\lambda}\right) e^{-\frac{2\pi\bar{h}}{\lambda}} \cdot \left(\frac{\sin\frac{\pi B}{\lambda}\sin\beta}{\frac{\pi B}{\lambda}\sin\beta}\right) \sin\beta \left[\cos\omega t \int_{\xi_s}^{\xi_b} \cos\left(\frac{2\pi}{\lambda} x \cos\beta\right) d\xi + \sin\omega t \int_{\xi_s}^{\xi_b} \sin\left(\frac{2\pi}{\lambda} x \cos\beta\right) d\xi\right] + \overline{OG}\, Y_w \quad \text{(A-127)}$$

For head-on waves, $\beta = \pi$, $\sin\beta = 0$, and $K_w = 0$.

For beam-on waves, $\beta = \pi/2$, $\sin\beta = 1$, and $\cos\beta = 0$, and K_w becomes

$$K_w = -\rho a \omega^2 e^{-\frac{2\pi\bar{h}}{\lambda}} \left(\frac{\sin\frac{\pi B}{\lambda}}{\frac{\pi B}{\lambda}}\right) \left\{ \cos\omega t \int_{\xi_s}^{\xi_b} \left[\frac{A_{42}'}{\rho} - S\bar{z}_{cb} - \frac{(B^*)^3}{12} \right] d\xi \right\}$$

$$- \frac{A_{44}}{L} a\omega^2 \left(\frac{2\pi}{\lambda}\right) e^{-\frac{2\pi\bar{h}}{\lambda}} \left(\frac{\sin\frac{\pi B}{\lambda}}{\frac{\pi B}{\lambda}}\right) \left[\cos\omega t \int_{\xi_s}^{\xi_b} \cos\left(\frac{2\pi x}{\lambda}\right) d\xi \right]$$

$$- \overline{OG} \left\{ \rho\omega^2 a e^{-\frac{2\pi\bar{h}}{\lambda}} \left(\frac{\sin\frac{\pi B}{\lambda}}{\frac{\pi B}{\lambda}}\right) \left[\cos\omega t \int_{\xi_s}^{\xi_b} \left(S + \frac{A_{22}'}{\rho} + \frac{2\pi A_{42}'}{\lambda\rho} \right) d\xi \right] \right.$$

$$\left. - C_y a\omega e^{-\frac{2\pi\bar{h}}{\lambda}} \left(\frac{\sin\frac{\pi B}{\lambda}}{\frac{\pi B}{\lambda}}\right) \left(\sin\omega t \int_{\xi_s}^{\xi_b} N_{yy}' \, d\xi \right) \right\} \qquad \text{(A-128)}$$

Summary

The wave exciting forces and moments are seen to consist of expressions of the form

$$F_r^{\,w} \quad \text{or} \quad M_r^{\,w} = A_r^{\,w} \cos\omega t + B_r^{\,w} \sin\omega t \qquad \text{(A-129)}$$

for the rth motion which are frequency- and heading-dependent and assume a surface wave elevation η of $\eta\,(x, y, t) = a\cos\left[\omega t + \pi/2 - (2\pi/\lambda)(x\cos\beta + y\sin\beta)\right]$ where a is the wave amplitude and β is the angle between the x-direction and the direction of propagation of the waves. Assuming a unit amplitude (a = 1), the coefficients $A_r^{\,w}$ and $B_r^{\,w}$ of the general expressions are as follows:

Surge:

$$A_x^{\,w} = -\rho\omega^2 e^{-\frac{2\pi\bar{h}}{\lambda}} \left(\frac{\sin\left(\frac{\pi B}{\lambda}\sin\beta\right)}{\frac{\pi B}{\lambda}\sin\beta}\right) \cos\beta \int_{\xi_s}^{\xi_b} S\cos\left(\frac{2\pi}{\lambda} x\cos\beta\right) d\xi \qquad \text{(A-130)}$$

$$B_x^{\,w} = -\rho\omega^2 e^{-\frac{2\pi\bar{h}}{\lambda}} \left(\frac{\sin\frac{\pi B}{\lambda}\sin\beta}{\frac{\pi B}{\lambda}\sin\beta}\right) \cos\beta \int_{\xi_s}^{\xi_b} S\sin\left(\frac{2\pi}{\lambda} x\cos\beta\right) d\xi \qquad \text{(A-131)}$$

Sway:

$$A_y{}^w = -\rho\,\omega^2\, e^{-\frac{2\pi\bar{h}}{\lambda}} \left(\frac{\sin\frac{\pi B}{\lambda}\sin\beta}{\frac{\pi B}{\lambda}\sin\beta}\right) \sin\beta \int_{\xi_s}^{\xi_b} \left(S + \frac{A_{22}'}{\rho} + \frac{2\pi A_{42}'}{\lambda\rho}\right) \cos\left(\frac{2\pi}{\lambda} x \cos\beta\right) d\xi$$

$$+ C_y\,\omega\, e^{-\frac{2\pi\bar{h}}{\lambda}} \left(\frac{\sin\frac{\pi B}{\lambda}\sin\beta}{\frac{\pi B}{\lambda}\sin\beta}\right) \sin\beta \int N_{yy}' \sin\left(\frac{2\pi}{\lambda} x \cos\beta\right) d\xi \qquad \text{(A-132)}$$

$$B_y{}^w = -\rho\,\omega^2\, e^{-\frac{2\pi\bar{h}}{\lambda}} \left(\frac{\sin\frac{\pi B}{\lambda}\sin\beta}{\frac{\pi B}{\lambda}\sin\beta}\right) \sin\beta \int_{\xi_s}^{\xi_b} \left(S + \frac{A_{22}'}{\rho} + \frac{2\pi A_{42}'}{\lambda\rho}\right) \sin\left(\frac{2\pi}{\lambda} x \cos\beta\right) d\xi$$

$$- C_y\,\omega\, e^{-\frac{2\pi\bar{h}}{\lambda}} \left(\frac{\sin\frac{\pi B}{\lambda}\sin\beta}{\frac{\pi B}{\lambda}\sin\beta}\right) \sin\beta \int_{\xi_s}^{\xi_b} N_{yy}' \cos\left(\frac{2\pi}{\lambda} x \cos\beta\right) d\xi \qquad \text{(A-133)}$$

Heave:

$$A_z{}^w = -\rho\,\omega^2\, e^{-\frac{2\pi\bar{h}}{\lambda}} \left[\frac{\sin\left(\frac{\pi B}{\lambda}\sin\beta\right)}{\frac{\pi B}{\lambda}\sin\beta}\right] \int_{\xi_s}^{\xi_b} \left(S + \frac{A_{33}'}{\rho}\right) \sin\left(\frac{2\pi}{\lambda} x \cos\beta\right) d\xi$$

$$- C_z\,\omega\, e^{-\frac{2\pi\bar{h}}{\lambda}} \left[\frac{\sin\left(\frac{\pi B}{\lambda}\sin\beta\right)}{\frac{\pi B}{\lambda}\sin\beta}\right] \int_{\xi_s}^{\xi_b} N_{zz}' \cos\left(\frac{2\pi}{\lambda} x \cos\beta\right) d\xi$$

$$+ \rho g \tanh\frac{2\pi d}{\lambda} \left[\frac{\sin\left(\frac{\pi B}{\lambda}\sin\beta\right)}{\frac{\pi B}{\lambda}\sin\beta}\right] \int_{\xi_s}^{\xi_b} B^* \sin\left(\frac{2\pi}{\lambda} x \cos\beta\right) d\xi \qquad \text{(A-134)}$$

$$B_z^{\,w} = \rho\,\omega^2\, e^{-\frac{2\pi\bar{h}}{\lambda}}\left[\frac{\sin\left(\frac{\pi B}{\lambda}\sin\beta\right)}{\frac{\pi B}{\lambda}\sin\beta}\right]\int_{\xi_s}^{\xi_b}\left(S + \frac{A_{33}'}{\rho}\right)\cos\left(\frac{2\pi}{\lambda}\,x\cos\beta\right)\,d\xi$$

$$- C_z\,\omega\, e^{-\frac{2\pi\bar{h}}{\lambda}}\left[\frac{\sin\left(\frac{\pi B}{\lambda}\sin\beta\right)}{\frac{\pi B}{\lambda}\sin\beta}\right]\int_{\xi_s}^{\xi_b} N_{zz}'\sin\left(\frac{2\pi}{\lambda}\,x\cos\beta\right)\,d\xi$$

$$- \rho\,g\,\tanh\frac{2\pi d}{\lambda}\left[\frac{\sin\left(\frac{\pi B}{\lambda}\sin\beta\right)}{\frac{\pi B}{\lambda}\sin\beta}\right]\int_{\xi_s}^{\xi_b} B^*\cos\left(\frac{2\pi}{\lambda}\,x\cos\beta\right)\,d\xi \qquad \text{(A-135)}$$

Yaw:

$$A_\psi^{\,w} = -\rho\omega^2\, e^{-\frac{2\pi\bar{h}}{\lambda}}\left[\frac{\sin\left(\frac{\pi B}{\lambda}\sin\beta\right)}{\frac{\pi B}{\lambda}\sin\beta}\right]\sin\beta\int\left(S + \frac{A_{22}'}{\rho} + \frac{2\pi A_{42}'}{\lambda\rho}\right)(\xi)\cos\left(\frac{2\pi}{\lambda}\,x\cos\beta\right)\,d\xi$$

$$+ C_y\,\omega\, e^{-\frac{2\pi\bar{h}}{\lambda}}\left[\frac{\sin\left(\frac{\pi B}{\lambda}\sin\beta\right)}{\frac{\pi B}{\lambda}\sin\beta}\right]\sin\beta\int_{\xi_s}^{\xi_b} N_{yy}'(\xi)\cos\left(\frac{2\pi}{\lambda}\,x\cos\beta\right)\,d\xi \qquad \text{(A-136)}$$

$$B_\psi^{\,w} = -\rho\,\omega^2\, e^{-\frac{2\pi\bar{h}}{\lambda}}\left[\frac{\sin\left(\frac{\pi B}{\lambda}\sin\beta\right)}{\frac{\pi B}{\lambda}\sin\beta}\right]\sin\beta\int_{\xi_s}^{\xi_b}\left(S + \frac{A_{22}'}{\rho} + \frac{2\pi A_{42}'}{\lambda\rho}\right)(\xi)\sin\left(\frac{2\pi}{\lambda}\,x\cos\beta\right)d\xi$$

$$- C_y\,\omega\, e^{-\frac{2\pi\bar{h}}{\lambda}}\left[\frac{\sin\left(\frac{\pi B}{\lambda}\sin\beta\right)}{\frac{\pi B}{\lambda}\sin\beta}\right]\sin\beta\int_{\xi_s}^{\xi_b} N_{yy}'(\xi)\sin\left(\frac{2\pi}{\lambda}\,x\cos\beta\right)\,d\xi \qquad \text{(A-137)}$$

Pitch:

$$A_\theta{}^w = \rho\,\omega^2\, e^{-\frac{2\pi\bar{h}}{\lambda}}\left[\frac{\sin\left(\frac{\pi B}{\lambda}\sin\beta\right)}{\frac{\pi B}{\lambda}\sin\beta}\right]\int_{\xi_s}^{\xi_b}\left(S + \frac{A_{33}'}{\rho}\right)(\xi)\,\sin\left(\frac{2\pi}{\lambda}\,x\cos\beta\right)\,d\xi$$

$$+\ C_z\,\omega\, e^{-\frac{2\pi\bar{h}}{\lambda}}\left[\frac{\sin\left(\frac{\pi B}{\lambda}\sin\beta\right)}{\frac{\pi B}{\lambda}\sin\beta}\right]\int_{\xi_s}^{\xi_b} N_{zz}'\,(\xi)\,\cos\left(\frac{2\pi}{\lambda}\,x\cos\beta\right)\,d\xi$$

$$-\ \rho\,g\,\tanh\frac{2\pi d}{\lambda}\left[\frac{\sin\left(\frac{\pi B}{\lambda}\sin\beta\right)}{\frac{\pi B}{\lambda}\sin\beta}\right]\int_{\xi_s}^{\xi_b} B^*\,(\xi)\,\sin\left(\frac{2\pi}{\lambda}\,x\cos\beta\right)\,d\xi \qquad \text{(A-138)}$$

$$B_\theta{}^w = -\rho\,\omega^2\, e^{-\frac{2\pi\bar{h}}{\lambda}}\left[\frac{\sin\left(\frac{\pi B}{\lambda}\sin\beta\right)}{\frac{\pi B}{\lambda}\sin\beta}\right]\int_{\xi_s}^{\xi_b}\left(S + \frac{A_{33}'}{\rho}\right)(\xi)\,\cos\left(\frac{2\pi}{\lambda}\,x\cos\beta\right)\,d\xi$$

$$+\ C_z\,\omega\, e^{-\frac{2\pi\bar{h}}{\lambda}}\left[\frac{\sin\left(\frac{\pi B}{\lambda}\sin\beta\right)}{\frac{\pi B}{\lambda}\sin\beta}\right]\int_{\xi_s}^{\xi_b} N_{zz}'\,(\xi)\,\sin\left(\frac{2\pi}{\lambda}\,x\cos\beta\right)\,d\xi$$

$$+\ \rho\,g\,\tanh\frac{2\pi d}{\lambda}\left[\frac{\sin\left(\frac{\pi B}{\lambda}\sin\beta\right)}{\frac{\pi B}{\lambda}\sin\beta}\right]\int_{\xi_s}^{\xi_b} B^*\,(\xi)\,\cos\left(\frac{2\pi}{\lambda}\,x\cos\beta\right)\,d\xi \qquad \text{(A-139)}$$

Roll:

$$A_{\phi}{}^{w} = -\rho\omega^2 e^{-\frac{2\pi\bar{h}}{\lambda}}\left[\frac{\sin\left(\frac{\pi B}{\lambda}\sin\beta\right)}{\frac{\pi B}{\lambda}\sin\beta}\right]\sin\beta\int_{\xi_s}^{\xi_b}\left[\frac{A_{42}'}{\rho} - S\,\bar{z}_{cb} - \frac{(B^*)^3}{12}\right]\cos\left(\frac{2\pi}{\lambda}x\cos\beta\right)\,d\xi$$

$$- \frac{A_{44}}{L}\omega^2\left(\frac{2\pi}{\lambda}\right)e^{-\frac{2\pi\bar{h}}{\lambda}}\left[\frac{\sin\left(\frac{\pi B}{\lambda}\sin\beta\right)}{\frac{\pi B}{\lambda}\sin\beta}\right]\sin\beta\int_{\xi_s}^{\xi_b}\cos\left(\frac{2\pi}{\lambda}x\cos\beta\right)\,d\xi$$

$$- \overline{OG}\,\rho\omega^2 e^{-\frac{2\pi\bar{h}}{\lambda}}\left[\frac{\sin\left(\frac{\pi B}{\lambda}\sin\beta\right)}{\frac{\pi B}{\lambda}\sin\beta}\right]\sin\beta\int_{\xi_s}^{\xi_b}\left(S + \frac{A_{22}'}{\rho} + \frac{2\pi A_{42}'}{\lambda\rho}\right)\cos\left(\frac{2\pi}{\lambda}x\cos\beta\right)\,d\xi$$

$$+ \overline{OG}\,C_y\,\omega\, e^{-\frac{2\pi\bar{h}}{\lambda}}\left[\frac{\sin\left(\frac{\pi B}{\lambda}\sin\beta\right)}{\frac{\pi B}{\lambda}\sin\beta}\right]\sin\beta\int_{\xi_s}^{\xi_b}N_{yy}'\sin\left(\frac{2\pi}{\lambda}x\cos\beta\right)\,d\xi \qquad \text{(A-140)}$$

$$B_{\phi}{}^{w} = -\rho\omega^2 e^{-\frac{2\pi\bar{h}}{\lambda}}\left[\frac{\sin\left(\frac{\pi B}{\lambda}\sin\beta\right)}{\frac{\pi B}{\lambda}\sin\beta}\right]\sin\beta\int_{\xi_s}^{\xi_b}\left[\frac{A_{42}'}{\rho} - S\,\bar{z}_{cb} - \frac{(B^*)^3}{12}\right]\sin\left(\frac{2\pi}{\lambda}x\cos\beta\right)\,d\xi$$

$$- \frac{A_{44}}{L}\omega^2\left(\frac{2\pi}{\lambda}\right)e^{-\frac{2\pi\bar{h}}{\lambda}}\left[\frac{\sin\left(\frac{\pi B}{\lambda}\sin\beta\right)}{\frac{\pi B}{\lambda}\sin\beta}\right]\sin\beta\int_{\xi_s}^{\xi_b}\sin\left(\frac{2\pi}{\lambda}x\cos\beta\right)\,d\xi$$

$$- \overline{OG}\,\rho\omega^2 e^{-\frac{2\pi\bar{h}}{\lambda}}\left[\frac{\sin\left(\frac{\pi B}{\lambda}\sin\beta\right)}{\frac{\pi B}{\lambda}\sin\beta}\right]\sin\beta\int_{\xi_s}^{\xi_b}\left(S + \frac{A_{22}'}{\rho} + \frac{2\pi A_{42}'}{\lambda\rho}\right)\sin\left(\frac{2\pi}{\lambda}x\cos\beta\right)\,d\xi$$

$$- \overline{OG}\,C_y\,\omega\, e^{-\frac{2\pi\bar{h}}{\lambda}}\left[\frac{\sin\left(\frac{\pi B}{\lambda}\sin\beta\right)}{\frac{\pi B}{\lambda}\sin\beta}\right]\sin\beta\int_{\xi_s}^{\xi_b}N_{yy}'\cos\left(\frac{2\pi}{\lambda}x\cos\beta\right)\,d\xi \qquad \text{(A-141)}$$

SOLUTION OF THE EQUATIONS OF MOTION

The equations of motion are thus formulated as linear combinations of terms proportional to accelerations, terms proportional to velocities, terms proportional to displacements, and terms sinusoidal in time. The method of undertermined coefficients is employed to obtain solutions to the equations of motion. Specifically, it is assumed that since the exciting forces are sinusoidal, the responses (i.e., the motions) will also consist of sinusoidal oscillations of the same frequency, but not necessarily in phase.

Recall that the time history of the surface wave elevation is

$$\eta(x,\ y,\ t) = a\ \cos\left[\omega t + \frac{\pi}{2} - \frac{2\pi}{\lambda}\ (x\ \cos\beta\ + y\ \sin\beta)\right]$$

which reduces to

$$\eta = (0,\ 0,\ t) = \cos\left(\omega t + \frac{\pi}{2}\right)$$

when evaluated at the center of gravity of the barge. Next, the rth component of the (known) excitation force or moment which is of the form

$$F_r^{\ w} \quad \text{or} \quad M_r^{\ w} = A_r^{\ w} \cos\omega t + B_r^{\ w} \sin\omega t$$

can also be written as

$$F_r^{\ w} \quad \text{or} \quad M_r^{\ w} = \sqrt{\left(A_r^{\ w}\right)^2 + \left(B_r^{\ w}\right)^2}\ \cos\left(\omega t + \gamma_r\right)$$

where

$$\gamma_r = \tan^{-1}\left(-\frac{B_r^{\ w}}{A_r^{\ w}}\right)$$

Since the motions are also sinusoidal, they are assumed to have the form

$$r(t) = a_r \cos\left(\omega t + \frac{\pi}{2} + \delta_r\right)$$

where $r(t)$ represents any of the six motions. Since the exciting waves are assumed to have unit amplitude and phase angle $\pi/2$, a_r and δ_r are by definition the amplitude-response operator and phase-response operator, respectively. Thus, the problem is reduced to finding a_r and δ_r for each of the motions.

The procedure is to substitute into the equations of motion the assumed solution and their derivatives, and then to solve for the amplitude-response and phase-response operators. Introducing the complex notation

$$\overline{X}_w = \sqrt{\left(A_x^w\right)^2 + \left(B_x^w\right)^2}\ e^{i\gamma_x}, \quad \overline{Y}_w = \sqrt{\left(A_y^w\right)^2 + \left(B_y^w\right)^2}\ e^{i\gamma_y},$$

$$\overline{Z}_w = \sqrt{\left(A_z^w\right)^2 + \left(B_z^w\right)^2}\ e^{i\gamma_z}, \quad \overline{\phi}_w = \sqrt{\left(A_\phi^w\right)^2 + \left(B_\phi^w\right)^2}\ e^{i\gamma_\phi},$$

$$\overline{\Theta}_w = \sqrt{\left(A_\theta^w\right)^2 + \left(B_\theta^w\right)^2}\ e^{i\gamma_\theta}, \quad \overline{\Psi}_w = \sqrt{\left(A_\psi^w\right)^2 + \left(B_\psi^w\right)^2}\ e^{i\gamma_\psi},$$

$$\overline{x} = a_x e^{i\left(\delta_x + \frac{\pi}{2}\right)}, \qquad \overline{y} = a_y e^{i\left(\delta_y + \frac{\pi}{2}\right)}, \qquad \overline{z} = a_z e^{i\left(\delta_z + \frac{\pi}{2}\right)},$$

$$\overline{\phi} = a_\phi e^{i\left(\delta_\phi + \frac{\pi}{2}\right)}, \qquad \overline{\theta} = a_\theta e^{i\left(\delta_\theta + \frac{\pi}{2}\right)}, \qquad \overline{\psi} = a_\psi e^{i\left(\delta_\psi + \frac{\pi}{2}\right)}$$

so that

$$F_x^w(t) = \mathrm{Re}\left(\overline{X}_w e^{i\omega t}\right), \quad F_y^w(t) = \mathrm{Re}\left(\overline{Y}_w e^{i\omega t}\right), \quad F_z^w(t) = \mathrm{Re}\left(\overline{Z}_w e^{i\omega t}\right),$$

$$M_\phi^w(t) = \mathrm{Re}\left(\overline{\phi}_w e^{i\omega t}\right), \quad M_\theta^w(t) = \mathrm{Re}\left(\overline{\Theta}_w e^{i\omega t}\right), \quad M_\psi^w(t) = \mathrm{Re}\left(\overline{\Psi}_w e^{i\omega t}\right)$$

and similarly the assumed solutions are

$$x(t) = \mathrm{Re}\left(\overline{x} e^{i\omega t}\right), \quad y(t) = \mathrm{Re}\left(\overline{y} e^{i\omega t}\right), \quad z(t) = \mathrm{Re}\left(\overline{z} e^{i\omega t}\right),$$

$$\phi(t) = \mathrm{Re}\left(\overline{\phi} e^{i\omega t}\right), \quad \theta(t) = \mathrm{Re}\left(\overline{\theta} e^{i\omega t}\right), \quad \psi(t) = \mathrm{Re}\left(\overline{\psi} e^{i\omega t}\right)$$

Thus, the known real functions, F_x^w, F_y^w, F_z^w, M_ϕ^w, M_θ^w, and M_ψ^w, and the unknown real functions, x, y, z, ϕ, θ, and ψ, may be replaced by both real and imaginary parts of the complex functions, $\overline{X}_w e^{i\omega t}$, $\overline{Y}_w e^{i\omega t}$, $\overline{Z}_w e^{i\omega t}$, $\overline{\Phi}_w e^{i\omega t}$, $\overline{\Theta}_w e^{i\omega t}$, and $\overline{\Psi}_w e^{i\omega t}$. The reason for substituting the complex functions is that their first and second time derivatives are just equal to the functions themselves multiplied by $i\omega$ and $-\omega^2$, respectively. After making the substitutions and solving for the unknowns $\overline{x}$, $\overline{y}$, $\overline{z}$, $\overline{\phi}$, $\overline{\theta}$, and $\overline{\psi}$ (and thus for a_x, δ_x, a_y, δ_y, a_z, δ_z, a_ϕ, δ_ϕ, a_θ, δ_θ, a_ψ, δ_ψ), the correct final solution can be found by taking the real parts of $\overline{x} e^{i\omega t}$, $\overline{y} e^{i\omega t}$, $\overline{z} e^{i\omega t}$, $\overline{\phi} e^{i\omega t}$, $\overline{\theta} e^{i\omega t}$, and $\overline{\psi} e^{i\omega t}$. By substituting the assumed complex function solutions and their appropriate time derivatives, canceling the factor $e^{i\omega t}$, and transposing all reaction terms to the left-hand side, the equations of motion are reduced to

$$\overline{X}_w = -m\omega^2 \overline{x} + m|BG|\omega^2 \overline{\theta} + i\omega N_x \overline{x} + K_x \overline{x}$$

$$\overline{Y}_w = -m\omega^2 \overline{y} - \omega^2 \rho \int_{\xi_s}^{\xi_b} \frac{A_{22}'}{\rho} d\xi\, \overline{y} - \omega^2 \rho \int_{\xi_s}^{\xi_b} \frac{A_{22}'}{\rho} \xi\, d\xi\, \overline{\psi} - \omega^2 \rho \int_{\xi_s}^{\xi_b} \frac{A_{42}'}{\rho} d\xi\, \overline{\phi}$$

$$- \omega^2 |\overline{OG}| \rho \int_{\xi_s}^{\xi_b} \frac{A_{22}'}{\rho} d\xi\, \overline{\phi} + i\omega C_y N_y \overline{y} + i\omega N_{y\psi} \overline{\psi} + i\omega C_y N_y |BG| \overline{\phi} + k_y \overline{y}$$

$$\overline{Z}_w = -m\omega^2 \overline{z} - \omega^2 \rho \int_{\xi_s}^{\xi_b} \frac{A_{33}'}{\rho} d\xi\, \overline{z} + \omega^2 \rho \int_{\xi_s}^{\xi_b} \frac{A_{33}'}{\rho} \xi\, d\xi\, \overline{\theta} + i\omega C_z N_z \overline{z}$$

$$- i\omega N_{z\theta} \overline{\theta} + \rho g \int_{\xi_s}^{\xi_b} B^*\, d\xi\, \overline{z} - \rho g \int_{\xi_s}^{\xi_b} B^* \xi\, d\xi\, \overline{\theta}$$

$$\overline{\Phi}_w = -\omega^2 I_{xT} \overline{\phi} - \omega^2 \rho \int_{\xi_s}^{\xi_b} \frac{A_{42}'}{\rho} d\xi\, \overline{y} - \omega^2 (\overline{OG}) \rho \int_{\xi_s}^{\xi_b} \frac{A_{22}'}{\rho} d\xi\, \overline{y}$$

$$- \omega^2 \rho \int_{\xi_s}^{\xi_b} \frac{A_{42}'}{\rho} \xi\, d\xi\, \overline{\psi} - \omega^2 (\overline{OG}) \rho \int_{\xi_s}^{\xi_b} \frac{A_{22}'}{\rho} \xi\, d\xi\, \overline{\psi} + i\omega N_\phi \overline{\phi}$$

$$+ i\omega C_y N_y |BG| \overline{y} + i\omega N_{y\psi} |BG| \overline{\psi} + W|GM| \overline{\phi}$$

$$\overline{\Theta}_w = -\omega^2 I_y \overline{\theta} + \omega^2 \rho \int_{\xi_s}^{\xi_b} \frac{A_{33}'}{\rho} \xi \, d\xi \, \overline{z} - \omega^2 \rho \int_{\xi_s}^{\xi_b} \frac{A_{33}'}{\rho} \xi^2 \, d\xi \, \overline{\theta} + m |BG| \omega^2 \overline{x}$$

$$- i \omega N_{z\theta} \overline{z} + i \omega C_\theta N_\theta \overline{\theta} - \rho g \int_{\xi_s}^{\xi_b} B^* \xi \, d\xi \, \overline{z} + \rho g \int_{\xi_s}^{\xi_b} B^* \xi^2 \, d\xi \, \overline{\theta}$$

$$\overline{\Psi}_w = -\omega^2 I_z \overline{\psi} - \omega^2 \rho \int_{\xi_s}^{\xi_b} \frac{A_{22}'}{\rho} \xi \, d\xi \, \overline{y} - \omega^2 \rho \int_{\xi_s}^{\xi_b} \frac{A_{22}'}{\rho} \xi \, d\xi \, \overline{\psi} - \omega^2 \rho \int_{\xi_s}^{\xi_b} \frac{A_{42}'}{\rho} \xi \, d\xi \, \overline{\phi}$$

$$- \omega^2 (\overline{OG}) \rho \int_{\xi_s}^{\xi_b} \frac{A_{22}'}{\rho} \xi \, d\xi \, \overline{\phi} + i \omega N_{y\psi} \overline{y} + i \omega C_\psi N_\psi \overline{\psi} + i \omega N_{y\psi} |BG| \overline{\phi} + k_\psi \overline{\psi}$$

The complex equations are conveniently represented in matrix form as

$$\begin{pmatrix} a_{11} & a_{12} & a_{13} \\ a_{21} & a_{22} & a_{23} \\ a_{31} & a_{32} & a_{33} \end{pmatrix} \begin{pmatrix} \overline{x} \\ \overline{z} \\ \overline{\theta} \end{pmatrix} = \begin{pmatrix} \overline{X}_w \\ \overline{Z}_w \\ \overline{M}_w \end{pmatrix}$$

for longitudinal motions and

$$\begin{pmatrix} b_{11} & b_{12} & b_{13} \\ b_{21} & b_{22} & b_{23} \\ b_{31} & b_{32} & b_{33} \end{pmatrix} \begin{pmatrix} \overline{y} \\ \overline{\psi} \\ \overline{\phi} \end{pmatrix} = \begin{pmatrix} \overline{Y}_w \\ \overline{\Psi}_w \\ \overline{\Phi}_w \end{pmatrix}$$

for lateral motions, where the matrix elements are given by

$$a_{11} = \left(-m \omega^2 + k_x\right) + i \left(\omega N_x\right)$$

$$a_{12} = a_{21} = 0$$

$$a_{13} = a_{31} = \left(m\,|BG|\,\omega^2\right)$$

$$a_{22} = \left(-m\,\omega^2 - \omega^2\,\rho\int_{\xi_s}^{\xi_b}\frac{A_{33}'}{\rho}\,d\xi + \rho\,g\int_{\xi_s}^{\xi_b}B^*\,d\xi\right) + i\left(\omega\,C_z\,N_z\right)$$

$$a_{23} = a_{32} = \left(\omega^2\,\rho\int_{\xi_s}^{\xi_b}\frac{A_{33}'}{\rho}\,\xi\,d\xi - \rho\,g\int_{\xi_s}^{\xi_b}B^*\,\xi\,d\xi\right) + i\left(-\omega\,N_{z\theta}\right)$$

$$a_{33} = \left(-\omega^2\,I_y - \omega^2\,\rho\int_{\xi_s}^{\xi_b}\frac{A_{33}'}{\rho}\,\xi^2\,d\xi + \rho\,g\int_{\xi_s}^{\xi_b}B^*\,\xi^2\,d\xi\right) + i\left(\omega\,C_\theta\,N_\theta\right)$$

$$b_{11} = \left(-m\,\omega^2 - \omega^2\,\rho\int_{\xi_s}^{\xi_b}\frac{A_{22}'}{\rho}\,d\xi + k_y\right) + i\left(\omega\,C_y\,N_y\right)$$

$$b_{12} = b_{21}\left(\omega^2\,\rho\int_{\xi_s}^{\xi_b}\frac{A_{22}'}{\rho}\,\xi\,d\xi\right) + \left(i\,\omega\,N_{y\psi}\right)$$

$$b_{13} = b_{31}\left[-\omega^2\,\rho\int_{\xi_s}^{\xi_b}\frac{A_{42}'}{\rho}\,d\xi - \omega^2\,(\overline{OG})\,\rho\int_{\xi_s}^{\xi_b}\frac{A_{22}'}{\rho}\,d\xi\right] + i\left(\omega\,C_y\,N_y\,|BG|\right)$$

$$b_{22} = \left(-\omega^2\,I_z - \omega^2\,\rho\int_{\xi_s}^{\xi_b}\frac{A_{22}'}{\rho}\,\xi^2\,d\xi - k_\psi\right) + i\left(\omega\,C_\psi\,N_\psi\right)$$

$$b_{23} = b_{32} = \left[-\omega^2\,\rho\int_{\xi_s}^{\xi_b}\frac{A_{42}'}{\rho}\,\xi\,d\xi - \omega^2\,(\overline{OG})\,\rho\int_{\xi_s}^{\xi_b}\frac{A_{22}'}{\rho}\,\xi\,d\xi\right] + i\left(\omega\,N_{y\psi}\,|BG|\right)$$

$$b_{33} = \left(-\omega^2\,I_{xT} + W\,|GM|\right) + i\left(\omega\,N_\phi\right)$$

In solving for x, y, z, ϕ, θ, and ψ, it is convenient to multiply both sides by the appropriate inverse matrix. Thus, if (A) and (B) represent the longitudinal and lateral component matrices respectively, then $(A)^{-1}$ and $(B)^{-1}$ represent their corresponding inverse matrices. Finally, the equations may be represented in the form

$$\begin{pmatrix} \overline{x} \\ \overline{z} \\ \overline{\theta} \end{pmatrix} = (A)^{-1} \begin{pmatrix} \overline{X}_w \\ \overline{Z}_w \\ \overline{\Theta}_w \end{pmatrix}$$

and

$$\begin{pmatrix} \overline{y} \\ \overline{\psi} \\ \overline{\phi} \end{pmatrix} = (B)^{-1} \begin{pmatrix} \overline{Y}_w \\ \overline{\Psi}_w \\ \overline{\Phi}_w \end{pmatrix}$$

The inverse matrices are obtained by application of the well-known formula from matrix theory,

$$(A)^{-1} = \frac{\text{Adj (A)}}{\text{Det (A)}}$$

where Det (A) is the determinant of the matrix (A), and Adj (A) ("adjunct of (A)") is the matrix whose elements are the cofactors (i.e., the signed minors) of the elements of (A), but placed in transposed position.

In order to carry out the matrix multiplication indicated, it is convenient to express the known (complex) quantities $\overline{X}_w$, $\overline{Z}_w$, $\overline{\Theta}_w$, $\overline{Y}_w$, $\overline{\Psi}_w$, $\overline{\Phi}_w$ in the form (u - iv) instead of the form $\sqrt{\left(A_r^w\right)^2 + \left(B_r^w\right)^2}\ e^{i\gamma_r}$ in which they were defined. This is done by applying the identity

$$\sqrt{\left(A_r^w\right)^2 + \left(B_r^w\right)^2}\ e^{i\gamma_r} = \left(A_r^w\right) + i\left(-B_r^w\right)$$

which is easily proved from the trigonometric equivalent of $e^{i\gamma_r}$ and the definition of δ_r.

The results are thus obtained in the form (u - iv). They are easily converted to imaginary exponential form, from which the desired amplitude-response operators a_r and phase response operators δ_r are obtained. These quantities are functions of both frequency and wave propagation direction for the various motions. From the response operators, the various motions are given by the formula

$$r(t) = a_r \cos\left(\omega t + \frac{\pi}{2} + \delta_r\right)$$

for imposed exciting waves of unit amplitude and phase angle $\pi/2$. For waves of amplitude a_o and phase angle δ_n, the motions will be given by

$$r(t) = a_o a_r \cos\left(\omega t + \delta_n + \delta_r\right)$$

It may be seen that a positive δ_r means that the peak amplitude of the motion lags behind the peak amplitude of the surface water elevation, and conversely, a negative δ_r means that the peak amplitude of the motion leads the peak amplitude of the surface elevation.

Appendix B

SUMMARY OF COMPUTATIONS

EVALUATION OF SECTIONAL AND GEOMETRIC PROPERTIES

The method described in Appendix A contains a number of terms whose coefficients must be evaluated for the large beam-draft ratios of the immediate problem. Table B-1 presents a brief summary of the coefficients required for the determination of each term appearing in the matrix equations of Appendix A, under the main heading of Solutions of the Equations of Motion. Certain architectural characteristics of general interest are required, and these also appear in Table B-1. Thus, with the exception of the wave-exciting and environmental properties (i.e., wave direction, β; wave frequency, ω; wave length, λ; water depth, d; and mass density of sea water, ρ) and the mooring restoring forces fully discussed in Appendix A, Table B-1 summarizes all the coefficients required to obtain solutions to the equations formulated in Appendix A and hence required to predict motion of the barge and mooring forces in the lines.

Values of the architectural characteristics appear in Table B-2. With the exception of the roll damping coefficient, N_ϕ, and the added and total moments of inertia in roll, A_{44} and I_{xt}, these values were obtained from the design (as-built) plans, stability calculations, and field experiments prepared and/or conducted by the Long Beach Naval Shipyard. The total moment of inertia in roll, I_{xt}, was determined in the usual manner from the effective radius of gyration, k_e. The actual radius of gyration, k, was calculated to be 40.6 feet. The transverse metacentric height was known to be 180.0 feet, and the natural period in roll was measured as 6.1 seconds. Thus, applying the well-known formula applicable to normal ship forms,

$$T = \frac{2\pi k_e}{(g\,\overline{GM})^{1/2}} \tag{B-1}$$

k_e was found to be 73.9 feet. Although Equation B-1 is not strictly applicable to catamaran-shaped hulls, its use to determine added mass effects is believed to be justified. Once the effective radius of gyration is known, the total moment of inertia, I_{xt}, and the added moment of inertia in roll, A_{44}, are easily calculated.

Table B-1. Evaluation of Coefficients

Equation Term	Sectional Coefficient									Barge Coefficient				Architectural Characteristic								
	S	ξ	B*	Z_{c_b}	A_{22}'	A_{42}'	A_{33}'	N_{yy}'	N_{zz}	C_y	C_z	C_θ	C_ψ	A_{44}	$\overline{BG}$	$\overline{OG}$	I_z	I_y	I_{xt}	GM	W	N_ϕ
Longitudinal Matrix																						
a_{11}									X													
$a_{12} = a_{21}$																						
$a_{13} = a_{31}$																						
a_{22}			X				X		X		X											
$a_{23} = a_{32}$		X	X				X		X		X											
a_{33}			X				X					X						X				
Lateral Matrix																						
b_{11}					X			X		X												
$b_{12} = b_{21}$		X			X			X														
$b_{13} = b_{31}$					X	X		X		X					X	X						
b_{22}					X			X		X			X				X					
$b_{23} = b_{32}$					X	X		X							X	X						
b_{33}																			X	X	X	X
Excitation Term																						
x	X																					
y	X				X	X		X		X												
z	X	X							X		X											
θ	X		X		X	X		X			X											
ϕ	X	X	X						X	X												
ψ	X			X	X	X		X		X				X		X						

The roll damping coefficient, N_ϕ, appears as part of one of the coefficients in the uncoupled equation for damped harmonic oscillation, viz

$$\ddot{\phi} + 2\mu\omega_\phi\dot{\phi} + \omega_\phi{}^2\phi = 0 \qquad \text{(B-2)}$$

where ϕ is the roll amplitude, ω_ϕ is the circular frequency of free undamped oscillations, and μ is termed the dimensionless coefficient of decay. The coefficient of decay, μ, is the quantity which appears most frequently in the literature on roll extinction properties and thus is a convenient basis for comparison. It is related to the roll damping coefficient, N_ϕ, by the expression

$$\mu = \frac{N_\phi}{2I_{xt}\omega_\phi} \qquad \text{(B-3)}$$

where I_{xt} is the total moment of inertia in roll.

Table B-2. Architectural Characteristics of Fishhook Prototype Barge

Weight, W	1,870,000 lb
Mass, m	58.075×10^3 slugs
Mean half draft, $\overline{h}$	2.50 ft
Vertical distance from center of buoyancy to center of gravity, $\overline{BG}$	17.28 ft
Vertical distance from center of gravity to free surface, $\overline{OG}$	14.95 ft
Longitudinal metacentric height, GM_L	167.50 ft
Transverse metacentric height, GM_T	180.00 ft
Pitch moment of inertia, I_{y_o}	1.296×10^8 slugs-ft^2
Yaw moment of inertia, I_{z_o}	1.130×10^8 slugs-ft^2
Roll moment of inertia, I_{x_o}	9.590×10^7 slugs-ft^2
Total roll moment of inertia (including added inertia due to fluid), I_{xt}	3.160×10^8 slugs-ft^2
Roll damping coefficient, N_ϕ	1.28×10^8 lb-ft-sec
Added moment of inertia in roll, A_{44}	2.20×10^8 slugs-ft^2

Korvin-Kroukovsky (1961) gives a comprehensive discussion on methods of obtaining values of μ and solutions to Equation B-2 for normal ship forms. Empirical data on damping in roll is given by both Korvin-Kroukovsky and by Blagoveshchensky (1962). One simplified method of obtaining values of μ from model and/or prototype tests is the "logarithmic decrement" method widely employed in general vibratory problems. The logarithmic decrement is measured by the slope of log ϕ versus the number of cycles of oscillation.

Thus,

$$2\pi\mu = \delta = \log\left(\frac{\phi_1}{\phi_2}\right) \tag{B-4}$$

where δ is the logarithmic decrement, and ϕ_1 and ϕ_2 are the amplitudes of any two succeeding oscillations. Model tests on the Fishhook barge indicated a value of 0.15 for μ. This compares with a mean value of 0.08 reported by Korvin-Kroukovsky for ships with bilge keels with a range of fluctuation of 40 percent from the mean value. Blagoveshchensky shows that the value of μ is highly dependent upon the maximum amplitude of oscillation.

If the circular frequency in roll for the undamped case is now assumed to be 1.96 radians/second (i.e., calculated from radius of gyration, k = 40.6 feet), N_ϕ is found to be 1.28×10^8 pounds-foot-second.

The sectional geometric properties of cross-sectional area, S; moment arm, ξ; beam width, B^*; and center of buoyancy, $\overline{z}_{cb}$, were obtained from detailed ship plans and are shown in Table B-3. To aid in the preparation of the remaining sectional quantities for the range of frequency of interest, Table B-4, listing frequency factors, was prepared. Using Table B-4, one may proceed to tabulate the remaining sectional quantities.

Added Mass in Heave, A_{33}'

In the plane case, the hydrodynamic mass of a plate of width B* and normal dimension $\Delta\ell$, in an otherwise unlimited fluid, is

$$A_{33}' = \frac{\rho\pi(B^*)^2}{4}\Delta\ell \tag{B-5}$$

In proximity to a free surface, this quantity is known to require modification. For a unit normal dimension (i.e., $\Delta\ell = 1$), Grim (1959a) has computed the quantity C which is related to the hydrodynamic mass, A_{33}', by the expression

$$A_{33}' = \frac{C}{2}\,\frac{\rho\pi(B^*)^2}{4} \tag{B-6}$$

Table B-3. Geometric Characteristics at 1-Foot Intervals Along ξ Axis

Index	Moment Arm, ξ	Beam		Total Beam, B*	Draft		Cross-Sectional Area		Total Area, S	Sectional Coefficient	Center of Buoyancy
		Barge	Catamaran		Barge	Catamaran	Barge	Catamaran			
1	-48.40	68.00	NA	90.00	0.00	NA	0.00	NA	0.00	1.00	0.00
2	-47.50	68.00	↑	↑	0.69	↑	46.92	↑	46.92	↑	0.35
3	-46.50	↑	↑	↑	1.24	↑	84.32	↑	81.32	↑	0.62
4	-45.50	↑	↑	↑	1.98	↑	134.64	↑	134.64	↑	0.99
5	-44.50	↑	↑	↑	2.38	↑	161.84	↑	161.84	↑	1.19
6	-43.50	↑	↑	↑	3.04	↑	206.72	↑	206.72	↑	1.52
7	-42.50	↑	↑	↑	3.59	↑	244.12	↑	244.12	↑	1.80
8	-41.50	↑	↑	↑	4.14	↑	281.52	↑	281.52	↑	2.07
9	-40.50	↑	↑	↑	4.54	↑	308.72	↑	308.72	↑	2.27
10	-39.50	↑	↑	↑	4.73	↑	321.64	↑	321.64	↑	2.36
11	-38.50	↑	↑	↑	4.87	↑	331.16	↑	331.16	↑	2.43
12	-37.50	↑	↑	↑	4.93	↑	335.24	↑	335.24	↑	2.47
13	-36.50	↑	↑	↑	5.00	↑	340.00	↑	340.00	↑	2.50
to		↑	↑	↑	↑	↑	↑	↑	↑	↑	↑
50	0.00	↑	↑	↑	↑	↑	↑	↑	↑	↑	↑
to		↑	↑	↑	↑	↑	↑	↑	↑	↑	↑
62	+11.50	↑	↓	↑	↑	NA	↑	NA	↓	↑	↓
63	+12.50	↑	NA	↑	↑	0.00	↑	0.00	340.00	↑	2.50
64	+13.50	↑	22.00	↑	↑	0.14	↑	3.08	343.08	↑	2.48
65	+14.50	↑	↑	↑	↑	0.32	↑	7.04	347.04	↑	2.45
66	+15.50	↑	↑	↑	↑	0.49	↑	10.78	350.78	↑	2.43
67	+16.50	↑	↑	↑	↑	0.67	↑	14.74	354.74	↑	2.41
68	+17.50	↑	↑	↑	↑	0.84	↑	18.48	358.48	↑	2.39
69	+18.50	↑	↑	↑	↑	1.02	↑	22.44	362.44	↑	2.38
70	+19.50	↑	↑	↑	↑	1.19	↑	26.18	366.18	↑	2.37
71	+20.50	↑	↑	↑	↑	1.37	↑	30.14	370.14	↑	2.36
72	+21.40	↑	↑	↑	↑	1.54	↑	33.88	373.88	↑	2.35
73	+22.50	↑	↑	↑	↑	1.72	↑	37.84	377.84	↑	2.34
74	+23.50	↑	↑	↑	↑	1.89	↑	41.58	381.58	↑	2.33
75	+24.50	↑	↑	↑	↑	2.07	↑	45.54	385.54	↑	↑
76	+25.50	↑	↑	↑	↑	2.24	↑	49.28	389.28	↑	↑
77	+26.50	↑	↑	↑	↑	2.42	↑	53.24	393.24	↑	↑
78	+27.50	↑	↑	↑	↑	2.59	↑	56.98	396.98	↑	↑
79	+28.50	↑	↑	↑	↑	2.77	↑	60.94	400.94	↑	↑
80	+29.50	↑	↑	↑	↑	2.94	↑	64.68	404.68	↑	↑
81	+30.50	↑	↑	↑	↑	3.00	↑	66.00	406.00	↑	↑
82	+31.50	↑	↑	↑	↓	↑	↓	↑	406.00	↑	↓
83	+32.50	↑	↑	↑	5.00	↑	340.00	↑	406.00	↑	2.33
84	+33.50	↑	↑	↑	4.93	↑	335.24	↑	401.24	↑	2.30
85	+34.50	↑	↑	↑	4.74	↑	322.42	↑	388.32	↑	2.22
86	+35.50	↑	↑	↑	4.54	↑	308.72	↑	374.72	↑	2.16
87	+36.50	↑	↑	↑	4.22	↑	286.96	↑	352.96	↑	2.00
88	+37.50	↑	↑	↑	3.75	↑	254.80	↑	320.80	↑	1.77
89	+38.50	↑	↑	↑	2.98	↑	202.50	↑	268.50	↑	1.39
90	+39.50	↑	↑	↑	2.52	↓	171.63	↓	237.63	↑	1.33
91	+40.50	↑	↑	↑	1.79	3.00	121.59	66.00	187.59	↑	1.11
92	+41.50	↑	↑	↑	1.39	2.70	94.66	59.40	154.06	↑	0.95
93	+42.50	↑	↑	↑	0.34	2.40	22.78	52.30	75.58	1.00	0.89
94	+43.50	↑	↑	↑	0.10	2.14	6.67	47.08	53.75	0.28	0.95
95	+44.50	↑	↑	↑	0.00	1.90	0.00	41.80	41.80	1.00	0.95
96	+45.50	↓	↑	↓	↑	1.64	↑	36.08	36.08	↑	0.82
97	+46.50	68.00	↑	90.00	↑	1.38	↑	30.36	30.36	↑	0.69
98	+47.50	67.81	↑	89.81	↑	1.12	↑	24.64	24.64	↑	0.56
99	+48.50	67.32	↑	89.32	↑	0.86	↑	18.92	18.92	↑	0.43
100	+49.50	66.31	↑	88.31	↑	0.60	↑	13.20	13.20	↑	0.30
101	+50.50	64.68	↑	86.68	↑	0.34	↑	7.48	7.48	↑	0.17
102	+51.50	62.07	↓	84.07	↓	0.06	↓	1.32	1.32	↓	0.03
103	+52.36	58.00	22.00	80.--	0.00	0.00	0.00	0.00	0.00	1.00	0.00

Table B-4. Frequency Factor, $\omega^2 B_b/2g$ or $\omega^2 B_c^*/2g$, at 1-Foot Intervals Along ξ Axis

Index	$\frac{B^*}{H}$	Frequency Factor Wave Length, λ (ft) Wave Frequency, ω (rad/sec) ω^2							
		25 2.84 8.08	50 2.01 4.04	75 1.64 2.69	100 1.42 2.02	150 1.16 1.35	250 0.90 0.81	350 0.76 0.57	450 0.66 0.44
1	6.8	4.26	2.14	1.42	1.17	0.71	0.43	0.30	0.24
2	↑	↑	↑	↑	↑	↑	↑	↑	↑
3	↑	↑	↑	↑	↑	↑	↑	↑	↑
4	↑	↑	↑	↑	↑	↑	↑	↑	↑
5	↑	↑	↑	↑	↑	↑	↑	↑	↑
6	↑	↑	↑	↑	↑	↑	↑	↑	↑
7	↑	↑	↑	↑	↑	↑	↑	↑	↑
8	↑	↑	↑	↑	↑	↑	↑	↑	↑
9	↑	↑	↑	↑	↑	↑	↑	↑	↑
10	↑	↑	↑	↑	↑	↑	↑	↑	↑
11	↑	↑	↑	↑	↑	↑	↑	↑	↑
12	↑	↑	↑	↑	↑	↑	↑	↑	↑
13	↑	↑	↑	↑	↑	↑	↑	↑	↑
to	↑	↑	↑	↑	↑	↑	↑	↑	↑
50	↑	↑	↑	↑	↑	↑	↑	↑	↑
to	↑	↑	↑	↑	↑	↑	↑	↑	↑
62	↑	↑	↑	↑	↑	↑	↑	↑	↑
63	6.8	4.26	2.14	1.42	1.17	0.71	0.43	0.30	0.24
64	18.0	11.30	5.65	3.76	2.82	1.89	1.13	0.80	0.62
65	↑	↑	↑	↑	↑	↑	↑	↑	↑
66	↑	↑	↑	↑	↑	↑	↑	↑	↑
67	↑	↑	↑	↑	↑	↑	↑	↑	↑
68	↑	↑	↑	↑	↑	↑	↑	↑	↑
69	↑	↑	↑	↑	↑	↑	↑	↑	↑
70	↑	↑	↑	↑	↑	↑	↑	↑	↑
71	↑	↑	↑	↑	↑	↑	↑	↑	↑
72	↑	↑	↑	↑	↑	↑	↑	↑	↑
73	↑	↑	↑	↑	↑	↑	↑	↑	↑
74	↑	↑	↑	↑	↑	↑	↑	↑	↑
75	↑	↑	↑	↑	↑	↑	↑	↑	↑
76	↑	↑	↑	↑	↑	↑	↑	↑	↑
77	↑	↑	↑	↑	↑	↑	↑	↑	↑
78	↑	↑	↑	↑	↑	↑	↑	↑	↑
79	↑	↑	↑	↑	↑	↑	↑	↑	↑
80	↑	↑	↑	↑	↑	↑	↑	↑	↑
81	↑	↑	↑	↑	↑	↑	↑	↑	↑
82	↓	↓	↓	↓	↓	↓	↓	↓	↓
83	18.0								
84	18.3								
85	19.0								
86	19.8								
87	21.3								
88	24.0								
89	30.0								
90	30.0								
91	30.0								
92	33.3								
93	37.5								
94	42.0	11.30	5.65	3.76	2.82	1.89	1.13	0.80	0.62
95	11.6	2.76	1.38	0.92	0.69	0.46	0.27	0.20	0.15
96	13.4	↑	↑	↑	↑	↑	↑	↑	↑
97	15.9	↑	↑	↑	↑	↑	↑	↑	↑
98	19.6	↑	↑	↑	↑	↑	↑	↑	↑
99	25.6	↑	↑	↑	↑	↑	↑	↑	↑
100	36.7	↑	↑	↑	↑	↑	↑	↑	↑
101	64.5	↑	↑	↑	↑	↑	↑	↑	↑
102	367.0	↓	↓	↓	↓	↓	↓	↓	↓
103	—	2.76	1.38	0.92	0.69	0.46	0.27	0.20	0.15

Thus, C, which is frequency-dependent, includes an improved evaluation of the free surface effect. Grim's computations were performed for cross-sectional profiles that could be represented by Lewis' transformation formula (i.e., $z = \xi + a\xi^{-1} + b\xi^{-3}$). His results are presented in graphs of varying sectional area coefficients as functions of the beam-draft ratios and frequency factors. An example is shown in Figure B-1.

In order to use Grim's results for the large beam-draft ratios of the immediate problem, a suitable extrapolation was required. For this purpose, Figure B-2 was prepared from Figure B-1 with the aid of an auxiliary logarithmic plot. The solid lines of Figure B-2 indicate that these values were obtained directly from Grim's results. The dashed lines indicate an extrapolation. Note that the ordinates and abscissas of Figure B-2 are given in terms of CH/B^* and $\omega^2 H/g$, respectively.

Values of the hydrodynamic mass coefficient, C, appearing in Table B-5, were obtained from Figure B-2. Table B-6 indicates values of the hydrodynamic mass, A_{33}'. Tables B-6a and B-6b present values of the terms $A_{33}'\xi^2$ and $A_{33}\xi^2$, respectively. These tabulations and their integrals will be used later to compute the matrix elements indicated by Table B-1.

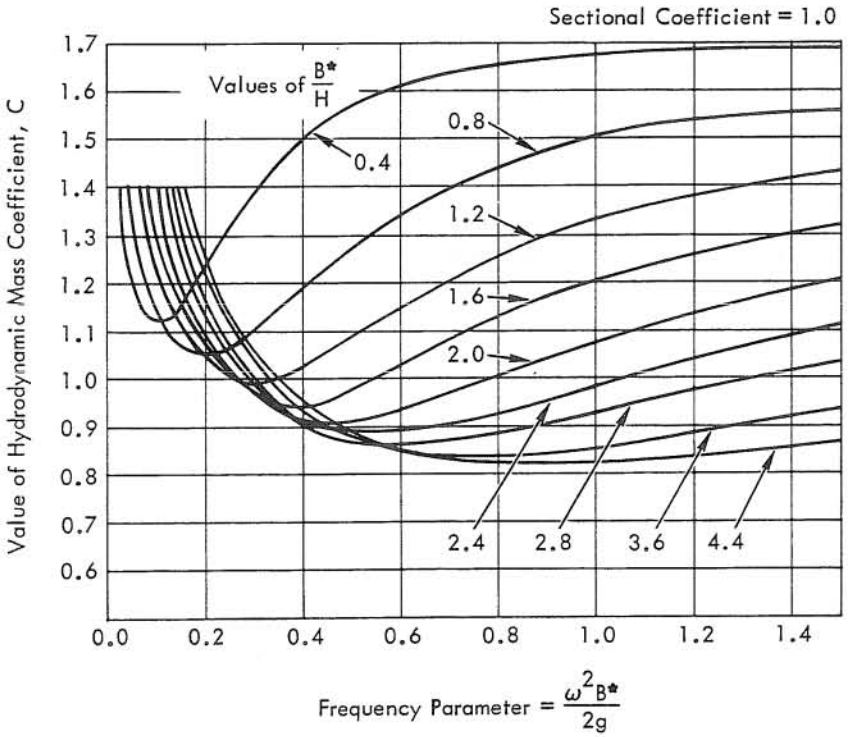

Figure B-1. Hydrodynamic mass coefficient, C, for heaving motion. (From Grim, 1959a.)

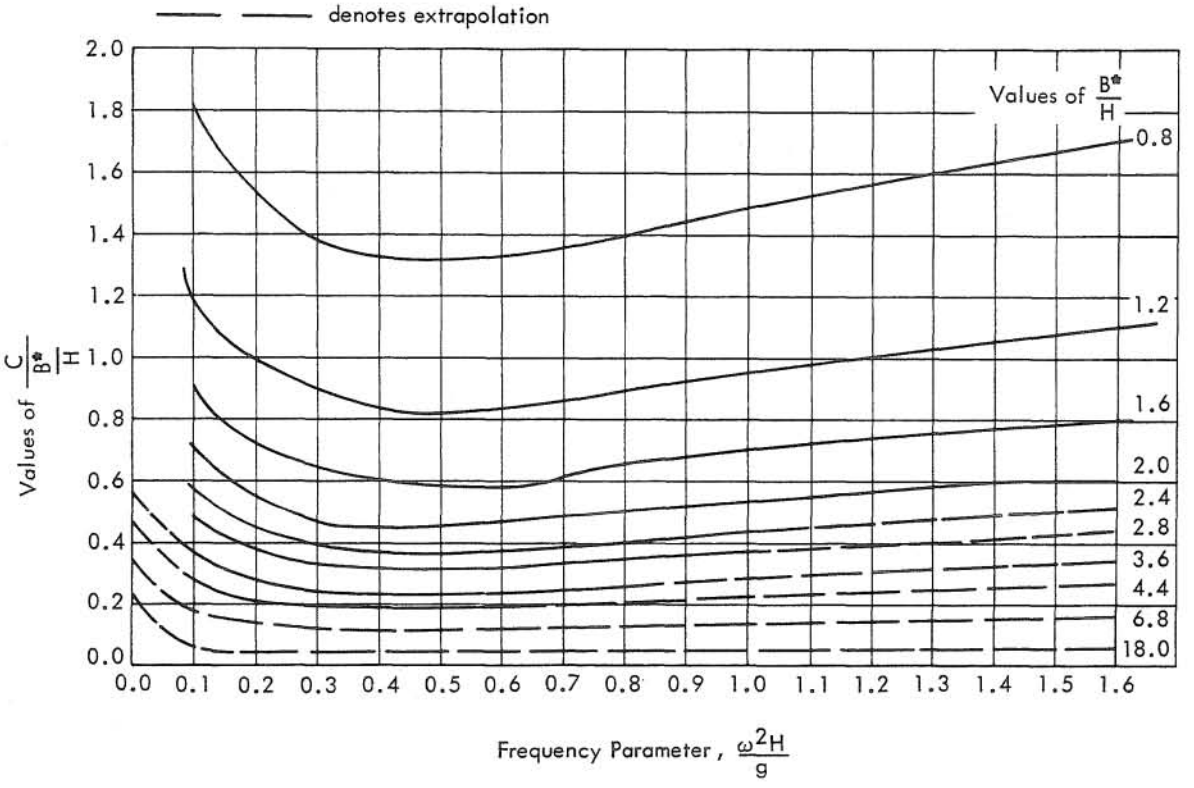

Figure B-2. Extrapolation of Grim's hydrodynamic mass coefficient, C (Grim, 1959a), for large beam-draft ratios.

Table B-5. Values of C at 1-Foot Intervals Along ξ Axis

Index	Wave Length, λ (ft)							
	25	50	75	100	150	250	350	450
1 to 63	1.02	0.82	0.75	0.82	0.88	1.09	1.29	1.50
64 to 82	1.08	0.90	0.72	0.72	0.72	0.90	1.26	1.62
83	1.08	0.90	0.72	0.72	0.72	0.90	1.26	1.62
84	1.10	0.92	0.73	0.73	0.73	0.92	1.28	1.65
85	1.14	0.95	0.76	0.76	0.76	0.95	1.33	1.70
86	1.19	0.99	0.79	0.79	0.79	0.99	1.38	1.78
87	1.26	1.06	0.85	0.85	0.85	1.06	1.49	1.92
88	1.20	0.96	0.96	0.96	0.96	1.20	1.44	1.92
89	1.20	1.20	1.20	1.20	1.20	1.50	1.56	1.94
90	1.20	1.20	1.20	1.20	1.20	1.50	1.68	1.96
91	1.20	1.20	1.20	1.20	1.20	1.50	1.80	2.00
92	1.33	1.33	1.33	1.33	1.33	1.66	1.92	2.00
93	1.50	1.50	1.50	1.50	1.50	1.88	2.00	2.00
94	1.30	1.30	1.30	1.30	1.74	1.93	2.00	2.00
95	0.81	1.05	1.05	1.28	1.61	1.97	2.00	2.00
96	0.94	1.21	1.21	1.47	1.87	2.00	2.00	1.98
97	0.95	1.11	1.11	1.25	1.43	1.75	1.80	1.86
98	1.16	0.98	0.79	0.79	0.79	0.98	1.37	1.76
99	0.86	0.73	0.59	0.59	0.59	0.73	1.00	1.26
100	0.56	0.48	0.39	0.39	0.39	0.48	0.65	0.86
101	0.26	0.23	0.19	0.19	0.19	0.23	0.30	0.46
102	0.00	0.00	0.00	0.00	0.00	0.00	0.00	0.00
103	0.00	0.00	0.00	0.00	0.00	0.00	0.00	0.00

Table B-6. Values of A_{33}' at 1-Foot Intervals Along ξ Axis

Index	Total Beam, B	B/2	πB²/8	Wave Length, λ (ft) 25	50	75	100	150	250	350	450
1	90.00	8.1000x10³	6.1709x10³	6.2943x10³	5.0601x10³	4.6282x10³	5.0601x10³	5.4304x10³	6.7263x10³	7.9605x10³	9.2564x10³
2	↓	↓	↓	↓	↓	↓	↓	↓	↓	↓	↓
3											
4											
5											
6											
7											
8											
9											
10											
11											
12											
13											
14											
15											
16											
17											
18											
19	↓	↓	↓	↓	↓	↓	↓	↓	↓	↓	↓
20	90.00	8.1000x10³	6.1709x10³	6.2943x10³	5.0601x10³	4.6282x10³	5.0601x10³	5.4304x10³	6.7263x10³	7.9605x10³	9.2564x10³
21	90.00	8.1000x10³	6.1709x10³	6.2943x10³	5.0601x10³	4.6282x10³	5.0601x10³	5.0304x10³	6.7263x10³	7.9605x10³	9.2564x10³
22	↓	↓	↓	↓	↓	↓	↓	↓	↓	↓	↓
23											
24											
25											
26											
27											
28											
29											
30											
31											
32											
33											
34											
35											
36											
37											
38											
39	↓	↓	↓	↓	↓	↓	↓	↓	↓	↓	↓
40	90.00	8.1000x10³	6.1709x10³	6.2943x10³	5.0601x10³	4.6282x10³	5.0601x10³	5.0304x10³	6.7263x10³	7.9605x10³	9.2564x10³
41	90.00	8.1000x10³	6.1709x10³	6.2943x10³	5.0601x10³	4.6282x10³	5.0601x10³	5.0304x10³	6.7263x10³	7.9605x10³	9.2564x10³
42	↓	↓	↓	↓	↓	↓	↓	↓	↓	↓	↓
43											
44											
45											
46											
47											
48											
49											
50											
51											
52											
53											
54											
55											

60	90.00	8.1000×10^{3}	6.1709×10^{3}	6.2948×10^{3}	5.0601×10^{3}	4.6282×10^{3}	5.0601×10^{3}	5.0304×10^{3}	6.7263×10^{3}	7.9605×10^{3}	9.2568×10^{3}		
61	90.00	8.1000×10^{3}	6.1709×10^{3}	6.2948×10^{3}	5.0601×10^{3}	4.6282×10^{3}	5.0601×10^{3}	5.4304×10^{3}	6.7263×10^{3}	7.9605×10^{3}	9.2568×10^{3}		
62				6.2948×10^{3}	5.0601×10^{3}	4.6282×10^{3}	5.0601×10^{3}	5.4304×10^{3}	6.7263×10^{3}	7.9605×10^{3}	9.2568×10^{3}		
63				6.2948×10^{3}	5.0601×10^{3}	4.6282×10^{3}	5.0601×10^{3}	5.4304×10^{3}	6.7263×10^{3}	7.9605×10^{3}	9.2568×10^{3}		
64				6.6646×10^{3}	5.5538×10^{3}	4.4430×10^{3}	4.4430×10^{3}	4.4430×10^{3}	5.5538×10^{3}	7.7753×10^{3}	9.9969×10^{3}		
65													
66													
67													
68													
69													
70													
71													
72													
73													
74													
75													
76													
77													
78													
79													
80	90.00	8.1000×10^{3}	6.1709×10^{3}	6.6646×10^{3}	5.5538×10^{3}	4.4430×10^{3}	4.4430×10^{3}	4.4430×10^{3}	5.5538×10^{3}	7.7753×10^{3}	9.9969×10^{3}		
81	90.00	8.1000×10^{3}	6.1709×10^{3}	6.6646×10^{3}	5.5538×10^{3}	4.4430×10^{3}	4.4430×10^{3}	4.4430×10^{3}	5.5538×10^{3}	7.7753×10^{3}	9.9969×10^{3}		
82				6.6646×10^{3}	5.5538×10^{3}	4.4430×10^{3}	4.4430×10^{3}	4.4430×10^{3}	5.5538×10^{3}	7.7753×10^{3}	9.9969×10^{3}		
83				6.6646×10^{3}	5.5538×10^{3}	4.4430×10^{3}	4.4430×10^{3}	4.4430×10^{3}	5.5538×10^{3}	7.7753×10^{3}	9.9969×10^{3}		
84				6.7880×10^{3}	5.4772×10^{3}	4.5048×10^{3}	4.5048×10^{3}	4.5048×10^{3}	5.4772×10^{3}	7.8988×10^{3}	1.0182×10^{4}		
85				7.0348×10^{3}	5.4624×10^{3}	4.6899×10^{3}	4.6899×10^{3}	4.6899×10^{3}	5.4624×10^{3}	8.2073×10^{3}	1.0491×10^{4}		
86				7.3934×10^{3}	6.1092×10^{3}	4.8750×10^{3}	4.8750×10^{3}	4.8750×10^{3}	6.1092×10^{3}	8.5158×10^{3}	1.0984×10^{4}		
87				7.7753×10^{3}	6.5412×10^{3}	5.2453×10^{3}	5.2453×10^{3}	5.2453×10^{3}	6.5412×10^{3}	9.1996×10^{3}	1.1848×10^{4}		
88				7.4051×10^{3}	5.9241×10^{3}	5.9241×10^{3}	5.9241×10^{3}	5.9241×10^{3}	7.4051×10^{3}	8.8861×10^{3}	1.1848×10^{4}		
89				7.4051×10^{3}	7.4051×10^{3}	7.4051×10^{3}	7.4051×10^{3}	7.4051×10^{3}	9.2564×10^{3}	9.4266×10^{3}	1.1977×10^{4}		
90				7.4051×10^{3}	7.4051×10^{3}	7.4051×10^{3}	7.4051×10^{3}	7.4051×10^{3}	9.2564×10^{3}	1.0367×10^{4}	1.2095×10^{4}		
91				7.4051×10^{3}	7.4051×10^{3}	7.4051×10^{3}	7.4051×10^{3}	7.4051×10^{3}	9.2564×10^{3}	1.1108×10^{4}	1.2342×10^{4}		
92				8.2073×10^{3}	8.2073×10^{3}	8.2073×10^{3}	8.2073×10^{3}	8.2073×10^{3}	1.0294×10^{4}	1.1848×10^{4}	1.2342×10^{4}		
93				9.2564×10^{3}	9.2564×10^{3}	9.2564×10^{3}	9.2564×10^{3}	9.2564×10^{3}	1.1601×10^{4}	1.2342×10^{4}	1.2342×10^{4}		
94				8.0222×10^{3}	8.0222×10^{3}	8.0222×10^{3}	8.0222×10^{3}	1.0782×10^{4}	1.1910×10^{4}	1.2342×10^{4}	1.2342×10^{4}		
95				6.9984×10^{3}	6.9794×10^{3}	6.9794×10^{3}	7.8988×10^{3}	9.9351×10^{3}	1.2157×10^{4}	1.2342×10^{4}	1.2342×10^{4}		
96				5.8006×10^{3}	7.4668×10^{3}	7.4668×10^{3}	9.0712×10^{3}	1.1540×10^{4}	1.2342×10^{4}	1.2342×10^{4}	1.2218×10^{4}		
97	90.00	8.1000×10^{3}	6.1709×10^{3}	5.8624×10^{3}	6.8997×10^{3}	6.8997×10^{3}	7.7134×10^{3}	8.8244×10^{3}	1.0799×10^{4}	1.1103×10^{4}	1.1478×10^{4}		
98	89.81	8.0658×10^{3}	6.1448×10^{3}	7.1280×10^{3}	6.0219×10^{3}	4.8544×10^{3}	4.8544×10^{3}	4.8544×10^{3}	6.0219×10^{3}	8.4184×10^{3}	1.0815×10^{4}		
99	89.32	7.9781×10^{3}	6.0780×10^{3}	5.2271×10^{3}	4.4369×10^{3}	3.5860×10^{3}	3.5860×10^{3}	3.5860×10^{3}	4.4369×10^{3}	6.0780×10^{3}	7.6583×10^{3}		
100	88.31	7.7987×10^{3}	5.9413×10^{3}	3.3271×10^{3}	2.8512×10^{3}	2.3171×10^{3}	2.3171×10^{3}	2.3171×10^{3}	2.8512×10^{3}	3.8618×10^{3}	5.1095×10^{3}		
101	86.68	7.5134×10^{3}	5.7240×10^{3}	1.4882×10^{3}	1.3165×10^{3}	1.0877×10^{3}	1.0877×10^{3}	1.0877×10^{3}	1.3165×10^{3}	1.7172×10^{3}	2.2330×10^{3}		
102	84.07	7.0678×10^{3}	5.3845×10^{3}	0.0000	0.0000	0.0000	0.0000	0.0000	0.0000	0.0000	0.0000		
103	80.00	6.4800×10^{3}	4.8758×10^{3}	0.0000	0.0000	0.0000	0.0000	0.0000	0.0000	0.0000	0.0000		
$\sum A_{83}\,d_i^2$				6.4645×10^{5}	5.4209×10^{5}	4.9609×10^{5}	5.1611×10^{5}	5.4969×10^{5}	6.7653×10^{5}	8.2163×10^{5}	9.7228×10^{5}		

$\pi\rho\,(B^*)^2 = 9.75666987\times10^{4}$

Table B-6a. Values of $A_{33}'\xi$ at 1-Foot Intervals Along ξ Axis

Index	Abscissa ξ, ft	Wave Length, λ, (ft)							
		25	50	75	100	150	200	300	400
1	-48.50	-3.0044x10^5	-2.6491x10^5	-2.2400x10^5	-2.0881x10^5	-2.0428x10^5	-2.0555x10^5	-2.1559x10^5	-1.9801x10^5
2	-47.50	-2.8998x10^5	-2.8055x10^5	-2.7984x10^5	-2.9035x10^5	-2.9794x10^5	-3.0930x10^5	-3.2812x10^5	-3.3768x10^5
3	-46.50	-2.9248x10^5	-2.9529x10^5	-3.0321x10^5	-3.0529x10^5	-3.0725x10^5	-3.1207x10^5	-3.2098x10^5	-3.3042x10^5
4	-45.50	-2.8349x10^5	-2.8023x10^5	-2.8052x10^5	-2.8285x10^5	-2.8708x10^5	-2.9065x10^5	-2.9620x10^5	-3.0117x10^5
5	-44.50	-2.8010x10^5	-2.8007x10^5	-2.8098x10^5	-2.8317x10^5	-2.8705x10^5	-2.8992x10^5	-2.9428x10^5	-2.9791x10^5
6	-43.50	-2.8388x10^5	-2.8701x10^5	-2.9033x10^5	-2.9201x10^5	-2.9522x10^5	-2.9859x10^5	-3.0428x10^5	-3.0965x10^5
7	-42.50	-2.6751x10^5	-2.7505x10^5	-2.8480x10^5	-2.9504x10^5	-3.0078x10^5	-3.0677x10^5	-3.1731x10^5	-3.2840x10^5
8	-41.50	-2.6121x10^5	-2.6999x10^5	-2.8207x10^5	-2.9098x10^5	-2.9853x10^5	-3.0418x10^5	-3.1240x10^5	-3.2488x10^5
9	-40.50	-2.5482x10^5	-2.6049x10^5	-2.7446x10^5	-2.8495x10^5	-2.9195x10^5	-2.9724x10^5	-3.0540x10^5	-3.1488x10^5
10	-39.50	-2.4862x10^5	-2.4987x10^5	-2.5689x10^5	-2.6487x10^5	-2.7480x10^5	-2.8569x10^5	-3.0444x10^5	-3.0563x10^5
11	-38.50	-2.4253x10^5	-2.3481x10^5	-2.3709x10^5	-2.4441x10^5	-2.5092x10^5	-2.5896x10^5	-2.7048x10^5	-2.8637x10^5
12	-37.50	-2.3604x10^5	-2.2995x10^5	-2.2586x10^5	-2.2995x10^5	-2.3634x10^5	-2.4224x10^5	-2.5285x10^5	-2.6712x10^5
13	-36.50	-2.3974x10^5	-2.3469x10^5	-2.1893x10^5	-2.1869x10^5	-2.2322x10^5	-2.2851x10^5	-2.3654x10^5	-2.5078x10^5
14	-35.50	-2.3345x10^5	-2.2963x10^5	-2.1430x10^5	-2.1063x10^5	-2.1227x10^5	-2.1877x10^5	-2.2760x10^5	-2.3860x10^5
15	-34.50	-2.1965x10^5	-2.1857x10^5	-2.0960x10^5	-2.0457x10^5	-2.0735x10^5	-2.1206x10^5	-2.2044x10^5	-2.3135x10^5
16	-33.50	-2.0886x10^5	-2.0695x10^5	-2.0504x10^5	-2.0478x10^5	-2.1192x10^5	-2.1538x10^5	-2.2448x10^5	-2.3609x10^5
17	-32.50	-2.0456x10^5	-2.0445x10^5	-2.0442x10^5	-2.0445x10^5	-2.1249x10^5	-2.1860x10^5	-2.2872x10^5	-3.0085x10^5
18	-31.50	-1.9827x10^5	-1.9739x10^5	-1.9579x10^5	-1.9739x10^5	-2.1206x10^5	-2.1188x10^5	-2.2074x10^5	-2.9158x10^5
19	-30.50	-1.9198x10^5	-1.9833x10^5	-1.9416x10^5	-1.9449x10^5	-1.9643x10^5	-2.0575x10^5	-2.1280x10^5	-2.8232x10^5
20	-29.50	-1.8548x10^5	-1.8927x10^5	-1.8653x10^5	-1.8927x10^5	-1.9020x10^5	-1.9843x10^5	-2.0483x10^5	-2.7306x10^5
21	-28.50	-1.7939x10^5	-1.8421x10^5	-1.8190x10^5	-1.8421x10^5	-1.8479x10^5	-1.9170x10^5	-2.0187x10^5	-2.6381x10^5
22	-27.50	-1.7309x10^5	-1.7915x10^5	-1.7728x10^5	-1.7915x10^5	-1.7934x10^5	-1.8477x10^5	-1.9391x10^5	-2.5455x10^5
23	-26.50	-1.6680x10^5	-1.7409x10^5	-1.7226x10^5	-1.7409x10^5	-1.7439x10^5	-1.7825x10^5	-1.8695x10^5	-2.4529x10^5
24	-25.50	-1.6050x10^5	-1.7903x10^5	-1.7102x10^5	-1.7903x10^5	-1.7848x10^5	-1.7152x10^5	-1.8099x10^5	-2.3604x10^5
25	-24.50	-1.5421x10^5	-1.7397x10^5	-1.7339x10^5	-1.7397x10^5	-1.7830x10^5	-1.6479x10^5	-1.7503x10^5	-2.2678x10^5
26	-23.50	-1.4792x10^5	-1.7191x10^5	-1.0876x10^5	-1.7191x10^5	-1.7761x10^5	-1.5809x10^5	-1.6907x10^5	-2.1753x10^5
27	-22.50	-1.4162x10^5	-1.7385x10^5	-1.0913x10^5	-1.7385x10^5	-1.7218x10^5	-1.5139x10^5	-1.6311x10^5	-2.0827x10^5
28	-21.50	-1.3533x10^5	-1.0879x10^5	-8.9506x10^4	-1.0879x10^5	-1.6675x10^5	-1.4462x10^5	-1.5715x10^5	-1.9901x10^5
29	-20.50	-1.2903x10^5	-1.0373x10^5	-9.4878x10^4	-1.0373x10^5	-1.1732x10^5	-1.3789x10^5	-1.4319x10^5	-1.8976x10^5
30	-19.50	-1.2274x10^5	-9.8672x10^4	-9.0250x10^4	-9.8672x10^4	-1.0589x10^5	-1.3146x10^5	-1.3523x10^5	-1.8050x10^5
31	-18.50	-1.1644x10^5	-9.3642x10^4	-8.5622x10^4	-9.3642x10^4	-1.0046x10^5	-1.2448x10^5	-1.2727x10^5	-1.7124x10^5
32	-17.50	-1.1015x10^5	-8.8632x10^4	-8.0994x10^4	-8.8632x10^4	-9.5082x10^4	-1.1771x10^5	-1.1931x10^5	-1.6199x10^5
33	-16.50	-1.0386x10^5	-8.3692x10^4	-7.6365x10^4	-8.3692x10^4	-8.9602x10^4	-1.1098x10^5	-1.1135x10^5	-1.5273x10^5
34	-15.50	-9.7562x10^4	-7.8832x10^4	-7.1737x10^4	-7.8832x10^4	-8.4171x10^4	-1.0422x10^5	-1.0339x10^5	-1.4347x10^5
35	-14.50	-9.1267x10^4	-7.3971x10^4	-6.7109x10^4	-7.3971x10^4	-7.8741x10^4	-9.7531x10^4	-9.5546x10^4	-1.3422x10^5
36	-13.50	-8.4973x10^4	-6.9311x10^4	-6.2481x10^4	-6.9311x10^4	-7.3310x10^4	-9.0805x10^4	-8.7747x10^4	-1.2496x10^5
37	-12.50	-7.8679x10^4	-6.4751x10^4	-5.7853x10^4	-6.4751x10^4	-6.7880x10^4	-8.4079x10^4	-8.0506x10^4	-1.1571x10^5
38	-11.50	-7.2384x10^4	-5.8191x10^4	-5.3224x10^4	-5.8191x10^4	-6.2450x10^4	-7.7352x10^4	-7.3546x10^4	-1.0646x10^5
39	-10.50	-6.6090x10^4	-5.3137x10^4	-4.8596x10^4	-5.3137x10^4	-5.7019x10^4	-7.0626x10^4	-6.8585x10^4	-9.7192x10^4
40	-9.50	-5.9796x10^4	-4.8071x10^4	-4.3968x10^4	-4.8071x10^4	-5.1589x10^4	-6.3900x10^4	-6.2625x10^4	-8.7936x10^4
41	-8.50	-5.3502x10^4	-4.3011x10^4	-3.9340x10^4	-4.3011x10^4	-4.6158x10^4	-5.7174x10^4	-5.7664x10^4	-7.8677x10^4
42	-7.50	-4.7207x10^4	-3.7951x10^4	-3.4712x10^4	-3.7951x10^4	-4.0728x10^4	-5.0447x10^4	-5.2704x10^4	-6.9423x10^4
43	-6.50	-4.0913x10^4	-3.2891x10^4	-3.0083x10^4	-3.2891x10^4	-3.5298x10^4	-4.3721x10^4	-4.7743x10^4	-6.0169x10^4
44	-5.50	-3.4619x10^4	-2.7831x10^4	-2.5455x10^4	-2.7831x10^4	-2.9867x10^4	-3.6995x10^4	-4.2782x10^4	-5.0910x10^4
45	-4.50	-2.8324x10^4	-2.2770x10^4	-2.0827x10^4	-2.2770x10^4	-2.4437x10^4	-3.0268x10^4	-3.7822x10^4	-4.1654x10^4
46	-3.50	-2.2030x10^4	-1.7710x10^4	-1.6199x10^4	-1.7710x10^4	-1.9006x10^4	-2.3542x10^4	-2.7862x10^4	-3.2397x10^4
47	-2.50	-1.5736x10^4	-1.2650x10^4	-1.1571x10^4	-1.2650x10^4	-1.3576x10^4	-1.6816x10^4	-1.9901x10^4	-2.3141x10^4
48	-1.50	-9.4415x10^3	-7.5902x10^3	-6.9423x10^3	-7.5902x10^3	-8.1456x10^3	-1.0089x10^4	-1.1941x10^4	-1.3885x10^4
49	-0.50	-3.1472x10^3	-2.5301x10^3	-2.3141x10^3	-2.5301x10^3	-2.7152x10^3	-3.3632x10^3	-3.9803x10^3	-4.6282x10^3
50	0.00	0.0000	0.0000	0.0000	0.0000	0.0000	0.0000	0.0000	0.0000
51	0.50	3.1472x10^3	2.5301x10^3	2.3141x10^3	2.5301x10^3	2.7152x10^3	3.3632x10^3	3.9803x10^3	4.6282x10^3
52	1.50	9.4415x10^3	7.5902x10^3	6.9423x10^3	7.5902x10^3	8.1456x10^3	1.0089x10^4	1.1941x10^4	1.3885x10^4
53	2.50	1.5736x10^4	1.2650x10^4	1.1571x10^4	1.2650x10^4	1.3576x10^4	1.6816x10^4	1.9901x10^4	2.3141x10^4
54	3.50	2.2030x10^4	1.7710x10^4	1.6199x10^4	1.7710x10^4	1.9006x10^4	2.3542x10^4	2.7862x10^4	3.2397x10^4
55	4.50	2.8324x10^4	2.2770x10^4	2.0827x10^4	2.2770x10^4	2.4437x10^4	3.0268x10^4	3.5822x10^4	4.1654x10^4
56	5.50	3.4619x10^4	2.7831x10^4	2.5455x10^4	2.7831x10^4	2.9867x10^4	3.6995x10^4	4.3782x10^4	5.0910x10^4
57	6.50	4.0913x10^4	3.2891x10^4	3.0083x10^4	3.2891x10^4	3.5298x10^4	4.3721x10^4	5.1743x10^4	6.0169x10^4

47	-2.50	-1.3738x10^3	-2.6682x10^3	-5.4271x10^3	-7.4053x10^3	-7.4053x10^3	-7.3376x10^3	-7.0876x10^3	-7.1701x10^3	-7.3194x10^3	
48	-1.50	-2.4415x10^3	-2.5902x10^3	-6.9483x10^3	-7.5782x10^3	-8.1456x10^3	-1.0089x10^4	-1.1941x10^4	-1.3825x10^4		
49	-0.50	-3.1472x10^3	-2.5304x10^3	-2.3141x10^3	-2.5304x10^3	-2.9152x10^3	-3.3632x10^3	-3.9933x10^3	-4.6282x10^3		
50	0.00	0.0000	0.0000	0.0000	0.0000	0.0000	0.0000	0.0000	0.0000		
51	0.50	3.1472x10^3	2.530x10^3	2.314x10^3	2.582x10^3	2.9152x10^3	3.3632x10^3	3.9933x10^3	4.6282x10^3		
52	1.50	2.4415x10^3	2.5902x10^3	6.9825x10^3	7.5902x10^3	8.1456x10^3	1.0089x10^4	1.1941x10^4	1.3825x10^4		
53	2.50	1.5736x10^4	1.7650x10^4	1.1671x10^4	1.2650x10^4	1.3576x10^4	1.6816x10^4	1.9901x10^4	2.3141x10^4		
54	3.50	2.2030x10^4	1.7710x10^4	1.6499x10^4	1.7710x10^4	1.9006x10^4	2.3542x10^4	2.7862x10^4	3.2397x10^4		
55	4.50	2.8324x10^4	2.2770x10^4	2.0827x10^4	2.2770x10^4	2.4437x10^4	3.0246x10^4	3.5822x10^4	4.1654x10^4		
56	5.50	3.4619x10^4	2.783x10^4	2.5455x10^4	2.7831x10^4	2.9869x10^4	3.6995x10^4	4.3788x10^4	5.0910x10^4		
57	6.50	4.0913x10^4	3.2891x10^4	3.0083x10^4	3.2891x10^4	3.5298x10^4	4.3721x10^4	5.1768x10^4	6.0167x10^4		
58	7.50	4.7207x10^4	3.7951x10^4	3.4712x10^4	3.7951x10^4	4.0722x10^4	5.0447x10^4	5.9734x10^4	6.9423x10^4		
59	8.50	5.3502x10^4	4.301x10^4	3.9340x10^4	4.301x10^4	4.6158x10^4	5.7174x10^4	6.7694x10^4	7.8679x10^4		
60	9.50	5.9796x10^4	4.807x10^4	4.3967x10^4	4.8071x10^4	5.1589x10^4	6.3900x10^4	7.5625x10^4	8.7931x10^4		
61	10.50	6.6090x10^4	5.313x10^4	4.8594x10^4	5.3151x10^4	5.7019x10^4	7.0626x10^4	8.3585x10^4	9.7182x10^4		
62	11.50	7.2384x10^4	5.8241x10^4	5.3221x10^4	5.8231x10^4	6.2450x10^4	7.7352x10^4	9.1546x10^4	1.0645x10^5		
63	12.50	7.8679x10^4	6.325x10^4	5.7853x10^4	6.325x10^4	6.7880x10^4	8.4079x10^4	9.9506x10^4	1.1571x10^5		
64	13.50	8.4973x10^4	6.8259x10^4	6.2484x10^4	6.8259x10^4	7.3311x10^4	9.0805x10^4	1.0746x10^5	1.2496x10^5		
65	14.50	9.1267x10^4	7.3268x10^4	6.7116x10^4	7.3268x10^4	7.8741x10^4	9.7532x10^4	1.1542x10^5	1.3422x10^5		
66	15.50	1.0330x10^5	8.1084x10^4	7.1747x10^4	7.8867x10^4	8.4172x10^4	1.0426x10^5	1.2337x10^5	1.4348x10^5		
67	16.50	1.0997x10^5	8.1638x10^4	7.3310x10^4	7.3310x10^4	8.3310x10^4	9.1638x10^4	1.2839x10^5	1.4995x10^5		
68	17.50	1.1663x10^5	8.7192x10^4	7.7853x10^4	7.7853x10^4	7.7853x10^4	9.7192x10^4	1.3607x10^5	1.7995x10^5		
69	18.50	1.2329x10^5	1.0275x10^5	8.2395x10^4	8.2395x10^4	8.2395x10^4	1.0275x10^5	1.4384x10^5	1.8994x10^5		
70	19.50	1.2996x10^5	1.0830x10^5	8.6938x10^4	8.6938x10^4	8.6938x10^4	1.0830x10^5	1.5762x10^5	1.9994x10^5		
71	20.50	1.3662x10^5	1.1385x10^5	9.1082x10^4	9.1082x10^4	9.1082x10^4	1.1385x10^5	1.5939x10^5	2.0494x10^5		
72	21.50	1.4329x10^5	1.1941x10^5	9.5524x10^4	9.5524x10^4	9.5524x10^4	1.1941x10^5	1.6719x10^5	2.1493x10^5		
73	22.50	1.4995x10^5	1.2496x10^5	9.9968x10^4	9.9968x10^4	9.9968x10^4	1.2496x10^5	1.7498x10^5	2.2493x10^5		
74	23.50	1.5662x10^5	1.3051x10^5	1.0441x10^5	1.0441x10^5	1.0441x10^5	1.3051x10^5	1.8278x10^5	2.3493x10^5		
75	24.50	1.6328x10^5	1.3607x10^5	1.0885x10^5	1.0885x10^5	1.0885x10^5	1.3607x10^5	1.9057x10^5	2.4492x10^5		
76	25.50	1.6995x10^5	1.4162x10^5	1.1330x10^5	1.1330x10^5	1.1330x10^5	1.4162x10^5	1.9837x10^5	2.5492x10^5		
77	26.50	1.7661x10^5	1.4718x10^5	1.1774x10^5	1.1774x10^5	1.1774x10^5	1.4718x10^5	2.0616x10^5	2.6492x10^5		
78	27.50	1.8328x10^5	1.5273x10^5	1.2218x10^5	1.2218x10^5	1.2218x10^5	1.5273x10^5	2.1382x10^5	2.7491x10^5		
79	28.50	1.8994x10^5	1.5828x10^5	1.2663x10^5	1.2663x10^5	1.2663x10^5	1.5828x10^5	2.2160x10^5	2.8491x10^5		
80	29.50	1.9661x10^5	1.6384x10^5	1.3107x10^5	1.3107x10^5	1.3107x10^5	1.6384x10^5	2.2937x10^5	2.9491x10^5		
81	30.50	2.0327x10^5	1.6939x10^5	1.3551x10^5	1.3551x10^5	1.3551x10^5	1.6939x10^5	2.3715x10^5	3.0491x10^5		
82	31.50	2.0993x10^5	1.7494x10^5	1.3995x10^5	1.3995x10^5	1.3995x10^5	1.7494x10^5	2.4492x10^5	3.1490x10^5		
83	32.50	2.1660x10^5	1.8050x10^5	1.4440x10^5	1.4440x10^5	1.4440x10^5	1.8050x10^5	2.5270x10^5	3.2490x10^5		
84	33.50	2.2326x10^5	1.9019x10^5	1.5091x10^5	1.5091x10^5	1.5091x10^5	1.9019x10^5	2.6441x10^5	3.4110x10^5		
85	34.50	2.2270x10^5	2.0225x10^5	1.6180x10^5	1.6180x10^5	1.6180x10^5	2.0225x10^5	2.8345x10^5	3.6194x10^5		
86	35.50	2.6069x10^5	2.1688x10^5	1.7806x10^5	1.7306x10^5	1.7306x10^5	2.1688x10^5	3.0931x10^5	3.8998x10^5		
87	36.50	2.8380x10^5	2.3875x10^5	1.9145x10^5	1.9145x10^5	1.7306x10^5	2.3875x10^5	3.3560x10^5	4.3245x10^5		
88	37.50	2.7769x10^5	2.2215x10^5	2.2215x10^5	2.2215x10^5	2.2215x10^5	2.7769x10^5	3.3323x10^5	4.4430x10^5		
89	38.50	2.8501x10^5	2.8501x10^5	2.8501x10^5	2.8051x10^5	2.8051x10^5	3.5639x10^5	3.7060x10^5	4.6099x10^5		
90	39.50	2.9250x10^5	2.9250x10^5	2.9250x10^5	2.9250x10^5	2.9250x10^5	3.6563x10^5	4.4950x10^5	4.7775x10^5		
91	40.50	2.9991x10^5	2.9991x10^5	2.9991x10^5	2.9991x10^5	2.9991x10^5	3.7488x10^5	4.4989x10^5	4.9985x10^5		
92	41.50	3.4060x10^5	3.4060x10^5	3.4060x10^5	3.4060x10^5	3.4060x10^5	4.2513x10^5	4.9169x10^5	5.1219x10^5		
93	42.50	3.9340x10^5	3.9340x10^5	3.9340x10^5	3.9340x10^5	3.9340x10^5	4.9304x10^5	5.2454x10^5	5.2454x10^5		
94	43.50	3.4899x10^5	3.4899x10^5	3.4899x10^5	3.4899x10^5	4.4706x10^5	5.1809x10^5	5.3688x10^5	5.3688x10^5		
95	44.50	2.2295x10^5	2.8813x10^5	2.8833x10^5	3.5150x10^5	4.421x10^5	5.4099x10^5	5.4922x10^5	5.4922x10^5		
96	45.50	2.6393x10^5	3.3974x10^5	3.3974x10^5	4.1274x10^5	5.2509x10^5	5.6156x10^5	5.6156x10^5	5.5592x10^5		
97	46.50	2.7260x10^5	3.1851x10^5	3.1851x10^5	3.5868x10^5	4.1033x10^5	5.0215x10^5	5.4652x10^5	5.3373x10^5		
98	47.50	3.3858x10^5	2.8604x10^5	2.3058x10^5	2.3058x10^5	2.3058x10^5	2.8604x10^5	3.9989x10^5	5.137x10^5		
99	48.50	2.5357x10^5	2.1519x10^5	1.7392x10^5	1.7392x10^5	1.7392x10^5	2.1519x10^5	2.9478x10^5	3.7143x10^5		
100	49.50	1.6969x10^5	1.4113x10^5	1.1470x10^5	1.1470x10^5	1.1470x10^5	1.4113x10^5	1.9116x10^5	2.5292x10^5		
101	50.50	7.5154x10^4	6.6483x10^4	5.4929x10^4	5.4929x10^4	5.4929x10^4	6.6483x10^4	8.6719x10^4	1.3297x10^5		
102	51.50	0.0000	0.0000	0.0000	0.0000	0.0000	0.0000	0.0000	0.0000		
103	52.36	0.0000	0.0000	0.0000	0.0000	0.0000	0.0000	0.0000	0.0000		
$\int \rho_{33} r^2 dr$		9.9203x10^5	1.6931x10^6	1.3044x10^6	9.9860x10^5	9.4318x10^5	1.0864x10^6	1.6914x10^6	2.2437x10^6		

Table B-6b. Values of $A_{33}' \xi^2$ at 1-Foot Intervals Along ξ Axis

Index	ξ^2	Wave Length, λ (ft)							
		25	50	75	100	150	250	350	450
1	2.34256x10^3	1.4745x10^7	1.1857x10^7	1.0842x10^7	1.1854x10^7	1.2721x10^7	1.5757x10^7	1.8648x10^7	2.1694x10^7
2	8.25625x10^3	1.4202x10^7	1.1417x10^7	1.0442x10^7	1.1417x10^7	1.2252x10^7	1.5176x10^7	1.7961x10^7	2.0885x10^7
3	2.16225x10^3	1.3610x10^7	1.0941x10^7	1.0007x10^7	1.0941x10^7	1.1742x10^7	1.4544x10^7	1.7213x10^7	2.0015x10^7
4	2.07025x10^3	1.3031x10^7	1.0476x10^7	9.5845x10^6	1.0476x10^7	1.1242x10^7	1.3925x10^7	1.6480x10^7	1.9163x10^7
5	1.98025x10^3	1.2464x10^7	1.0020x10^7	9.1650x10^6	1.0020x10^7	1.0754x10^7	1.3320x10^7	1.5764x10^7	1.8330x10^7
6	1.89225x10^3	1.1910x10^7	9.5750x10^6	8.7577x10^6	9.5750x10^6	1.0276x10^7	1.2728x10^7	1.5063x10^7	1.7515x10^7
7	1.80625x10^3	1.1369x10^7	9.1398x10^6	8.3597x10^6	9.1398x10^6	9.8087x10^6	1.2149x10^7	1.4379x10^7	1.6719x10^7
8	1.72225x10^3	1.0840x10^7	8.7148x10^6	7.9709x10^6	8.7148x10^6	9.3525x10^6	1.1584x10^7	1.3710x10^7	1.5942x10^7
9	1.64025x10^3	1.0324x10^7	8.2998x10^6	7.5914x10^6	8.2998x10^6	8.9072x10^6	1.1033x10^7	1.3057x10^7	1.5183x10^7
10	1.56025x10^3	9.8207x10^6	7.8950x10^6	7.2211x10^6	7.8950x10^6	8.4728x10^6	1.0495x10^7	1.2420x10^7	1.4442x10^7
11	1.48225x10^3	9.3297x10^6	7.5003x10^6	6.8601x10^6	7.5003x10^6	8.0492x10^6	9.9701x10^6	1.1799x10^7	1.3720x10^7
12	1.40625x10^3	8.8514x10^6	7.1158x10^6	6.5084x10^6	7.1158x10^6	7.6365x10^6	9.4589x10^6	1.1194x10^7	1.3017x10^7
13	1.33225x10^3	8.3856x10^6	6.7413x10^6	6.1659x10^6	6.7413x10^6	7.2347x10^6	8.9611x10^6	1.0605x10^7	1.2332x10^7
14	1.26025x10^3	7.9324x10^6	6.3790x10^6	5.8337x10^6	6.3790x10^6	6.8437x10^6	8.4768x10^6	1.0032x10^7	1.1665x10^7
15	1.19025x10^3	7.4918x10^6	6.0288x10^6	5.5087x10^6	6.0288x10^6	6.4635x10^6	8.0060x10^6	9.4750x10^6	1.1017x10^7
16	1.12225x10^3	7.0638x10^6	5.6787x10^6	5.1940x10^6	5.6787x10^6	6.0943x10^6	7.5486x10^6	8.9332x10^6	1.0388x10^7
17	1.05625x10^3	6.6484x10^6	5.3447x10^6	4.8885x10^6	5.3447x10^6	5.7359x10^6	7.1047x10^6	8.4083x10^6	9.7771x10^6
18	9.9225x10^2	6.2455x10^6	5.0209x10^6	4.5923x10^6	5.0209x10^6	5.3883x10^6	6.6742x10^6	7.8988x10^6	9.1847x10^6
19	9.3025x10^2	5.8553x10^6	4.7072x10^6	4.3054x10^6	4.7072x10^6	5.0516x10^6	6.2571x10^6	7.4053x10^6	8.6108x10^6
20	8.7025x10^2	5.4776x10^6	4.4036x10^6	4.0277x10^6	4.4036x10^6	4.7258x10^6	5.8536x10^6	6.9276x10^6	8.0554x10^6
21	8.1225x10^2	5.1125x10^6	4.1101x10^6	3.7593x10^6	4.1101x10^6	4.4108x10^6	5.4634x10^6	6.4659x10^6	7.5185x10^6
22	7.5625x10^2	4.7601x10^6	3.8267x10^6	3.5001x10^6	3.8267x10^6	4.1067x10^6	5.0868x10^6	6.0201x10^6	7.0002x10^6
23	7.0225x10^2	4.4202x10^6	3.5535x10^6	3.2502x10^6	3.5535x10^6	3.8135x10^6	4.7235x10^6	5.5903x10^6	6.5003x10^6
24	6.5025x10^2	4.0929x10^6	3.2903x10^6	3.0085x10^6	3.2903x10^6	3.5311x10^6	4.3738x10^6	5.1743x10^6	6.0190x10^6
25	6.0025x10^2	3.7782x10^6	3.0373x10^6	2.7781x10^6	3.0373x10^6	3.2596x10^6	4.0375x10^6	4.7783x10^6	5.5562x10^6
26	5.5225x10^2	3.4760x10^6	2.7944x10^6	2.5559x10^6	2.7944x10^6	2.9989x10^6	3.7146x10^6	4.3962x10^6	5.1118x10^6
27	5.0625x10^2	3.2494x10^6	2.5647x10^6	2.3430x10^6	2.5647x10^6	2.7491x10^6	3.4052x10^6	4.0300x10^6	4.6861x10^6
28	4.6225x10^2	2.9095x10^6	2.3390x10^6	2.394x10^6	2.3390x10^6	2.5102x10^6	3.1092x10^6	3.6797x10^6	4.2788x10^6
29	4.2025x10^2	2.6452x10^6	2.1265x10^6	1.9450x10^6	2.1265x10^6	2.2831x10^6	2.8267x10^6	3.3454x10^6	3.8900x10^6
30	3.8025x10^2	2.3934x10^6	1.9241x10^6	1.7589x10^6	1.9241x10^6	2.0649x10^6	2.5577x10^6	3.0270x10^6	3.5197x10^6
31	3.4225x10^2	2.1542x10^6	1.7318x10^6	1.5840x10^6	1.7318x10^6	1.8586x10^6	2.3021x10^6	2.7245x10^6	3.1680x10^6
32	3.0625x10^2	1.9276x10^6	1.5497x10^6	1.4174x10^6	1.5497x10^6	1.6631x10^6	2.0599x10^6	2.4379x10^6	2.8348x10^6
33	2.7225x10^2	1.7136x10^6	1.3776x10^6	1.2600x10^6	1.3776x10^6	1.4784x10^6	1.8312x10^6	2.1672x10^6	2.5201x10^6
34	2.4025x10^2	1.5122x10^6	1.2157x10^6	1.1119x10^6	1.2157x10^6	1.3047x10^6	1.6160x10^6	1.9125x10^6	2.2239x10^6
35	2.1025x10^2	1.3234x10^6	1.0639x10^6	9.7308x10^5	1.0639x10^6	1.1417x10^6	1.4142x10^6	1.6737x10^6	1.9462x10^6
36	1.8225x10^2	1.1471x10^6	9.2220x10^5	8.4349x10^5	9.2220x10^5	9.8969x10^5	1.2259x10^6	1.4508x10^6	1.6870x10^6
37	1.5625x10^2	9.8348x10^5	7.9064x10^5	7.2316x10^5	7.9064x10^5	8.4850x10^5	1.0510x10^6	1.2438x10^6	1.4463x10^6
38	1.3225x10^2	8.3242x10^5	6.6930x10^5	6.1208x10^5	6.6930x10^5	7.1817x10^5	8.8955x10^5	1.0528x10^6	1.2242x10^6
39	1.1025x10^2	6.9395x10^5	5.5788x10^5	5.1006x10^5	5.5788x10^5	5.9870x10^5	7.4157x10^5	8.7765x10^5	1.0205x10^6
40	9.0250x10^1	5.6806x10^5	4.5667x10^5	4.1770x10^5	4.5667x10^5	4.9009x10^5	6.0705x10^5	7.1844x10^5	8.3539x10^5
41	7.2250x10^1	4.5476x10^5	3.6559x10^5	3.3439x10^5	3.6559x10^5	3.9235x10^5	4.8598x10^5	5.7515x10^5	6.6877x10^5
42	5.6250x10^1	3.5405x10^5	2.8463x10^5	2.6034x10^5	2.8463x10^5	3.0546x10^5	3.7835x10^5	4.4778x10^5	5.2067x10^5
43	4.2250x10^1	2.6593x10^5	2.1379x10^5	1.9554x10^5	2.1379x10^5	2.2943x10^5	2.8419x10^5	3.3633x10^5	3.9108x10^5
44	3.0250x10^1	1.9040x10^5	1.5031x10^5	1.4000x10^5	1.5031x10^5	1.6427x10^5	2.0347x10^5	2.4081x10^5	2.8001x10^5
45	2.0250x10^1	1.2746x10^5	1.0247x10^5	9.3721x10^4	1.0247x10^5	1.0999x10^5	1.3621x10^5	1.6120x10^5	1.8744x10^5
46	1.2250x10^1	7.7105x10^4	6.1986x10^4	5.6695x10^4	6.1986x10^4	6.6522x10^4	8.2397x10^4	9.7516x10^4	1.1339x10^5
47	6.2500	3.9339x10^4	3.1626x10^4	2.8926x10^4	3.1626x10^4	3.3940x10^4	4.2039x10^4	4.9753x10^4	5.7853x10^4
48	2.2500	1.4162x10^4	1.1385x10^4	1.0413x10^4	1.1385x10^4	1.2218x10^4	1.5134x10^4	1.7911x10^4	2.0822x10^4
49	0.2500	1.5736x10^3	1.2650x10^3	1.1571x10^3	1.2650x10^3	1.3576x10^3	1.6816x10^3	1.9901x10^3	2.3141x10^3
50	0.0000	0.0000	0.0000	0.0000	0.0000	0.0000	0.0000	0.0000	0.0000
51	0.2500	1.5736x10^3	1.2650x10^3	1.1571x10^3	1.2650x10^3	1.3576x10^3	1.6816x10^3	1.9901x10^3	2.3141x10^3
52	2.2500	1.4162x10^4	1.1385x10^4	1.0413x10^4	1.1385x10^4	1.2218x10^4	1.5134x10^4	1.7911x10^4	2.0822x10^4
53	6.2500	3.9339x10^4	3.1626x10^4	2.8926x10^4	3.1626x10^4	3.3940x10^4	4.2039x10^4	4.9753x10^4	5.7853x10^4
54	12.2500x10^1	7.7105x10^4	6.1986x10^4	5.6695x10^4	6.1986x10^4	6.6522x10^4	8.2397x10^4	9.7516x10^4	1.1339x10^5
55	20.2500x10^1	1.2746x10^5	1.0247x10^5	9.3721x10^4	1.0247x10^5	1.0999x10^5	1.3621x10^5	1.6120x10^5	1.8744x10^5

46	1.2250×10^{1}	7.7105×10^{4}	6.1986×10^{4}	5.6695×10^{4}	6.1986×10^{4}	6.6522×10^{4}	8.2397×10^{4}	9.7516×10^{4}	1.1339×10^{5}
47	6.2500	3.9339×10^{4}	3.1626×10^{4}	2.8926×10^{4}	3.1626×10^{4}	3.3940×10^{4}	4.2089×10^{4}	4.9753×10^{4}	5.7853×10^{4}
48	2.2500	1.4162×10^{4}	1.1385×10^{4}	1.0413×10^{4}	1.1385×10^{4}	1.2218×10^{4}	1.5134×10^{4}	1.7911×10^{4}	2.0827×10^{4}
49	0.2500	1.5736×10^{3}	1.2650×10^{3}	1.1571×10^{3}	1.2650×10^{3}	1.3576×10^{3}	1.6816×10^{3}	1.9901×10^{3}	2.3141×10^{3}
50	0.0000	0.0000	0.0000	0.0000	0.0000	0.0000	0.0000	0.0000	0.0000
51	0.2500	1.5736×10^{3}	1.2650×10^{3}	1.1571×10^{3}	1.2650×10^{3}	1.3576×10^{3}	1.6816×10^{3}	1.9901×10^{3}	2.3141×10^{3}
52	2.2500	1.4162×10^{4}	1.1385×10^{4}	1.0413×10^{4}	1.1385×10^{4}	1.2218×10^{4}	1.5134×10^{4}	1.7911×10^{4}	2.0827×10^{4}
53	6.2500	3.9339×10^{4}	3.1626×10^{4}	2.8926×10^{4}	3.1626×10^{4}	3.3940×10^{4}	4.2089×10^{4}	4.9753×10^{4}	5.7853×10^{4}
54	1.2250×10^{1}	7.7105×10^{4}	6.1986×10^{4}	5.6695×10^{4}	6.1986×10^{4}	6.6522×10^{4}	8.2397×10^{4}	9.7516×10^{4}	1.1339×10^{5}
55	2.0250×10^{1}	1.2746×10^{5}	1.0247×10^{5}	9.3721×10^{4}	1.0247×10^{5}	1.0997×10^{5}	1.3621×10^{5}	1.6120×10^{5}	1.8744×10^{5}
56	3.0250×10^{1}	1.9040×10^{5}	1.5031×10^{5}	1.4000×10^{5}	1.5031×10^{5}	1.6427×10^{5}	2.0347×10^{5}	2.4081×10^{5}	2.8001×10^{5}
57	4.2250×10^{1}	2.6593×10^{5}	2.1379×10^{5}	1.9554×10^{5}	2.1379×10^{5}	2.2943×10^{5}	2.8419×10^{5}	3.3633×10^{5}	3.9108×10^{5}
58	5.6250×10^{1}	3.5405×10^{5}	2.8463×10^{5}	2.6039×10^{5}	2.8463×10^{5}	3.0546×10^{5}	3.7835×10^{5}	4.4778×10^{5}	5.2062×10^{5}
59	7.2250×10^{1}	4.5476×10^{5}	3.6559×10^{5}	3.3439×10^{5}	3.6559×10^{5}	3.9225×10^{5}	4.8578×10^{5}	5.7515×10^{5}	6.6877×10^{5}
60	9.0250×10^{1}	5.6806×10^{5}	4.5667×10^{5}	4.1770×10^{5}	4.5667×10^{5}	4.9009×10^{5}	6.0705×10^{5}	7.1844×10^{5}	8.3539×10^{5}
61	1.1025×10^{2}	6.9385×10^{5}	5.5788×10^{5}	5.1006×10^{5}	5.5788×10^{5}	5.9870×10^{5}	7.4157×10^{5}	8.7765×10^{5}	1.0205×10^{6}
62	1.3225×10^{2}	8.3292×10^{5}	6.6920×10^{5}	6.1208×10^{5}	6.6920×10^{5}	7.1817×10^{5}	8.8955×10^{5}	1.0528×10^{6}	1.2242×10^{6}
63	1.5625×10^{2}	9.8348×10^{5}	7.9064×10^{5}	7.2316×10^{5}	7.9064×10^{5}	8.4850×10^{5}	1.0510×10^{6}	1.2438×10^{6}	1.4463×10^{6}
64	1.8225×10^{2}	1.2146×10^{6}	1.0122×10^{6}	8.0994×10^{5}	8.0994×10^{5}	8.0994×10^{5}	1.0122×10^{6}	1.4170×10^{6}	1.8219×10^{6}
65	2.1025×10^{2}	1.4012×10^{6}	1.1677×10^{6}	9.3414×10^{5}	9.3414×10^{5}	9.3414×10^{5}	1.1677×10^{6}	1.6348×10^{6}	2.1018×10^{6}
66	2.4025×10^{2}	1.6012×10^{6}	1.3343×10^{6}	1.0674×10^{6}	1.0674×10^{6}	1.0674×10^{6}	1.3343×10^{6}	1.8680×10^{6}	2.4018×10^{6}
67	2.7225×10^{2}	1.8144×10^{6}	1.5120×10^{6}	1.2096×10^{6}	1.2096×10^{6}	1.2096×10^{6}	1.5120×10^{6}	2.1168×10^{6}	2.7217×10^{6}
68	3.0625×10^{2}	2.0410×10^{6}	1.7009×10^{6}	1.3607×10^{6}	1.3607×10^{6}	1.3607×10^{6}	1.7009×10^{6}	2.3812×10^{6}	3.0616×10^{6}
69	3.4225×10^{2}	2.2810×10^{6}	1.9008×10^{6}	1.5206×10^{6}	1.5206×10^{6}	1.5206×10^{6}	1.9008×10^{6}	2.6611×10^{6}	3.4214×10^{6}
70	3.8025×10^{2}	2.5342×10^{6}	2.1118×10^{6}	1.6895×10^{6}	1.6895×10^{6}	1.6895×10^{6}	2.1118×10^{6}	2.9566×10^{6}	3.8013×10^{6}
71	4.2025×10^{2}	2.8008×10^{6}	2.3340×10^{6}	1.8672×10^{6}	1.8672×10^{6}	1.8672×10^{6}	2.3340×10^{6}	3.2676×10^{6}	4.2012×10^{6}
72	4.6225×10^{2}	3.0807×10^{6}	2.5672×10^{6}	2.0538×10^{6}	2.0538×10^{6}	2.0538×10^{6}	2.5672×10^{6}	3.5941×10^{6}	4.6211×10^{6}
73	5.0625×10^{2}	3.3740×10^{6}	2.8061×10^{6}	2.2493×10^{6}	2.2493×10^{6}	2.2493×10^{6}	2.8061×10^{6}	3.9362×10^{6}	5.0609×10^{6}
74	5.5225×10^{2}	3.6805×10^{6}	3.0671×10^{6}	2.4536×10^{6}	2.4536×10^{6}	2.4536×10^{6}	3.0671×10^{6}	4.2939×10^{6}	5.5208×10^{6}
75	6.0025×10^{2}	4.0004×10^{6}	3.3337×10^{6}	2.6669×10^{6}	2.6669×10^{6}	2.6669×10^{6}	3.3337×10^{6}	4.6671×10^{6}	6.0006×10^{6}
76	6.5025×10^{2}	4.3337×10^{6}	3.6114×10^{6}	2.8891×10^{6}	2.8891×10^{6}	2.8891×10^{6}	3.6114×10^{6}	5.0559×10^{6}	6.5005×10^{6}
77	7.0225×10^{2}	4.6802×10^{6}	3.9002×10^{6}	3.1201×10^{6}	3.1201×10^{6}	3.1201×10^{6}	3.9002×10^{6}	5.4602×10^{6}	7.0203×10^{6}
78	7.5625×10^{2}	5.0401×10^{6}	4.2000×10^{6}	3.3600×10^{6}	3.3600×10^{6}	3.3600×10^{6}	4.2000×10^{6}	5.8801×10^{6}	7.5602×10^{6}
79	8.1225×10^{2}	5.4133×10^{6}	4.5111×10^{6}	3.6088×10^{6}	3.6088×10^{6}	3.6088×10^{6}	4.5111×10^{6}	6.3155×10^{6}	8.1200×10^{6}
80	8.7025×10^{2}	5.7999×10^{6}	4.8332×10^{6}	3.8665×10^{6}	3.8665×10^{6}	3.8665×10^{6}	4.8332×10^{6}	6.7665×10^{6}	8.6998×10^{6}
81	9.3025×10^{2}	6.1997×10^{6}	5.1664×10^{6}	4.1331×10^{6}	4.1331×10^{6}	4.1331×10^{6}	5.1664×10^{6}	7.2330×10^{6}	9.2996×10^{6}
82	9.9225×10^{2}	6.6063×10^{6}	5.5107×10^{6}	4.4086×10^{6}	4.4086×10^{6}	4.4086×10^{6}	5.5107×10^{6}	7.7150×10^{6}	9.9194×10^{6}
83	1.0562×10^{3}	7.0395×10^{6}	5.8662×10^{6}	4.6929×10^{6}	4.6929×10^{6}	4.6929×10^{6}	5.8662×10^{6}	8.2127×10^{6}	1.0559×10^{7}
84	1.1222×10^{3}	7.6178×10^{6}	6.3472×10^{6}	5.0555×10^{6}	5.0555×10^{6}	5.0555×10^{6}	6.3472×10^{6}	8.8644×10^{6}	1.1427×10^{7}
85	1.1902×10^{3}	8.3732×10^{6}	6.9777×10^{6}	5.5822×10^{6}	5.5822×10^{6}	5.5822×10^{6}	6.9777×10^{6}	9.7687×10^{6}	1.2487×10^{7}
86	1.2602×10^{3}	9.2545×10^{6}	7.6991×10^{6}	6.1437×10^{6}	6.1437×10^{6}	6.1437×10^{6}	7.6991×10^{6}	1.0732×10^{7}	1.3843×10^{7}
87	1.3322×10^{3}	1.0359×10^{7}	8.7145×10^{6}	6.9881×10^{6}	6.9881×10^{6}	6.9881×10^{6}	8.7145×10^{6}	1.2250×10^{7}	1.5784×10^{7}
88	1.4062×10^{3}	1.0413×10^{7}	8.3308×10^{6}	8.3308×10^{6}	8.3308×10^{6}	8.3308×10^{6}	1.0413×10^{7}	1.2496×10^{7}	1.6661×10^{7}
89	1.4822×10^{3}	1.0976×10^{7}	1.0976×10^{7}	1.0976×10^{7}	1.0976×10^{7}	1.0976×10^{7}	1.3720×10^{7}	1.4269×10^{7}	1.7745×10^{7}
90	1.5602×10^{3}	1.1554×10^{7}	1.1554×10^{7}	1.1554×10^{7}	1.1554×10^{7}	1.1554×10^{7}	1.4442×10^{7}	1.6175×10^{7}	1.8871×10^{7}
91	1.6402×10^{3}	1.2146×10^{7}	1.2146×10^{7}	1.2146×10^{7}	1.2146×10^{7}	1.2146×10^{7}	1.5183×10^{7}	1.8220×10^{7}	2.2244×10^{7}
92	1.7222×10^{3}	1.4135×10^{7}	1.4135×10^{7}	1.4135×10^{7}	1.4135×10^{7}	1.4135×10^{7}	1.7643×10^{7}	2.0905×10^{7}	2.2256×10^{7}
93	1.8062×10^{3}	1.4719×10^{7}	1.4719×10^{7}	1.4719×10^{7}	1.4719×10^{7}	1.4719×10^{7}	2.0954×10^{7}	2.2293×10^{7}	2.2293×10^{7}
94	1.8922×10^{3}	1.5180×10^{7}	1.5180×10^{7}	1.5180×10^{7}	1.5180×10^{7}	2.0317×10^{7}	2.2537×10^{7}	2.3354×10^{7}	2.3354×10^{7}
95	1.9802×10^{3}	9.8981×10^{6}	1.2831×10^{7}	1.2831×10^{7}	1.5642×10^{7}	1.9674×10^{7}	2.4074×10^{7}	2.4440×10^{7}	2.4440×10^{7}
96	2.0702×10^{3}	1.2008×10^{7}	1.5458×10^{7}	1.5458×10^{7}	1.7780×10^{7}	2.3891×10^{7}	2.5551×10^{7}	2.5551×10^{7}	2.5294×10^{7}
97	2.1622×10^{3}	1.2676×10^{7}	1.4811×10^{7}	1.4811×10^{7}	1.6679×10^{7}	1.9081×10^{7}	2.3350×10^{7}	2.4018×10^{7}	2.4818×10^{7}
98	2.2562×10^{3}	1.4083×10^{7}	1.3587×10^{7}	1.0953×10^{7}	1.0953×10^{7}	1.0953×10^{7}	1.3587×10^{7}	1.7994×10^{7}	2.4401×10^{7}
99	2.3522×10^{3}	1.2295×10^{7}	1.0437×10^{7}	8.4352×10^{6}	8.4352×10^{6}	8.4352×10^{6}	1.0437×10^{7}	1.4297×10^{7}	1.8014×10^{7}
100	2.4502×10^{3}	8.1522×10^{6}	6.9862×10^{6}	5.6775×10^{6}	5.6775×10^{6}	5.6775×10^{6}	6.9862×10^{6}	9.4624×10^{6}	1.2520×10^{7}
101	2.5502×10^{3}	3.7953×10^{6}	3.3524×10^{6}	2.7739×10^{6}	2.7739×10^{6}	2.7739×10^{6}	3.3524×10^{6}	4.3793×10^{6}	6.7148×10^{6}
102	2.6522×10^{3}	0.0000	0.0000	0.0000	0.0000	0.0000	0.0000	0.0000	0.0000
103	2.7457×10^{3}	0.0000	0.0000	0.0000	0.0000	0.0000	0.0000	0.0000	0.0000
$\int A_{337}\,\rho^2\,dA$		5.2504×10^{8}	4.5841×10^{8}	4.1635×10^{8}	4.4141×10^{8}	4.7181×10^{8}	5.7990×10^{8}	6.9162×10^{8}	8.0789×10^{8}

Added Mass in Sway, A_{22}'

The sectional added mass, A_{22}', for lateral motion is determined by modifying the values appropriate for zero frequency by a frequency-dependent function. The total added mass for lateral motion at zero frequency is equal to one-half of the total added mass of the reflected body about the free surface. Kaplan and Putz (1962) give the following expression for the added mass for zero frequency:

$$\rho Sk_y = \frac{1}{2} \rho C_z' \pi H^2 \tag{B-7}$$

where C_z' is a factor taken from the work of Prohaska (1947). The coefficient C_z', originally derived for vertical motions at infinite frequency, was studied for analytic forms that resemble ship sections which were derived by conformal transformation of the known flow about an elliptic cylinder. Lewis (1929) studied the transformation, $z = \xi + a\xi^{-1} + b\xi^{-3}$. Prohaska also studied the transformation more generally (i.e., $z = \xi + a\xi^{-m} + b\xi^{-n}$) for values of (m, n) = (1, 5), (1, 7), (3, 7). Prohaska's experimental work, which included the testing of 10 representative model ship sections vibrated vertically, supported the results of the analytic investigation. His results, slightly extrapolated for the present problem, are shown in Figure B-3 in the form of a graph of contours of the coefficient C_z' for varying beam-draft ratios and sectional (area) coefficients ($C_S = S/B^*H$). Kaplan and Putz (1962) point out that the value of C_z' found for an effective beam-draft ratio appropriate for lateral motion is "obtained by 'turning' the ship section by 90 degrees and interpreting the effective beam-draft ratio as $4H/B^*$."

The frequency correction factor, k_4', given by Kaplan and Putz is

$$k_4' = 1 - \frac{2}{\pi} \left(\frac{\omega^2 H}{g} \right) \tag{B-8}$$

It was derived by Kaplan and Ulc (1961) as an approximation based on energy considerations and has been successfully applied to the analysis of lateral bending moments in waves. Putting all the foregoing together, the sectional added mass for lateral motion emerges as

$$A_{22}' = \frac{1}{2} \rho C_z' \pi H^2 \left(1 - \frac{2}{\pi} \frac{\omega^2 H}{g} \right) \tag{B-9}$$

where C_z' is taken from Prohaska's chart, but which for lateral motions has the abscissa B^*/H interpreted as $4H/B^*$.

Table B-7 presents values of the coefficient C_z' at 1-foot intervals along the ξ axis as obtained from Figure B-3. Table B-7 also includes values of the term $C_z'\xi$ and $C_z'\xi^2$.

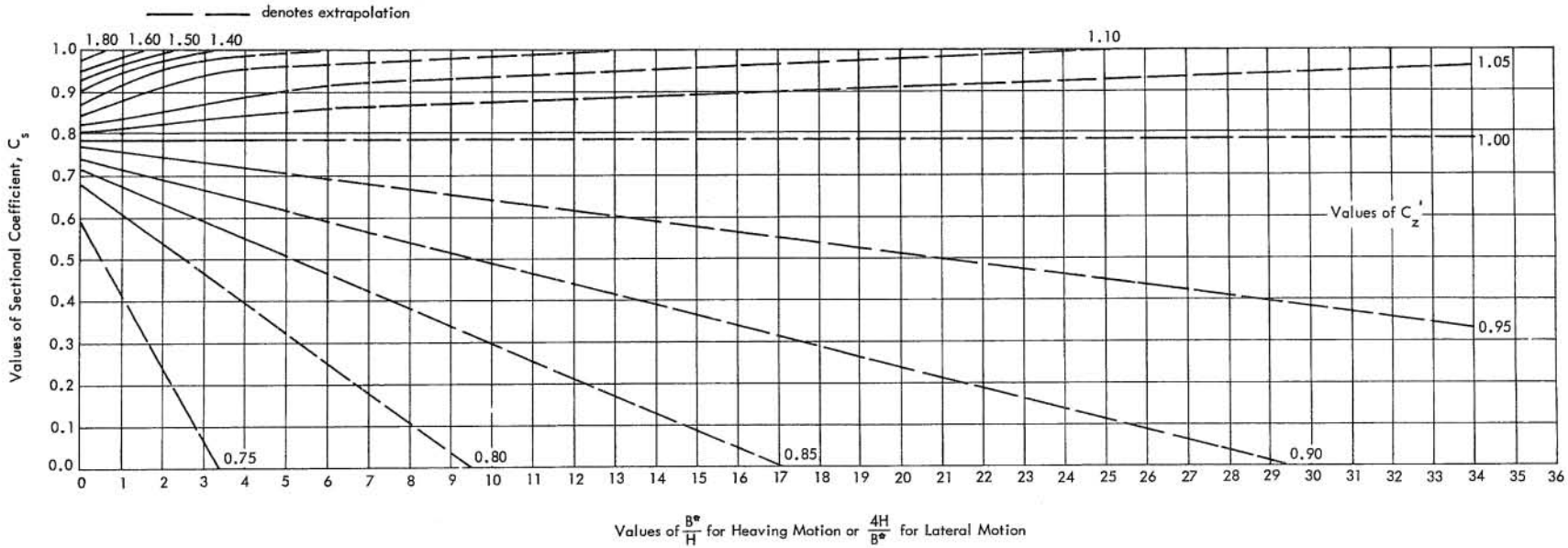

Figure B-3. Extrapolation of coefficient C_z' from data by Prohaska (1947).

Table B-7. Coefficient C_z' for Lateral Motions at 1-Foot Intervals Along ξ Axis

Index	Moment Arm, ξ	ξ^2	C_z'	$C_z'\xi$	$C_z'\xi^2$
1	-48.50	2.34256×10^3	1.80	-8.2120×10^1	4.2166×10^3
2	-47.50	2.25625×10^3		-8.5500×10^1	4.0613×10^3
3	-46.50	2.16225×10^3		-8.3900×10^1	3.8921×10^3
4	-45.50	2.07025×10^3		-8.1900×10^1	3.7265×10^3
5	-44.50	1.98025×10^3		-8.0100×10^1	3.5644×10^3
6	-43.50	1.89225×10^3		-7.8300×10^1	3.4061×10^3
7	-42.50	1.80625×10^3		-7.6500×10^1	3.2513×10^3
8	-41.50	1.72225×10^3		-7.4700×10^1	3.1000×10^3
9	-40.50	1.64025×10^3		-7.2900×10^1	2.9525×10^3
10	-39.50	1.56025×10^3	1.80	-7.1100×10^1	2.8084×10^3
11	-38.50	1.48225×10^3	1.80	-6.9300×10^1	2.6681×10^3
12	-37.50	1.40625×10^3		-6.7500×10^1	2.5312×10^3
13	-36.50	1.33225×10^3		-6.5700×10^1	2.3981×10^3
14	-35.50	1.26025×10^3		-6.3900×10^1	2.2685×10^3
15	-34.50	1.19025×10^3		-6.2100×10^1	2.1424×10^3
16	-33.50	1.12225×10^3		-6.0300×10^1	2.0200×10^3
17	-32.50	1.05625×10^3		-5.8500×10^1	1.9013×10^3
18	-31.50	9.9225×10^2		-5.6700×10^1	1.7860×10^3
19	-30.50	9.3025×10^2		-5.4900×10^1	1.6745×10^3
20	-29.50	8.7025×10^2	1.80	-5.3100×10^1	1.5664×10^3
21	-28.50	8.1225×10^2	1.80	-5.1300×10^1	1.4621×10^3
22	-27.50	7.5625×10^2		-4.9500×10^1	1.3612×10^3
23	-26.50	7.0225×10^2		-4.7700×10^1	1.2641×10^3
24	-25.50	6.5025×10^2		-4.5900×10^1	1.1704×10^3
25	-24.50	6.0025×10^2		-4.4100×10^1	1.0805×10^3
26	-23.50	5.5225×10^2		-4.2300×10^1	9.9405×10^2
27	-22.50	5.0625×10^2		-4.0500×10^1	9.1125×10^2
28	-21.50	4.6225×10^2		-3.8700×10^1	8.3205×10^2
29	-20.50	4.2025×10^2		-3.6900×10^1	7.5645×10^2
30	-19.50	3.8025×10^2	1.80	-3.5100×10^1	6.8445×10^2
31	-18.50	3.4225×10^2	1.80	-3.3300×10^1	6.1605×10^2
32	-17.50	3.0625×10^2		-3.1500×10^1	5.5125×10^2
33	-16.50	2.7225×10^2		-2.9700×10^1	4.9005×10^2
34	-15.50	2.4025×10^2		-2.7900×10^1	4.3245×10^2
35	-14.50	2.1025×10^2		-2.6100×10^1	3.7845×10^2
36	-13.50	1.8225×10^2		-2.4300×10^1	3.2805×10^2
37	-12.50	1.5625×10^2		-2.2500×10^1	2.8125×10^2
38	-11.50	1.3225×10^2		-2.0700×10^1	2.3805×10^2
39	-10.50	1.1025×10^2		-1.8900×10^1	1.9845×10^2
40	-9.50	9.0250×10^1	1.80	-1.7100×10^1	1.6245×10^2
41	-8.50	7.2250×10^1	1.80	-1.5300×10^1	1.3005×10^2
42	-7.50	5.6250×10^1		-1.3500×10^1	1.0125×10^2
43	-6.50	4.2250×10^1		-1.1700×10^1	7.6050×10^1
44	-5.50	3.0250×10^1		-9.9000	5.4950×10^1
45	-4.50	2.0250×10^1		-8.1000	3.6450×10^1
46	-3.50	1.2250×10^1		-6.3000	2.2050×10^1
47	-2.50	6.2500		-4.5000	1.1250×10^1
48	-1.50	2.2500		-2.7000	4.0500
49	-0.50	0.2500		-0.9000	0.4500
50	0.000	0.0000	1.80	0.0000	0.0000
51	0.50	0.2500	1.80	0.9000	0.4500
52	1.50	2.2500		2.7000	4.0500
53	2.50	6.2500		4.5000	1.1250×10^1
54	3.50	1.2250×10^1		6.3000	2.2050×10^1
55	4.50	2.0250×10^1		8.1000	3.6450×10^1
56	5.50	3.0250×10^1		9.9000	5.4450×10^1
57	6.50	4.2250×10^1		1.1700×10^1	7.6050×10^1
58	7.50	5.6250×10^1		1.3500×10^1	1.0125×10^2
59	8.50	7.2250×10^1		1.5300×10^1	1.3005×10^2
60	9.50	9.0250×10^1	1.80	1.7100×10^1	1.6245×10^2

Index	Moment Arm, ξ	ξ^2	C_z'	$C_z'\xi$	$C_z'\xi^2$
61	10.50	1.1025×10^2	1.80	1.8900×10^1	1.9845×10^2
62	11.50	1.3225×10^2	1.80	2.0700×10^1	2.3805×10^2
63	12.50	1.5625×10^2	1.80	2.2500×10^1	2.8125×10^2
64	13.50	1.8225×10^2	1.87	2.5245×10^1	3.4081×10^2
65	14.50	2.1025×10^2		2.7115×10^1	3.9317×10^2
66	15.50	2.4025×10^2		2.8985×10^1	4.4926×10^2
67	16.50	2.7225×10^2		3.0855×10^1	5.0911×10^2
68	17.50	3.0625×10^2		3.2725×10^1	5.7248×10^2
69	18.50	3.4225×10^2		3.4595×10^1	6.4001×10^2
70	19.50	3.8025×10^2	1.87	3.6465×10^1	7.1106×10^2
71	20.50	4.2025×10^2	1.87	3.8335×10^1	7.8587×10^2
72	21.50	4.6225×10^2		4.0205×10^1	8.6440×10^2
73	22.50	5.0625×10^2		4.2075×10^1	9.4669×10^2
74	23.50	5.5225×10^2		4.3945×10^1	1.0327×10^3
75	24.50	6.0025×10^2		4.5815×10^1	1.1225×10^3
76	25.50	6.5025×10^2		4.7685×10^1	1.2160×10^3
77	26.50	7.0225×10^2		4.9555×10^1	1.3132×10^3
78	27.50	7.5625×10^2		5.1425×10^1	1.4142×10^3
79	28.50	8.1225×10^2		5.3295×10^1	1.5189×10^3
80	29.50	8.7025×10^2	1.87	5.5165×10^1	1.6274×10^3
81	30.50	9.3025×10^2	1.87	5.7035×10^1	1.7396×10^3
82	31.50	9.9225×10^2	1.87	5.8905×10^1	1.8555×10^3
83	32.50	1.05625×10^3	1.87	6.0775×10^1	1.9752×10^3
84	33.50	1.12225×10^3	1.87	6.2645×10^1	2.0986×10^3
85	34.50	1.19025×10^3	1.87	6.4515×10^1	2.2258×10^3
86	35.50	1.26025×10^3	1.87	6.6385×10^1	2.3567×10^3
87	36.50	1.33225×10^3	1.88	6.8620×10^1	2.5096×10^3
88	37.50	1.40625×10^3	1.90	7.1250×10^1	2.6719×10^3
89	38.50	1.48225×10^3	1.91	7.3535×10^1	2.8311×10^3
90	39.50	1.56025×10^3	1.91	7.5445×10^1	2.9801×10^3
91	40.50	1.64025×10^3	1.91	7.7355×10^1	3.1329×10^3
92	41.50	1.72225×10^3	1.91	7.9265×10^1	3.2895×10^3
93	42.50	1.80625×10^3	1.92	8.1600×10^1	3.4680×10^3
94	43.50	1.89225×10^3	1.92	8.3520×10^1	3.6331×10^3
95	44.50	1.98025×10^3	1.84	8.1880×10^1	3.6437×10^3
96	45.50	2.07025×10^3	1.85	8.4175×10^1	3.8299×10^3
97	46.50	2.16225×10^3	1.86	8.6490×10^1	4.0218×10^3
98	47.50	2.25625×10^3	1.87	8.8825×10^1	4.2191×10^3
99	48.50	2.35225×10^3	1.88	9.1180×10^1	4.4222×10^3
100	49.50	2.45025×10^3	1.89	9.3555×10^1	4.6310×10^3
101	50.50	2.55025×10^3	1.90	9.5950×10^1	4.8455×10^3
102	51.50	2.65225×10^3	1.92	9.8880×10^1	5.0923×10^3
103	52.36	2.74157×10^3	1.92	1.0053×10^2	5.2638×10^3
$\Sigma C_B'$			1.8777×10^2	4.6646×10^2	1.6174×10^3
$\omega = 2.84$	$\rho(1-\frac{2}{\pi}\frac{\omega^2 H}{g})\frac{\pi H^2}{2} = 15.4302$			2.8973×10^3	7.1996×10^3	2.4957×10^6
$\omega = 2.01$	"	$= 45.7283$		8.5862×10^3	2.7330×10^4	7.3959×10^6
$\omega = 1.64$	"	$= 55.8913$		1.0495×10^4	2.6071×10^4	9.0399×10^6
$\omega = 1.42$	"	$= 60.9579$		1.1446×10^4	2.8434×10^4	9.8593×10^6
$\omega = 1.16$	"	$= 66.0064$		1.2394×10^4	3.0789×10^4	1.0676×10^7
$\omega = 0.90$	"	$= 70.0374$		1.3157×10^4	3.2670×10^4	1.1328×10^7
$\omega = 0.76$	"	$= 71.7865$		1.3479×10^4	3.3486×10^4	1.1611×10^7
$\omega = 0.66$	"	$= 72.8552$		1.3680×10^4	3.3984×10^4	1.1784×10^7

Added Mass in Sway Due to Motion in Roll, A_{42}'

The added mass in sway due to motion in roll is given by Hu (1961) as

$$A_{42}' = C_{42}' \frac{\rho \pi H^3}{2} \tag{B-10}$$

Values of C_{42}' were computed by Hu for Lewis-form sections as functions of the parameters, beam-draft ratios, and section coefficients. Kaplan and Putz performed additional computations to enlarge the range of parameters given by Hu. The large beam-draft ratios of the present problem required a further extension of Hu's work. These results are shown in Figure B-4. Hu* states that the extrapolation employed is reasonable and the large negative values of C_{42}' confirm the fact that swaying does not induce rolling on craft with large beam-draft ratios. Table B-8 presents values of C_{42}' and $C_{42}'\xi$ for the various beam-draft ratios as obtained from Figure B-4.

Sectional Damping Factor, N_{zz}'

Vossers (1960) states that there is a direct connection between the sectional damping coefficients and the amplitude of the waves emitted, since "damping is exclusively due to the fact that waves are sent out which carry off energy." For heaving motions, the following formula has been adopted:

$$N_{zz}' = \frac{\rho g^2}{\omega^3} (\overline{A}_z)^2 \tag{B-11}$$

$\overline{A}_z$ is the ratio of the amplitude of heave-generated two-dimensional waves to the amplitude of heaving motion of the section. Values of $\overline{A}_z$ are given by Grim (1959a), which were derived for Lewis from ship sections, as functions of varying beam-draft ratios and a frequency parameter. An example for a sectional coefficient of 1.0 is given in Figure B-5. In order to use Grim's results, Figure B-6 was prepared from Figure B-5 with the aid of an auxiliary logarithmic plot. For ease in tabulating values of $\overline{A}_z$, Figures B-7, B-8 and B-8a were prepared. Values of $\overline{A}_z$ are presented in Table B-9.

Sectional Damping Factor, N_{yy}'

As in the case for heaving motion, the sectional damping factor for swaying motion, N_{yy}', is related to $\overline{A}_y$ by the following formula:

$$N_{yy}' = \frac{\rho g^2}{\omega^3} (\overline{A}_y)^2 \tag{B-12}$$

*Personal communication with Dr. J. P. Breslin, 15 April, 1964.

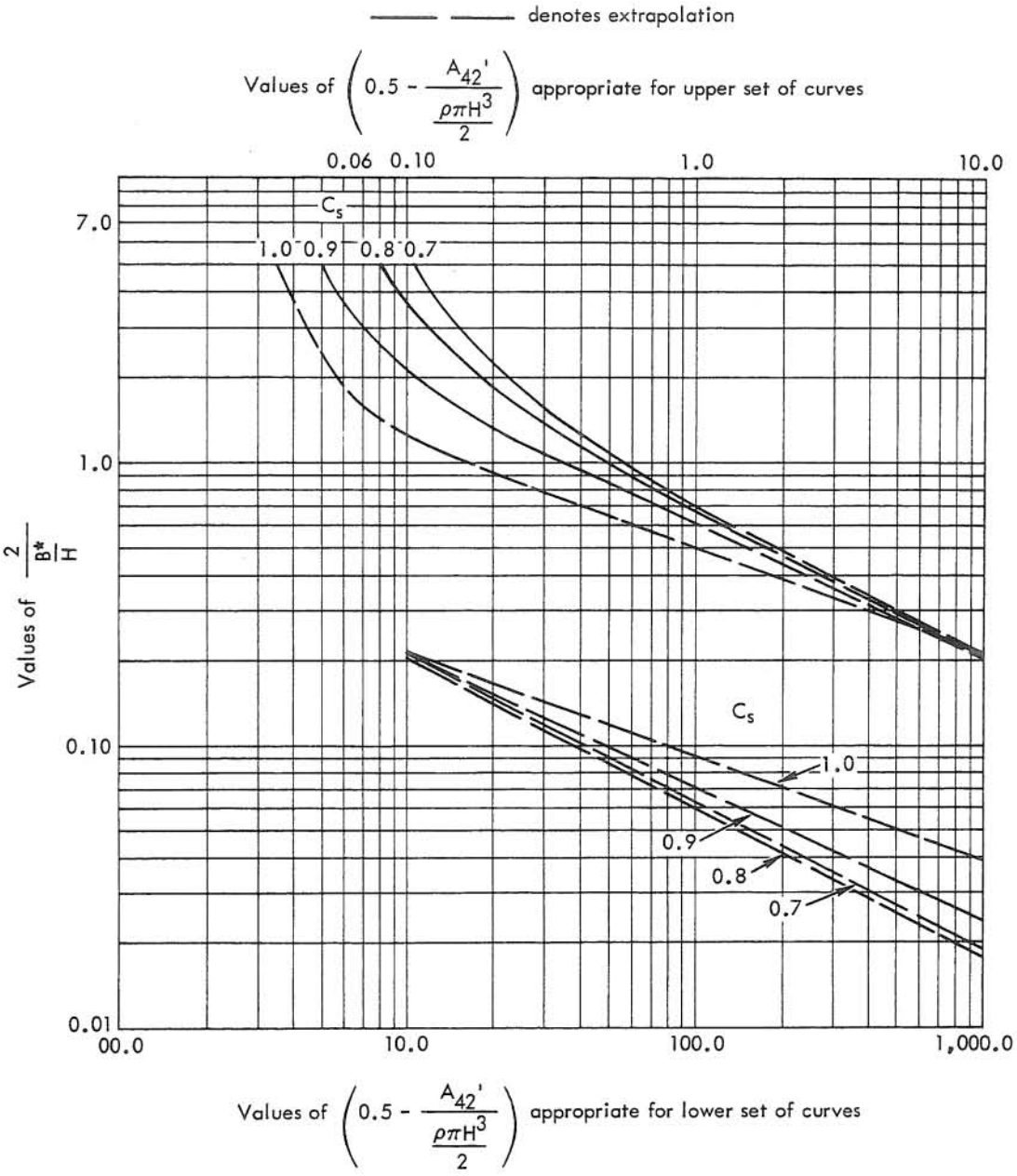

Figure B-4. Extrapolation of added mass coefficient in sway due to motion in roll. (Based on data from Kaplan and Putz, 1962, and Hu, 1961.)

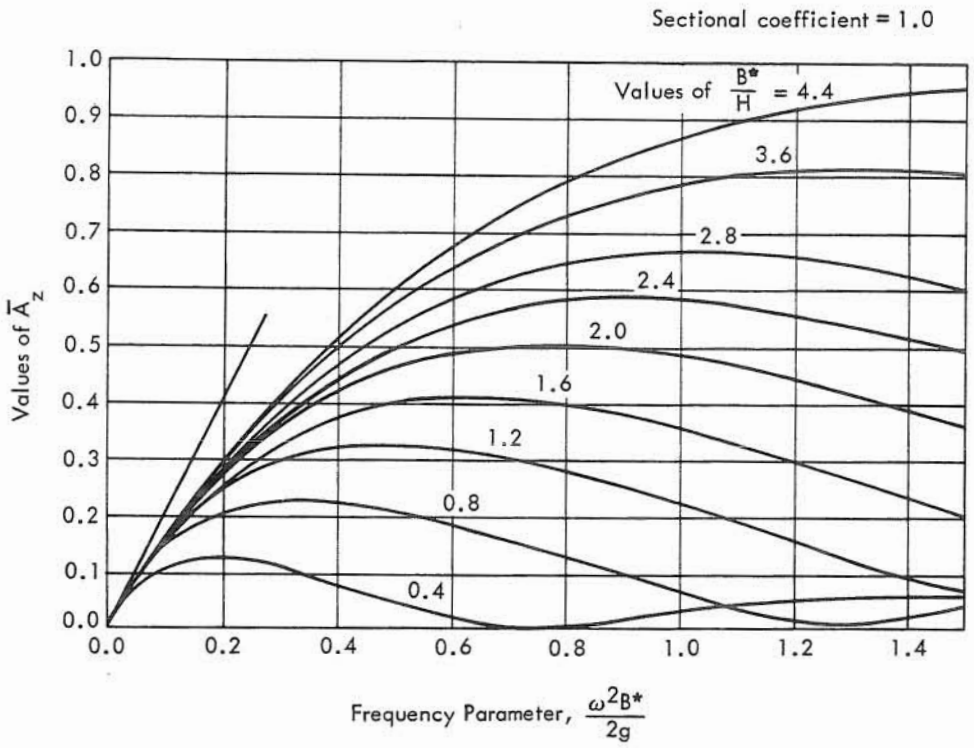

Figure B-5. Ratio of amplitude of two-dimensional heave-generated wave to amplitude of heaving motion. (From Grim, (1959a.)

In Equation B-12, $\bar{A}_y$ is the ratio of the amplitude of the sway-generated wave to the amplitude of swaying motion of the section. Vossers (1960) gives the following formula for calculating $\bar{A}_y$:

$$\bar{A}_y = \left(\frac{\omega^2 B^*}{2g}\right)^2 d_y \qquad \text{(B-13)}$$

where d_y is a coefficient whose values were calculated by Grim for Lewis-form sections and is a function of the beam-draft ratio and sectional (area) coefficient. Vossers states that these calculations are reliable for values up to $\omega^2 B^*/2g = 0.3$ and that a few calculations have been made for special shapes for higher values, but that little is as yet known about them. Values of d_y presented by Vossers are shown in Figure B-9 as the solid lines. The extrapolated values required for the present study were obtained with the use of an auxiliary logarithmic plot and are shown as the dashed curves in Figure B-9. Sectional values of d_y at 1-foot intervals along the ξ axis are shown in Table B-10. Table B-10 also includes values of other terms which will be used in the computation of the matrix elements.

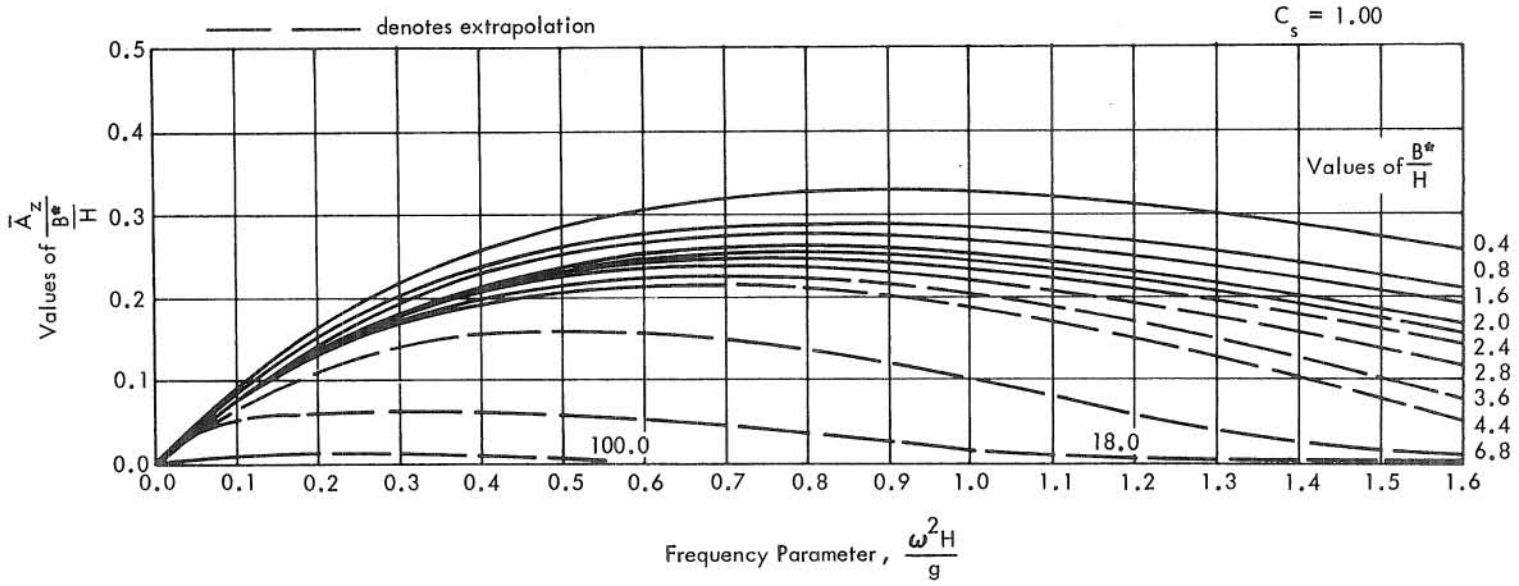

Figure B-6. Extrapolation of Grim's amplitude ratio, A_z (Grim, 1959a), for large beam-draft ratios.

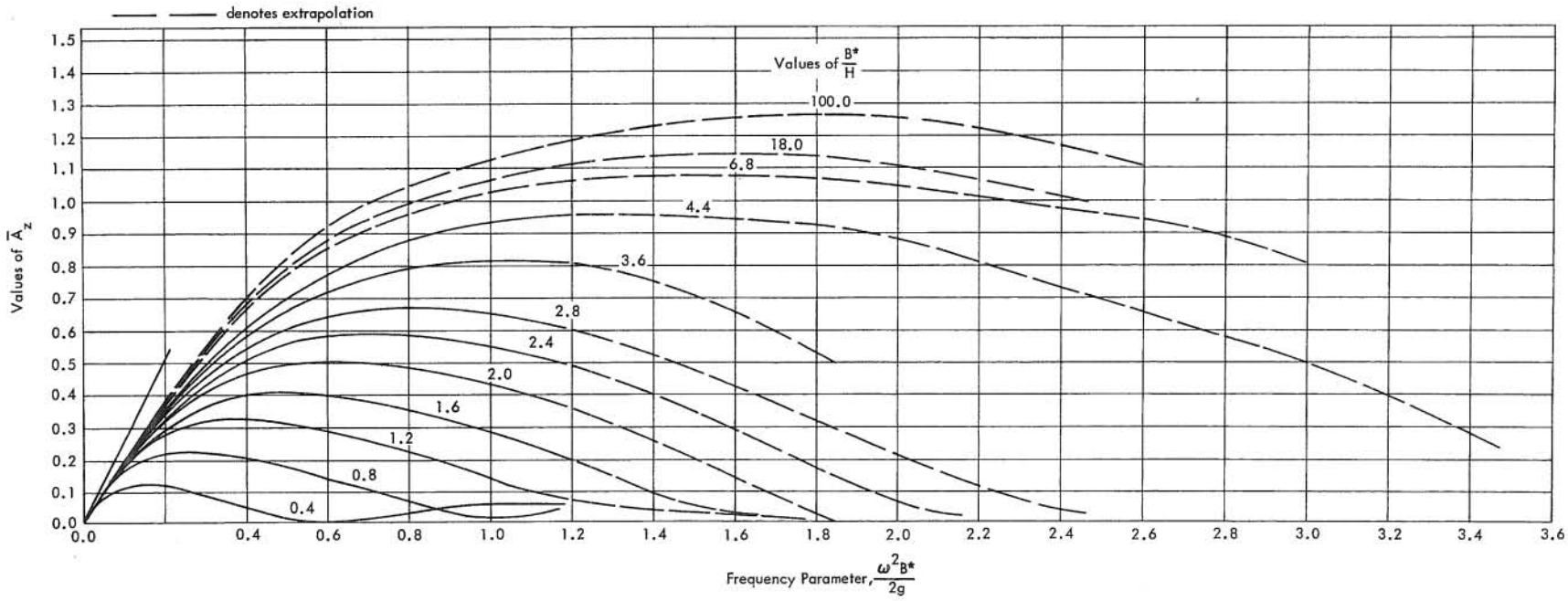

Figure B-7. Extrapolation of Grim's amplitude ratio, $\bar{A}_Z$ (Grim, 1959a) for large beam-draft ratios.

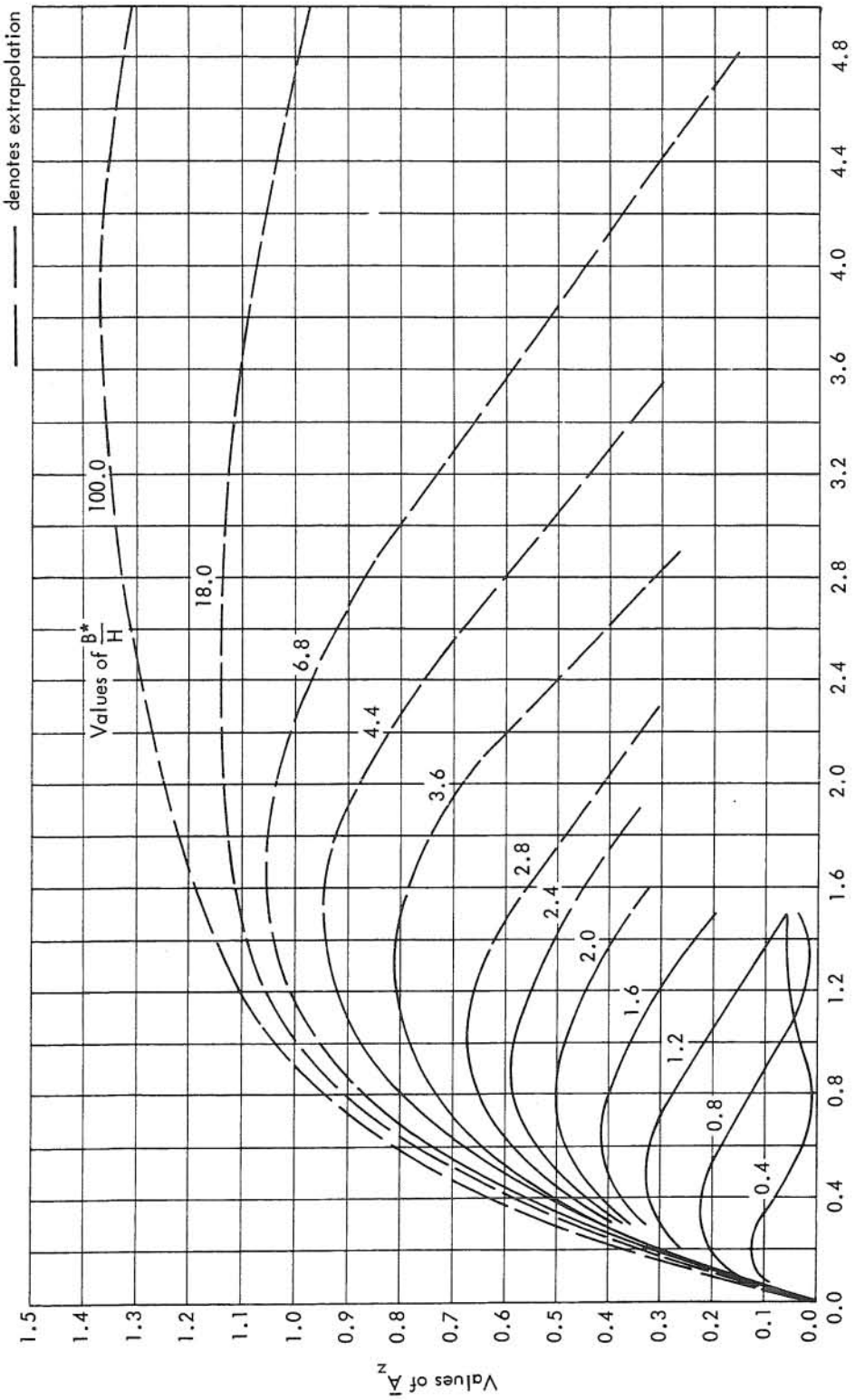

Figure B-8. Extrapolation of Grim's amplitude ratio, $\bar{A}_z$ (Grim, 1959a), for large beam-draft ratios.

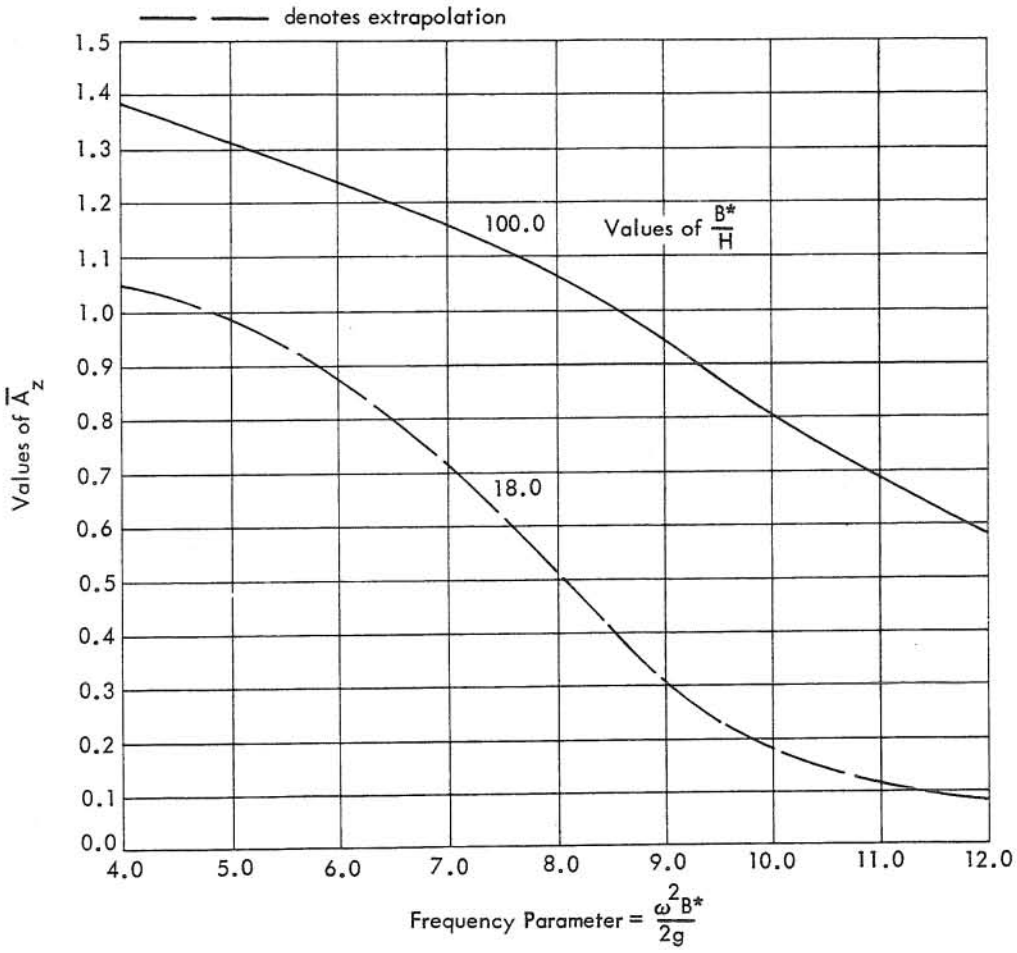

Figure B-8a. Extrapolation of Grim's amplitude ratio, $\bar{A}_z$ (Grim, 1959a), for large beam-draft ratios.

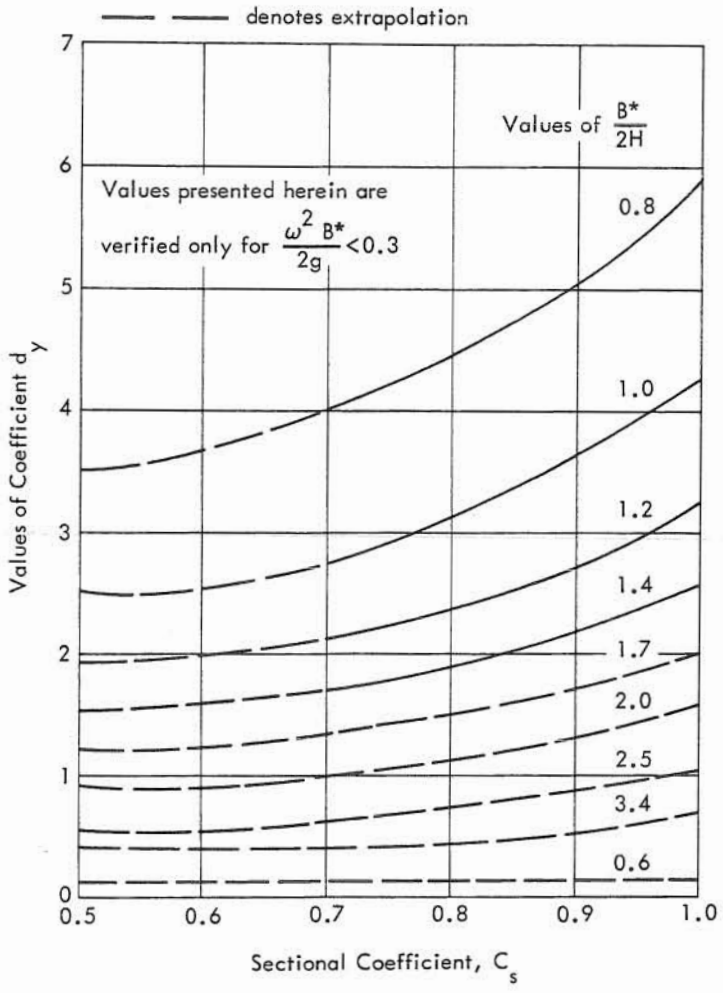

Figure B-9. Extrapolation of coefficient d_y from data by Vossers (1960).

Table B-8. Values of C_{42}' at 1-Foot Intervals Along ξ Axis

Index	Moment Arm, ξ	C_{42}'	$C_{42}'\xi$
1	-48.50	-3.50	1.6940×10^{2}
2	-47.50		1.6625×10^{2}
3	-46.50		1.6275×10^{2}
4	-45.50		1.5925×10^{2}
5	-44.50		1.5575×10^{2}
6	-43.50		1.5225×10^{2}
7	-42.50		1.4875×10^{2}
8	-41.50		1.4525×10^{2}
9	-40.50		1.4175×10^{2}
10	-39.50	-3.50	1.3825×10^{2}
11	-38.50	-3.50	1.3475×10^{2}
12	-37.50		1.3125×10^{2}
13	-36.50		1.2775×10^{2}
14	-35.50		1.2425×10^{2}
15	-34.50		1.2075×10^{2}
16	-33.50		1.1725×10^{2}
17	-32.50		1.1375×10^{2}
18	-31.50		1.1025×10^{2}
19	-30.50		1.0675×10^{2}
20	-29.50	-3.50	1.0325×10^{2}
21	-28.50	-3.50	9.9750×10^{1}
22	-27.50		9.6250×10^{1}
23	-26.50		9.2750×10^{1}
24	-25.50		8.9250×10^{1}
25	-24.50		8.5750×10^{1}
26	-23.50		8.2250×10^{1}
27	-22.50		7.8750×10^{1}
28	-21.50		7.5250×10^{1}
29	-20.50		7.1750×10^{1}
30	-19.50	-3.50	6.8250×10^{1}
31	-18.50	-3.50	6.4750×10^{1}
32	-17.50		6.1250×10^{1}
33	-16.50		5.7750×10^{1}
34	-15.50		5.4250×10^{1}
35	-14.50		5.0750×10^{1}
36	-13.50		4.7250×10^{1}
37	-12.50		4.3750×10^{1}
38	-11.50		4.0250×10^{1}
39	-10.50		3.6750×10^{1}
40	-9.50	-3.50	3.3250×10^{1}
41	-8.50	-3.50	2.9750×10^{1}
42	-7.50		2.6250×10^{1}
43	-6.50		2.2750×10^{1}
44	-5.50		1.9250×10^{1}
45	-4.50		1.5750×10^{1}
46	-3.50		1.2250×10^{1}
47	-2.50		8.7500
48	-1.50		5.2500
49	-0.50		1.7500
50	0.0000	-3.50	0.0000
51	0.50	-3.50	-1.7500
52	1.50		-5.2500
53	2.50		-8.7500
54	3.50		-1.2250×10^{1}
55	4.50		-1.5750×10^{1}
56	5.50		-1.9250×10^{1}
57	6.50		-2.2750×10^{1}
58	7.50		-2.6250×10^{1}
59	8.50		-2.9750×10^{1}
60	9.50	-3.50	-3.3250×10^{1}
61	10.50	-3.50	-4.0250×10^{1}
62	11.50	-3.50	-4.3750×10^{1}
63	12.50	-3.50	-4.7250×10^{1}
64	13.50	-52.50	-7.7625×10^{2}
65	14.50		-8.3375×10^{2}
66	15.50		-8.9125×10^{2}
67	16.50		-9.4875×10^{2}
68	17.50		-1.0063×10^{3}
69	18.50		-1.0638×10^{3}
70	19.50	-52.50	-1.1212×10^{3}
71	20.50	-52.50	-1.1788×10^{3}
72	21.50		-1.2362×10^{3}
73	22.50		-1.2938×10^{3}
74	23.50		-1.3512×10^{3}
75	24.50		-1.4088×10^{3}
76	25.50		-1.4662×10^{3}
77	26.50		-1.5238×10^{3}
78	27.50		-1.5812×10^{3}
79	28.50		-1.6388×10^{3}
80	29.50	-52.50	-1.6962×10^{3}
81	30.50	-52.50	-1.7538×10^{3}
82	31.50	-52.50	-1.8112×10^{3}
83	32.50	-52.50	-1.8688×10^{3}
84	33.50	-52.50	-1.9263×10^{3}
85	34.50	-67.00	-2.3115×10^{3}
86	35.50	-74.50	-2.6447×10^{3}
87	36.50	-94.50	-3.4493×10^{3}
88	37.50	-135.00	-5.0625×10^{3}
89	38.50	-235.00	-9.0475×10^{3}
90	39.50	-235.00	-9.2825×10^{3}
91	40.50	-235.00	-9.5175×10^{3}
92	41.50	-315.00	-1.3073×10^{4}
93	42.50	-435.00	-1.8487×10^{4}
94	43.50	-600.00	-2.6100×10^{4}
95	44.50	-19.00	-8.4550×10^{2}
96	45.50	-27.50	-1.2513×10^{3}
97	46.50	-41.50	-1.9297×10^{3}
98	47.50	-76.00	-3.6100×10^{3}
99	48.50	-153.00	-7.4205×10^{3}
100	49.50	-410.00	-2.0295×10^{4}
101	50.50	-1860.00	-9.3930×10^{4}
102	51.50	0.00	0.0000
103	52.36	0.00	0.0000
$\int C_{42}' \xi \rho$		-6.4421×10^{3}	
$\int C_{42}' \xi d\rho$			-2.5283×10^{5}
$\int A_{42}' \xi \rho$		-2.4539×10^{6}	
$\int A_{42}' \xi d\rho$			-9.6309×10^{7}

Table B-9. Values of $\bar{A}_z$ at 1-Foot Intervals Along ξ Axis

INDEX \ λ	25'	50'	75'	100'	150'	250'	350'	450'
001	0.35	1.02	1.04	1.00	0.82	0.57	0.44	0.34
002	0.35	1.02	1.04	1.00	0.82	0.57	0.44	0.34
003	0.35	1.02	1.04	1.00	0.82	0.57	0.44	0.34
004	0.35	1.02	1.04	1.00	0.82	0.57	0.44	0.34
005	0.35	1.02	1.04	1.00	0.82	0.57	0.44	0.34
006	0.35	1.02	1.04	1.00	0.82	0.57	0.44	0.34
007	0.35	1.02	1.04	1.00	0.82	0.57	0.44	0.34
008	0.35	1.02	1.04	1.00	0.82	0.57	0.44	0.34
009	0.35	1.02	1.04	1.00	0.82	0.57	0.44	0.34
010	0.35	1.02	1.04	1.00	0.82	0.57	0.44	0.34
011	0.35	1.02	1.04	1.00	0.82	0.57	0.44	0.34
012	0.35	1.02	1.04	1.00	0.82	0.57	0.44	0.34
013	0.35	1.02	1.04	1.00	0.82	0.57	0.44	0.34
014	0.35	1.02	1.04	1.00	0.82	0.57	0.44	0.34
015	0.35	1.02	1.04	1.00	0.82	0.57	0.44	0.34
016	0.35	1.02	1.04	1.00	0.82	0.57	0.44	0.34
017	0.35	1.02	1.04	1.00	0.82	0.57	0.44	0.34
018	0.35	1.02	1.04	1.00	0.82	0.57	0.44	0.34
019	0.35	1.02	1.04	1.00	0.82	0.57	0.44	0.34
020	0.35	1.02	1.04	1.00	0.82	0.57	0.44	0.34
021	0.35	1.02	1.04	1.00	0.82	0.57	0.44	0.34
022	0.35	1.02	1.04	1.00	0.82	0.57	0.44	0.34
023	0.35	1.02	1.04	1.00	0.82	0.57	0.44	0.34
024	0.35	1.02	1.04	1.00	0.82	0.57	0.44	0.34
025	0.35	1.02	1.04	1.00	0.82	0.57	0.44	0.34
026	0.35	1.02	1.04	1.00	0.82	0.57	0.44	0.34
027	0.35	1.02	1.04	1.00	0.82	0.57	0.44	0.34
028	0.35	1.02	1.04	1.00	0.82	0.57	0.44	0.34
029	0.35	1.02	1.04	1.00	0.82	0.57	0.44	0.34
030	0.35	1.02	1.04	1.00	0.82	0.57	0.44	0.34
031	0.35	1.02	1.04	1.00	0.82	0.57	0.44	0.34
032	0.35	1.02	1.04	1.00	0.82	0.57	0.44	0.34
033	0.35	1.02	1.04	1.00	0.82	0.57	0.44	0.34
034	0.35	1.02	1.04	1.00	0.82	0.57	0.44	0.34
035	0.35	1.02	1.04	1.00	0.82	0.57	0.44	0.34
036	0.35	1.02	1.04	1.00	0.82	0.57	0.44	0.34
037	0.35	1.02	1.04	1.00	0.82	0.57	0.44	0.34
038	0.35	1.02	1.04	1.00	0.82	0.57	0.44	0.34
039	0.35	1.02	1.04	1.00	0.82	0.57	0.44	0.34
040	0.35	1.02	1.04	1.00	0.82	0.57	0.44	0.34
041	0.35	1.02	1.04	1.00	0.82	0.57	0.44	0.34
042	0.35	1.02	1.04	1.00	0.82	0.57	0.44	0.34
043	0.35	1.02	1.04	1.00	0.82	0.57	0.44	0.34
044	0.35	1.02	1.04	1.00	0.82	0.57	0.44	0.34
045	0.35	1.02	1.04	1.00	0.82	0.57	0.44	0.34
046	0.35	1.02	1.04	1.00	0.82	0.57	0.44	0.34
047	0.35	1.02	1.04	1.00	0.82	0.57	0.44	0.34
048	0.35	1.02	1.04	1.00	0.82	0.57	0.44	0.34
049	0.35	1.02	1.04	1.00	0.82	0.57	0.44	0.34
050	0.35	1.02	1.04	1.00	0.82	0.57	0.44	0.34
051	0.35	1.02	1.04	1.00	0.82	0.57	0.44	0.34
052	0.35	1.02	1.04	1.00	0.82	0.57	0.44	0.34
053	0.35	1.02	1.04	1.00	0.82	0.57	0.44	0.34
054	0.35	1.02	1.04	1.00	0.82	0.57	0.44	0.34
055	0.35	1.02	1.04	1.00	0.82	0.57	0.44	0.34
056	0.35	1.02	1.04	1.00	0.82	0.57	0.44	0.34
057	0.35	1.02	1.04	1.00	0.82	0.57	0.44	0.34
058	0.35	1.02	1.04	1.00	0.82	0.57	0.44	0.34
059	0.35	1.02	1.04	1.00	0.82	0.57	0.44	0.34
060	0.35	1.02	1.04	1.00	0.82	0.57	0.44	0.34
061	0.35	1.02	1.04	1.00	0.82	0.57	0.44	0.34
062	0.35	1.02	1.04	1.00	0.82	0.57	0.44	0.34
063	0.35	1.02	1.04	1.00	0.82	0.57	0.44	0.34
064	0.10	0.93	1.09	1.14	1.13	1.04	0.90	0.78
065	0.10	0.93	1.09	1.14	1.13	1.04	0.90	0.78
066	0.10	0.93	1.09	1.14	1.13	1.04	0.90	0.78
067	0.10	0.93	1.09	1.14	1.13	1.04	0.90	0.78
068	0.10	0.93	1.09	1.14	1.13	1.04	0.90	0.78
069	0.10	0.93	1.09	1.14	1.13	1.04	0.90	0.78
070	0.10	0.93	1.09	1.14	1.13	1.04	0.90	0.78
071	0.10	0.93	1.09	1.14	1.13	1.04	0.90	0.78
072	0.10	0.93	1.09	1.14	1.13	1.04	0.90	0.78
073	0.10	0.93	1.09	1.14	1.13	1.04	0.90	0.78
074	0.10	0.93	1.09	1.14	1.13	1.04	0.90	0.78
075	0.10	0.93	1.09	1.14	1.13	1.04	0.90	0.78
076	0.10	0.93	1.09	1.14	1.13	1.04	0.90	0.78
077	0.10	0.93	1.09	1.14	1.13	1.04	0.90	0.78
078	0.10	0.93	1.09	1.14	1.13	1.04	0.90	0.78
079	0.10	0.93	1.09	1.14	1.13	1.04	0.90	0.78
080	0.10	0.93	1.09	1.14	1.13	1.04	0.90	0.78
081	0.10	0.93	1.09	1.14	1.13	1.04	0.90	0.78
082	0.10	0.93	1.09	1.14	1.13	1.04	0.90	0.78
083	0.10	0.93	1.09	1.14	1.13	1.04	0.90	0.78
084	0.10	0.93	1.09	1.14	1.13	1.04	0.90	0.78
085	0.11	0.93	1.10	1.14	1.13	1.04	0.90	0.78
086	0.11	0.94	1.10	1.14	1.13	1.04	0.90	0.78
087	0.12	0.95	1.11	1.14	1.13	1.04	0.90	0.78
088	0.14	0.98	1.12	1.15	1.13	1.04	0.90	0.78
089	0.19	1.02	1.15	1.17	1.14	1.04	0.90	0.78
090	0.19	1.02	1.15	1.17	1.14	1.04	0.90	0.78
091	0.19	1.02	1.15	1.17	1.14	1.04	0.90	0.78
092	0.21	1.04	1.18	1.18	1.15	1.04	0.90	0.78
093	0.24	1.05	1.19	1.18	1.15	1.05	0.91	0.78
094	0.27	1.07	1.21	1.19	1.16	1.05	0.91	0.78
095	0.99	1.06	1.04	0.82	0.59	0.41	0.30	0.26
096	1.03	1.07	1.04	0.82	0.60	0.41	0.30	0.26
097	1.09	1.08	1.04	0.83	0.61	0.41	0.30	0.26
098	1.15	1.09	1.07	0.83	0.62	0.41	0.30	0.26
099	1.16	1.11	1.08	0.83	0.62	0.41	0.30	0.26
100	1.18	1.12	1.09	0.84	0.62	0.41	0.30	0.26
101	1.24	1.14	1.10	0.86	0.63	0.41	0.30	0.26
102	1.35	1.15	1.13	0.88	0.64	0.41	0.30	0.26
103	1.40	1.17	1.14	0.89	0.65	0.41	0.30	0.26

Table B-10. Coefficient d_y at 1-Foot Intervals Along ξ Axis

Index	B^{*4}	d_y^2	$B^{*4}d_y^2$	ξ_i	ξ_i^2	$B^{*4}d_y^2\xi_i^2$	$B^{*4}d_y^2\xi_i^4$
1	6.5640×10^7	0.49	3.21489×10^7	-48.50	2.35225×10^3	$-.5560 \times 10^9$	9.5311×10^{10}
2				-47.50	2.25625×10^3	-1.5221×10^9	7.3536×10^{10}
3				-46.50	2.16225×10^3	-1.4949×10^9	6.9574×10^{10}
4				-45.50	2.07025×10^3	-1.4685×10^9	6.4556×10^{10}
5				-44.50	1.98025×10^3	-1.4306×10^9	6.3643×10^{10}
6				-43.50	1.89225×10^3	-1.3985×10^9	6.0834×10^{10}
7				-42.50	1.80625×10^3	-1.3663×10^9	5.8069×10^{10}
8				-41.50	1.72225×10^3	-1.3342×10^9	5.5346×10^{10}
9				-40.50	1.64025×10^3	-1.3020×10^9	5.2732×10^{10}
10	6.5640×10^7	0.49	3.21489×10^7	-39.50	1.56025×10^3	-1.2699×10^9	5.0160×10^{10}
11	6.5640×10^7	0.49	3.21489×10^7	-38.50	1.48225×10^3	-1.2397×10^9	4.7653×10^{10}
12				-37.50	1.40625×10^3	-1.2056×10^9	4.5209×10^{10}
13				-36.50	1.33225×10^3	-1.1734×10^9	4.2830×10^{10}
14				-35.50	1.26025×10^3	-1.1413×10^9	4.0576×10^{10}
15				-34.50	1.19025×10^3	-1.1091×10^9	3.8265×10^{10}
16				-33.50	1.12225×10^3	-1.0770×10^9	3.6079×10^{10}
17				-32.50	1.05625×10^3	-1.0448×10^9	3.3957×10^{10}
18				-31.50	9.9225×10^2	-1.0127×10^9	3.1900×10^{10}
19				-30.50	9.3025×10^2	-9.8054×10^8	2.9907×10^{10}
20	6.5640×10^7	0.49	3.21489×10^7	-29.50	8.7025×10^2	-9.4839×10^8	2.7978×10^{10}
21	6.5640×10^7	0.49	3.21489×10^7	-28.50	8.1225×10^2	$-.9624 \times 10^8$	2.6113×10^{10}
22				-27.50	7.5625×10^2	-8.8409×10^8	2.4313×10^{10}
23				-26.50	7.0225×10^2	-8.5195×10^8	2.2577×10^{10}
24				-25.50	6.5025×10^2	-8.1980×10^8	2.0905×10^{10}
25				-24.50	6.0025×10^2	-7.8765×10^8	1.9297×10^{10}
26				-23.50	5.5225×10^2	-2.5550×10^8	1.7754×10^{10}
27				-22.50	5.0625×10^2	-7.2335×10^8	1.6275×10^{10}
28				-21.50	4.6225×10^2	-6.9120×10^8	1.4861×10^{10}
29				-20.50	4.2025×10^2	-6.5905×10^8	1.3511×10^{10}
30	6.5640×10^7	0.49	3.21489×10^7	-19.50	3.8025×10^2	-6.2690×10^8	1.2225×10^{10}
31	6.5640×10^7	0.49	3.21489×10^7	-18.50	3.4225×10^2	-5.9475×10^8	1.1005×10^{10}
32				-17.50	3.0625×10^2	-5.6261×10^8	9.8456×10^9
33				-16.50	2.7225×10^2	-5.3046×10^8	8.7525×10^9
34				-15.50	2.4025×10^2	-4.9831×10^8	7.7238×10^9
35				-14.50	2.1025×10^2	-4.6616×10^8	6.7543×10^9
36				-13.50	1.8225×10^2	-4.3401×10^8	5.8591×10^9
37				-12.50	1.5625×10^2	-4.0186×10^8	5.0283×10^9
38				-11.50	1.3225×10^2	-3.6971×10^8	4.2517×10^9
39				-10.50	1.1025×10^2	-3.3756×10^8	3.5444×10^9
40	6.5640×10^7	0.49	3.21489×10^7	-9.50	9.0250×10^1	-3.0541×10^8	2.9014×10^9
41	6.5640×10^7	0.49	3.21489×10^7	-8.50	7.2250×10^1	-2.7327×10^8	2.3228×10^9
42				-7.50	5.6250×10^1	-2.4112×10^8	1.8084×10^9
43				-6.50	4.2250×10^1	-2.0897×10^8	1.3583×10^9
44				-5.50	3.0250×10^1	-1.7682×10^8	9.7250×10^8
45				-4.50	2.0250×10^1	-1.4467×10^8	6.5702×10^8
46				-3.50	1.2250×10^1	-1.1252×10^8	3.9382×10^8
47				-2.50	6.2500	-8.0372×10^7	2.0093×10^8
48				-1.50	2.2500	-4.8223×10^7	7.2335×10^7
49				-0.50	0.2500	-1.6074×10^7	8.0372×10^6
50	6.5640×10^7	0.49	3.21489×10^7	0.00	0.0000	0.0000	0.0000
51	6.5640×10^7	0.49	3.21489×10^7	0.50	0.2500	1.6074×10^7	8.0372×10^6
52				1.50	2.2500	4.8223×10^7	7.2335×10^7
53				2.50	6.2500	8.0372×10^7	2.0093×10^8
54				3.50	1.2250×10^1	1.1252×10^8	3.9382×10^8
55				4.50	2.0250×10^1	1.4467×10^8	6.5102×10^8
56				5.50	3.0250×10^1	1.7682×10^8	9.7250×10^8
57				6.50	4.2250×10^1	2.0897×10^8	1.3583×10^9
58				7.50	5.6250×10^1	2.4112×10^8	1.8084×10^9
59				8.50	7.2250×10^1	2.7327×10^8	2.3228×10^9
60	6.5640×10^7	0.49	3.21489×10^7	9.50	9.0250×10^1	3.0541×10^8	2.9014×10^9
61	6.5640×10^7	0.49	3.21489×10^7	10.50	1.1025×10^2	3.3756×10^8	3.5444×10^9
62		0.49	3.21489×10^7	11.50	1.3225×10^2	3.6971×10^8	4.2517×10^9
63		0.49	3.21489×10^7	12.50	1.5625×10^2	4.0186×10^8	5.0283×10^9

52					1.50	2.2500	4.8223 x10^7	7.2335 x10^7	
53					2.50	6.2500	8.0372 x10^7	2.0093 x10^8	
54					3.50	1.2250 x10^1	1.1252 x10^8	3.9382 x10^8	
55					4.50	2.0250 x10^1	1.4467 x10^8	6.5102 x10^8	
56					5.50	3.0250 x10^1	1.7682 x10^8	9.7250 x10^8	
57					6.50	4.2250 x10^1	2.0897 x10^8	1.3583 x10^9	
58					7.50	5.6250 x10^1	2.4112 x10^8	1.8084 x10^9	
59					8.50	7.2250 x10^1	2.7327 x10^8	2.3228 x10^9	
60	6.5610 x10^7	0.49	3.21489 x10^7		9.50	9.0850 x10^1	3.0541 x10^8	2.9014 x10^9	
61	6.5610 x10^7	0.49	3.21489 x10^7		10.50	7.1025 x10^2	8.3256 x10^8	8.5448 x10^9	
62		0.49	3.21489 x10^7		11.50	1.3225 x10^2	3.6971 x10^8	4.2517 x10^9	
63		0.49	3.21489 x10^7		12.50	1.5625 x10^2	4.0186 x10^8	5.0233 x10^9	
64		0.0225	1.476225 x10^6		13.50	1.8225 x10^2	1.9939 x10^7	2.6904 x10^8	
65					14.50	2.1025 x10^2	2.1405 x10^7	3.1038 x10^8	
66					15.50	2.4025 x10^2	2.2881 x10^7	3.5446 x10^8	
67					16.50	2.7225 x10^2	2.4358 x10^7	4.0190 x10^8	
68					17.50	3.0625 x10^2	2.5834 x10^7	4.5269 x10^8	
69					18.50	3.4225 x10^2	2.7310 x10^7	5.0684 x10^8	
70	6.5610 x10^7	0.0225	1.476225 x10^6		19.50	3.8025 x10^2	2.8786 x10^7	5.6433 x10^8	
71	6.5610 x10^7	0.0225	1.476225 x10^6		20.50	4.2025 x10^2	3.0263 x10^7	6.2058 x10^8	
72					21.50	4.6225 x10^2	3.1739 x10^7	6.8239 x10^8	
73					22.50	5.0625 x10^2	3.3215 x10^7	7.4734 x10^8	
74					23.50	5.5225 x10^2	3.4691 x10^7	8.1525 x10^8	
75					24.50	6.0025 x10^2	3.6168 x10^7	8.8610 x10^8	
76					25.50	6.5025 x10^2	3.7644 x10^7	9.5992 x10^8	
77					26.50	7.0225 x10^2	3.9120 x10^7	1.0367 x10^9	
78					27.50	2.5625 x10^2	4.0596 x10^7	1.1169 x10^9	
79					28.50	8.1225 x10^2	4.2072 x10^7	1.1991 x10^9	
80	6.5610 x10^7	0.0225	1.476225 x10^6		29.50	8.7025 x10^2	4.3549 x10^7	1.2847 x10^9	
81	6.5610 x10^7	0.0225	1.476225 x10^6		30.50	9.3025 x10^2	4.5025 x10^7	1.3733 x10^9	
82		0.0225	1.476225 x10^6		31.50	9.9225 x10^2	4.6501 x10^7	1.4647 x10^9	
83		0.0225	1.476225 x10^6		32.50	1.0562 5x10^3	4.7977 x10^7	1.5592 x10^9	
84		0.0196	1.285956 x10^6		33.50	1.1222 5x10^3	4.8080 x10^7	1.4431 x10^9	
85		0.0196	1.285956 x10^6		34.50	1.1902 5x10^3	4.8365 x10^7	1.5306 x10^9	
86		0.0169	1.108809 x10^6		35.50	1.2602 5x10^3	3.9363 x10^7	1.3974 x10^9	
87		0.0121	7.93881 x10^5		36.50	1.3322 5x10^3	2.8979 x10^7	1.0576 x10^9	
88		0.0100	6.5610 x10^5		37.50	1.4062 5x10^3	2.4604 x10^7	9.2264 x10^8	
89		0.0049	3.21489 x10^5		38.50	1.4822 5x10^3	1.2373 x10^7	4.7653 x10^8	
90	6.5610 x10^7	0.0049	3.21489 x10^5		39.50	1.5602 5x10^3	1.2695 x10^7	5.0160 x10^8	
91	6.5610 x10^7	0.0049	3.21489 x10^5		40.50	1.6402 5x10^3	1.3016 x10^7	5.2732 x10^8	
92		0.0036	2.36196 x10^5		41.50	1.7222 5x10^3	9.8021 x10^6	4.0679 x10^8	
93		0.0025	1.64025 x10^5		42.50	1.8062 5x10^3	6.9711 x10^6	2.9791 x10^8	
94		0.0016	1.04976 x10^5		43.50	1.8922 5x10^3	4.5645 x10^6	1.9864 x10^8	
95		0.0900	5.9049 x10^6		44.50	1.9802 5x10^3	2.6277 x10^8	1.1693 x10^10	
96		0.0676	4.43534 x10^6		45.50	2.0702 5x10^3	2.0180 x10^8	9.1820 x10^9	
97	6.5610 x10^7	0.0324	2.125764 x10^6		46.50	2.1622 5x10^3	9.8895 x10^7	4.5964 x10^9	
98	6.50579 x10^7	0.0169	1.099775 x10^6		47.50	2.2562 5x10^3	5.2225 x10^7	2.4807 x10^9	
99	6.36495 x10^7	0.0100	6.36495 x10^5		48.50	2.3522 5x10^3	3.0870 x10^7	1.4772 x10^9	
100	6.08890 x10^7	0.0036	2.189484 x10^5		49.50	2.4502 5x10^3	1.0839 x10^7	5.3648 x10^8	
101	5.645715 x10^7	0.0004	2.25886 x10^4		50.50	2.5502 5x10^3	6.1908 x10^6	3.2586 x10^7	
102	4.99533 x10^7	0.0000	0.0000		51.50	2.6522 5x10^3	0.0000	0.0000	
103	4.0940 x10^7	0.0000	0.0000		52.36	2.74157 x10^3	0.0000	0.0000	
			2.06852 x10^9						
							-3.3980 x10^10		
								1.32417 x10^12	

λ=25' ω=2.64	$N_y = \frac{\rho\omega\pi^2}{g\lambda^2}\int$ WHEN $\frac{\rho\omega\pi^2}{g\lambda^2}$ = 2.1751 x10^-2	4.5014 x10^7	-7.3913 x10^8	2.8862 x10^10
λ=50' ω=8.01	$N_y = \frac{\rho\omega\pi^2}{g\lambda^2}\int$ WHEN $\frac{\rho\omega\pi^2}{g\lambda^2}$ = 3.8185 5x10^-3	7.9647 x10^6	-1.3099 x10^8	5.0961 x10^9
λ=75' ω=1.68	$N_y = \frac{\rho\omega\pi^2}{g\lambda^2}\int$ WHEN $\frac{\rho\omega\pi^2}{g\lambda^2}$ = 1.393 x10^-3	2.8862 x10^6	-4.7434 x10^7	1.8480 x10^9
λ=100' ω=1.42	$N_y = \frac{\rho\omega\pi^2}{g\lambda^2}\int$ WHEN $\frac{\rho\omega\pi^2}{g\lambda^2}$ = 6.7994 x10^-4	1.4067 x10^6	-2.3098 x10^7	9.0006 x10^8
λ=150' ω=1.16	$N_y = \frac{\rho\omega\pi^2}{g\lambda^2}\int$ WHEN $\frac{\rho\omega\pi^2}{g\lambda^2}$ = 2.4768 x10^-4	5.1072 x10^5	-8.5860 x10^6	3.2678 x10^8
λ=200' ω=0.90	$N_y = \frac{\rho\omega\pi^2}{g\lambda^2}\int$ WHEN $\frac{\rho\omega\pi^2}{g\lambda^2}$ = 1.2795 x10^-4	2.6245 x10^5	-4.3423 x10^6	1.6794 x10^8
λ=250' ω=0.74	$N_y = \frac{\rho\omega\pi^2}{g\lambda^2}\int$ WHEN $\frac{\rho\omega\pi^2}{g\lambda^2}$ = 7.6994 x10^-5	1.4859 x10^5	-1.7092 x10^6	5.9324 x10^7
λ=300' ω=0.66	$N_y = \frac{\rho\omega\pi^2}{g\lambda^2}\int$ WHEN $\frac{\rho\omega\pi^2}{g\lambda^2}$ = 4.8287 x10^-5	9.3287 x10^4	-3.3816 x10^5	2.0859 x10^7

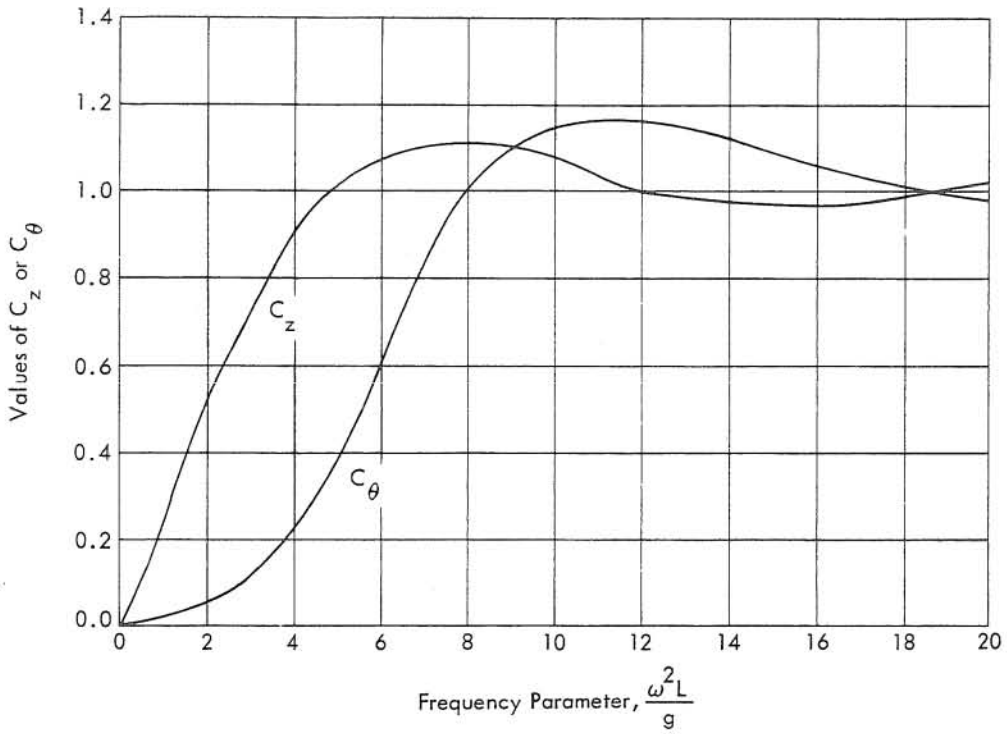

Figure B-10. Three-dimensional damping factors in heave and pitch. (From Havelock, 1956.)

Three-Dimensional Damping Factors, C_z, C_θ, C_y, and C_ψ

Havelock (1956) has determined the ratio of three-dimensional to two-dimensional damping for pure heave, C_z, and pitch, C_θ, for a submerged spheroid at zero forward speed. Although the results are generally applicable only to representative surface-ship forms, their use in the present study is justified in the absence of more precise information.

In accordance with the treatment in Appendix A (i.e., due to the relative degree of wave interference for the two motions), these factors are applied only to pure heave and pitch damping and not to any associated coupling terms. Figure B-10 presents the damping coefficients for heave and pitch as determined by Havelock.

The sway, C_y, and yaw, C_ψ, damping factors were determined by Hu and Kaplan (1962) for the case of a submerged spheroid at zero forward speed. The same argument for their use in the present study applies as in the case for the heave and pitch motions.

Sway and yaw damping factors are shown in Figures B-11 and B-12, respectively. The information presented in Figures B-11 and B-12 has been replotted in Figure B-13 for ease in extracting necessary information. Values of the three-dimensional damping factors appropriate for use in this study as obtained from Figures B-10 and B-13 are presented in Table B-11.

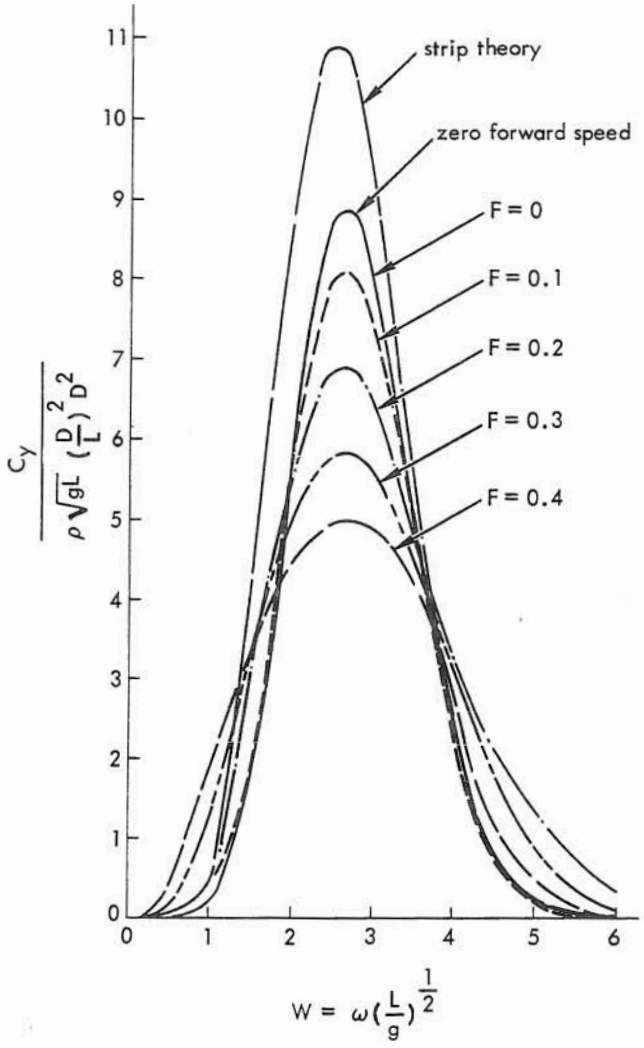

Figure B-11. Sway damping coefficient for the spheroid L/D = 8, L/f = 5. (From Hu and Kaplan, 1962.)

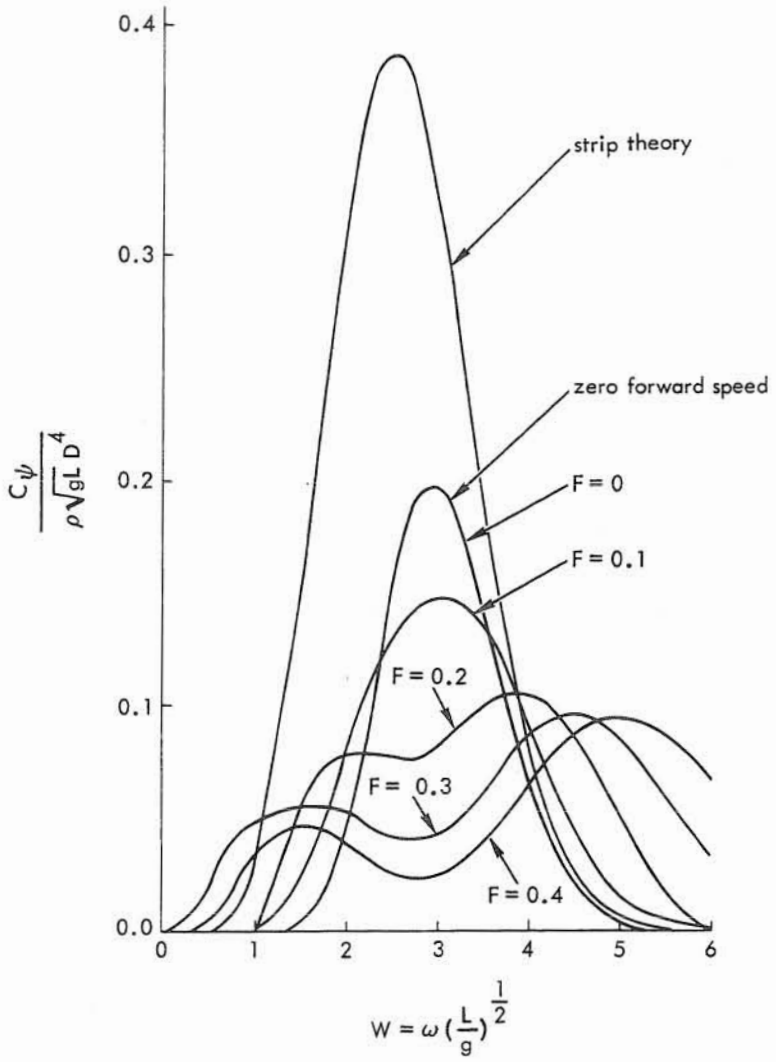

Figure B-12. Yaw damping coefficient for the spheroid L/D = 8, L/f = 5. (From Hu and Kaplan, 1962.)

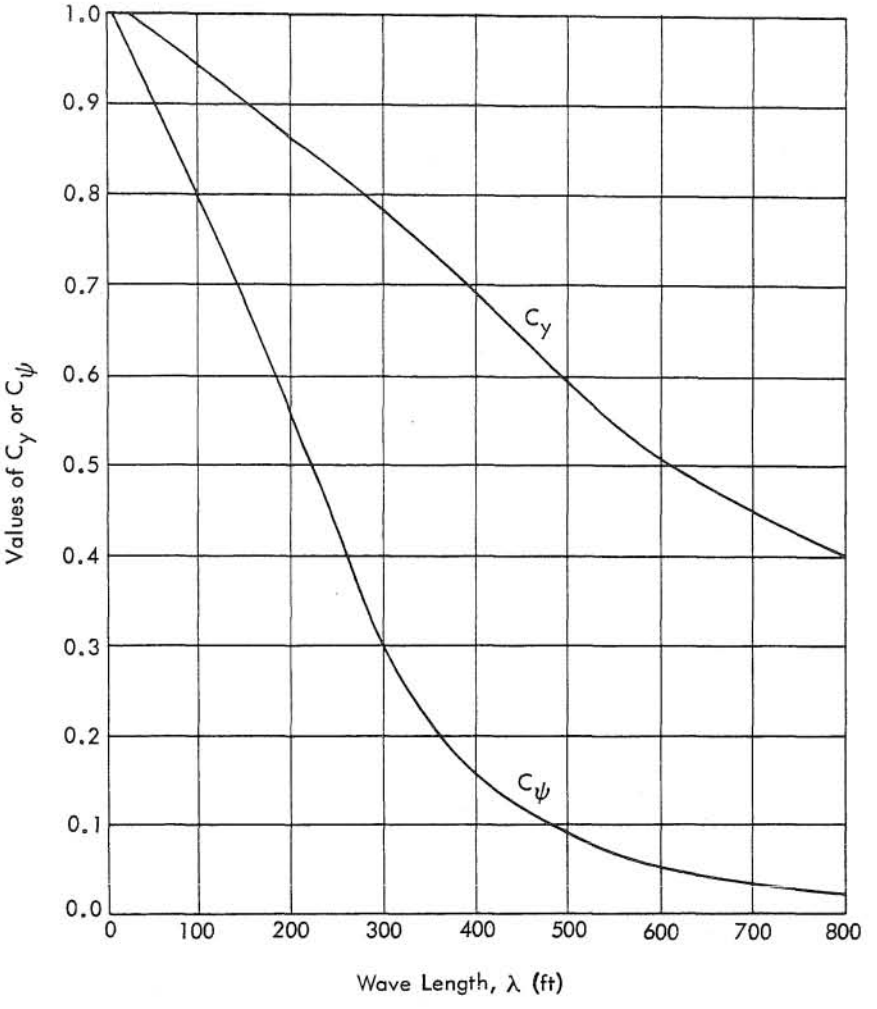

Figure B-13. Three-dimensional damping factors in sway and yaw. (From personal communication with Marine Advisers, Inc., La Jolla, California, 1962.)

Table B-11. Three-Dimensional Damping Factors for Heave, C_z, Pitch, C_θ, Sway, C_y, and Yaw, C_ψ

Wave Length λ	Wave Frequency ω	Three-Dimensional Damping Factors			
		Heave C_z	Pitch C_θ	Sway C_y	Yaw C_ψ
25	2.84	0.10	0.23	1.00	0.94
50	2.01	0.50	0.47	0.98	0.89
75	1.64	0.80	0.71	0.96	0.84
100	1.42	0.95	0.95	0.94	0.79
150	1.16	0.99	1.10	0.90	0.67
250	0.90	1.05	1.08	0.82	0.43
350	0.76	1.08	0.72	0.74	0.23
450	0.66	1.05	0.43	0.64	0.13

COMPUTATION OF THE LONGITUDINAL AND LATERAL BODY COMPONENT MATRIX ELEMENTS

Additional information required to compute the matrix elements includes tabulations of B^*, $B^*\xi$, $B^*\xi^2$ and $\overline{A}_z{}^2$, $\overline{A}_z{}^2\xi$, and $\overline{A}_z{}^2\xi^2$. The first three are shown in Table B-12 and the last three in Tables B-13, B-13a, and B-13b respectively. With this information and the appropriate integrals together with the tabulations appearing in the first section of this appendix, under the main heading of Evaluation of Sectional and Geometric Properties, values of the matrix elements a_{ii} and b_{ii} may be determined. The results of the calculations are shown in Tables B-14 and B-15, respectively. One set (matrix) of values (complex numbers) for each of the eight different wave lengths considered is given. The inverted matrix elements $a_{ii}{}^{-1}$ and $b_{ii}{}^{-1}$ are also shown in Tables B-14 and B-15, respectively.

COMPUTATION OF THE WAVE-EXCITING FORCES

The data tabulated thus far is sufficient to permit computation of the exciting forces due to the imposed surface gravity wave system. These forces are highly dependent on the directionality of the waves with respect to the orientation of the barge. Thus, the one-dimensional matrix elements have different values for each condition of wave direction and wave frequency. This is in contrast to the longitudinal and/or lateral component body matrix elements which have different values for each wave frequency only. Values of the wave-exciting forces for the indicated wave direction are shown in Tables B-16, B-17, and B-18. Calculations were performed at 15-degree intervals clockwise for exciting waves incident from a starboard beam-on direction (β = 270 degrees) to a port beam-on direction (β = 90 degrees).

COMPUTATION OF THE AMPLITUDE AND PHASE RESPONSE OPERATORS

As indicated by Appendix A, multiplication of the longitudinal and/or lateral body matrix and the appropriate one-dimensional wave-exciting force matrix yields the complex response operator. The amplitude response operator and the phase response operator are given, respectively, by the modulus and argument of the complex response operator. The results for the various incident wave directions are presented in Tables B-19 and B-20. The phase angle, positive (lead) or negative (lag), is interpreted to mean that the peak amplitude of the motion leads or lags the peak amplitude of the surface water elevation. It should be recalled that the vertical axis of the coordinate system describing the imposed waves occupies the mean position of the body's center of gravity.

Table B-12. Values of B*, B*ξ, and B*ξ^2 at 1-Foot Intervals Along ξ Axis

Index	Moment Arm, ξ	ξ^2	Total Beam, B*	B*ξ	B*ξ^2
1	-48.50	2.3426 x10^3	90.00	-4.3560 x10^3	2.1083 x10^5
2	-47.50	2.2563 x10^3		-4.2750 x10^3	2.0306 x10^5
3	-46.50	2.1623 x10^3		-4.1850 x10^3	1.9440 x10^5
4	-45.50	2.0703 x10^3		-4.0950 x10^3	1.8632 x10^5
5	-44.50	1.9803 x10^3		-4.0050 x10^3	1.7822 x10^5
6	-43.50	1.8923 x10^3		-3.9150 x10^3	1.7030 x10^5
7	-42.50	1.8063 x10^3		-3.8250 x10^3	1.6256 x10^5
8	-41.50	1.7223 x10^3		-3.7350 x10^3	1.5500 x10^5
9	-40.50	1.6403 x10^3		-3.6450 x10^3	1.4762 x10^5
10	-39.50	1.5603 x10^3		-3.5550 x10^3	1.4042 x10^5
11	-38.50	1.4823 x10^3		-3.4650 x10^3	1.3340 x10^5
12	-37.50	1.4063 x10^3		-3.3750 x10^3	1.2656 x10^5
13	-36.50	1.3323 x10^3		-3.2850 x10^3	1.1990 x10^5
14	-35.50	1.2603 x10^3	90.00	-3.1950 x10^3	1.1342 x10^5
15	-34.50	1.1903 x10^3		-3.1050 x10^3	1.0712 x10^5
16	-33.50	1.1223 x10^3		-3.0150 x10^3	1.0100 x10^5
17	-32.50	1.0563 x10^3		-2.9250 x10^3	9.5063 x10^4
18	-31.50	9.9225 x10^2		-2.8350 x10^3	8.9303 x10^4
19	-30.50	9.3025 x10^2		-2.7450 x10^3	8.3723 x10^4
20	-29.50	8.7025 x10^2		-2.6550 x10^3	7.8323 x10^4
21	-28.50	8.1225 x10^2		-2.5650 x10^3	7.3103 x10^4
22	-27.50	7.5625 x10^2		-2.4750 x10^3	6.8063 x10^4
23	-26.50	7.0225 x10^2		-2.3850 x10^3	6.3203 x10^4
24	-25.50	6.5025 x10^2		-2.2950 x10^3	5.8523 x10^4
25	-24.50	6.0025 x10^2		-2.2050 x10^3	5.4023 x10^4
26	-23.50	5.5225 x10^2		-2.1150 x10^3	4.9703 x10^4
27	-22.50	5.0625 x10^2		-2.0250 x10^3	4.5563 x10^4
28	-21.50	4.6225 x10^2		-1.9350 x10^3	4.1603 x10^4
29	-20.50	4.2025 x10^2		-1.8450 x10^3	3.7823 x10^4
30	-19.50	3.8025 x10^2		-1.7550 x10^3	3.4223 x10^4
31	-18.50	3.4225 x10^2		-1.6650 x10^3	3.0803 x10^4
32	-17.50	3.0625 x10^2		-1.5750 x10^3	2.7563 x10^4
33	-16.50	2.7225 x10^2		-1.4850 x10^3	2.4508 x10^4
34	-15.50	2.4025 x10^2		-1.3950 x10^3	2.1623 x10^4
35	-14.50	2.1025 x10^2		-1.3050 x10^3	1.8923 x10^4
36	-13.50	1.8225 x10^2	90.00	-1.2150 x10^3	1.6403 x10^4
37	-12.50	1.5625 x10^2		-1.1250 x10^3	1.4063 x10^4
38	-11.50	1.3225 x10^2		-1.0350 x10^3	1.1903 x10^4
39	-10.50	1.1025 x10^2		-9.4500 x10^2	9.9225 x10^3
40	-9.50	9.0250 x10^1		-8.5500 x10^2	8.1225 x10^3
41	-8.50	7.2250 x10^1		-7.6500 x10^2	6.5025 x10^3
42	-7.50	5.6250 x10^1		-6.7500 x10^2	5.0625 x10^3
43	-6.50	4.2250 x10^1		-5.8500 x10^2	3.8025 x10^3
44	-5.50	3.0250 x10^1		-4.9500 x10^2	2.7225 x10^3
45	-4.50	2.0250 x10^1		-4.0500 x10^2	1.8225 x10^3
46	-3.50	1.2250 x10^1		-3.1500 x10^2	1.1025 x10^3
47	-2.50	6.2500		-2.2500 x10^2	5.6250 x10^2
48	-1.50	2.2500		-1.3500 x10^2	2.0250 x10^2
49	-0.50	0.2500		-4.5000 x10^1	2.2500 x10^1
50	0.00	0.0000		0.0000	0.0000
51	0.50	0.2500		4.5000 x10^1	2.2500 x10^1
52	1.50	2.2500		1.3500 x10^2	2.0250 x10^2
53	2.50	6.2500		2.2500 x10^2	5.6250 x10^2
54	3.50	1.2250 x10^1		3.1500 x10^2	1.1025 x10^3
55	4.50	2.0250 x10^1		4.0500 x10^2	1.8225 x10^3
56	5.50	3.0250 x10^1		4.9500 x10^2	2.7225 x10^3
57	6.50	4.2250 x10^1		5.8500 x10^2	3.8025 x10^3
58	7.50	5.6250 x10^1		6.7500 x10^2	5.0625 x10^3
59	8.50	7.2250 x10^1		7.6500 x10^2	6.5025 x10^3
60	9.50	9.0250 x10^1		8.5500 x10^2	8.1225 x10^3
61	10.50	1.1025 x10^2	90.00	9.4500 x10^2	9.9225 x10^3
62	11.50	1.3225 x10^2		1.0350 x10^3	1.1903 x10^4
63	12.50	1.5625 x10^2		1.1250 x10^3	1.4063 x10^4
64	13.50	1.8225 x10^2		1.2150 x10^3	1.6403 x10^4
65	14.50	2.1025 x10^2		1.3050 x10^3	1.8923 x10^4
66	15.50	2.4025 x10^2		1.3950 x10^3	2.1623 x10^4
67	16.50	2.7225 x10^2		1.4850 x10^3	2.4503 x10^4
68	17.50	3.0625 x10^2		1.5750 x10^3	2.7563 x10^4
69	18.50	3.4225 x10^2		1.6650 x10^3	3.0803 x10^4
70	19.50	3.8025 x10^2		1.7550 x10^3	3.4223 x10^4
71	20.50	4.2025 x10^2		1.8450 x10^3	3.7823 x10^4
72	21.50	4.6225 x10^2		1.9350 x10^3	4.1603 x10^4
73	22.50	5.0625 x10^2		2.0250 x10^3	4.5563 x10^4
74	23.50	5.5225 x10^2		2.1150 x10^3	4.9703 x10^4
75	24.50	6.0025 x10^2		2.2050 x10^3	5.4023 x10^4
76	25.50	6.5025 x10^2		2.2950 x10^3	5.8523 x10^4
77	26.50	7.0225 x10^2		2.3850 x10^3	6.3203 x10^4
78	27.50	7.5625 x10^2		2.4750 x10^3	6.8063 x10^4
79	28.50	8.1225 x10^2		2.5650 x10^3	7.3103 x10^4
80	29.50	8.7025 x10^2		2.6550 x10^3	7.8323 x10^4
81	30.50	9.3025 x10^2		2.7450 x10^3	8.3723 x10^4
82	31.50	9.9225 x10^2		2.8350 x10^3	8.9303 x10^4
83	32.50	1.0563 x10^3		2.9250 x10^3	9.5063 x10^4
84	33.50	1.1223 x10^3		3.0150 x10^3	1.0100 x10^5
85	34.50	1.1903 x10^3		3.1050 x10^3	1.0712 x10^5
86	35.50	1.2603 x10^3		3.1950 x10^3	1.1342 x10^5
87	36.50	1.3323 x10^3		3.2850 x10^3	1.1990 x10^5
88	37.50	1.4063 x10^3		3.3750 x10^3	1.2656 x10^5
89	38.50	1.4823 x10^3		3.4650 x10^3	1.3340 x10^5
90	39.50	1.5603 x10^3		3.5550 x10^3	1.4042 x10^5
91	40.50	1.6403 x10^3		3.6450 x10^3	1.4762 x10^5
92	41.50	1.7223 x10^3		3.7350 x10^3	1.5500 x10^5
93	42.50	1.8063 x10^3		3.8250 x10^3	1.6256 x10^5
94	43.50	1.8923 x10^3		3.9150 x10^3	1.7030 x10^5
95	44.50	1.9803 x10^3		4.0050 x10^3	1.7822 x10^5
96	45.50	2.0703 x10^3		4.0950 x10^3	1.8632 x10^5
97	46.50	2.1623 x10^3	90.00	4.1850 x10^3	1.9460 x10^5
98	47.50	2.2563 x10^3	89.81	4.2660 x10^3	2.0263 x10^5
99	48.50	2.3523 x10^3	89.32	4.3302 x10^3	2.1010 x10^5
100	49.50	2.4503 x10^3	88.31	4.3713 x10^3	2.1632 x10^5
101	50.50	2.5503 x10^3	86.68	4.3773 x10^3	2.2106 x10^5
102	51.50	2.6523 x10^3	84.07	4.3296 x10^3	2.2298 x10^5
103	52.36	2.7417 x10^3	80.00	4.1112 x10^3	2.1933 x10^5

Table B-13. Values of $\overline{A}_z^2$ at 1-Foot Intervals Along ξ Axis

Index	Wave Length λ (ft) / Wave Frequency, ω (rad/sec): 25 / 2.84	50 / 2.01	75 / 1.64	100 / 1.42	150 / 1.16	250 / 0.90	350 / 0.76	450 / 0.68
1	0.1225	1.0404	1.0816	1.00	0.6724	0.3249	0.1936	0.1156
2	1	1	1	1	1	1	1	1
3								
4								
5								
6								
7								
8								
9								
10								
11								
12								
13								
70								
50								
70								
62	1	1	1	1	1	1	1	1
63	0.1225	1.0404	1.0816	1.0000	0.6724	0.3249	0.1936	0.1156
64	0.0100	0.8649	1.1881	1.2996	1.2769	1.0816	0.8100	0.6084
65	1	1	1	1	1	1	1	1
66								
67								
68								
69								
70								
71								
72								
73								
74								
75								
76								
77								
78								
79								
80								
81								
82								
83	1	1	1	1	1	1	1	1
84	0.0100	0.8649	1.1881	1.2996	1.2769	1.0816	0.8100	0.6084
85	0.0121	0.8649	1.2100	1.2996	1.2769	1.0816	0.8100	0.6084
86	0.0121	0.8836	1.2100	1.2996	1.2769	1.0816	0.8100	0.6084
87	0.0144	0.9025	1.2321	1.2996	1.2769	1.0816	0.8100	0.6084
88	0.0144	0.9025	1.2544	1.3225	1.2769	1.0816	0.8100	0.6084
89	0.0361	1.0404	1.3225	1.3689	1.2996	1.0816	0.8100	0.6084
90	0.0361	1.0404	1.3225	1.3689	1.2996	1.0816	0.8100	0.6084
91	0.0361	1.0404	1.3225	1.3689	1.2996	1.0816	0.8100	0.6084
92	0.0441	1.0816	1.3924	1.3924	1.3225	1.0816	0.8100	0.6084
93	0.0576	1.1025	1.4161	1.3924	1.3225	1.1025	0.8281	0.6084
94	0.0728	1.1449	1.4641	1.4161	1.3456	1.1025	0.8281	0.6084
95	0.9801	1.1836	1.0816	0.6724	0.3481	0.1681	0.0900	0.0676
96	1.0609	1.1449	1.0816	0.6724	0.3600	0.1681	0.0900	0.0676
97	1.1881	1.1449	1.0816	0.6889	0.3721	0.1681	0.0900	0.0676
98	1.3225	1.1881	1.1449	0.6889	0.3844	0.1681	0.0900	0.0676
99	1.3456	1.2321	1.1664	0.6889	0.3844	0.1681	0.0900	0.0676
100	1.3924	1.2544	1.1881	0.7056	0.3844	0.1681	0.0900	0.0676
101	1.5376	1.2996	1.2100	0.7396	0.3969	0.1681	0.0900	0.0676
102	1.8225	1.3225	1.2769	0.7744	0.4096	0.1681	0.0900	0.0676
103	1.9600	1.3689	1.2996	0.7921	0.4225	0.1681	0.0900	0.0676
$\int_{\xi_a}^{\xi_b} \overline{A}_z^2 \, d\xi$	1.9680×10^1	1.0422×10^2	1.1619×10^2	1.0932×10^2	8.5383×10^1	5.5442×10^1	3.8089×10^1	2.6910×10^1
$\rho\omega\left(\frac{\lambda}{2\pi}\right)^2$	8.7252×10^1	2.4693×10^2	4.5332×10^2	6.9780×10^2	1.2826×10^3	2.9642×10^3	4.5750×10^3	6.5697×10^3
$N_z = \rho\omega\left(\frac{\lambda}{2\pi}\right)^2 \int_{\xi_a}^{\xi_b} \overline{A}_z^2 \, d\xi$	1.7171×10^3	2.5735×10^4	5.2671×10^4	7.6634×10^4	1.0951×10^5	1.5325×10^5	1.7426×10^5	1.7547×10^5

Table B-13a. Values of $\overline{A}_z^2 \xi$ at 1-Foot Intervals Along ξ Axis

Index	ξ ft	Wave Length, λ (ft) / Wave Frequency, ω (rad/sec): 35 / 2.84	50 / 2.01	75 / 1.64	100 / 1.42	150 / 1.16	250 / 0.90	350 / 0.76	450 / 0.66
1	-48.50	-5.9290	-5.0353 x10'	-3.2599 x10'	-4.8400 x10'	-3.2544 x10'	-1.5725 x10'	-9.3702	-5.5850
2	-47.50	-5.8188	-4.9419 x10'	-5.1326 x10'	-4.7500 x10'	-8.1989 x10'	-1.5433 x10'	-7.1960	-5.4910
3	-46.50	-5.6962	-4.8379 x10'	-5.0298 x10'	-4.6500 x10'	-3.1267 x10'	-1.5109 x10'	-9.0026	-5.3754
4	-45.50	-5.5738	-4.7338 x10'	-4.9213 x10'	-4.5500 x10'	-3.0594 x10'	-1.4783 x10'	-8.8089	-5.2598
5	-44.50	-5.4512	-4.6298 x10'	-4.8131 x10'	-4.4500 x10'	-2.9922 x10'	-1.4458 x10'	-8.6152	-5.1442
6	-43.50	-5.3288	-4.5257 x10'	-4.7050 x10'	-4.3500 x10'	-2.9249 x10'	-1.4133 x10'	-8.4216	-5.0286
7	-42.50	-5.2062	-4.4217 x10'	-4.5968 x10'	-4.2500 x10'	-2.8577 x10'	-1.3808 x10'	-8.2280	-4.9130
8	-41.50	-5.0838	-4.3177 x10'	-4.4886 x10'	-4.1500 x10'	-2.7905 x10'	-1.3483 x10'	-8.0344	-4.7974
9	-40.50	-4.9612	-4.2136 x10'	-4.3805 x10'	-4.0500 x10'	-2.7232 x10'	-1.3158 x10'	-7.8408	-4.6818
10	-39.50	-4.8388	-4.1096 x10'	-4.2723 x10'	-3.9500 x10'	-2.6560 x10'	-1.2834 x10'	-7.6472	-4.5662
11	-38.50	-4.7162	-4.0055 x10'	-4.1642 x10'	-3.8500 x10'	-2.5887 x10'	-1.2509 x10'	-7.4536	-4.4506
12	-37.50	-4.5938	-3.9015 x10'	-4.0560 x10'	-3.7500 x10'	-2.5215 x10'	-1.2184 x10'	-7.2600	-4.3350
13	-36.50	-4.4712	-3.7975 x10'	-3.9478 x10'	-3.6500 x10'	-2.4543 x10'	-1.1859 x10'	-7.0664	-4.2194
14	-35.50	-4.3488	-3.6934 x10'	-3.8397 x10'	-3.5500 x10'	-2.3870 x10'	-1.1534 x10'	-6.8728	-4.1038
15	-34.50	-4.2262	-3.5894 x10'	-3.7315 x10'	-3.4500 x10'	-2.3198 x10'	-1.1209 x10'	-6.6792	-3.9882
16	-33.50	-4.1038	-3.4853 x10'	-3.6234 x10'	-3.3500 x10'	-2.2525 x10'	-1.0884 x10'	-6.4856	-3.8726
17	-32.50	-3.9812	-3.3813 x10'	-3.5152 x10'	-3.2500 x10'	-2.1853 x10'	-1.0559 x10'	-6.2920	-3.7570
18	-31.50	-3.8588	-3.2773 x10'	-3.4070 x10'	-3.1500 x10'	-2.1181 x10'	-1.0234 x10'	-6.0984	-3.6414
19	-30.50	-3.7362	-3.1732 x10'	-3.2989 x10'	-3.0500 x10'	-2.0508 x10'	-9.9095	-5.9048	-3.5258
20	-29.50	-3.6138	-3.0692 x10'	-3.1907 x10'	-2.9500 x10'	-1.9836 x10'	-9.5845	-5.7112	-3.4102
21	-28.50	-3.4912	-2.9657 x10'	-3.0826 x10'	-2.8500 x10'	-1.9163 x10'	-9.2596	-5.5176	-3.2946
22	-27.50	-3.3688	-2.8611 x10'	-2.9744 x10'	-2.7500 x10'	-1.8491 x10'	-8.9348	-5.3240	-3.1790
23	-26.50	-3.2462	-2.7571 x10'	-2.8662 x10'	-2.6500 x10'	-1.7819 x10'	-8.6098	-5.1304	-3.0634
24	-25.50	-3.1238	-2.6530 x10'	-2.7580 x10'	-2.5500 x10'	-1.7146 x10'	-8.2849	-4.9368	-2.9478
25	-24.50	-3.0012	-2.5490 x10'	-2.6499 x10'	-2.4500 x10'	-1.6474 x10'	-7.9601	-4.7432	-2.8322
26	-23.50	-2.8788	-2.4449 x10'	-2.5418 x10'	-2.3500 x10'	-1.5801 x10'	-7.6351	-4.5496	-2.7166
27	-22.50	-2.7562	-2.3409 x10'	-2.4336 x10'	-2.2500 x10'	-1.5129 x10'	-7.3103	-4.3560	-2.6010
28	-21.50	-2.6338	-2.2369 x10'	-2.3254 x10'	-2.1500 x10'	-1.4457 x10'	-6.9853	-4.1624	-2.4854
29	-20.50	-2.5112	-2.1328 x10'	-2.2173 x10'	-2.0500 x10'	-1.3784 x10'	-6.6605	-3.9688	-2.3698
30	-19.50	-2.3888	-2.0288 x10'	-2.1091 x10'	-1.9500 x10'	-1.3112 x10'	-6.3356	-3.7752	-2.2542
31	-18.50	-2.2662	-1.9247 x10'	-2.0010 x10'	-1.8500 x10'	-1.2439 x10'	-6.0106	-3.5816	-2.1386
32	-17.50	-2.1438	-1.8207 x10'	-1.8928 x10'	-1.7500 x10'	-1.1767 x10'	-5.6858	-3.3880	-2.0230
33	-16.50	-2.0212	-1.7167 x10'	-1.7846 x10'	-1.6580 x10'	-1.1095 x10'	-5.3608	-3.1944	-1.9074
34	-15.50	-1.8988	-1.6126 x10'	-1.6765 x10'	-1.5500 x10'	-1.0422 x10'	-5.0360	-3.0008	-1.7918
35	-14.50	-1.7762	-1.5086 x10'	-1.5683 x10'	-1.4500 x10'	-9.7498	-4.7110	-2.8072	-1.6762
36	-13.50	-1.6538	-1.4045 x10'	-1.4602 x10'	-1.3500 x10'	-9.0774	-4.3862	-2.6136	-1.5606
37	-12.50	-1.5312	-1.3005 x10'	-1.3520 x10'	-1.2500 x10'	-8.4050	-4.0612	-2.4200	-1.4450
38	-11.50	-1.4088	-1.1965 x10'	-1.2438 x10'	-1.1500 x10'	-7.7326	-3.7364	-2.2264	-1.3294
39	-10.50	-1.2862	-1.0924 x10'	-1.1357 x10'	-1.0500 x10'	-7.0602	-3.4114	-2.0328	-1.2138
40	-9.50	-1.1638	-9.8838	-1.0275 x10'	-9.5000	-6.3878	-3.0866	-1.8392	-1.0982
41	-8.50	-1.0412	-8.8434	-9.1936	-8.5000	-5.7154	-2.7617	-1.6456	-0.9826
42	-7.50	-0.9188	-7.8030	-8.1120	-7.5000	-5.0430	-2.4367	-1.4520	-0.8670
43	-6.50	-0.7962	-6.7626	-7.0304	-6.5000	-4.3706	-2.1118	-1.2584	-0.7514
44	-5.50	-0.6738	-5.7222	-5.9488	-5.5000	-3.6982	-1.7870	-1.0648	-0.6358
45	-4.50	-0.5512	-4.6818	-4.8672	-4.5000	-3.0258	-1.4620	-0.8712	-0.5202
46	-3.50	-0.4288	-3.6414	-3.7856	-3.5000	-2.3534	-1.1372	-0.6776	-0.4046
47	-2.50	-0.3062	-2.6010	-2.7040	-2.5000	-1.6810	-0.8122	-0.4840	-0.2890
48	-1.50	-0.1838	-1.5606	-1.6224	-1.5000	-1.0086	-0.4874	-0.2904	-0.1734
49	-0.50	-0.0612	-0.5202	-0.5408	-0.5000	-0.3362	-0.1624	-0.0968	-0.0578
50	0.00	0.0000	0.0000	0.0000	0.0000	0.0000	0.0000	0.0000	0.0000
51	0.50	0.0612	0.5202	0.5408	0.5000	0.3362	0.1624	0.0968	0.0578
52	1.50	0.1838	1.5606	1.6224	1.5000	1.0086	0.4874	0.2904	0.1734
53	2.50	0.3062	2.6010	2.7040	2.5000	1.6810	0.8122	0.4840	0.2890
54	3.50	0.4288	3.6414	3.7856	3.5000	2.3534	1.1372	0.6776	0.4046
55	4.50	0.5512	4.6818	4.8672	4.5000	3.0258	1.4620	0.8712	0.5202

46	-3.50	-0.4288	-3.6414	-3.7856	-3.5000	-2.3534	-1.1372	-0.6776	-0.4046
47	-2.50	-0.3062	-2.6010	-2.7040	-2.5000	-1.6810	-0.8122	-0.4840	-0.2890
48	-1.50	-0.1838	-1.5606	-1.6224	-1.5000	-1.0086	-0.4874	-0.2904	-0.1734
49	-0.50	-0.0612	-0.5202	-0.5408	-0.5000	-0.3362	-0.1624	-0.0968	-0.0578
50	0.00	0.0000	0.0000	0.0000	0.0000	0.0000	0.0000	0.0000	0.0000
51	0.50	0.0612	0.5202	0.5408	0.5000	0.3362	0.1624	0.0968	0.0578
52	1.50	0.1838	1.5606	1.6224	1.5000	1.0086	0.4874	0.2904	0.1734
53	2.50	0.3062	2.6010	2.7040	2.5000	1.6810	0.8122	0.4840	0.2890
54	3.50	0.4288	3.6414	3.7856	3.5000	2.3534	1.1372	0.6776	0.4046
55	4.50	0.5512	4.6818	4.8672	4.5000	3.0258	1.4620	0.8712	0.5202
56	5.50	0.6738	5.7222	5.9488	5.5000	3.6982	1.7870	1.0648	0.6358
57	6.50	0.7962	6.7626	7.0304	6.5000	4.3706	2.1118	1.2584	0.7514
58	7.50	0.9188	7.8030	8.1120	7.5000	5.0430	2.4367	1.4520	0.8670
59	8.50	1.0412	8.8434	9.1196	8.5000	5.7154	2.7617	1.6456	0.9826
60	9.50	1.1638	9.8838	1.0275x10'	9.5000	6.3878	3.0866	1.8392	1.0982
61	10.50	1.2862	1.0924x10'	1.1356x10'	1.0500x10'	7.0602	3.4114	2.0328	1.2138
62	11.50	1.4088	1.1965x10'	1.2438x10'	1.1500x10'	7.7326	3.7363	2.2264	1.3294
63	12.50	1.5312	1.3005x10'	1.3520x10'	1.2500x10'	8.4050	4.0612	2.4200	1.4450
64	13.50	0.1350	1.1676x10'	1.6039x10'	1.7545x10'	1.7238x10'	1.4602x10'	1.0935x10'	8.2134
65	14.50	0.1450	1.2541x10'	1.9227x10'	1.8844x10'	1.8515x10'	1.5683x10'	1.1745x10'	8.8218
66	15.50	0.1550	1.3406x10'	1.8416x10'	2.0144x10'	1.9792x10'	1.6765x10'	1.2555x10'	9.4302
67	16.50	0.1650	1.4271x10'	1.9603x10'	2.1443x10'	2.1069x10'	1.7846x10'	1.3365x10'	1.0039x10'
68	17.50	0.1750	1.5136x10'	2.0792x10'	2.2743x10'	2.2346x10'	1.8928x10'	1.4175x10'	1.0649x10'
69	18.50	0.1850	1.6000x10'	2.1980x10'	2.4043x10'	2.3623x10'	2.0010x10'	1.4985x10'	1.1255x10'
70	19.50	0.1950	1.6866x10'	2.3168x10'	2.5342x10'	2.4900x10'	2.1091x10'	1.5795x10'	1.1864x10'
71	20.50	0.2050	1.7730x10'	2.4356x10'	2.6642x10'	2.6176x10'	2.2173x10'	1.6605x10'	1.2472x10'
72	21.50	0.2150	1.8595x10'	2.5544x10'	2.7941x10'	2.7453x10'	2.3254x10'	1.7415x10'	1.3081x10'
73	22.50	0.2250	1.9460x10'	2.6732x10'	2.9241x10'	2.8730x10'	2.4336x10'	1.8225x10'	1.3689x10'
74	23.50	0.2350	2.0325x10'	2.7920x10'	3.0541x10'	3.0007x10'	2.5418x10'	1.9035x10'	1.4297x10'
75	24.50	0.2450	2.1190x10'	2.9108x10'	3.1840x10'	3.1284x10'	2.6499x10'	1.9845x10'	1.4906x10'
76	25.50	0.2550	2.2055x10'	3.0297x10'	3.3140x10'	3.2561x10'	2.7580x10'	2.0655x10'	1.5514x10'
77	26.50	0.2650	2.2920x10'	3.1485x10'	3.4439x10'	3.3838x10'	2.8662x10'	2.1465x10'	1.6123x10'
78	27.50	0.2750	2.3785x10'	3.2673x10'	3.5739x10'	3.5115x10'	2.9744x10'	2.2275x10'	1.6731x10'
79	28.50	0.2850	2.4649x10'	3.3861x10'	3.7039x10'	3.6392x10'	3.0826x10'	2.3085x10'	1.7339x10'
80	29.50	0.2950	2.5515x10'	3.5049x10'	3.8338x10'	3.7669x10'	3.1907x10'	2.3895x10'	1.7948x10'
81	30.50	0.3050	2.6379x10'	3.6237x10'	3.9638x10'	3.8945x10'	3.2989x10'	2.4705x10'	1.8556x10'
82	31.50	0.3150	2.7244x10'	3.7425x10'	4.0937x10'	4.0222x10'	3.4070x10'	2.5515x10'	1.9165x10'
83	32.50	0.3250	2.8109x10'	3.8613x10'	4.2237x10'	4.1499x10'	3.5152x10'	2.6325x10'	1.9773x10'
84	33.50	0.3350	2.8974x10'	3.9801x10'	4.3537x10'	4.2776x10'	3.6234x10'	2.7135x10'	2.0381x10'
85	34.50	4.1745x10^{-1}	2.9819x10'	4.1745x10'	4.4836x10'	4.4053x10'	3.7315x10'	2.7945x10'	2.0990x10'
86	35.50	4.2955x10^{-1}	3.1348x10'	4.2955x10'	4.6136x10'	4.5330x10'	3.8397x10'	2.8755x10'	2.1598x10'
87	36.50	5.2560x10^{-1}	3.2941x10'	4.4992x10'	4.7435x10'	4.6607x10'	3.9478x10'	2.9565x10'	2.2207x10'
88	37.50	5.4000x10^{-1}	3.3844x10'	4.7040x10'	4.9544x10'	4.7884x10'	4.0560x10'	3.0375x10'	2.2815x10'
89	38.50	1.3899	4.0055x10'	5.0916x10'	5.2705x10'	6.0055x10'	4.1642x10'	3.1185x10'	2.3423x10'
90	39.50	1.4259	4.1096x10'	5.2239x10'	5.4072x10'	5.1334x10'	4.2723x10'	3.1995x10'	2.4032x10'
91	40.50	1.4621	4.2136x10'	5.3561x10'	5.6440x10'	5.2684x10'	4.3805x10'	3.2805x10'	2.4640x10'
92	41.50	1.8301	4.4886x10'	5.7785x10'	5.7784x10'	5.4884x10'	4.4886x10'	3.3615x10'	2.5249x10'
93	42.50	2.4438	4.6856x10'	6.0188x10'	5.9177x10'	5.6206x10'	4.6856x10'	3.5194x10'	2.5857x10'
94	43.50	3.1668	4.9803x10'	6.3688x10'	6.1600x10'	5.8534x10'	4.7959x10'	3.6022x10'	2.6465x10'
95	44.50	4.3614x10'	5.0003x10'	4.8131x10'	2.9922x10'	1.5890x10'	7.4805	4.0450	3.0082
96	45.50	4.8271x10'	5.2093x10'	4.9213x10'	3.0594x10'	1.6380x10'	7.6486	4.0950	3.0758
97	46.50	5.5246x10'	5.4238x10'	5.0294x10'	3.2034x10'	1.7303x10'	7.8167	4.1850	3.1434
98	47.50	6.2819x10'	5.6435x10'	5.4783x10'	3.2723x10'	1.8259x10'	7.9848	4.2750	3.2110
99	48.50	6.5261x10'	5.9737x10'	5.6570x10'	3.3411x10'	1.8643x10'	8.1529	4.3650	3.2786
100	49.50	6.8924x10'	6.2092x10'	5.8811x10'	3.4927x10'	1.9628x10'	8.3210	4.4550	3.3462
101	50.50	7.7648x10'	6.5629x10'	6.1105x10'	3.7850x10'	2.0093x10'	8.4890	4.5450	3.4138
102	51.50	9.3859x10'	6.8109x10'	6.5760x10'	3.9882x10'	2.1094x10'	8.6571	4.6350	3.4814
103	52.36	1.0263x10^{2}	7.1675x10'	6.8047x10'	4.1474x10'	2.2122x10'	8.8619	4.7124	3.5395
$\int A_e^2 \rho dl$		#.4659x10^{2}	1.8868x10^{2}	3.9819x10^{2}	3.6661x10^{2}	5.5600x10^{3}	6.6887x10^{3}	5.4098x10^{3}	4.3815x10^{2}
$\rho\omega\left(\frac{\lambda}{2\pi}\right)^2$		8.9252x10'	2.4603x10^{2}	4.5332x10^{2}	6.9880x10^{2}	1.2826x10^{3}	2.7642x10^{3}	4.5750x10^{3}	6.5677x10^{3}
$\frac{1}{2}\rho\omega\left(\frac{\lambda}{2\pi}\right)^2\int A_e^2 \rho dl$		4.0711x10^{4}	2.2723x10^{4}	1.8051x10^{5}	2.5582x10^{5}	7.1313x10^{5}	1.8439x10^{6}	2.4750x10^{6}	2.8776x10^{6}

Table B-13b. Values of $A_z^2 \xi^2$ at 1-Foot Intervals Along ξ Axis

Index	ξ^2	25 2.34	50 2.01	75 1.69	100 1.42	125 1.16	150 0.92	175 0.74	200 0.66
1	2.3426×10^{3}	2.8676×10^{3}	2.4837×10^{3}	2.5338×10^{3}	2.3926×10^{3}	1.5705×10^{3}	7.6117×10^{2}	4.5353×10^{2}	2.7080×10^{2}
2	2.2563×10^{3}	2.7639×10^{3}	2.3994×10^{3}	2.4409×10^{3}	2.2563×10^{3}	1.4791×10^{3}	7.3306×10^{2}	4.3681×10^{2}	2.6082×10^{2}
3	2.1623×10^{3}	2.6488×10^{3}	2.2996×10^{3}	2.3397×10^{3}	2.1622×10^{3}	1.4539×10^{3}	7.0252×10^{2}	4.1861×10^{2}	2.4996×10^{2}
4	2.0703×10^{3}	2.5361×10^{3}	2.1939×10^{3}	2.2349×10^{3}	2.0703×10^{3}	1.3926×10^{3}	6.7262×10^{2}	4.0080×10^{2}	2.3932×10^{2}
5	1.9803×10^{3}	2.4258×10^{3}	2.0988×10^{3}	2.1418×10^{3}	1.9802×10^{3}	1.3315×10^{3}	6.4338×10^{2}	3.8338×10^{2}	2.2892×10^{2}
6	1.8983×10^{3}	2.3180×10^{3}	1.9677×10^{3}	2.0462×10^{3}	1.8923×10^{3}	1.2723×10^{3}	6.1477×10^{2}	3.6634×10^{2}	2.1874×10^{2}
7	1.8063×10^{3}	2.2127×10^{3}	1.8792×10^{3}	1.9536×10^{3}	1.8062×10^{3}	1.2145×10^{3}	5.8685×10^{2}	3.4970×10^{2}	2.0880×10^{2}
8	1.7223×10^{3}	2.1098×10^{3}	1.7918×10^{3}	1.8628×10^{3}	1.7223×10^{3}	1.1580×10^{3}	5.5956×10^{2}	3.3343×10^{2}	1.9909×10^{2}
9	1.6403×10^{3}	2.0093×10^{3}	1.7065×10^{3}	1.7741×10^{3}	1.6402×10^{3}	1.1029×10^{3}	5.3292×10^{2}	3.1755×10^{2}	1.8961×10^{2}
10	1.5603×10^{3}	1.9113×10^{3}	1.6233×10^{3}	1.6876×10^{3}	1.5603×10^{3}	1.0491×10^{3}	5.0693×10^{2}	3.0206×10^{2}	1.8036×10^{2}
11	1.4823×10^{3}	1.8157×10^{3}	1.5421×10^{3}	1.6032×10^{3}	1.4822×10^{3}	9.9666×10^{2}	4.8158×10^{2}	2.8696×10^{2}	1.7155×10^{2}
12	1.4063×10^{3}	1.7227×10^{3}	1.4631×10^{3}	1.5210×10^{3}	1.4063×10^{3}	9.4556×10^{2}	4.5689×10^{2}	2.7225×10^{2}	1.6256×10^{2}
13	1.3323×10^{3}	1.6320×10^{3}	1.3861×10^{3}	1.4410×10^{3}	1.3322×10^{3}	8.9580×10^{2}	4.3285×10^{2}	2.5792×10^{2}	1.5401×10^{2}
14	1.2603×10^{3}	1.5438×10^{3}	1.3112×10^{3}	1.3631×10^{3}	1.2603×10^{3}	8.4939×10^{2}	4.0946×10^{2}	2.4398×10^{2}	1.4568×10^{2}
15	1.1903×10^{3}	1.4580×10^{3}	1.2383×10^{3}	1.2874×10^{3}	1.1902×10^{3}	8.0032×10^{2}	8.8671×10^{2}	2.3043×10^{2}	1.3759×10^{2}
16	1.1223×10^{3}	1.3748×10^{3}	1.1676×10^{3}	1.2138×10^{3}	1.1223×10^{3}	7.5460×10^{2}	3.6462×10^{2}	2.1727×10^{2}	1.2973×10^{2}
17	1.0563×10^{2}	1.2939×10^{2}	1.0989×10^{3}	1.1429×10^{3}	1.0562×10^{3}	7.1022×10^{2}	3.4318×10^{2}	2.0449×10^{2}	1.2210×10^{2}
18	9.9225×10^{2}	1.2155×10^{3}	1.0323×10^{3}	1.0732×10^{3}	9.9225×10^{2}	6.6719×10^{2}	3.2238×10^{2}	1.9210×10^{2}	1.1470×10^{2}
19	9.3025×10^{2}	1.1365×10^{2}	9.6785×10^{2}	1.0062×10^{3}	9.3025×10^{2}	6.2550×10^{2}	3.0224×10^{2}	1.8010×10^{2}	1.0754×10^{2}
20	8.7025×10^{2}	1.0661×10^{2}	9.0541×10^{2}	9.4126×10^{2}	8.7025×10^{2}	5.8516×10^{2}	2.8274×10^{2}	1.6848×10^{2}	1.0060×10^{2}
21	8.1225×10^{2}	9.9499×10^{1}	8.4506×10^{2}	8.7853×10^{2}	8.1225×10^{2}	5.4616×10^{2}	2.6390×10^{2}	1.5725×10^{2}	9.3896×10^{1}
22	7.5625×10^{2}	9.2642×10^{1}	7.8680×10^{2}	8.1796×10^{2}	7.5625×10^{2}	5.0850×10^{2}	2.4571×10^{2}	1.4641×10^{2}	8.7423×10^{1}
23	7.0225×10^{2}	8.6024×10^{1}	7.3046×10^{2}	7.5955×10^{2}	7.0225×10^{2}	4.7219×10^{2}	2.2816×10^{2}	1.3789×10^{2}	8.2336×10^{1}
24	6.5025×10^{2}	7.9657×10^{1}	6.7652×10^{2}	7.0331×10^{2}	6.5025×10^{2}	4.3723×10^{2}	2.1127×10^{2}	1.2589×10^{2}	7.5769×10^{1}
25	6.0025×10^{2}	7.3536×10^{1}	6.2450×10^{2}	6.4923×10^{2}	6.0025×10^{2}	4.1100×10^{2}	1.9502×10^{2}	1.1621×10^{2}	6.9389×10^{1}
26	5.5225×10^{2}	6.7651×10^{1}	5.7456×10^{2}	5.9731×10^{2}	5.5225×10^{2}	3.7133×10^{2}	1.7943×10^{2}	1.0692×10^{2}	6.3840×10^{1}
27	5.0625×10^{2}	6.2016×10^{1}	5.2670×10^{2}	5.4756×10^{2}	5.0625×10^{2}	3.4040×10^{2}	1.6448×10^{2}	9.8010×10^{1}	5.8523×10^{1}
28	4.6225×10^{2}	5.6627×10^{1}	4.8092×10^{2}	4.9997×10^{2}	4.6225×10^{2}	3.1082×10^{2}	1.5019×10^{2}	8.9492×10^{1}	5.3436×10^{1}
29	4.2025×10^{2}	5.1480×10^{1}	4.3723×10^{2}	4.5458×10^{2}	4.2025×10^{2}	2.8258×10^{2}	1.3654×10^{2}	8.1340×10^{1}	4.8581×10^{1}
30	3.8025×10^{2}	4.6582×10^{1}	3.9561×10^{2}	4.1128×10^{2}	3.8025×10^{2}	2.5568×10^{2}	1.2354×10^{2}	7.3616×10^{1}	4.3957×10^{1}
31	3.4225×10^{2}	4.1925×10^{1}	3.5608×10^{2}	3.7018×10^{2}	3.4225×10^{2}	2.3018×10^{2}	1.1120×10^{2}	6.6260×10^{1}	3.9564×10^{1}
32	3.0625×10^{2}	3.7517×10^{1}	3.1862×10^{2}	3.3129×10^{2}	3.0625×10^{2}	2.0592×10^{2}	9.9501×10^{1}	5.9290×10^{1}	3.5403×10^{1}
33	2.7225×10^{2}	3.3350×10^{1}	2.8325×10^{2}	2.9447×10^{2}	2.7225×10^{2}	1.8306×10^{2}	8.8454×10^{1}	5.2708×10^{1}	3.1472×10^{1}
34	2.4025×10^{2}	2.9431×10^{1}	2.4996×10^{2}	2.5985×10^{2}	2.4025×10^{2}	1.6154×10^{2}	7.8057×10^{1}	4.6512×10^{1}	2.7773×10^{1}
35	2.1025×10^{2}	2.5755×10^{1}	2.1874×10^{2}	2.2741×10^{2}	2.1025×10^{2}	1.4137×10^{2}	6.8310×10^{1}	4.0704×10^{1}	2.4305×10^{1}
36	1.8225×10^{2}	2.2326×10^{1}	1.8961×10^{2}	1.9712×10^{2}	1.8225×10^{2}	1.2254×10^{2}	5.9213×10^{1}	3.5284×10^{1}	2.1062×10^{1}
37	1.5625×10^{2}	1.9140×10^{1}	1.6256×10^{2}	1.6900×10^{2}	1.5625×10^{2}	1.0506×10^{2}	5.0766×10^{1}	3.0250×10^{1}	1.8063×10^{1}
38	1.3225×10^{2}	1.6201×10^{1}	1.3759×10^{2}	1.4304×10^{2}	1.3225×10^{2}	8.8925×10^{1}	4.2968×10^{1}	2.5604×10^{1}	1.5288×10^{1}
39	1.1025×10^{2}	1.3505×10^{1}	1.1470×10^{2}	1.1925×10^{2}	1.1025×10^{2}	7.4132×10^{1}	3.5820×10^{1}	2.1348×10^{1}	1.2745×10^{1}
40	9.0250×10^{1}	1.1056×10^{1}	9.3896×10^{1}	9.7614×10^{1}	9.0250×10^{1}	6.0684×10^{1}	2.9322×10^{1}	1.7472×10^{1}	1.0433×10^{1}
41	7.2250×10^{1}	8.8506	7.5169×10^{1}	7.8146×10^{1}	7.2250×10^{1}	4.8581×10^{1}	2.3474×10^{1}	1.3988×10^{1}	8.3521
42	5.6250×10^{1}	6.8906	5.8523×10^{1}	6.0840×10^{1}	5.6250×10^{1}	3.7823×10^{1}	1.8276×10^{1}	1.0890×10^{1}	6.5025
43	4.2250×10^{1}	5.1756	4.3957×10^{1}	4.5698×10^{1}	4.2250×10^{1}	2.8409	1.3727×10^{1}	8.1796	4.8841
44	3.0250×10^{1}	3.7057	3.1472×10^{1}	3.2718×10^{1}	3.0250×10^{1}	2.0340	9.8282	5.8564	3.4969
45	2.0250×10^{1}	2.4806	2.1068×10^{1}	2.1902×10^{1}	2.0250×10^{1}	1.3616	6.5792	3.9204	2.3409
46	1.2250×10^{1}	1.5006	1.2745×10^{1}	1.3250×10^{1}	1.2250×10^{1}	8.2369	3.9800	2.3716	1.4161
47	6.2500	0.7656	6.5025	6.7600	6.2500	4.2025	2.0306	1.2100	0.7225
48	2.2500	0.2757	2.3409	2.4336	2.2500	1.5129	0.7311	0.4356	0.2601
49	0.2500	0.0306	0.2601	0.2704	0.2500	0.1681	8.1225×10^{-2}	0.0484	0.0289
50	0.0000	0.0000	0.0000	0.0000	0.0000	0.0000	0.0000	0.0000	0.0000
51	0.2500	0.0306	0.2601	0.2704	0.2500	0.1681	8.1225×10^{-2}	0.0484	0.0289
52	2.2500	0.2757	2.3409	2.4336	2.2500	1.5129	0.7311	0.4356	0.2601
53	6.2500	0.7656	6.5025	6.7600	6.2500	4.2025	2.0306	1.2100	0.7225
54	1.2250×10^{1}	1.5006	1.2745×10^{1}	1.3250×10^{1}	1.2250×10^{1}	8.2369	3.9800	2.3716	1.4161
55	2.0250×10^{1}	2.4806	2.1068×10^{1}	2.1902×10^{1}	2.0250×10^{1}	1.3616	6.5792	3.9204	2.3409
56	3.0250×10^{1}	3.7057	3.1472×10^{1}	3.2718×10^{1}	3.0250×10^{1}	2.0340	9.8282	5.8564	3.4969
57	4.2250×10^{1}	5.1756	4.3957×10^{1}	4.5698×10^{1}	4.2250×10^{1}	2.8409	1.3727	8.1794	4.8841
58	5.6250×10^{1}	6.8906	5.8523×10^{1}	6.0840×10^{1}	5.6250×10^{1}	3.7823	1.8276	1.0890	6.5025

49	0.2500	0.0306	0.2601	0.2704	0.2500	0.1681	8.1225x10⁻²	0.0484	0.0289
50	0.0000	0.0000	0.0000	0.0000	0.0000	0.0000	0.0000	0.0000	0.0000
51	0.2500	0.0306	0.2610	0.2704	0.2500	0.1681	8.1225x10⁻²	0.0484	0.0289
52	2.2500	0.2757	2.3409	2.4336	2.2500	1.5129	0.7311	0.4356	0.2601
53	6.2500	0.7656	6.5025	6.7600	6.2500	4.2025	2.0306	1.2100	0.7225
54	1.2250x10¹	1.5006	1.2795x10¹	1.3250x10¹	1.2250x10¹	8.2369	3.9800	2.3716	1.4161
55	2.0250x10¹	2.4806	2.1048x10¹	2.1902x10¹	2.0250x10¹	1.3616x10¹	6.5792	3.9204	2.4161
56	3.0250x10¹	3.7057	3.1472x10¹	3.2718x10¹	3.0250x10¹	2.0340x10¹	9.8282	5.8564	3.4969
57	4.2250x10¹	5.1756	4.3952x10¹	4.5698x10¹	4.2250x10¹	2.8409x10¹	1.3727x10¹	8.1796	4.8841
58	5.6250x10¹	6.8906	5.8523x10¹	6.0844x10¹	5.6250x10¹	3.7823x10¹	1.8276x10¹	1.0890x10¹	6.5025
59	7.2250x10¹	8.8506	7.5169x10¹	7.8146x10¹	7.2250x10¹	4.8581x10¹	2.3474x10¹	1.3988x10¹	8.3521
60	9.0250x10¹	1.1056x10¹	9.3896x10¹	9.7614x10¹	9.0250x10¹	6.0684x10¹	2.9322x10¹	1.7492x10¹	1.0443x10¹
61	1.1025x10²	1.3505x10¹	1.1470x10²	1.1925x10²	1.1025x10²	7.4132x10¹	3.5820x10¹	2.1364x10¹	1.2755x10¹
62	1.3225x10²	1.6201x10¹	1.3756x10²	1.4304x10²	1.3225x10²	8.8923x10¹	4.2968x10¹	2.5624x10¹	1.5298x10¹
63	1.5625x10²	1.9140x10¹	1.6256x10²	1.6900x10²	1.5625x10²	1.0506x10²	5.0766x10¹	3.0275x10¹	1.8068x10¹
64	1.8225x10²	1.8225	1.5463x10²	2.1659x10²	2.3685x10²	2.3872x10²	1.4712x10²	1.4762x10²	1.1088x10²
65	2.1025x10²	2.1025	1.8185x10²	2.4980x10²	2.7384x10²	2.6848x10²	2.2741x10²	1.7030x10²	1.2792x10²
66	2.4025x10²	2.4025	2.0779x10²	2.8544x10²	3.1223x10²	3.0678x10²	2.5985x10²	1.9460x10²	1.4619x10²
67	2.7225x10²	2.7225	2.3540x10²	3.2346x10²	3.5382x10²	3.4764x10²	2.9447x10²	2.2052x10²	1.6564x10²
68	3.0625x10²	3.0625	2.6487x10²	3.6386x10²	3.9800x10²	3.9105x10²	3.3124x10²	2.4806x10²	1.8632x10²
69	3.4225x10²	3.4225	2.9601x10²	4.0663x10²	4.4479x10²	4.3702x10²	3.7018x10²	2.7722x10²	2.0822x10²
70	3.8025x10²	3.8025	3.2888x10²	4.5178x10²	4.9417x10²	4.8554x10²	4.1128x10²	3.0800x10²	2.3134x10²
71	4.2025x10²	4.3025	3.6347x10²	4.9930x10²	5.4616x10²	5.3662x10²	4.5454x10²	3.4040x10²	2.5568x10²
72	4.6225x10²	4.6225	3.9980x10²	5.4980x10²	6.0079x10²	5.9025x10²	4.9997x10²	3.7442x10²	2.8123x10²
73	5.0625x10²	5.0625	4.3786x10²	6.0148x10²	6.5792x10²	6.4643x10²	5.4736x10²	4.1007x10²	3.0800x10²
74	5.5225x10²	5.5225	4.7764x10²	6.5613x10²	7.1770x10²	7.0517x10²	5.9731x10²	4.4732x10²	3.3599x10²
75	6.0025x10²	6.0025	5.1916x10²	7.1423x10²	7.8038x10²	7.6651x10²	6.4923x10²	4.8620x10²	3.6519x10²
76	6.5025x10²	6.5025	5.6240x10²	7.7256x10²	8.4506x10²	8.3030x10²	7.0331x10²	5.2671x10²	3.9561x10²
77	7.0225x10²	7.0225	6.0738x10²	8.3434x10²	9.1264x10²	8.9670x10²	7.5955x10²	5.6882x10²	4.2725x10²
78	7.5625x10²	7.5625	6.5408x10²	8.9850x10²	9.8282x10²	9.6546x10²	8.1796x10²	6.1256x10²	4.6010x10²
79	8.1225x10²	8.1225	7.0252x10²	9.6503x10²	1.0556x10³	1.0372x10³	8.7853x10²	6.5792x10²	4.9417x10²
80	8.7025x10²	8.7025	7.5268x10²	1.0339x10³	1.1310x10³	1.1112x10³	9.4126x10²	7.0491x10²	5.2946x10²
81	9.3025x10²	9.3025	8.0457x10²	1.1523x10³	1.2090x10³	1.1878x10³	1.0062x10³	7.5350x10²	5.6596x10²
82	9.9225x10²	9.9225	8.5820x10²	1.1790x10³	1.2895x10³	1.2670x10³	1.0732x10³	8.0377x10²	6.0348x10²
83	1.0563x10³	1.0563x10¹	9.1355x10²	1.2549x10³	1.3729x10³	1.3489x10³	1.1424x10³	8.5556x10²	6.4262x10²
84	1.1223x10³	1.1223x10¹	9.7063x10²	1.3333x10³	1.4585x10³	1.4330x10³	1.2138x10³	9.0903x10²	6.8278x10²
85	1.1903x10³	1.1903x10¹	1.0294x10³	1.4402x10³	1.5468x10³	1.5198x10³	1.2874x10³	9.6410x10²	7.2415x10²
86	1.2603x10³	1.5258x10¹	1.0905x10³	1.5249x10³	1.6378x10³	1.6092x10³	1.3631x10³	1.0208x10³	7.6674x10²
87	1.3323x10³	1.9185x10¹	1.2024x10³	1.6415x10³	1.7314x10³	1.7012x10³	1.4410x10³	1.0791x10³	8.1054x10²
88	1.4063x10³	2.0251x10¹	1.2691x10³	1.7640x10³	1.8598x10³	1.7956x10³	1.5210x10³	1.1391x10³	8.5556x10²
89	1.4823x10³	5.3511x10¹	1.3382x10³	1.9603x10³	2.0291x10³	1.9263x10³	1.6032x10³	1.2006x10³	9.0180x10²
90	1.5605x10³	6.6327x10¹	1.4233x10³	2.0634x10³	2.1958x10³	2.0277x10³	1.6876x10³	1.2638x10³	9.4926x10²
91	1.6403x10³	5.9813x10¹	1.7065x10³	2.1698x10³	2.2953x10³	2.1317x10³	1.7741x10³	1.3286x10³	9.9793x10²
92	1.7223x10³	7.5951x10¹	1.8628x10³	2.3981x10³	2.3981x10³	2.2777x10³	1.8628x10³	1.3950x10³	1.0478x10³
93	1.8063x10³	1.0404x10²	1.9914x10³	2.5578x10³	2.5150x10³	2.3888x10³	1.9914x10³	1.4958x10³	1.0989x10³
94	1.8923x10³	1.3776x10²	2.1227x10³	2.7204x10³	2.6796x10³	2.5462x10³	2.0862x10³	1.5670x10³	1.1512x10³
95	1.9803x10³	1.9403x10²	2.2250x10³	2.8418x10³	1.3315x10³	6.3139x10²	3.8288x10²	1.7822x10³	1.3386x10²
96	2.0703x10³	2.1963x10³	2.3702x10³	2.8392x10³	1.3920x10³	7.4529x10²	3.4801x10²	1.8632x10²	1.3995x10²
97	2.1623x10³	2.5690x10³	2.5220x10³	2.9387x10³	1.4896x10³	8.0457x10²	3.6342x10²	1.9460x10²	1.4617x10²
98	2.2563x10³	2.9839x10³	2.6807x10³	2.9832x10³	1.5543x10³	8.6730x10²	3.7928x10²	2.0306x10²	1.5252x10²
99	2.3523x10³	3.1652x10³	2.8982x10³	2.7437x10³	1.6205x10³	9.0420x10²	3.954x10²	2.1171x10²	1.5901x10²
100	2.4503x10³	3.4117x10³	3.0736x10³	2.9111x10³	1.7289x10³	9.4188x10²	4.1189x10²	2.2052x10²	1.6564x10²
101	2.5503x10³	3.9213x10³	3.3145x10³	3.0858x10³	1.8862x10³	1.0122x10³	4.2870x10²	2.2952x10²	1.7240x10²
102	2.6523x10³	4.8330x10³	3.5076x10³	3.2587x10³	2.0539x10³	1.0864x10³	4.4584x10²	2.3871x10²	1.7929x10²
103	2.7416x10³	5.8736x10³	3.7530x10³	3.5630x10³	2.1716x10³	1.1383x10³	4.6086x10²	2.4674x10²	1.8533x10²
$\int_{R_i}^{R_2} r^2 dr$		9.1885x10⁴	9.2504x10⁴	1.0175x10⁵	9.0981x10⁴	7.0169x10⁴	4.6249x10⁴	3.1954x10⁴	2.2774x10⁴
$\rho\omega\left(\frac{\lambda}{2\pi}\right)^2$		8.725²x10¹	2.8603x10⁵	4.5372x10⁵	6.9990x10⁵	1.2826x10⁶	2.7642x10⁶	4.5750x10⁶	6.5677x10⁶
$N_0 = \rho\omega\left(\frac{\lambda}{2\pi}\right)^2 \int_{R_i}^{R_2} r^2 \rho^2 dr$		1.0370x10⁶	2.2382x10⁷	4.6126x10⁷	6.3487x10⁷	8.9999x10⁷	1.2783x10⁸	1.4619x10⁸	1.4957x10⁸

Table B-14. Longitudinal Body Component and Inverted Matrix Elements

OMEGA ω	A_{11} REAL	A_{11} IMAGINARY	A_{12} REAL	A_{12} IMAGINARY	A_{13} REAL	A_{13} IMAGINARY
	A_{21} REAL	A_{21} IMAGINARY	A_{22} REAL	A_{22} IMAGINARY	A_{23} REAL	A_{23} IMAGINARY
	A_{31} REAL	A_{31} IMAGINARY	A_{32} REAL	A_{32} IMAGINARY	A_{33} REAL	A_{33} IMAGINARY
2.84	-4.6534E+05	4.8766E+03	0.0000E+00	0.0000E+00	8.0941E+06	0.0000E+00
	0.0000E+00	0.0000E+00	-5.1102E+06	4.8766E+02	6.5458E+06	-1.1562E+05
	8.0941E+06	0.0000E+00	6.5458E+06	-1.1562E+05	-4.7934E+09	6.7737E+05
2.01	-2.3156E+05	5.1727E+04	0.0000E+00	0.0000E+00	4.0544E+06	0.0000E+00
	0.0000E+00	0.0000E+00	-1.8525E+06	2.5864E+04	5.5861E+06	-5.5723E+04
	4.0544E+06	0.0000E+00	5.5861E+06	-5.5723E+04	-1.8889E+09	2.1579E+07
1.64	-1.5313E+05	8.6380E+04	0.0000E+00	0.0000E+00	2.6991E+06	0.0000E+00
	0.0000E+00	0.0000E+00	-8.9107E+05	6.9104E+04	2.4830E+06	-2.9603E+05
	2.6991E+06	0.0000E+00	2.4830E+06	-2.9603E+05	-9.8173E+08	5.3709E+07
1.42	-1.1403E+05	1.0882E+05	0.0000E+00	0.0000E+00	2.0235E+06	0.0000E+00
	0.0000E+00	0.0000E+00	-5.8557E+05	1.0338E+05	9.6140E+05	-3.6326E+05
	2.0235E+06	0.0000E+00	9.6140E+05	-3.6326E+05	-6.6473E+08	8.5644E+07
1.16	-7.5073E+04	1.2703E+05	0.0000E+00	0.0000E+00	1.3504E+06	0.0000E+00
	0.0000E+00	0.0000E+00	-2.4289E+05	1.2576E+05	2.1690E+05	-8.2723E+05
	1.3504E+06	0.0000E+00	2.1690E+05	-8.2723E+05	-3.2259E+08	1.1484E+08
0.90	-4.3968E+04	1.3793E+05	0.0000E+00	0.0000E+00	8.1286E+05	0.0000E+00
	0.0000E+00	0.0000E+00	-2.2800E+04	1.4482E+05	-1.7222E+05	-1.6640E+06
	8.1286E+05	0.0000E+00	-1.7222E+05	-1.6640E+06	-8.8030E+07	1.2425E+08
0.76	-3.0471E+04	1.3244E+05	0.0000E+00	0.0000E+00	5.7964E+05	0.0000E+00
	0.0000E+00	0.0000E+00	6.4110E+04	1.4303E+05	-8.7800E+04	-1.8810E+06
	5.7964E+05	0.0000E+00	-8.7800E+04	-1.8810E+06	1.2330E+07	7.9995E+07
0.66	-2.2224E+04	1.1578E+05	0.0000E+00	0.0000E+00	4.3714E+05	0.0000E+00
	0.0000E+00	0.0000E+00	1.2341E+05	1.2157E+05	-7.4840E+04	-1.8992E+06
	4.3714E+05	0.0000E+00	-7.4840E+04	-1.8992E+06	7.8300E+07	4.2448E+07

OMEGA ω	$(A_{11})^{-1}$ REAL	$(A_{11})^{-1}$ IMAGINARY	$(A_{12})^{-1}$ REAL	$(A_{12})^{-1}$ IMAGINARY	$(A_{13})^{-1}$ REAL	$(A_{13})^{-1}$ IMAGINARY
	$(A_{21})^{-1}$ REAL	$(A_{21})^{-1}$ IMAGINARY	$(A_{22})^{-1}$ REAL	$(A_{22})^{-1}$ IMAGINARY	$(A_{23})^{-1}$ REAL	$(A_{23})^{-1}$ IMAGINARY
	$(A_{31})^{-1}$ REAL	$(A_{31})^{-1}$ IMAGINARY	$(A_{32})^{-1}$ REAL	$(A_{32})^{-1}$ IMAGINARY	$(A_{33})^{-1}$ REAL	$(A_{33})^{-1}$ IMAGINARY
2.84	-2.2138E-06	-2.3909E-08	-4.7977E-09	3.2082E-11	-3.7448E-09	-4.0742E-11
	-4.7977E-09	3.2082E-11	-1.9604E-07	-6.4021E-12	-2.7581E-10	4.7350E-12
	-3.7448E-09	-4.0742E-11	-2.7581E-10	4.7350E-12	-2.1532E-10	-8.6105E-14
2.01	-4.2582E-06	-9.9064E-07	-2.7702E-08	-6.8978E-09	-9.1964E-09	-2.2509E-09
	-2.7702E-08	-6.8978E-09	-5.4474E-07	-7.6774E-09	-1.6702E-09	-4.0521E-11
	-9.1964E-09	-2.2509E-09	-1.6702E-09	-4.0521E-11	-5.5396E-10	-1.1230E-11
1.64	-5.0664E-06	-3.0181E-06	-3.8893E-08	-2.3840E-08	-1.3537E-08	-9.0871E-09
	-3.8893E-08	-2.3840E-08	-1.1238E-06	-8.6470E-08	-2.9695E-09	-1.0782E-10
	-1.3537E-08	-9.0871E-09	-2.9695E-09	-1.0782E-10	-1.0588E-09	-8.2290E-11
1.42	-4.5616E-06	-4.6310E-06	-2.5259E-08	-2.2763E-08	-1.1918E-08	-1.5651E-08
	-2.5259E-08	-2.2763E-08	-1.6605E-06	-2.9140E-07	-2.6475E-09	7.5607E-11
	-1.1918E-08	-1.5651E-08	-2.6475E-09	7.5607E-11	-1.5133E-09	-2.4107E-10
1.16	-3.2597E-06	-5.9922E-06	-7.0664E-08	-4.5333E-08	-4.3782E-09	-2.6492E-08
	-7.0664E-08	-4.5333E-08	-3.2542E-06	-1.6533E-06	-8.1929E-09	4.1270E-09
	-4.3782E-09	-2.6492E-08	-8.1929E-09	4.1270E-09	-2.7354E-09	-1.0609E-09
0.90	-1.8872E-06	-6.5268E-06	1.3163E-07	-4.2218E-07	2.0636E-08	-3.2803E-08
	1.3163E-07	-4.2218E-07	-1.9045E-06	-7.0475E-06	-6.4517E-08	-4.5172E-08
	2.0636E-08	-3.2803E-08	-6.4517E-08	-4.5172E-08	-4.4500E-09	-5.2760E-09
0.76	-1.6123E-06	-6.8903E-06	7.1187E-07	3.5986E-07	6.6107E-08	6.1869E-09
	7.1187E-07	3.5986E-07	4.5792E-06	-6.9027E-06	1.1964E-07	-1.4373E-07
	6.6107E-08	6.1869E-09	1.1964E-07	-1.4373E-07	4.8888E-09	-1.4779E-08
0.66	-1.7100E-06	-8.2409E-06	-1.1100E-07	4.0670E-07	1.7983E-08	3.3955E-08
	-1.1100E-07	4.0670E-07	4.5532E-06	-2.8841E-06	1.0207E-07	5.0076E-08
	1.7983E-08	3.3955E-08	1.0207E-07	5.0076E-08	9.9075E-09	-3.0369E-09

Table B-15. Lateral Body Component and Inverted Matrix Elements

OMEGA ω	B_{11} REAL	B_{11} IMAGINARY	B_{12} REAL	B_{12} IMAGINARY	B_{13} REAL	B_{13} IMAGINARY
	B_{21} REAL	B_{21} IMAGINARY	B_{22} REAL	B_{22} IMAGINARY	B_{23} REAL	B_{23} IMAGINARY
	B_{31} REAL	B_{31} IMAGINARY	B_{32} REAL	B_{32} IMAGINARY	B_{33} REAL	B_{33} IMAGINARY
2.84	5.4917E+05	1.2784E+08	-5.7900E+04	-2.0991E+09	2.0141E+07	2.2091E+09
	5.7900E+04	-2.0991E+09	-9.2264E+08	7.6890E+10	7.7764E+08	-3.6300E+10
	2.0141E+07	2.2091E+09	7.7764E+08	-3.6300E+10	-2.2120E+09	3.6400E+08
2.01	2.6574E+05	1.5689E+07	-8.6100E+04	-2.6289E+08	1.0433E+07	2.7110E+08
	8.6100E+04	-2.6289E+08	-4.9769E+08	9.1084E+09	3.9038E+08	-4.5500E+09
	1.0433E+07	2.7110E+08	3.9038E+08	-4.5500E+09	-9.4010E+08	2.5730E+08
1.64	1.8085E+05	4.5472E+06	-7.0300E+04	-7.7775E+07	7.0220E+06	7.8575E+07
	7.0300E+04	-7.7775E+07	-3.1930E+08	2.5458E+09	2.6008E+08	-1.3400E+09
	7.0220E+06	7.8575E+07	2.6008E+08	-1.3430E+09	-5.1331E+08	2.1000E+08
1.42	1.3660E+05	1.8777E+06	-5.7100E+04	-3.2799E+07	5.2931E+06	3.2446E+07
	5.7100E+04	-3.2799E+07	-2.3880E+08	1.0097E+09	1.9505E+08	-5.6700E+08
	5.2931E+06	3.2446E+07	1.9505E+08	-5.6700E+08	-3.0058E+08	1.8180E+08
1.16	9.1247E+04	5.3319E+05	-4.1400E+04	-9.7287E+06	3.5513E+06	9.2135E+06
	4.1400E+04	-9.7287E+06	-1.5748E+08	2.5397E+08	1.3021E+08	-1.6810E+08
	3.5513E+06	9.2135E+06	1.3021E+08	-1.6810E+08	-8.8610E+07	1.4830E+08
0.90	5.4117E+04	1.0528E+05	-2.6400E+04	-2.1081E+06	2.1469E+06	1.8192E+06
	2.6400E+04	-2.1081E+06	-9.1767E+07	3.5323E+07	7.8404E+07	-3.6650E+07
	2.1469E+06	1.8192E+06	7.8404E+07	-3.6650E+07	8.0640E+07	1.1510E+08
0.76	3.7754E+04	3.4565E+04	-1.9342E+04	-7.6699E+05	1.5338E+06	5.9727E+05
	1.9342E+04	-7.6699E+05	-6.3035E+07	6.8738E+06	5.5916E+07	-1.3250E+07
	1.5338E+06	5.9727E+05	5.5916E+07	-1.3250E+07	1.5408E+08	0.9720E+08
0.66	2.7680E+04	1.3638E+04	-1.4803E+04	-3.4990E+05	1.1580E+06	2.3567E+05
	1.4803E+04	-3.4990E+05	-4.5414E+07	1.7725E+06	4.2173E+07	-6.0400E+06
	1.1580E+06	2.3567E+05	4.2173E+07	-6.0400E+06	1.9895E+08	0.8450E+08

OMEGA ω	$(B_{11})^{-1}$ REAL	$(B_{11})^{-1}$ IMAGINARY	$(B_{12})^{-1}$ REAL	$(B_{12})^{-1}$ IMAGINARY	$(B_{13})^{-1}$ REAL	$(B_{13})^{-1}$ IMAGINARY
	$(B_{21})^{-1}$ REAL	$(B_{21})^{-1}$ IMAGINARY	$(B_{22})^{-1}$ REAL	$(B_{22})^{-1}$ IMAGINARY	$(B_{23})^{-1}$ REAL	$(B_{23})^{-1}$ IMAGINARY
	$(B_{31})^{-1}$ REAL	$(B_{31})^{-1}$ IMAGINARY	$(B_{32})^{-1}$ REAL	$(B_{32})^{-1}$ IMAGINARY	$(B_{33})^{-1}$ REAL	$(B_{33})^{-1}$ IMAGINARY
2.84	-2.3017E-10	-6.3012E-09	2.1389E-12	-3.8686E-10	1.7928E-11	-4.5540E-10
	2.1389E-12	-3.8686E-10	-5.9594E-13	-2.3579E-11	-7.8660E-13	-2.5734E-14
	1.7928E-11	-4.5540E-10	-7.8660E-13	-2.5734E-14	-2.1379E-12	2.6305E-11
2.01	-5.8034E-09	-5.7105E-08	2.5506E-11	-3.5117E-09	4.4843E-10	-3.7662E-09
	2.5506E-11	-3.5117E-09	-2.5497E-11	-2.1348E-10	-2.9520E-11	-4.9455E-12
	4.4843E-10	-3.7662E-09	-2.9520E-11	-4.9455E-12	-6.6360E-11	2.1018E-10
1.64	-2.9382E-08	-2.0846E-07	1.7638E-10	-1.3222E-08	2.5854E-09	-1.3451E-08
	1.6885E-10	-1.3190E-08	-2.2689E-10	-8.4359E-10	-2.5699E-10	-9.4840E-11
	2.5752E-09	-1.3420E-08	-2.5766E-10	-9.3070E-11	-4.9178E-10	6.3490E-10
1.42	-6.3368E-08	-4.8903E-07	1.7942E-09	-3.4593E-08	9.1895E-09	-3.5726E-08
	1.7942E-09	-3.4593E-08	-1.0838E-09	-2.5132E-09	-1.2280E-09	-7.4461E-10
	9.1895E-09	-3.5726E-08	-1.2280E-09	-7.4461E-10	-2.0782E-09	9.3927E-10
1.16	-1.0292E-06	-4.6444E-07	5.4810E-08	-9.0603E-09	1.2548E-07	-3.2912E-08
	5.4810E-08	-9.0603E-09	2.9986E-09	-1.0925E-08	3.7565E-09	-1.0120E-08
	1.2548E-07	-3.2912E-08	3.7565E-09	-1.0120E-08	1.7748E-10	-9.9729E-09
0.90	-4.8569E-06	-4.2153E-06	-5.3879E-08	7.5831E-08	7.5239E-08	1.6189E-08
	-5.3879E-08	7.5831E-08	-4.5607E-09	-5.7126E-09	4.6088E-09	-3.9002E-09
	7.5239E-06	1.6189E-08	4.6088E-09	-3.9002E-09	4.4181E-09	-2.5477E-09
0.76	-1.2172E-05	-8.4789E-06	-2.6116E-08	1.4264E-07	9.6183E-08	1.6902E-08
	-2.6116E-08	1.4264E-07	-1.1231E-08	-4.2454E-09	3.4226E-09	-2.9030E-09
	9.6183E-08	1.6902E-08	3.4226E-09	-2.9030E-09	3.6586E-09	-1.5012E-09
0.66	-2.3712E-05	-1.0889E-05	2.5850E-08	1.7668E-07	1.1653E-07	5.3113E-09
	2.5850E-08	1.7668E-07	-1.7992E-08	-3.3905E-09	3.0492E-09	-2.1816E-09
	1.1653E-07	5.3113E-09	3.0492E-09	-2.1816E-09	3.3363E-09	-1.0309E-09

Table B-16. Values of Wave-Exciting Forces for Indicated Wave Direction

BETA= 4.712389RADIANS, 270.000EGREES

OMEGA RADS/SEC	SURGE REAL	SURGE IMAGINARY	HEAVE REAL	HEAVE IMAGINARY	PITCH REAL	PITCH IMAGINARY
2.84	-0.	-0.	0.2332E 07	-0.2068E 06	-0.5611E 03	0.2650E 06
2.01	-0.	-0.	0.1977E 04	-0.1245E 06	-0.3942E 04	0.3955E 06
1.64	-0.	-0.	0.8817E 04	-0.0517E 05	-0.3155E 05	0.2735E 06
1.42	0.	0.	-0.9741E 04	0.4529E 05	0.3330E 05	-0.6888E 05
1.16	0.	0.	-0.5748E 05	0.7980E 05	0.3779E 06	-0.2901E 05
0.90	0.	0.	-0.1087E 06	-0.1495E 05	0.1315E 07	0.2358E 06
0.76	0.	0.	-0.1236E 06	-0.7872E 05	0.1744E 07	0.1711E 06
0.66	0.	0.	-0.1171E 06	-0.1237E 06	0.1923E 07	0.1426E 06

OMEGA RADS/SEC	SWAY REAL	SWAY IMAGINARY	YAW REAL	YAW IMAGINARY	ROLL REAL	ROLL IMAGINARY
2.84	0.1076E 06	-0.5746E 07	-0.8159E 08	0.	-0.1633E 08	0.8590E 08
2.01	0.7259E 05	-0.1197E 07	-0.1512E 08	0.	-0.4436E 07	0.1790E 08
1.64	0.4533E 05	-0.5765E 06	-0.6322E 07	0.	-0.1505E 07	0.8619E 07
1.42	-0.1538E 05	0.1757E 06	0.1623E 07	-0.	-0.1118E 06	-0.2627E 07
1.16	-0.1827E 05	0.2432E 06	0.1360E 07	-0.	-0.3432E 07	-0.3636E 07
0.90	0.7052E 04	0.7989E 05	-0.2142E 06	-0.	-0.5861E 07	-0.1196E 07
0.76	0.1453E 05	0.2078E 05	-0.1939E 06	-0.	-0.5609E 07	-0.4452E 06
0.66	0.1548E 05	0.1167E 05	-0.3438E 06	-0.	-0.4864E 07	-0.1744E 06

BETA= 5.235988RADIANS, 300.000EGREES

OMEGA RADS/SEC	SURGE REAL	SURGE IMAGINARY	HEAVE REAL	HEAVE IMAGINARY	PITCH REAL	PITCH IMAGINARY
2.84	-0.5005E 03	0.5830E 02	-0.1775E 04	0.2917E 04	0.7611E 06	-0.5378E 04
2.01	0.2410E 04	0.2439E 03	0.1479E 05	-0.1350E 03	-0.4031E 07	-0.5565E 06
1.64	0.1291E 04	-0.7930E 01	0.2507E 04	-0.9482E 04	-0.5045E 06	-0.5348E 05
1.42	-0.9408E 04	0.1024E 03	-0.1862E 05	0.6819E 05	0.2176E 07	0.4338E 06
1.16	-0.1027E 05	0.1771E 03	-0.5831E 05	0.7216E 05	0.1784E 07	0.1068E 07
0.90	-0.1843E 05	0.1115E 03	-0.1048E 06	-0.3023E 05	0.1022E 07	0.1368E 07
0.76	-0.1490E 05	0.6587E 02	-0.1204E 06	-0.9355E 05	0.9915E 06	0.1072E 07
0.66	-0.1186E 05	0.4112E 02	-0.1156E 06	-0.1363E 06	0.1051E 07	0.9183E 06

OMEGA RADS/SEC	SWAY REAL	SWAY IMAGINARY	YAW REAL	YAW IMAGINARY	ROLL REAL	ROLL IMAGINARY
2.84	0.3364E 06	-0.2579E 06	0.5821E 07	0.9715E 07	-0.4947E 07	0.3593E 07
2.01	-0.8794E 06	-0.3866E 04	0.9636E 07	-0.2554E 08	0.1227E 08	0.6006E 07
1.64	-0.5834E 05	-0.5432E 05	-0.3798E 06	-0.1698E 07	0.7086E 06	0.9335E 06
1.42	0.1484E 06	0.2114E 04	0.2165E 07	0.3806E 07	-0.2328E 07	-0.3971E 07
1.16	0.7430E 05	0.1755E 06	0.1426E 07	0.1536E 07	-0.4042E 07	-0.3895E 07
0.90	0.2796E 05	0.5360E 05	-0.1014E 06	0.1727E 06	-0.5187E 07	-0.1629E 07
0.76	0.1710E 05	0.1926E 05	-0.3022E 06	0.4323E 05	-0.4860E 07	-0.7815E 06
0.66	0.1483E 05	0.6930E 04	-0.2851E 06	0.2161E 05	-0.4183E 07	-0.4167E 06

BETA= 4.974188RADIANS, 285.000EGREES

OMEGA RADS/SEC	SURGE REAL	SURGE IMAGINARY	HEAVE REAL	HEAVE IMAGINARY	PITCH REAL	PITCH IMAGINARY
2.84	0.6049E 03	0.1042E 03	0.6131E 04	0.1237E 04	-0.3468E 07	-0.1752E 06
2.01	0.4259E 04	-0.4494E 02	0.1427E 05	-0.9979E 05	-0.3259E 07	0.1218E 06
1.64	0.3823E 04	-0.3595E 02	0.1043E 05	-0.6516E 05	-0.1280E 07	0.2821E 05
1.42	-0.3598E 04	0.2724E 02	-0.1303E 05	0.5168E 05	0.7738E 06	0.9260E 05
1.16	-0.2670E 04	0.5107E 02	-0.5805E 05	0.7615E 05	0.1063E 07	0.5002E 06
0.90	-0.9500E 04	0.3075E 02	-0.1059E 06	-0.2245E 05	0.1171E 07	0.8211E 06
0.76	-0.7703E 04	0.1791E 02	-0.1217E 06	-0.9659E 05	0.1362E 07	0.6420E 06
0.66	-0.6133E 04	0.1112E 02	-0.1164E 06	-0.1304E 06	0.1478E 07	0.4976E 06

OMEGA RADS/SEC	SWAY REAL	SWAY IMAGINARY	YAW REAL	YAW IMAGINARY	ROLL REAL	ROLL IMAGINARY
2.84	-0.2372E 07	-0.1002E 07	0.4104E 08	-0.7468E 08	0.3523E 08	0.1617E 08
2.01	-0.5981E 06	-0.9528E 06	-0.9207E 07	-0.1940E 08	0.6035E 07	0.1463E 08
1.64	-0.1267E 06	-0.3636E 06	-0.4056E 07	-0.4117E 07	0.1216E 07	0.5833E 07
1.42	0.4170E 05	0.1869E 06	0.1801E 07	0.1368E 07	-0.9521E 06	-0.3132E 07
1.16	0.2728E 05	0.2127E 06	0.1390E 07	0.7835E 06	-0.3921E 07	-0.3892E 07
0.90	0.1560E 05	0.6810E 05	-0.1821E 06	0.9200E 05	-0.5753E 07	-0.1489E 07
0.76	0.1439E 05	0.2496E 05	-0.3618E 06	0.2346E 05	-0.5435E 07	-0.6581E 06
0.66	0.1568E 05	0.9432E 04	-0.3283E 06	0.1203E 05	-0.4680E 07	-0.3217E 06

BETA= 5.497787RADIANS, 315.000EGREES

OMEGA RADS/SEC	SURGE REAL	SURGE IMAGINARY	HEAVE REAL	HEAVE IMAGINARY	PITCH REAL	PITCH IMAGINARY
2.84	-0.2766E 04	0.1047E 04	-0.1825E 04	0.3115E 05	0.1285E 07	-0.1618E 06
2.01	-0.4072E 04	0.8343E 03	-0.2012E 04	0.5550E 05	-0.3630E 06	-0.5922E 06
1.64	-0.3145E 04	-0.1700E 03	-0.5491E 04	0.5419E 04	0.1920E 07	0.3988E 06
1.42	-0.1582E 05	0.5255E 03	-0.2079E 05	0.6452E 05	0.4112E 07	0.1039E 07
1.16	-0.2781E 05	0.2975E 03	-0.5673E 05	0.6580E 05	0.2506E 07	0.1656E 07
0.90	-0.2414E 05	0.2129E 03	-0.1022E 06	-0.3710E 05	0.8802E 06	0.1852E 07
0.76	-0.2111E 05	0.1288E 03	-0.1191E 06	-0.9933E 05	0.6615E 06	0.1438E 07
0.66	-0.1678E 05	0.8110E 02	-0.1148E 06	-0.1411E 06	0.6797E 06	0.1089E 07

OMEGA RADS/SEC	SWAY REAL	SWAY IMAGINARY	YAW REAL	YAW IMAGINARY	ROLL REAL	ROLL IMAGINARY
2.84	-0.1919E 05	0.6693E 06	0.1682E 08	0.2766E 08	0.1214E 07	-0.9510E 07
2.01	-0.2438E 04	-0.6440E 05	0.1426E 08	-0.6958E 07	0.4299E 07	0.6874E 06
1.64	0.2207E 06	0.9641E 05	-0.1063E 07	0.5901E 07	-0.2916E 07	-0.1701E 07
1.42	0.2698E 06	0.1940E 06	0.1537E 07	0.6544E 07	-0.3625E 07	-0.4000E 07
1.16	0.1072E 06	0.1324E 06	0.1341E 07	0.2063E 07	-0.3647E 07	-0.3476E 07
0.90	0.2627E 05	0.3871E 05	-0.1160E 06	0.2211E 06	-0.4217E 07	-0.1525E 07
0.76	0.1594E 05	0.1352E 05	-0.2216E 06	0.5410E 05	-0.3941E 07	-0.7728E 06
0.66	0.1275E 05	0.4501E 04	-0.2223E 06	0.2618E 05	-0.3397E 07	-0.4303E 06

Table B-17. Values of Wave-Exciting Forces for Indicated Wave Direction

BETA= 5.759586RADIANS, 330.00DEGREES

OMEGA RADS/SEC	SURGE REAL	SURGE IMAGINARY	HEAVE REAL	HEAVE IMAGINARY	PITCH REAL	PITCH IMAGINARY
2.84	0.4403E 03	0.3278E 02	0.2040E 04	0.1925E 05	-0.5141E 06	-0.1057E 06
2.01	0.3411E 04	-0.5276E 03	0.6280E 04	-0.2307E 05	-0.9802E 06	0.1459E 06
1.64	0.6940E 03	-0.1393E 04	-0.3709E 03	-0.4614E 05	0.3524E 07	0.1238E 07
1.42	-0.1787E 05	-0.4131E 03	-0.1576E 05	0.4108E 05	0.5794E 07	0.1662E 07
1.16	-0.3393E 05	0.3275E 03	-0.5298E 05	0.5719E 05	0.3118E 07	0.2183E 07
0.90	-0.3207E 05	0.3024E 03	-0.9962E 05	-0.4258E 05	0.7625E 06	0.2235E 07
0.76	-0.2587E 05	0.1987E 03	-0.1179E 06	-0.1036E 06	0.3999E 06	0.1720E 07
0.66	-0.2056E 05	0.1201E 03	-0.1141E 06	-0.1447E 06	0.3869E 06	0.1294E 07

OMEGA RADS/SEC	SWAY REAL	SWAY IMAGINARY	YAW REAL	YAW IMAGINARY	ROLL REAL	ROLL IMAGINARY
2.84	0.7538E 05	0.1137E 06	0.8122E 07	-0.9246E 07	-0.6719E 06	-0.1655E 07
2.01	-0.4468E 05	0.4554E 05	-0.4702E 07	-0.1016E 07	0.3982E 06	-0.4856E 06
1.64	0.3594E 06	0.9734E 05	-0.5533E 07	0.9845E 07	-0.4712E 07	-0.1509E 07
1.42	0.3028E 06	0.1372E 06	0.1777E 06	0.7380E 07	-0.3713E 07	-0.2955E 07
1.16	0.1073E 06	0.8690E 05	0.1046E 07	0.2042E 07	-0.2724E 07	-0.2591E 07
0.90	0.2328E 05	0.2460E 05	0.4360E 05	0.2109E 06	-0.2949E 07	-0.1187E 07
0.76	0.1248E 05	0.8372E 04	-0.1385E 06	0.5055E 05	-0.2763E 07	-0.6196E 06
0.66	0.9405E 04	0.2669E 04	-0.1496E 06	0.2376E 05	-0.2387E 07	-0.3532E 06

BETA= 6.283185RADIANS, 360.00DEGREES

OMEGA RADS/SEC	SURGE REAL	SURGE IMAGINARY	HEAVE REAL	HEAVE IMAGINARY	PITCH REAL	PITCH IMAGINARY
2.84	0.1186E 05	-0.9833E 04	0.2154E 05	-0.7792E 05	-0.9089E 07	0.9764E 06
2.01	0.2195E 05	-0.2167E 04	0.6266E 05	-0.3129E 05	-0.1123E 08	-0.7083E 06
1.64	0.1771E 05	-0.4308E 04	0.2542E 05	-0.1457E 06	0.2652E 07	0.2145E 07
1.42	-0.1402E 05	-0.1535E 04	-0.2634E 04	-0.5631E 04	0.6914E 07	0.2326E 07
1.16	-0.3810E 05	0.2340E 03	-0.4703E 05	0.4612E 05	0.3651E 07	0.2677E 07
0.90	-0.3699E 05	0.3770E 03	-0.9683E 05	-0.4739E 05	0.6562E 06	0.2570E 07
0.76	-0.2988E 05	0.2452E 03	-0.1167E 06	-0.1072E 06	0.1729E 06	0.1959E 07
0.66	-0.2375E 05	0.1579E 03	-0.1134E 06	-0.1476E 06	0.1355E 06	0.1465E 07

OMEGA RADS/SEC	SWAY REAL	SWAY IMAGINARY	YAW REAL	YAW IMAGINARY	ROLL REAL	ROLL IMAGINARY
2.84	0.	-0.	0.	-0.	-0.	-0.
2.01	0.	-0.	0.	-0.	-0.	-0.
1.64	-0.	-0.	-0.	-0.	-0.	-0.
1.42	-0.	0.	-0.	0.	0.	0.
1.16	-0.	0.	-0.	0.	0.	0.
0.90	-0.	0.	0.	0.	0.	0.
0.76	-0.	0.	0.	0.	0.	0.
0.66	-0.	0.	0.	0.	0.	0.

BETA= 6.021386RADIANS, 345.00DEGREES

OMEGA RADS/SEC	SURGE REAL	SURGE IMAGINARY	HEAVE REAL	HEAVE IMAGINARY	PITCH REAL	PITCH IMAGINARY
2.84	0.7524E 03	-0.6236E 03	0.9706E 03	-0.1077E 05	-0.5123E 06	0.8995E 05
2.01	0.1744E 05	-0.2171E 04	0.4390E 05	-0.5413E 05	-0.7683E 07	-0.1370E 06
1.64	0.1174E 05	-0.3339E 04	0.1624E 05	-0.1159E 06	0.3197E 07	0.1917E 07
1.42	-0.1571E 05	-0.1158E 04	-0.6982E 04	0.8776E 04	0.6685E 07	0.2151E 07
1.16	-0.3717E 05	0.2730E 03	-0.4884E 05	0.4933E 05	0.3516E 07	0.2547E 07
0.90	-0.3575E 05	0.3591E 03	-0.9760E 05	-0.4615E 05	0.6839E 06	0.2484E 07
0.76	-0.2886E 05	0.2304E 03	-0.1170E 06	-0.1063E 06	0.2312E 06	0.1898E 07
0.66	-0.2294E 05	0.1479E 03	-0.1135E 06	-0.1469E 06	0.1998E 06	0.1422E 07

OMEGA RADS/SEC	SWAY REAL	SWAY IMAGINARY	YAW REAL	YAW IMAGINARY	ROLL REAL	ROLL IMAGINARY
2.84	-0.1303E 06	-0.3864E 05	-0.2524E 07	-0.1442E 07	0.1860E 07	0.6771E 06
2.01	-0.3175E 06	0.2352E 06	-0.9479E 07	-0.7485E 07	0.4176E 07	-0.2892E 07
1.64	0.2307E 06	0.5709E 05	-0.6100E 07	0.6617E 07	-0.3096E 07	-0.6382E 06
1.42	0.1967E 06	0.6861E 05	-0.5313E 06	0.4878E 07	-0.2289E 07	-0.1461E 07
1.16	0.6719E 05	0.4257E 05	0.5662E 06	0.1288E 07	-0.1439E 07	-0.1370E 07
0.90	0.1373E 05	0.1183E 05	0.4261E 05	0.1302E 06	-0.1509E 07	-0.6493E 06
0.76	0.6890E 04	0.3949E 04	-0.6467E 05	0.1078E 05	-0.1419E 07	-0.3444E 06
0.66	0.5007E 04	0.1194E 04	-0.7457E 05	0.1418E 05	-0.1230E 07	-0.1987E 06

BETA= 0.261799RADIANS, 15.00DEGREES

OMEGA RADS/SEC	SURGE REAL	SURGE IMAGINARY	HEAVE REAL	HEAVE IMAGINARY	PITCH REAL	PITCH IMAGINARY
2.84	0.7524E 03	-0.6236E 03	0.9706E 03	-0.1077E 05	-0.5123E 06	0.8995E 05
2.01	0.1744E 05	-0.2171E 04	0.4390E 05	-0.5413E 05	-0.7683E 07	-0.1370E 06
1.64	0.1174E 05	-0.3339E 04	0.1624E 05	-0.1159E 06	0.3197E 07	0.1917E 07
1.42	-0.1571E 05	-0.1158E 04	-0.6982E 04	0.8776E 04	0.6685E 07	0.2151E 07
1.16	-0.3717E 05	0.2730E 03	-0.4884E 05	0.4933E 05	0.3516E 07	0.2547E 07
0.90	-0.3575E 05	0.3591E 03	-0.9760E 05	-0.4615E 05	0.6839E 06	0.2484E 07
0.76	-0.2886E 05	0.2304E 03	-0.1170E 06	-0.1063E 06	0.2312E 06	0.1898E 07
0.66	-0.2294E 05	0.1479E 03	-0.1135E 06	-0.1469E 06	0.1998E 06	0.1422E 07

OMEGA RADS/SEC	SWAY REAL	SWAY IMAGINARY	YAW REAL	YAW IMAGINARY	ROLL REAL	ROLL IMAGINARY
2.84	0.1303E 06	0.3864E 05	0.2524E 07	0.1442E 07	-0.1860E 07	-0.6771E 06
2.01	0.3175E 06	-0.2352E 06	0.9479E 07	0.7485E 07	-0.4176E 07	0.2892E 07
1.64	-0.2307E 06	-0.5709E 05	0.6100E 07	-0.6617E 07	0.3096E 07	0.6382E 06
1.42	-0.1967E 06	-0.6861E 05	0.5313E 06	-0.4878E 07	0.2289E 07	0.1461E 07
1.16	-0.6719E 05	-0.4257E 05	-0.5662E 06	-0.1288E 07	0.1439E 07	0.1370E 07
0.90	-0.1373E 05	-0.1183E 05	-0.4261E 05	-0.1302E 06	0.1509E 07	0.6493E 06
0.76	-0.6890E 04	-0.3949E 04	0.6467E 05	-0.1078E 05	0.1419E 07	0.3444E 06
0.66	-0.5007E 04	-0.1194E 04	0.7457E 05	-0.1418E 05	0.1230E 07	0.1987E 06

Table B-18. Values of Wave-Exciting Forces for Indicated Wave Direction

BETA= 0.523599RADIANS, 30.000EGREES

OMEGA RADS/SEC	SURGE REAL	SURGE IMAGINARY	HEAVE REAL	HEAVE IMAGINARY	PITCH REAL	PITCH IMAGINARY
2.84	0.4404E 03	0.3278E 02	0.2040E 04	0.1925E 05	-0.5142E 06	-0.1057E 06
2.01	0.3411E 04	-0.5277E 03	0.6282E 04	-0.2307E 05	-0.9804E 06	0.1458E 06
1.64	0.6940E 03	-0.1393E 04	-0.3709E 03	-0.4615E 05	0.3524E 07	0.1238E 07
1.42	-0.1787E 05	-0.4131E 03	-0.1576E 05	0.4108E 05	0.5794E 07	0.1662E 07
1.16	-0.3393E 05	0.3275E 03	-0.5298E 05	0.5719E 05	0.3118E 07	0.2183E 07
0.90	-0.3207E 05	0.3024E 03	-0.9962E 05	-0.4258E 05	0.7625E 06	0.2235E 07
0.76	-0.2587E 05	0.1887E 03	-0.1179E 06	-0.1036E 06	0.3999E 06	0.1720E 07
0.66	-0.2056E 05	0.1201E 03	-0.1141E 06	-0.1447E 06	0.3869E 06	0.1294E 07

OMEGA RADS/SEC	SWAY REAL	SWAY IMAGINARY	YAW REAL	YAW IMAGINARY	ROLL REAL	ROLL IMAGINARY
2.84	-0.7539E 05	-0.1137E 06	-0.8173E 07	0.9247E 07	0.6720E 06	0.1655E 07
2.01	0.4469E 05	-0.4555E 05	0.4703E 07	0.1017E 07	-0.3983E 06	0.4857E 06
1.64	-0.3594E 06	-0.9734E 05	0.5533E 07	-0.9845E 07	0.4712E 07	0.1509E 07
1.42	-0.3028E 06	-0.1372E 06	-0.1777E 06	-0.7380E 07	0.3713E 07	0.2955E 07
1.16	-0.1072E 06	-0.8690E 05	-0.1046E 07	-0.2042E 07	0.2724E 07	0.2591E 07
0.90	-0.2328E 05	-0.2460E 05	-0.4360E 05	-0.2109E 06	0.2949E 07	0.1187E 07
0.76	-0.1248E 05	-0.8372E 04	0.1385E 06	-0.5055E 05	0.2761E 07	0.6196E 06
0.66	-0.9405E 04	-0.2669E 04	0.1496E 06	-0.2376E 05	0.2387E 07	0.3532E 06

BETA= 1.04719RADIANS, 60.000EGREES

OMEGA RADS/SEC	SURGE REAL	SURGE IMAGINARY	HEAVE REAL	HEAVE IMAGINARY	PITCH REAL	PITCH IMAGINARY
2.84	-0.5904E 03	0.5829E 02	-0.1775E 04	0.2915E 04	0.7611E 06	-0.5370E 04
2.01	0.2410E 04	0.2639E 03	0.1479E 05	-0.1299E 03	-0.4031E 07	-0.5566E 06
1.64	0.1291E 04	-0.7929E 01	0.2507E 04	-0.9482E 04	-0.5045E 06	-0.5348E 05
1.42	-0.9608E 04	0.1024E 03	-0.1862E 05	0.6818E 05	0.2176E 07	0.4338E 06
1.16	-0.1927E 05	0.1771E 03	-0.5931E 05	0.7216E 05	0.1784E 07	0.1069E 07
0.90	-0.1943E 05	0.1115E 03	-0.1048E 06	-0.3023E 05	0.1022E 07	0.1368E 07
0.76	-0.1490E 05	0.6587E 02	-0.1204E 06	-0.9355E 05	0.9915E 06	0.1072E 07
0.66	-0.1186E 05	0.4112E 02	-0.1156E 06	-0.1363E 06	0.1053E 07	0.8183E 06

OMEGA RADS/SEC	SWAY REAL	SWAY IMAGINARY	YAW REAL	YAW IMAGINARY	ROLL REAL	ROLL IMAGINARY
2.84	-0.3364E 06	0.2579E 06	-0.5819E 07	-0.9715E 07	0.4947E 07	-0.3593E 07
2.01	0.8794E 06	0.3863E 06	-0.9636E 07	0.2554E 08	-0.1227E 08	-0.6006E 07
1.64	0.5834E 05	0.5432E 05	0.3798E 06	0.1608E 07	-0.7086E 06	-0.9335E 06
1.42	-0.1484E 06	-0.2114E 06	-0.2165E 07	-0.3806E 07	0.2328E 07	0.3971E 07
1.16	-0.7430E 05	-0.1755E 06	-0.1426E 07	-0.1536E 07	0.4042E 07	0.3895E 07
0.90	-0.2297E 05	-0.5369E 05	0.1014E 06	-0.1727E 06	0.5187E 07	0.1620E 07
0.76	-0.1710E 05	-0.1924E 05	0.3022E 06	-0.4323E 05	0.4860E 07	0.7815E 06
0.66	-0.1483E 05	-0.6930E 04	0.2851E 06	-0.2161E 05	0.4183E 07	0.4167E 06

BETA= 0.785398RADIANS, 45.000EGREES

OMEGA RADS/SEC	SURGE REAL	SURGE IMAGINARY	HEAVE REAL	HEAVE IMAGINARY	PITCH REAL	PITCH IMAGINARY
2.84	-0.2766E 04	0.1047E 04	-0.1825E 04	0.3115E 05	0.1285E 07	-0.1619E 06
2.01	-0.4072E 04	0.8343E 03	-0.2012E 04	0.5550E 05	-0.3630E 06	-0.5922E 06
1.64	-0.3145E 04	-0.1790E 03	-0.5691E 04	0.5419E 04	0.1929E 07	0.3988E 06
1.42	-0.1582E 05	0.5255E 02	-0.2079E 05	0.6652E 05	0.4112E 07	0.1009E 07
1.16	-0.3781E 05	0.2975E 03	-0.5673E 05	0.6580E 05	0.2506E 07	0.1656E 07
0.90	-0.2616E 05	0.2129E 03	-0.1022E 06	-0.3710E 05	0.8802E 06	0.1852E 07
0.76	-0.2111E 05	0.1289E 03	-0.1191E 06	-0.9933E 05	0.6615E 06	0.1438E 07
0.66	-0.1678E 05	0.8119E 02	-0.1148E 06	-0.1411E 06	0.6797E 06	0.1099E 07

OMEGA RADS/SEC	SWAY REAL	SWAY IMAGINARY	YAW REAL	YAW IMAGINARY	ROLL REAL	ROLL IMAGINARY
2.84	0.1918E 05	-0.6693E 06	-0.1682E 08	-0.2266E 08	-0.1214E 07	0.9510E 07
2.01	0.2438E 06	0.6440E 05	-0.1426E 08	0.6958E 07	-0.4209E 07	-0.6874E 06
1.64	-0.2207E 06	-0.9641E 05	0.1063E 07	-0.5901E 07	0.2816E 07	0.1701E 07
1.42	-0.2698E 06	-0.1040E 06	-0.1537E 07	-0.6564E 07	0.3625E 07	0.4000E 07
1.16	-0.1072E 06	-0.1324E 06	-0.1361E 07	-0.2063E 07	0.3647E 07	0.3476E 07
0.90	-0.2627E 05	-0.3871E 05	0.1160E 05	-0.2211E 06	0.4217E 07	0.1525E 07
0.76	-0.1594E 05	-0.1352E 05	0.2216E 06	-0.5410E 05	0.3961E 07	0.7728E 06
0.66	-0.1275E 05	-0.4591E 04	0.2223E 06	-0.2618E 05	0.3397E 07	0.4303E 06

BETA= 1.30899?RADIANS, 75.000EGREES

OMEGA RADS/SEC	SURGE REAL	SURGE IMAGINARY	HEAVE REAL	HEAVE IMAGINARY	PITCH REAL	PITCH IMAGINARY
2.84	0.6049E 03	0.1042E 03	0.6131E 04	0.1237E 04	-0.3468E 07	-0.1752E 06
2.01	0.4359E 04	-0.4494E 02	0.1427E 05	-0.9979E 05	-0.3259E 07	0.1218E 06
1.64	0.3823E 04	-0.3595E 02	0.1043E 05	-0.6534E 05	-0.1280E 07	0.2821E 05
1.42	-0.3596E 04	0.2724E 02	-0.1303E 05	0.5368E 05	0.7738E 06	0.9260E 05
1.16	-0.9670E 04	0.5107E 02	-0.5805E 05	0.7615E 05	0.1063E 07	0.5002E 06
0.90	-0.9500E 04	0.3075E 02	-0.1069E 06	-0.2245E 05	0.1171E 07	0.8211E 06
0.76	-0.7703E 04	0.1791E 02	-0.1217E 06	-0.8658E 05	0.1362E 07	0.6420E 06
0.66	-0.6133E 04	0.1112E 02	-0.1164E 06	-0.1304E 06	0.1479E 07	0.4974E 06

OMEGA RADS/SEC	SWAY REAL	SWAY IMAGINARY	YAW REAL	YAW IMAGINARY	ROLL REAL	ROLL IMAGINARY
2.84	0.2372E 07	0.1092E 07	-0.4104E 08	0.7468E 08	-0.3523E 08	-0.1617E 08
2.01	0.5981E 06	0.9528E 06	0.9207E 07	0.1940E 08	-0.6035E 07	-0.1463E 08
1.64	0.1267E 06	0.3638E 06	0.4056E 07	0.4117E 07	-0.1216E 07	-0.5833E 07
1.42	-0.4179E 05	-0.1869E 06	-0.1891E 07	-0.1368E 07	0.9521E 06	0.3132E 07
1.16	-0.2728E 05	-0.2127E 06	-0.1390E 07	-0.7835E 06	0.3921E 07	0.3892E 07
0.90	-0.1560E 05	-0.6810E 05	0.1821E 06	-0.9200E 05	0.5751E 07	0.1449E 07
0.76	-0.1639E 05	-0.3496E 05	0.3619E 06	-0.2346E 05	0.5435E 07	0.6581E 06
0.66	-0.1568E 05	-0.9432E 04	0.3283E 06	-0.1203E 05	0.4680E 07	0.3217E 06

Table B-19. Results for the Various Incident Wave Directions

SURGE $\beta = 270^{\circ}$

OMEGA ω	COMPLEX RESPONSE OPERATOR REAL	COMPLEX RESPONSE OPERATOR IMAGINARY	AMPLITUDE RESPONSE OPERATOR MODULUS IN FEET/FOOT	PHASE RESPONSE OPERATOR ARGUMENT IN RADIANS
2.84	-1.5441862E-05	2.3124000E-07	1.5443598E-05	1.5705720
2.01	-4.9969500E-05	1.8351330E-04	1.9019494E-04	7.4008392E-02
1.64	-1.3229630E-04	7.7423500E-05	1.5328640E-04	1.2408258
1.42	-1.0371690E-04	2.3624300E-05	1.0637345E-04	1.5189605
1.16	-4.4179960E-04	-1.8936160E-03	1.9444648E-03	5.4379254E-07
0.90	1.1024841E-02	-2.6154600E-04	1.1027942E-02	1.5762335
0.76	7.4574000E-04	1.1398616E-02	1.1422984E-02	4.2802330E-03
0.66	2.1126020E-03	1.3758200E-03	2.5211049E-03	1.1696720

$\beta = 315^{\circ}$

2.84	1.3526826E-03	-2.7605887E-03	3.0741834E-03	.23563795
2.01	2.2510065E-02	-2.5964223E-03	2.2659312E-02	1.5574926
1.64	-1.4251068E-02	-1.3857170E-03	1.4318232E-02	1.5613485
1.42	6.6201360E-03	2.2844529E-02	2.3784421E-02	8.3782153E-02
1.16	3.8618272E-02	.11375610	.12013251	.11474253
0.90	1.0381650E-02	.15127856	.15163431	4.7094950E-03
0.76	-3.2978257E-02	8.2127900E-02	8.8511739E-02	.15986448
0.66	3.3920348E-02	7.9287937E-02	8.6239020E-02	.18101978

$\beta = 360^{\circ}$

2.84	7.4001000E-03	2.5138316E-02	2.6204894E-02	8.6440888E-02
2.01	7.7357000E-03	4.9477570E-03	9.1826664E-03	1.1824794
1.64	-.15563504	-3.2959346E-02	.15908672	1.5259784
1.42	-6.1765520E-02	-8.6433490E-03	6.2367356E-02	1.5512161
1.16	3.9925410E-02	.14792924	.15322239	7.2715048E-02
0.90	8.7730150E-03	.21327095	.21345131	1.6921280E-03
0.76	-4.8237163E-02	.11136973	.12136737	.18544301
0.66	4.6652989E-02	.11120381	.12059348	.17421852

HEAVE $\beta = 270^{\circ}$

OMEGA ω	COMPLEX RESPONSE OPERATOR REAL	COMPLEX RESPONSE OPERATOR IMAGINARY	AMPLITUDE RESPONSE OPERATOR MODULUS IN FEET/FOOT	PHASE RESPONSE OPERATOR ARGUMENT IN RADIANS
2.84	-1.8381666F-06	-4.0467986E-02	4.0467986E-02	2.0632248E-09
2.01	-1.3056682E-04	-6.7174585E-02	6.7174713E-02	3.7773665E-06
1.64	-1.6149958E-03	-.10689890	.10691110	2.2823900E-04
1.42	2.8840555E-03	7.7862730E-02	7.7916123E-02	1.3719790E-03
1.16	5.1902259E-02	.35603875	.35980193	2.1247731E-02
0.90	.21054511	.69511696	.72630360	9.1487226E-02
0.76	.16603058	.93561010	.95022764	3.1480586E-02
0.66	2.7004890E-02	.98269991	.98307092	7.5515900E-04

$\beta = 315^{\circ}$

2.84	1.5628450E-05	6.0630042E-03	6.0630246E-03	6.6444047E-06
2.01	1.4187577E-03	2.9279109E-02	2.9313462E-02	2.3480050E-03
1.64	2.7385190E-04	7.6401634E-03	7.6450699E-03	1.2847690E-03
1.42	4.7284270E-03	.11965566	.11994889	1.5563780E-03
1.16	6.4105187E-02	.33306744	.33918046	3.7027418E-02
0.90	.31230220	.74039489	.80356538	.17607688
0.76	-2.3533700E-03	1.0023390	1.0023417	5.5125324E-06
0.66	9.9784400E-03	.88960019	.88965620	1.2580900E-04

$\beta = 360^{\circ}$

2.84	-1.7673277E-03	-1.5001754E-02	1.5105498E-02	1.3877849E-02
2.01	-1.5731142E-02	-1.8345307E-02	2.4166488E-02	.63403308
1.64	-2.4866201E-02	-.16010674	.16202627	2.4115563E-02
1.42	-1.1795134E-02	-1.5439863E-03	1.1895759E-02	1.5536631
1.16	6.0633447E-02	.26654911	.27335846	5.1699080E-02
0.90	.35525623	.74398819	.82445464	.22417626
0.76	-7.6663430E-02	1.0266317	1.0294900	5.5762520E-03
0.66	-8.7586300E-04	.84668535	.84668585	1.0701096E-06

PITCH $\beta = 270^{\circ}$

OMEGA ω	COMPLEX RESPONSE OPERATOR REAL	COMPLEX RESPONSE OPERATOR IMAGINARY	AMPLITUDE RESPONSE OPERATOR MODULUS IN RADIANS/FOOT	PHASE RESPONSE OPERATOR ARGUMENT IN RADIANS
2.84	-8.8763165F-07	2.2450000E-08	8.8791573E-07	1.5701566
2.01	-5.1487560E-07	1.1115430E-05	1.1127344E-05	2.1456060E-03
1.64	-5.0220280E-06	8.6230800E-06	9.9763032E-06	.32721727
1.42	-4.5744490E-06	6.9050700E-06	8.2828459E-06	.41356443
1.16	-2.0266860E-04	-6.3694600E-05	2.1244201E-04	1.4723440
0.90	5.5183370E-04	-1.8848974E-03	1.9640168E-03	8.5502895F-02
0.76	2.6439423E-03	4.2830900E-04	2.6784112E-03	1.5445595
0.66	4.7226400E-04	-4.9066820E-04	6.8077740E-04	.74732730

$\beta = 315^{\circ}$

2.84	-2.6562065E-04	-3.0174694E-05	2.6732912E-04	1.5578919
2.01	2.4817507E-04	-2.2970789E-04	3.3816657E-04	.86241768
1.64	-2.0179800E-03	3.1121940E-04	2.0418378E-03	1.5470160
1.42	-6.2164931E-03	9.5715227E-04	6.2897500E-03	1.5470940
1.16	-7.7457839E-03	2.9116151E-03	8.2749432E-03	1.4304272
0.90	-5.9513780E-03	6.6829823E-03	8.9488077E-03	.67048187
0.76	-1.9387900E-02	1.2073598E-02	2.2830166E-02	1.2008167
0.66	-1.5660927E-02	-4.7684000E-03	1.6370774E-02	1.4783539

$\beta = 360^{\circ}$

2.84	1.9058357E-03	2.2597134E-04	1.9191862E-03	1.5567388
2.01	5.9187995E-03	-3.5053522E-04	5.9291735E-03	1.5672888
1.64	-3.3231124E-03	1.5148810E-03	3.6521163E-03	1.3659023
1.42	-1.0874071E-02	2.0757917E-03	1.1070425E-02	1.5343720
1.16	-1.2078317E-02	4.6410044E-03	1.2939411E-02	1.4241879
0.90	-8.8424580E-03	1.0912114E-02	1.5736579E-02	.61578461
0.76	-2.8637714E-02	1.7297596E-02	3.3456374E-02	1.2209683
0.66	-2.2505004F-02	-6.3426650E-03	2.3381715E-02	1.4915326

Table B-20. Results for the Various Incident Wave Directions

SWAY $\beta = 270^{\circ}$

OMEGA ω	COMPLEX RESPONSE OPERATOR REAL	COMPLEX RESPONSE OPERATOR IMAGINARY	AMPLITUDE RESPONSE OPERATOR MODULUS IN FEET/FOOT	PHASE RESPONSE OPERATOR ARGUMENT IN RADIANS
2.84	2.4012010E-03	4.0577503E-02	4.0643496E-02	3.5026050E-03
2.01	-3.7370550E-03	8.0632009E-02	8.0718569E-02	2.1480360E-03
1.64	-1.0581580E-02	.13360186	.13402024	6.2729270E-03
1.42	-5.0704320E-03	-7.9903567E-02	8.0064288E-02	4.0267480E-03
1.16	-.34401850	-.59742943	.68939881	.32017313
0.90	-.10759577	-.61870612	.62799214	3.0233554E-02
0.76	-.44631441	-.67807958	.81178108	.40882246
0.66	-.81241939	-.55207410	.98224802	1.1381902

$\beta = 315^{\circ}$

2.84	8.7149420E-03	-7.2150643E-03	1.1314033E-02	.96992851
2.01	-2.1857124E-02	-5.1501817E-02	5.5947933E-02	.17820072
1.64	6.1287916E-02	-2.6378500E-04	6.1286487E-02	1.5707778
1.42	.13138533	-9.2877240E-02	.16089838	1.1073744
1.16	-.52867446	-.40126929	.66371212	1.0481384
0.90	-.27315238	-.49454730	.56496839	.29609832
0.76	-.44732774	-.47369552	.69152865	.72824975
0.66	-.65627550	-.35448109	.74589170	1.2869236

YAW $\beta = 270^{\circ}$

OMEGA ω	COMPLEX RESPONSE OPERATOR REAL	COMPLEX RESPONSE OPERATOR IMAGINARY	AMPLITUDE RESPONSE OPERATOR MODULUS IN RADIANS/FOOT	PHASE RESPONSE OPERATOR ARGUMENT IN RADIANS
2.84	-2.1588753E-03	1.7679258E-03	2.7903954E-03	.98006558
2.01	-3.5966638E-03	2.4359030E-03	4.3439184E-03	1.1407384
1.64	-4.9577832E-03	2.9654049E-03	5.7821990E-03	1.3091786
1.42	2.4725879E-03	7.7560900E-05	2.4738046E-03	1.5698123
1.16	-4.4408446E-02	1.9710529E-02	4.8586159E-02	1.3762874
0.90	-3.7130206E-02	1.4810171E-02	3.9974910E-02	1.4130204
0.76	-2.0806604E-02	1.7683395E-02	2.7305995E-02	.94524784
0.66	-1.0626844E-02	1.4238219E-02	1.7766729E-02	.50824278

$\beta = 315^{\circ}$

2.84	7.8196115E-04	-3.9380102E-04	8.7552487E-04	1.3224125
2.01	-2.2022029E-03	-2.0534145E-03	3.0110151E-03	.85512520
1.64	7.0904826E-03	-2.6326866E-03	7.5634646E-03	1.4337972
1.42	2.3499022E-02	-1.2350756E-02	2.6547038E-02	1.3012771
1.16	-1.5242464E-02	2.1671312E-02	2.6494877E-02	.45939683
0.90	-2.8417974E-02	8.3820426E-03	2.9628647E-02	1.4839953
0.76	-1.5358222E-02	1.1049514E-02	1.8920010E-02	1.0931584
0.66	-7.6900400E-03	8.7928492E-03	1.1651140E-02	.65736735

ROLL $\beta = 270^{\circ}$

OMEGA ω	COMPLEX RESPONSE OPERATOR REAL	COMPLEX RESPONSE OPERATOR IMAGINARY	AMPLITUDE RESPONSE OPERATOR MODULUS IN RADIANS/FOOT	PHASE RESPONSE OPERATOR ARGUMENT IN RADIANS
2.84	-4.7739087E-03	-8.0147745E-04	4.8407216E-03	1.5476177
2.01	-7.4970966E-03	-2.8555856E-03	8.0225201E-03	1.4767226
1.64	-1.0722992E-02	-6.6989876E-03	1.2643536E-02	1.1986893
1.42	6.8424847E-03	6.3099801E-03	9.3078167E-03	.86606433
1.16	-2.6050057E-02	5.0936514E-02	5.7211311E-02	.25582172
0.90	-3.0686395E-02	1.6617290E-02	3.4896837E-02	1.2855494
0.76	-2.1608817E-02	1.1015509E-02	2.4254534E-02	1.3165550
0.66	-1.5647239E-02	6.6039869E-03	1.6983778E-02	1.3945153

$\beta = 315^{\circ}$

2.84	5.3937303E-04	5.4742280E-05	5.4214396E-04	1.5604959
2.01	-1.2310234E-03	1.8632297E-03	2.2331693E-03	.41158393
1.64	5.1500848E-03	-5.0863980E-03	7.2384271E-03	.79784010
1.42	2.3700910E-02	-1.2193223E-02	2.6635201E-02	1.3136785
1.16	8.4109610E-03	4.3018371E-02	4.3852914E-02	3.8209544E-02
0.90	-2.0357646E-02	8.4080837E-03	2.2025658E-02	1.4018383
0.76	-1.4875424E-02	5.4871425E-03	1.5855188E-02	1.4355595
0.66	-1.0936357E-02	3.2338634E-03	1.1404463E-02	1.4835805

NOTE: For $\beta = 360^{\circ}$, all entries equal zero.

Appendix C

COMPUTER PROGRAMS

Appendix C contains listings and writeups of the major computer programs employed in this study. The following programs are included:

1. Spectral and Cross-Spectral Program for 7094
2. Wave Excitation Force Program for 7094
3. Complex Matrix Inversion Program for 1620
4. Complex Matrix Multiplication Program for 1620
5. Mooring Force Catenary Program for 7094
6. Derivation of Linear and Angular Displacements from Acceleration Records Program for 1620

All of the listings are given in the original Fortran II source language.

SPECTRAL AND CROSS-SPECTRAL PROGRAM FOR 7094

This program consists of a spectral package of 11 subroutines: SPC, CQG, CSTAB, CSTR, LPRG, PTG, RMG, SMOOTH, SPG, SPMAP, and WRITES. These subroutines assume a maximum lag of 300 and a minimum of 30 for cross-spectra which can be changed by repunching the needed dimension cards. Nine hundred common locations are used to conserve working storage for the subroutines. Those, too, can be omitted by recompiling.

Calling sequence is SPC (DATUM, NSER, N, LABEL, IDV, SPM) with definitions:

DATUM	data matrix consisting of at least NSER columns and exactly N rows
LABEL	12-word hollerith page heading
IDV	hollerith vector of at least NSER elements. It identifies each data column
SPM	spectral matrix of NSER rows and M+1 columns where M is the maximum lag. This lag is read in by the subroutine itself

After the input program has called the first subroutine SPC, the following data are read in by the subroutine:

DELT, TEST, M, MAXCS, (LR(I), LS(I), I = 1, MAXCS
FORMAT (2E10.3, 215.8 (IX, 212)/14(IX, 212)

DELT	time between observations
TEST	zero if the computer finds its own bounds for the graphing routines. Otherwise, TEST is the upper bound. In that case, zero is assumed to be the lower bound
MAXCS	total number of cross-spectra needed. If only spectra are wanted, MAXCS = 0

For each I, from 1 to MAXCS, the computer will find the cross-spectra between the LF (I)'th and LS (I)'th data columns. Covariances, raw and smooth, are printed. Both normalized covariances and spectra are graphed. Coherencies, phase angle, and the complex gain are printed for each cross-spectrum. The spectra themselves are also repeated. Finally, the coherencies are graphed on a fixed scale of zero to one.

The following is an example of the use of this program:

Call SPC (X, 76, 127, LABEL, IDV, SPM) followed by the following cards:

3	0	12	23	1364	4264	etc.
xxxx	xxxx	xxxx	xxxx	xxxx	xxxx	

The data, X, consists of 127 rows and 76 columns. The identification of the Jth column is IDV (j). The time between observations is 3 time units (seconds, hours, etc.). No fixed scale is used in graphing except for coherencies. All 76 spectra of 12 lags will be computed. Twenty-three cross-spectra will be found - 13th versus 64th, 42nd versus 64th, etc.

Listing of the subroutines along with a sample master input program is given in Tables C-1 through C-4.

WAVE EXCITATION FORCE PROGRAM FOR 7094

This program, which consists of one input program and one subroutine, computes the wave-exciting forces as outlined in Appendix B. Input data punched on cards in the indicated format are as follows:

JM	number of wave directions to be computed
IM	number of wave frequencies (or lengths) to be computed
KM	number of cross sections to be considered in the computations
D	depth of water in feet
H	barge draft in feet
G	acceleration of gravity in feet/second^2
RO	density of sea water in slugs/foot^3
GO	distance in feet from the free surface to the center of gravity
EL	length of the barge in feet
B	barge width in feet
P	value of $\pi = 3.1415926536$
A44	added moment of inertia in roll in slugs-feet^2
CO(1)	coefficients of the terminal stern sectional elements
CO(3)	coefficients of the terminal bow sectional elements
BET(J)	incident wave directions in degrees to be considered
RAM(I)	wave lengths in feet to be considered
W(I)	wave frequencies in radians/second to be considered
CY(I)	three-dimensional damping factors in sway

Table C-1. Spectral and Cross-Spectral Program for 7094

```
C     PROGRAM NCEL
      DIMENSION D(1801,10), SPM(10,61), IDV(10), LABEL (12)
      READ INPUT TAPE 7, 10, (LABEL (I), I = 1, 12)
   10 FORMAT (12 A6)
   12 FORMAT (3X, 10F4.0, 29X)
      READ INPUT TAPE 7, 11, (IDV(I), I = 1,10)
   11 FORMAT (10(1X,A6), 2X)
      READ INPUT TAPE 7,12, ((D(I,J), J = 1,10), I = 1,1801)
      CONV = 5.74/797.0
      DO 13 I = 1, 1801
      D(I, 1) = CONV*(800    -D(I, 1))*20.95
      D(I, 2) = CONV*(800    -D(I, 2))*14.05
      D(I, 3) = CONV*(800    -D(I, 3))*14.85
      D(I, 4) = CONV*(800    -D(I, 4))*17.65
      D(I, 5) = CONV*(800    -D(I, 5))*10.80
      D(I, 6) = CONV*(800    -D(I, 6))* 9.20
      D(I, 7) = CONV*(800    -D(I, 7))* 11.40
      D(I, 8) = CONV*(800    -D(I, 8))* 9.90
      D(I, 9) = CONV*(800    -D(I, 9))*9.80
   13 D(I,10) = CONV*(800    -D(I,10))*9.60
      CALL SPC (D,10,1801, LABEL, IDV, SPM)
      END
```

```
*     SUBROUTINE SPC                                                    SPC30002
      SUBROUTINE  SPC(DATAM,NSER, N,LABEL, IDV,SPM)                     SPC30002
      DIMENSION  A(301),B(301),C(301),CS(600),SN(600),CO(301),QUOD(301),SPC30004
     X DATAM(1),SPM(1),LABEL(12),IDV(30),LF(30),LS(30),AV(30),SIG(30)   SPC30005
      COMMON A,B,C                                                      SPC30003
  200 FORMAT(2E10.3,2I5,8(1X,2I2)/   14(1X,2I2) )                       SPC30007
      READ INPUT TAPE 5,200,DELT,TEST,M,MAXCS,(LF(I),LS(I),I=1,MAXCS)   SPC30006
      CALL CSTAB(CS,SN,M)                                               SPC30008
        CALL   RMG(DATAM,NSER,N,AV)                                     SPC30009
      DO 6 J=1, NSER                                                    SPC30010
    4 WRITE OUTPUT TAPE 6, 105, LABEL                                   SPC30011
  105 FORMAT(1H1,25X, 12A6)                                             SPC30012
      CALL SPG (DATAM,M,N,J,SPM,CS,DELT,AV,SIG,IDV,NSER        )        SPC30013
      WRITE OUTPUT TAPE 6, 105, LABEL                                   SPC30014
      WRITE OUTPUT TAPE 6, 79, IDV(J)                                   SPC30015
   79  FORMAT  (  1H0 25X,  19HSPECTRAL  GRAPH  OF  3X,  A6  )          SPC30016
       CALL  SPMAP (TEST  ,  M,  C)                                     SPC30017
   80 FORMAT (1H0 25X,32HGRAPH OF NORMALIZED COVARIANCES 5X A6)         SPC30018
      WRITE OUTPUT TAPE 6, 105, LABEL                                   SPC30019
      WRITE OUTPUT TAPE 6, 80, IDV(J)                                   SPC30020
      CALL SPMAP(0.0 ,M,A)                                              SPC30021
    6 CONTINUE                                                          SPC30022
      IF (MAXCS) 8,11,8                                                 SPC30023
    8 DO  10  K=1,MAXCS                                                 SPC30024
      JF=LF(K)                                                          SPC30025
      JS= LS(K)                                                         SPC30026
    7 WRITE  OUTPUT  TAPE  6, 105,LABEL                                 SPC30027
      WRITE OUTPUT TAPE 6, 91,IDV(JF), AV(JF),SIG(JF),IDV(JS),AV(JS),   SPC30028
     1  SIG(JS),N,M                                                    SPC30029
   91 FORMAT(1H0,40X,14HIDENTIFICATION, 11X,7HAVERAGE,10X,              SPC30030
     1     18HSTANDARD DEVIATION//24X21HDRIVING FUNCTION....., A6,     SPC30031
     2     1P2E23.3//24X21HOUTPUT FUNCTION.....,A6,1P2E23.3// 29X,     SPC30032
     3     30HNUMBER OF OBSERVATIONS.....  , I4,12X, 9HNUMBER OF       SPC30033
     4 11H LAGS....., I2///)                                            SPC30034
      CALL COG (DATAM,CS,SN,M,N,JF,JS,CO,QUOD)                          SPC30035
      CALL PTG(SPM,M,N,CO,QUOD,JF,JS,NSER)                              SPC30036
      WRITE OUTPUT TAPE 6, 105,  LABEL                                  SPC30037
        WRITE OUTPUT TAPE 6, 88, IDV(JF) , IDV(JS)                      SPC30038
   88   FORMAT ( 1H0  25X, 16HCOHERENCY  GRAPH  20X,A6,3X,3HAND3XA6)     SPC30039
   10 CALL SPMAP (1.0, M , A )                                          SPC30040
   11 CONTINUE                                                          SPC30041
        RETURN                                                          SPC30042
      END
```

Continued

Table C-1. Spectral and Cross-Spectral Program for 7094 (Contd)

```
      SUBROUTINE SPG                                                    SPG30002
      SUBROUTINE  SPG(DATAM,M,N, J, SPM, CS,DELT,AV,SIG,IDV,NSER)       SPG30003
       XSPECF(I,J)  =  NSER * (J-1)  +  I                               SPG30004
      DIMENSION  A(301), B(301), C(301)                                 SPG30005
      DIMENSION DATAM(1),SPM(1),CS(1),SN(1),AV(1),SIG(1),IDV(1)         SPG30006
      COMMON  A,B,C                                                     SPG30007
      M1 = 1+M                                                          SPG30008
      CALL LPRG(DATAM, M, N, J, J, A)                                   SPG30009
      SIG(J) = SQRTF(A(1))                                              SPG30010
      CALL CSTR (A, CS, M, B)                                           SPG30011
      CALL SMOOTH ( B, M, C)                                            SPG30012
  200 FORMAT (1H0, 8X,7HMEAN = 1P E12.4,26X,A6,26X, 21HSTANDARD DEVIATIOSPG30013
     1N =    1P E12.4)                                                  SPG30014
      WRITE OUTPUT TAPE 6,200, AV(J), IDV(J),SIG(J)                     SPG30015
      WRITE OUTPUT TAPE 6, 100                                          SPG30016
  100 FORMAT(12H0    LAG NO.9X,11HCYCLES/TIME  12X,8HRAD/TIME   10X ,10HSPG30017
     1COVARIANCE  8X,  12HRAW SPECTRUM   5X,  15HSMOOTH SPECTRUM//)     SPG30018
      FM = M                                                            SPG30019
         A1  =  A(1)
      DO  10   JM1 = 1,M1                                               SPG30020
      JM = JM1-1                                                        SPG30021
      FJM = JM                                                          SPG30022
      CPS = FJM / (2.* DELT * FM)                                       SPG30023
      RADPS = 6.283186 * CPS                                            SPG30024
      A(JM1) = A(JM1) / A  1
      WRITE OUTPUT TAPE 6,101, JM, CPS,RADPS,A(JM1), B(JM1), C(JM1)     SPG30026
  101 FORMAT  (1H  I10,2F20.4 , 1P 3E20.4  )                            SPG30027
       JJM1  =  XSPECF(J,JM1)                                           SPG30028
   10  SPM(JJM1)  =  C(JM1)                                             SPG30029
      RETURN                                                            SPG30030
       END
```

```
*     SUBROUTINE WRITES
      SUBROUTINE WRITES (B1,B2,B3,B4,B5,B6,  FX,N,XMAX,XMIN)            WRITES04
      DIMENSION X(1),FX(1),B(6),OV(17)                                  WRITES05
  100 FORMAT (8X,I3,     2X,1H=,1X,17A6,1H=)                            WRITES06
      B(1)=B1                                                           WRITES07
      B(2)=B2                                                           WRITES08
      B(3)=B3                                                           WRITES09
      B(4)=B4                                                           WRITES10
      B(5)=B5                                                           WRITES11
      B(6)=B6                                                           WRITES12
      FACTOR=100.0/(XMAX-XMIN)                                          WRITES13
      DO 2 K=1,17                                                       WRITES14
B     2 OV(K)=606060606060                                              WRITES15
      DO 1 I=1,N                                                        WRITES16
      JSCALE=(FX(I)-XMIN)*FACTOR+.5                                     WRITES17
      M=XMODF(JSCALE,6)+1                                               WRITES18
      L=JSCALE/6+1                                                      WRITES19
      IM=I-1                                                            WRITES20
      OV(L)=B(M)                                                        WRITES21
      WRITE OUTPUT TAPE 6,100,IM  ,(OV(K),K=1,17)                       WRITES22
B     1 OV(L)=606060606060                                              WRITES23
      RETURN                                                            WRITES24
      END                                                               WRITES25
```

```
*     SUBROUTINE PTG                                                    PTG30002
      SUBROUTINE PTG(SPM,M,N,CO,QUOD,JF,JS,NSER)                        PTG30003
       XSPECF(I,J)  =  NSER * (J-1)  +  I                               PTG30004
      DIMENSION COHER(301),B(301),C(301)
      DIMENSION            SPM(602),CO(1),QUOD(1)                       PTG30005
      COMMON   COHER,B,C                                                PTG30006
  100 FORMAT (7X,I3,1P5E14.3, 3H  + E9.3,3H I   0PF10.4,0P F9.1,1PE14.3) PTG30007
  900 FORMAT (7X,I3,1P5E14.3, 2H   E10.3,3H I   0PF10.4,0P F9.1,1PE14.3) PTG30008
      M1= M+1                                                           PTG30009
      PI = 3.141592636                                                  PTG30010
      WRITE OUTPUT TAPE 6,666                                           PTG30011
  666 FORMAT(1H0 6X,3HLAG 12X, 7HSPECTRA 20X, 5HCROSS 2X, 7HSPECTRA 12X,PTG30012
     1 13HCOMPLEX  GAIN  8X,9HCOHERENCE3X5HPHASE6X8HRESPONSE/8X3HNO.7X  PTG30013
     2 5HINPUT 7X, 6HOUTPUT  10X 2HCO 12X,4HQUAD 55X,8HOPERATOR/1H0)    PTG30014
      DO  6   K = 1, M1                                                 PTG30015
      K1= K-1                                                           PTG30016
       JFK = XSPECF(JF,K)                                               PTG30017
       JSK = XSPECF(JS,K)                                               PTG30018
      A = SPM(JFK)                                                      PTG30019
      G = SPM(JSK)
      COHER(K) = (CO(K)**2 +QUOD(K)** 2 )  /  ( A * G)                  PTG30020
      RESP = G/A
      S  = SIGNF- ( PI, QUOD(K))                                        PTG30021
      IF  (CO(K))    3, 2, 4                                            PTG30022
    2     AT  = .5  * 5                                                 PTG30023
      GO  TO  9                                                         PTG30024
    3   S  =  0.0                                                       PTG30025
    4   AT  =  ATAN F(QUOD(K) / CO(K) )                                 PTG30026
      9 PHASE=AT+PI-S                                                   X+700  7
    5   PHASE  =  PHASE *  57.2957795                                   PTG30028
      GAINR  =  CO(K) / A                                               PTG30029
      GAINI  =  QUOD(K) /A                                              PTG30030
      IF (GAINI)21,31,31                                                PTG30031
   21 WRITE OUTPUT TAPE 6,900,K1,A        ,G        ,CO(K),QUOD(K)      PTG30032
     1GAINR, GAINI, COHER(K), PHASE, RESP                               PTG30033
       GO  TO  6                                                        PTG30034
   31 WRITE OUTPUT TAPE 6,100,K1,A        ,G        ,CO(K),QUOD(K),     PTG30035
     1GAINR, GAINI, COHER(K), PHASE, RESP                               PTG30036
    6    CONTINUE                                                      PTG30037
      RETURN                                                            PTG30038
       END
```

Continued

Table C-1. Spectral and Cross-Spectral Program for 7094 (Contd)

```
*     SUBROUTINE CSTAR
      SUBROUTINE   CSTR (Q, TABLE, M, U)                                  CSTR 003
      DIMENSION  Q(1), TABLE(1), U(1)                                     CSTR 004
      DIMENSION A(301),B(301),C(301)
      COMMON A,B,C
      U IS EITHER A COS OR SIN TRANSFORM DEPENDING ON TABLE.              CSTR 005
      M1 = 1+M                                                            CSTR 006
      FM=M                                                                CSTR 007
      Q(1) =  .5 *  Q(1)                                                  CSTR 008
      Q(M1) = .5 *  Q(M1)                                                 CSTR 009
      MM    =  M*2                                                        CSTR 010
      C = 2.0 /FM                                                         CSTR 011
      DO5 J=1,M1                                                          CSTR
      JM1=J                                                               CSTR
       JM = JM1-1                                                         CSTR 013
      U(JM1) =0.0                                                         CSTR 014
      DO4 I=1,M1                                                          CSTR
      IM1=I                                                               CSTR
      IM = IM1-1                                                          CSTR 016
      K = XMODF ( IM *JM ,MM)                                             CSTR 017
      IF (K)   3,3,4                                                      CSTR 018
    3 K=MM                                                                CSTR 019
    4 U(JM1) = U(JM1) +Q(IM1)*TABLE(K)                                    CSTR 020
    5 U(JM1) = U(JM1) *C                                                  CSTR 021
        Q(1)  =  2.0  *  Q(1)                                             CSTR 022
        Q(M1)  =  2.0  *  Q(M1)                                           CSTR 023
      RETURN                                                              CSTR 024
       END

*     SUBROUTINE CSTAB
      SUBROUTINE      CSTAB (CS,SN,M)                                     CSTAB 04
      DIMENSION A(301),B(301),C(301)
      COMMON A,B,C
      FM= M                                                               CSTAB 05
      MM=M*2                                                              CSTAB 06
      DIMENSION   CS(1), SN(1)                                            CSTAB 07
      ANG =  3.141592654  /FM                                             CSTAB 08
      DO  1    K=  1, MM                                                  CSTAB 09
      FK = K                                                              CSTAB 10
      G = FK * ANG                                                        CSTAB 11
      CS(K)  =COSF(G)                                                     CSTAB 12
    1 SN(K) =SINF (G)                                                     CSTAB 13
      RETURN                                                              CSTAB 14
       END

*     SUBROUTINE SMOOTH
      SUBROUTINE  SMOOTH (U,M,W)                                          SMOOTH03
      DIMENSION  U(1), W(1)                                               SMOOTH04
      DIMENSION A(301),B(301),C(301)
      COMMON A,B,C
      M1 = M+1                                                            SMOOTH05
      W(1) = .5 *( U(1)+U(2))                                             SMOOTH06
      W(M1)= .5 *( U(M)+U(M1))                                            SMOOTH07
      DO  1    I = 2, M                                                   SMOOTH08
    1 W(I)  = .25 * (U(I-1) + U(I+1)) + .5 * U(I)                         SMOOTH09
      RETURN                                                              SMOOTH10
       END

*     SUBROUTINE SPMAP
      SUBROUTINE SPMAP(FNTEST,M,FX)                                       SPMAP 02
      DIMENSION X(1),FX(1),B(6),OV(17)  ,S(11)                            SPMAP 03
  101 FORMAT(15X1HA,9X,1HB,9X,1HC,9X,1HD,9X1HE,9X1HF,9X1HG,9X1HH,9X1HI,9SPMAP 04
     1X,1HJ,9X,1HK)                                                       SPMAP 05
  103 FORMAT(15X,101H----------                                          SPMAP 06
     1----------)                                                         SPMAP 07
  104  FORMAT(3H0A=1PE8.1,3H,B=E8.1,3H,C=E8.1,3H,D=E8.1,3H,E=E8.1,3H,F=   SPMAP 08
     X  E8.1,3H,G=1PE8.1,3H,H=E8.1,3H,I=E8.1,3H,J=E8.1,3H,K=E8.1//)       SPMAP 09
       N=M+1                                                              SPMAP 10
       IF(FNTEST) 10,9,10                                                 SPMAP 11
    9  XMAX=FX(1)                                                         SPMAP 12
       XMIN=FX(1)                                                         SPMAP 13
       DO 1 I=1,N                                                         SPMAP 14
       IF (XMAX-FX(I)) 2,3,3                                              SPMAP 15
    3  IF (XMIN-FX(I)) 1,1,5                                              SPMAP 16
    2  XMAX=FX(I)                                                         SPMAP 17
       GO TO 1                                                            SPMAP 18
    5  XMIN=FX(I)                                                         SPMAP 19
    1  CONTINUE                                                           SPMAP 20
       GO TO 17                                                           SPMAP 21
   10  XMAX=FNTEST                                                        SPMAP 22
       XMIN=0.0                                                           SPMAP 23
       DO 11 I=1,N                                                        SPMAP 24
       IF (XMAX-FX(I)) 12,13,13                                           SPMAP 25
   13  IF (XMIN-FX(I)) 11,11,15                                           SPMAP 26
   12  FX(I)=XMAX                                                         SPMAP 27
       GO TO 11                                                           SPMAP 28
   15  FX(I)=XMIN                                                         SPMAP 29
   11  CONTINUE                                                           SPMAP 30
   17  DELT=(XMAX-XMIN)/10.0                                              SPMAP 31
       DO 6 K=1,11                                                        SPMAP 32
       FK=K                                                               SPMAP 33
    6  S(K)=XMIN+(FK-1.0)*DELT                                            SPMAP 34
       WRITE OUTPUT TAPE 6,104,(S(I),I=1,11)                              SPMAP 35
       WRITE OUTPUT TAPE 6,101                                            SPMAP 36
       WRITE OUTPUT TAPE 6,103                                            SPMAP 37
       CALL WRITES (6H*     ,6H *    ,6H  *   ,6H   *  ,6H    * ,6H     *
     X,FX,N,XMAX,XMIN)
       WRITE OUTPUT TAPE 6,103                                            SPMAP 40
       WRITE OUTPUT TAPE 6,101                                            SPMAP 41
       RETURN                                                             SPMAP 42
        END
```

Continued

Table C-1. Spectral and Cross-Spectral Program for 7094 (Contd)

```
*     SUBROUTINE CQG
      SUBROUTINECQG(DATAM,CS,SN,M,N,JF,JS,CO,QUOD)                    CQG   02
      DIMENSION              DATAM(1),CO(1),QUOD(1),CS(1),SN(1)       CQG   03
      DIMENSION A(301),B(301),C(301)
      COMMON A,B,C
      M1=M+1                                                          CQG   05
      CALL LPRG(DATAM,M,N,JF,JS,CO )                                  CQG   06
      CALL LPRG(DATAM,M,N,JS,JF,QUOD)                                 CQG   07
      DO   1   J = 1, M1                                              CQG   08
      CO(J) = .5 * (CO(J) + QUOD (J))                                 CQG   09
    1 QUOD(J) = CO(J)  - QUOD (J)                                     CQG   10
      CALL   CSTR  (CO , CS,  M,  A  )                                CQG   11
      CALL   CSTR  (QUOD, SN, M,  B )                                 CQG   12
      CALL  SMOOTH  (A,  M,  CO  )                                    CQG   13
      CALL  SMOOTH  (B,  M,  QUOD )                                   CQG   14
      QUOD(1)=0.0                                                     CQG   15
      QUOD(M1)=0.0                                                    CQG   16
      RETURN                                                          CQG   17
       END
```

```
*     SUBROUTINE RMG
      SUBROUTINE RMG(DATAM, NSER,N,AV)                                RMG   02
      DIMENSION A(301),B(301),C(301)
      COMMON A,B,C
      XFINDF(I,J) = N * (J-1) + I                                     RMG   03
      DIMENSION   DATAM(1), AV(1)                                     RMG   04
      FN=N                                                            RMG   05
      DO 1  J = 1, NSER                                               RMG   06
      AV(J)= 0.0                                                      RMG   07
      DO 2  K = 1, N                                                  RMG   08
      KJ = XFINDF (K,J)                                               RMG   09
    2 AV(J) = AV(J) + DATAM (KJ)                                      RMG   10
      AV(J) =AV(J) / FN                                               RMG   11
      DO 3   K = 1,N                                                  RMG   12
      KJ = XFINDF(K,J)                                                RMG   13
    3 DATAM(KJ) = DATAM(KJ) - AV(J)                                   RMG   14
    1 CONTINUE                                                        RMG   15
      RETURN                                                          RMG   16
       END
```

```
*     SUBROUTINE LPRG
      SUBROUTINE  LPRG(DATA, M, N, J, K, Q)                           LPRG  02
      XFINDF(I,J) = N *(J-1) + I                                      LPRG  03
      DIMENSION DATA(1), Q(1)                                         LPRG  04
      M1 = M + 1                                                      LPRG  05
      DO  10   JM1  = 1, M1                                           LPRG  06
      JM  = JM1  -  1                                                 LPRG  07
      Q(JM1) = 0.0                                                    LPRG  08
      NJM = N - JM                                                    LPRG  09
      FNJM = NJM                                                      LPRG  10
      DO  1    I = 1, NJM                                             LPRG  11
      IJM   = I + JM                                                  LPRG  12
      IJ = XFINDF(I,J)                                                LPRG  13
      IJMK = XFINDF(IJM,K)                                            LPRG  14
    1 Q(JM1) = DATA(IJ) * DATA(IJMK) + Q(JM1)                         LPRG  15
   10 Q(JM1) = Q(JM1)  /FNJM                                          LPRG  16
      RETURN                                                          LPRG  17
      END
```

Table C-2. Wave Excitation Force Program for 7094

```
C     MUGA MAIN PROGRAM
      DIMENSION XI(103),ZCB(103),BET(24),RAM(8),W(8),CY(8),CZ(8),
     1YYN(103,8),CO(3),ES(103),A22(103,8),A42(103),A33(103,8),
     2ZZN(103,8),BS(103)
      COMMON ES,A22,A42,A33,ZZN,BS,XI,CO,A44,ZCB,BET,RAM,W,CY,CZ,YYN,D,
     1H,G,RO,GO,EL,B,P,JM,IM,KM
      READ INPUT TAPE 5,101,JM,IM,KM
      READ INPUT TAPE 5,100,D,H,G,RO,GO
      READ INPUT TAPE 5,100,EL,B,P,A44
      READ INPUT TAPE 5,100,CO(1),CO(3)
      READ INPUT TAPE 5,100,(BET(J),J=1,JM)
      READ INPUT TAPE 5,100,(RAM(I),W(I),CY(I),CZ(I),I=1,IM)
      READ INPUT TAPE 5,102,(XI(K),BS(K),ES(K),ZCB(K),A42(K),K=1,KM)
      READ INPUT TAPE 5,100,((A33(K,I),I=1,IM),K=1,KM)
      READ INPUT TAPE 5,100,((ZZN(K,I),I=1,IM),K=1,KM)
      READ INPUT TAPE 5,100,((A22(K,I),I=1,IM),K=1,KM)
      READ INPUT TAPE 5,100,((YYN(K,I),I=1,IM),K=1,KM)
  100 FORMAT(8E10.3)
  101 FORMAT(3I5)
  102 FORMAT(5E10.3)
      CALL WEF
      CALL EXIT
      END
C     SUBROUTINE WEF     MUGA-SHOEMAKER
      SUBROUTINE WEF
      DIMENSION XI(103),ZCB(103),BET(24),RAM(8),W(8),CY(8),CZ(8),
     1YYN(103,8),CO(3),ES(103),A22(103,8),A42(103),A33(103,8),
     2ZZN(103,8),BS(103),SS(16),A(8,12),S(26)
      COMMON ES,A22,A42,A33,ZZN,BS,XI,CO,A44,ZCB,BET,RAM,W,CY,CZ,YYN,D,
     1H,G,RO,GO,EL,B,P,JM,IM,KM
      DO 3 J=1,JM
      P=3.1415926536
      BT=BET(J)/180.*P
      SB=INTF(SINF(BT)*100000.)/100000.
      CB=INTF(COSF(BT)*100000.)/100000.
      WRITE OUTPUT TAPE 6,201,BT,BET(J)
  201 FORMAT(1H1/30X5HBETA=F10.6,8HRADIANS,F10.2,7HDEGREES)
      DO 2 I=1,IM
      PL=P/RAM(I)
      PL2=2.*PL
      PLD2=PL2*D
      PLH2=PL2*H
      E=EXPF(-PLH2)
      PBL=PL*B
      RTERM=RO*W(I)**2*E
      TANT=RO*G*TANHF(PLD2)
      IF(SB)4,5,4
    4 GLUMP=SINF(PBL*SB)/(PBL*SB)
      GO TO 11
    5 GLUMP=1.
   11 RED=-RTERM*GLUMP
      REDC=RED*CB
      REDS=RED*SB
      GRN=W(I)*E*GLUMP
      GRNY=CY(I)*GRN*SB
      GRNZ=CZ(I)*GRN
      BLK=TANT*GLUMP
      BOX=A44/EL*W(I)*PL2*GRN*SB
      DO 20 K=1,26
   20 S(K)=0.
      KMM=KM-1
      LL=2*KMM-2
      DO 1 K=1,KM
      KK=(LL+K)/KMM
      BRAK=PL2*XI(K)*CB
      CBRAK=COSF(BRAK)
      SBRAK=SINF(BRAK)
      GWIG=ES(K)+A22(K,I)/RO+PL2*A42(K)/RO
      RL=ES(K)+A33(K,I)/RO
      BWIG=A42(K)/RO-ES(K)*ZCB(K)-BS(K)**3/12.
      SS(1)=ES(K)*CBRAK
      SS(2)=ES(K)*SBRAK
      SS(3)=GWIG*CBRAK
      SS(4)=YYN(K,I)*SBRAK
      SS(5)=GWIG*SBRAK
      SS(6)=YYN(K,I)*CBRAK
      SS(7)=RL*SBRAK
      SS(8)=ZZN(K,I)*CBRAK
      SS(9)=BS(K)*SBRAK
      SS(10)=RL*CBRAK
      SS(11)=ZZN(K,I)*SBRAK
      SS(12)=BS(K)*CBRAK
      SS(13)=BWIG*CBRAK/X
      SS(14)=CBRAK/X
      SS(15)=BWIG*SBRAK/X
      SS(16)=SBRAK/X
      GO TO(6,7,6),KK
    6 DO 8 L=1,16
    8 SS(L)=SS(L)*CO(KK)
    7 DO 9 L=1,12
    9 S(L)=S(L)+SS(L)
      X=XI(K)
      DO 10 L=13,26
   10 S(L)=S(L)+SS(L-10)*X
    1 CONTINUE
      A(I,1)=REDC*S(1)
      A(I,2)=REDC*S(2)
      A(I,3)=REDS*S(3)+GRNY*S(4)
      A(I,4)=REDS*S(5)-GRNY*S(6)
      A(I,5)=RED*S(7)-GRNZ*S(8)+BLK*S(9)
      A(I,6)=-RED*S(10)-GRNZ*S(11)-BLK*S(12)
      A(I,7)=REDS*S(13)+GRNY*S(16)
      A(I,8)=REDS*S(15)-GRNY*S(14)
      A(I,9)=-RED*S(17)+GRNZ*S(18)-BLK*S(19)
      A(I,10)=RED*S(20)+GRNZ*S(21)+BLK*S(22)
      A(I,11)=REDS*(S(23)+GO*S(3))-BOX*S(24)+GO*GRNY*S(4)
      A(I,12)=REDS*S(25)-BOX*S(26)+GO*(REDS*S(5)-GRNY*S(6))
    2 CONTINUE
      WRITE OUTPUT TAPE 6,202
      WRITE OUTPUT TAPE 6,204
      WRITE OUTPUT TAPE 6,203,(W(L),A(L,1),A(L,2),A(L,5),A(L,6),A(L,9),
     1A(L,10),L=1,IM)
      WRITE OUTPUT TAPE 13,206,(    A(L,1),A(L,2),A(L,5),A(L,6),A(L,9),
     1A(L,10),L=1,IM)
      WRITE OUTPUT TAPE 6,205
      WRITE OUTPUT TAPE 6,204
      WRITE OUTPUT TAPE 6,203,(W(L),A(L,3),A(L,4),A(L,7),A(L,8),
     1A(L,11),A(L,12),L=1,IM)
      WRITE OUTPUT TAPE 13,206,(    A(L,3),A(L,4),A(L,7),A(L,8),
     1A(L,11),A(L,12),L=1,IM)
    3 CONTINUE
  202 FORMAT(1H /7H  OMEGA12X5HSURGE23X5HHEAVE23X5HPITCH)
  205 FORMAT(1H /7H  OMEGA13X4HSWAY24X3HYAW24X4HROLL)
  204 FORMAT(9H RADS/SEC4X4HREAL7X9HIMAGINARY8X4HREAL7X9HIMAGINARY8X,
     14HREAL7X9HIMAGINARY/1H )
  203 FORMAT(F6.2,6E14.4)
  206 FORMAT(6E12.4)
      END FILE 13
      RETURN
      END
```

Table C-3. Sample Output From Wave Excitation Force Program for 7094

BETA= 5.323254RADIANS, 305.00DEGREES

OMEGA RADS/SEC	SURGE REAL	SURGE IMAGINARY	HEAVE REAL	HEAVE IMAGINARY	PITCH REAL	PITCH IMAGINARY
2.84	-0.5173E 01	0.4476E 02	0.6430E 03	0.4211E 04	-0.2159E 06	-0.2096E 05
2.01	-0.1251E 03	0.5226E 03	0.9749E 04	0.3414E 05	-0.3048E 07	-0.7091E 06
1.64	-0.5278E 03	-0.1426E 01	-0.9790E 03	0.2936E 04	0.2279E 06	0.3149E 05
1.42	-0.1189E 05	0.1158E 03	-0.2002E 05	0.7032E 05	0.2795E 07	0.6034E 06
1.16	-0.2230E 05	0.2229E 03	-0.5805E 05	0.7036E 05	0.2029E 07	0.1265E 07
0.90	-0.2117E 05	0.1447E 03	-0.1039E 06	-0.3264E 05	0.9728E 06	0.1538E 07
0.76	-0.1711E 05	0.8610E 02	-0.1200E 06	-0.9562E 05	0.8756E 06	0.1202E 07
0.66	-0.1361E 05	0.5390E 02	-0.1154E 06	-0.1381E 06	0.9216E 06	0.9148E 06

OMEGA RADS/SEC	SWAY REAL	SWAY IMAGINARY	YAW REAL	YAW IMAGINARY	ROLL REAL	ROLL IMAGINARY
2.84	-0.1379E 06	0.1658E 06	0.1706E 07	-0.2525E 07	0.2252E 07	-0.2323E 07
2.01	-0.7305E 06	-0.2211E 06	0.1471E 08	-0.2088E 08	0.1079E 08	0.3327E 07
1.64	0.2657E 05	0.1873E 05	0.6163E 05	0.7190E 06	-0.3300E 06	-0.3275E 06
1.42	0.1920E 06	0.2113E 06	0.2082E 07	0.4789E 07	-0.2829E 07	-0.4110E 07
1.16	0.8783E 05	0.1616E 06	0.1417E 07	0.1751E 07	-0.3972E 07	-0.3808E 07
0.90	0.2466E 05	0.4867E 05	-0.7011E 05	0.1937E 06	-0.4905E 07	-0.1615E 07
0.76	0.1695E 05	0.1729E 05	-0.2767E 06	0.4814E 05	-0.4589E 07	-0.7947E 06
0.66	0.1428E 05	0.6115E 04	-0.2658E 06	0.2381E 05	-0.3950E 07	-0.4312E 06

Table C-4. Complex Matrix Inversion Program for 1620

```
    DIMENSION AR(3,3),AI(3,3),BR(3,3),BI(3,3)
    DIMENSION WR(4),WI(4)
  1 DO 2 I=1,3
  2 READ 10,AR(I,1),AI(I,1),AR(I,2),AI(I,2),AR(I,3),AI(I,3)
    Z=-1.
    N=0
 51 N=N+1
    DO 6 J=1,3
    M=0
    K=0
 60 K=K+1
    IF (K-N) 3,61,3
  3 DO 5 L=1,3
    IF (L-J) 4,5,4
  4 M=M+1
    WR(M)=AR(K,L)
    WI(M)=AI(K,L)
  5 CONTINUE
 61 IF (K-3) 60,62,62
 62 CONTINUE
    UR=WR(1)*WR(4)-WI(1)*WI(4)
    UI=WI(1)*WR(4)+WR(1)*WI(4)
    VR=WR(2)*WR(3)-WI(2)*WI(3)
    VI=WI(2)*WR(3)+WR(2)*WI(3)
    Z=(-1.)*Z
    BR(J,N)=Z*(UR-VR)
    BI(J,N)=Z*(UI-VI)
  6 CONTINUE
    IF (N-3) 51,52,52
 52 CONTINUE
    DETR=0.
    DETI=0.
    DO 7 J=1,3
    DETR=DETR+AR(1,J)*BR(J,1)-AI(1,J)*BI(J,1)
  7 DETI=DETI+AI(1,J)*BR(J,1)+AR(1,J)*BI(J,1)
    DO 8 I=1,3
    DO 8 J=1,3
    P=BR(I,J)
    Q=BI(I,J)
    BR(I,J)=(P*DETR+Q*DETI)/(DETR*DETR+DETI*DETI)
  8 BI(I,J)=(Q*DETR-P*DETI)/(DETR*DETR+DETI*DETI)
    DO 9 I=1,3
    PUNCH 10,BR(I,1),BI(I,1),BR(I,2),BI(I,2),BR(I,3),BI(I,3)
  9 PRINT 10,BR(I,1),BI(I,1),BR(I,2),BI(I,2),BR(I,3),BI(I,3)
    GO TO 1
 10 FORMAT (E11.4,1X,E11.4,1X,E11.4,1X,E11.4,1X,E11.4,1X,E11.4)
    END
```

CZ(I)	three-dimensional damping factors in heave
XI(K)	index numbers of the cross-sectional elements
BS(K)	local barge beam widths of the cross-sectional elements
ES(K)	moment arms of the cross-sectional elements referenced to the center of gravity of the barge
ZCB(K)	local centers of buoyancy of the cross-sectional elements measured from the free surface
A42(K)	sectional added moments of inertia in roll due to motion in sway
A33	local added masses in heave due to motion in heave
ZZN	local vertical damping forces per unit vertical velocity of the cross-sectional elements
A22	local added masses in sway due to motion in sway
YYN	local lateral damping forces per unit lateral velocity of the cross-sectional elements

The wave excitation force program for 7094 is presented in Table C-2.

After the data is read in, the program branches to a subroutine where all the required operations including printing and punching of the output are completed. For each wave direction, β, and each wave frequency, ω, the program computes the real A_r and imaginary parts, B_r, of the wave-exciting forces described in Appendix B. The longitudinal and lateral elements are tabulated and punched separately. A sample output is given in Table C-3.

COMPLEX MATRIX INVERSION PROGRAM FOR 1620

This program inverts a 3 by 3 matrix with complex entries. Data is entered on punched cards, the ith card containing six values representing A_{i1}', A_{i1}'', A_{i2}', A_{i2}'', A_{i3}', A_{i3}'', respectively, where the single prime designates the real part and the double prime the imaginary part of the matrix element A_{ii}. The values must be punched in the form prescribed in the statement "10 format."

After the required operations have been performed, the elements of the inverted matrix are printed and punched in the same order and form as the input data.

More than one matrix can be inverted with one loading of the program. After punching and printing the results for one matrix, the program branches back to the beginning and attempts to read three more data cards. Listing is given in Table C-4.

COMPLEX MATRIX MULTIPLICATION PROGRAM FOR 1620

This program multiplies a 3 by 3 matrix by a 1 by 3 matrix with complex entries. After each operation, the resulting matrix is printed on-line and punched on cards. More than one pair of matrices can be multiplied with one loading of the program. After punching and printing the results for one matrix, the program branches back to the beginning and attempts to read four more cards. Listing is given in Table C-5.

Table C-5. Complex Matrix Multiplication Program for 1620

```
      DIMENSION AR(3,3),AI(3,3),XR(3),XI(3),YR(3),YI(3)
    1 DO 2 J=1,3
    2 READ,XR(J),XI(J)
      DO 4 I=1,3
      DO 3 J=1,3
      READ,AR(I,J),AI(I,J)
      YR(J)=XR(J)*AR(I,J)-XI(J)*AI(I,J)
    3 YI(J)=XR(J)*AI(I,J)+XI(J)*AR(I,J)
      ZR=YR(1)+YR(2)+YR(3)
      ZI=YI(1)+YI(2)+YI(3)
      ZR1= ZR*ZR
      ZI1 = ZI*ZI
      RO = SQR  (ZR1 +ZI1)
      PHASE = ATN  (ZR1/ZI1)
    4 PUNCH,ZR,ZI, RO, PHASE
      GO TO 1
      END
```

MOORING FORCE CATENARY PROGRAM FOR 7094

This program computes the horizontal, vertical, and total tension versus the horizontal distance, X, in a mooring chain with an attached sinker, given the following input data:

S1	chain length from the lower mooring point to the sinker
S2	chain length from the sinker to the upper mooring point
W	submerged weight of the sinker
U	submerged unit (per length) weight of the chain
Y	vertical distance from the lower mooring point to the upper mooring point
TO	horizontal component of force in the mooring chain. It may initially be set equal to zero when the upper mooring point is directly above the lower mooring point
TOP	increment in the horizontal component of force in the mooring chain corresponding to increments in the horizontal distance, X, by which the upper mooring point is moved
TEST	absolute error in feet allowed in the iteration scheme

The values must be punched on cards prescribed by the statement "100 format." After the required operations, output data is tabulated in four columns as follows:

X	horizontal distance from the lower to the upper mooring point
TO	horizontal component of force in the mooring chain
TV	vertical component of force in the mooring chain
T	total tension in the mooring chain

A listing is given in Table C-6.

Table C-6. Mooring Force Catenary Program for 7094

```
      DIMENSION H(2)
      CALL FTRAP
    1 READ 100,S1,S2,W,U,Y,DELTA,T0,TOP,TEST
      READ 150, THETA
      WRITE OUTPUT TAPE 6,100,S1,S2,W,U,Y,DELTA,T0,TOP,TEST
  150 FORMAT (F12.8)
  100 FORMAT (9F8.1)
      K=0
      TB=T0
      SP=0
      VP=0
      I=1
      S=0
      V=0
      DS=1
      DV=1
      A=1./U
      XMAX=((S1+S2)**2)-(Y**2)
      XMAX=SQRT(XMAX)
      ADJTE=XMAX-TEST
      GO TO 50
   81 T0=TOP
      K=1
      XB=X
   50 IF (S1-Y) 40,40,31
   31 II=2
      S=SQRT(Y*(2.*T0/U+Y))
      IF (S-S1) 32,33,33
   32 X=T0/U*ELOG(U*Y/T0*(SQRT(1.+2.*T0/U/Y)+1.)+1.)
      X=X+S1-S+S2
      TV=U*S
      T=SQRT(T0**2+TV**2)
      GO TO 201
   33 II=3
      I=3
      S=0
      B=T0**2
      C=U*S1
      D=0
      E=0
      GO TO 15
   40 II=1
      B=T0**2
   11 C=U*S+W+U*S1
      D=U*S+W
      E=U*S
   15 Y1=A*(SQRT(B+(V+C)**2)-SQRT(B+(V+D)**2))
      Y2=A*(SQRT(B+(V+E)**2)-SQRT(B+V**2))
      FRAC=(Y-(Y1+Y2))/Y
      GO TO (3,4,6,16),I
    3 IF (FRAC) 4,12,5
    5 SL=S
      DS=2.*DS
      S=S+DS
      GO TO 11
    4 I=2
      IF (ABSF(FRAC)-.00001) 12,12,10
   10 IF (FRAC) 7,12,9
    7 SU=S
      GO TO 8
    9 SL=S
    8 S=(SL+SU)/2.
      GO TO 11
    6 IF (FRAC) 16,17,21
   21 VL=V
      DV=2.*DV
      V=V+DV
      GO TO 15
   16 I=4
      IF (ABSF(FRAC)-.00001) 17,17,18
   18 IF (FRAC) 20,17,19
   20 VU=V
      GO TO 22
   19 VL=V
   22 V=(VL+VU)/2.
      GO TO 15
   12 IF (S2-S) 14,14,13
   14 S=S2
      I=3
      GO TO 11
   13 DS=S-SP
      SP=S
      I=1
      GO TO 23
   17 DV=V-VP
      VP=V
      I=3
   23 Q=S1**2-Y1**2
      IF (T0) 26, 26 , 25
   25 DO 2 J=1,2
   61 Q=(U/T0)**2*Q
   62 X1=SQRT(Q+4.)
   63 X2=SQRT(Q)
      X=X1*X2
   64 X=(X+Q)/2.+1.
   65 X=T0/U*ELOG(X)
   66 Q=S**2-Y2**2
    2 H(J)=X
   67 X=H(1)+H(2)+S2-S
   60 GO TO 27
   26 X=S2-S
   27 TV=V+C
      T=SQRT(T0**2+TV**2)
   24 IF (W-V) 203,201,201
  203 IF (S) 201,204,201
  204 V=0
      I=1
      GO TO 40
  201 CONTINUE
      HLO =  T0*COS(THETA)
      HLA = T0*SIN(THETA)
      WRITE OUTPUT TAPE 6, 101, X, T0, TV, T, HLO, HLA
  101 FORMAT (6F12.2    )
      IF (K) 81,81,70
   70 IF (X-ADJTE) 71,99,99
   71 X0=X+DELTA
      XA=XB
      TA=TB
      TB=T0
   82 XB=X
      T0=((X0-XA)/(XB-XA))*(TB-TA)+TA
      GO TO (40,31,33),II
   99 GO TO 1
      END
```

DERIVATION OF LINEAR AND ANGULAR DISPLACEMENTS FROM ACCELERATION RECORDS PROGRAM FOR 1620

This program computes the spectra of any pair of linear and angular displacements from the appropriate pair of acceleration spectra and cross-spectra. For example, the spectra of heave and pitch may be determined from the spectra, cospectra, and quadrature spectra of the vertical acceleration measurements recorded from pickups located on the centerline at the bow and stern. For completeness, the mathematic derivation of the heave and pitch spectra from the routine spectra and cross-spectra obtained from the record of vertical accelerations as measures at the bow and stern is given below.

In this example, M_b and M_s denote the vertical displacements of the bow and stern, respectively. Then

$$M_b = z(t) + X_b\theta(t)$$

$$M_s = z(t) - X_s\theta(t)$$

where $z(t)$ is the vertical displacement of the barge due to heave alone, and $X_b\theta(t)$ and $X_s\theta(t)$ are, respectively, the vertical displacement of the bow and stern due to pitch, $\theta(t)$, alone. X_b and X_s are known distances from the pitch point (assumed to be at the CG) to the bow accelerometer and stern accelerometer, respectively. The accelerations, $\ddot{M}_b$ and $\ddot{M}_s$, are

$$\ddot{M}_b = \ddot{z}(t) + X_b\ddot{\theta}(t) \qquad \text{(C-1)}$$

$$\ddot{M}_s = \ddot{z}(t) - X_s\ddot{\theta}(t) \qquad \text{(C-2)}$$

Simultaneous solution of Equations C-1 and C-2 yields

$$z(t) = \frac{X_s M_b + X_b M_s}{\ddot{X}_b + \ddot{X}_s} \qquad \text{(C-3)}$$

$$\theta(t) = \frac{\ddot{M}_b - \ddot{M}_s}{\ddot{X}_b + \ddot{X}_s} \qquad \text{(C-4)}$$

where $\ddot{z}(t)$ and $\ddot{\theta}(t)$ are acceleration in heave and pitch, respectively.

The covariance function, $F(\ddot{z})$, of heave acceleration is

$$F(\ddot{z}) = \sum \frac{\left[X_s \ddot{M}_b(t) + X_b \ddot{M}_s(t)\right]\left[X_s \ddot{M}_b(t+\tau) + X_b \ddot{M}_s(t+\tau)\right]}{\left(X_b + X_s\right)^2}$$

or

$$F(\ddot{z}) = \left(\frac{1}{X_b + X_s}\right)^2 \sum \left[X_s^2 \ddot{M}_b(t)\ddot{M}_b(t+\tau) + X_b^2 \ddot{M}_s(t) M_s(t+\tau)\right.$$

$$\left. + X_b X_s \ddot{M}_s(t)\ddot{M}_b(t+\tau) + X_b X_s \ddot{M}_b(t)\ddot{M}_s(t+\tau)\right] \qquad \text{(C-5)}$$

where τ is the lag used for auto-correlated analysis. $\tau = \rho \Delta t$ where Δt is the time interval between ordinates read from the original record, and ρ is an integer varying from 0 to m (maximum number of lags).

It can be shown that

$$X_b X_s \ddot{M}_s(t)\ddot{M}_b(t+\tau) = X_b X_s \ddot{M}_b(t)\ddot{M}_s(t-\tau) \qquad \text{(C-6)}$$

and further that

$$\sum \left[X_b X_s \ddot{M}_b(t)\ddot{M}_s(t-\tau) + X_b X_s \ddot{M}_b(t)\ddot{M}_s(t+\tau)\right] = 2X_b X_s C_{\ddot{M}_b \ddot{M}_s}(\omega) \qquad \text{(C-7)}$$

where C denotes the cospectra and ω is the frequency. Substituting Equations C-6 and C-7 in Equation C-5 and performing standard transformations as given in Blackman and Tukey (1958, pp 11, 12), the spectrum $S_{z(t)}(\omega)$ of heave acceleration is found to be

$$S_{\ddot{z}(t)}(\omega) = \left[X_s^2 S_{\ddot{M}_b}(\omega) + X_b^2 S_{\ddot{M}_s}(\omega) + 2X_b X_s C_{\ddot{M}_s \ddot{M}_b}(\omega)\right] \frac{1}{\left(X_b + X_s\right)^2} \qquad \text{(C-8)}$$

The spectrum of pitch acceleration, $S_{\ddot{\theta}(t)}(\omega)$, obtained in a similar fashion, is

$$S_{\ddot{\theta}(t)} = \frac{S_{\ddot{M}_b}(\omega) + S_{\ddot{M}_s}(\omega) - 2C_{\ddot{M}_b \ddot{M}_s}(\omega)}{\left(X_b + X_s\right)^2} \tag{C-9}$$

Based on simple harmonic motion, an assumption which seems reasonable, the acceleration spectra are divided by $(\omega^2)^2$ to obtain the displacement spectra of heave, S_z, and rotation of spectra of pitch, S_θ; specifically

$$S_{z(t)} = \frac{1}{\omega^4} S_{z(t)}(\omega) \tag{C-10}$$

$$S_{\theta(t)} = \frac{1}{\omega^4} S_{z(t)}(\omega) \tag{C-11}$$

The same method was used to obtain the spectra of sway and yaw from spectra and cross-spectra of transverse accelerations as measured at the bow and stern.

Dr. W. J. Pierson, Jr., of New York University, assisted in obtaining the above information. It is based on a method given by Cartwright (1957). However, in a more recent publication, Cartwright (1963) states that the final step in obtaining the displacement spectra from the acceleration spectra is probably defective in vigor. He suggests that the acceleration spectra should first be highly resolved by passing them through very narrow-banded filters. The resulting acceleration spectra can then be divided by ω^4 to obtain the displacement spectra.

Input data punched on cards is as follows:

X1	distance from the center of gravity to the forward (or port) accelerometer
X2	distance from the center of gravity to the stern (or starboard) accelerometer
M	number of lags for which computations are to be made
DT	incremental frequency corresponding to the resolution for which computations are to be made
SM1	spectral ordinate of the acceleration record taken at the forward (or port) location
SM2	spectral ordinate of the acceleration record taken at the stern (or starboard) location
C & Q	cospectral and quadrature spectral ordinates, respectively, where SM1 is the driving function and SM2 is the output function

Output data is printed on-line and punched on cards as follows:

W	frequency
HEAVE	spectral ordinate of heave corresponding to frequency, ω
PITCH	spectral ordinate of pitch corresponding to frequency, ω
COSP	cospectral ordinate where heave is the driving function and pitch is the output function
QUAD	quadrature spectral ordinate where heave is the driving function and pitch is the output function

The Fortran listing is given in Table C-7.

Table C-7. Derivation of Linear and Angular Displacements From Acceleration Records Program for 1620

```
      READ, X1, X2, M, DT
      EM=M
      PI= 3.1415927
      COR = 180./PI
      COR = COR*COR
      DIV = 2.0*EM*DT
      FAC = (2.0*PI)/DIV
      DO 1  K= 1, M
      EK = K
      W = (EK*FAC)**4.
      EMUS = X1 - X2
      SUM = X1 + X2
      SUMSQ = SUM**2.0
      DEN = W*SUMSQ
      READ, SM1, SM2, C, Q
      FIRST = X2*SM1
      SECON  = X2*FIRST
      RIF = X1*SM2
      CES = X1*RIF
      EMUL = X1*X2
      HEAVE = (SECON  + CES + 2.0*EMUL*C)/DEN
      PITCH = (SM1 + SM2 - 2.0*C)/DEN
      COSP = (FIRST - RIF + EMUS*C)/DEN
      QUAD = (Q*(-SUM))/DEN
      PITCH = PITCH*COR
      PRINT, W, HEAVE, PITCH, COSP, QUAD
      PUNCH, HEAVE, PITCH, COSP, QUAD
    1 CONTINUE
      PAUSE
      END
```

REFERENCES

Blackman, R. B., and Tukey, J. W. (1958): "The Measurement of Power Spectra from the Point of View of Communications Engineering," Dover Publications, Inc., New York, 1958.

Blagoveshchensky, S. N. (1962): "Theory of Ship Motion," translated from the first Russian edition by Theodor and Leonilla Strelkoff under the editorship of Louis Landweber, Iowa Institute of Hydraulic Research, 2 vol., Dover Publications, Inc., New York, 1962.

Bureau of Yards and Docks, Department of the Navy (1962): "Design Manual - Harbor and Coastal Facilities," NAVDOCKS DM-26, U. S. Government Printing Office, Washington, D. C., 19 February 1962.

Canham, H. J. S., Cartwright, D. E., Goodrich, G. J., and Hogben, N. (1962): "Seakeeping Trials on O. W. S. Weather Reporter," Paper No. 8 of the meeting of The Royal Institution of Naval Architects, 29 March 1962, London, 1962.

Cartwright, D. E. (1957): "On the Vertical Motions of a Ship in Sea Waves," Proceedings of Symposium on the Behavior of Ships in a Seaway, Vol. 1, Netherlands Ship Model Basin, Wageningen, The Netherlands, September 1957, pp. 1-27, 791-799.

Cartwright, D. E. (1963): "The Use of Directional Spectra in Studying the Output of a Wave Recorder on a Moving Ship," Proceedings of Conference on Ocean Wave Spectra, Prentice-Hall, Inc., New York, 1963, pp. 203-218.

Den Hartog, J. P. (1957): "Mechanical Vibrations," McGraw-Hill Book Company, Inc., New York, 1947.

Goodman, N. R. (1957): "On the Joint Estimation of the Spectra, Cospectrum, and Quadrature Spectrum of a Two-Dimensional Stationary Gaussian Process," New York University Engineering Statistics Laboratory, Technical Report No. 8, Nonr (285) 17, March 1957.

Grim, O. (1959a): "Die Schwingungen von schwimmenden, zweidimensionalen Körpern," Hamburgische Schiffbau-Versuchsanstalt Gesselschaft, Report No. 1171, September 1959.

Grim, O. (1959b): "The Hydrodynamic Forces in Roll Research," translated from German by Stevens Institute of Technology, Davidson Laboratory, Note 533, 7 May 1959.

Havelock, T. H., Sir (1956): "The Damping of Heave and Pitch: A Comparison of Two-Dimensional and Three-Dimensional Calculations," Transactions, The Institution of Naval Architects, Vol. 98, No. 4, October 1956, pp. 464-468.

Hogner, Von Einar (1932): "Eine Interpolationsformel für den Wellenwiderstand von Schiffen," Jahrbuch der Schiffenbautechnischen Gesellschaft, Vol. 33, 1932, pp. 452-460.

Hu, Pung Nien (1961): "Lateral Forces and Moments on Ships in Oblique Waves," Stevens Institute of Technology, Davidson Laboratory Report 831, June 1961.

Hu, Pung Nien, and Kaplan, Paul (1962): "On the Lateral Damping Coefficients of Submerged Slender Bodies of Revolution," Stevens Institute of Technology, Davidson Laboratory Report No. 830, February 1962.

Kaplan, Paul (1957): "Application of Slender-Body Theory to the Forces Acting on Submerged Bodies and Surface Ships in Regular Waves," Journal of Ship Research, Vol. 1, No. 3, November 1957, pp. 40-49.

Kaplan, Paul, and Putz, Robert R. (1962): "The Motions of a Moored Construction Type Barge in Irregular Waves and Their Influence on Construction Operation," Contract Nby-32206, an investigation conducted by Marine Advisers, Inc., La Jolla, California, for U. S. Naval Civil Engineering Laboratory, Port Hueneme, California, August 1962 (unpublished).

Kaplan, Paul, and Ulc, Stanley (1961): "A Dimensional Method for Calculating Lateral Bending Moments on Ships in Oblique Waves," Technical Research Group, Inc., Report TRG-147-SR-1, November 1961 (unpublished).

Korvin-Kroukovsky, B. V. (1961): "Theory of Seakeeping," Society of Naval Architects and Marine Engineers, New York, 1961.

Kotik, Jack, and Thomsen, Peter (1963): "Various Wave Resistance Theories for Slender Ships," Schiffstechnik, Bd. 10 Heft 54, 1963, pp. 178-186.

Lamb, Sir Horace (1945): "Hydrodynamics," Dover Publications, Inc., New York, 1945.

Lewis, F. M. (1929): "The Inertia of the Water Surrounding a Vibrating Ship," Transactions, The Society of Naval Architects and Marine Engineers, Vol. 37, 1929, pp. 1-20.

Longuet-Higgins, M. S. (1952): "On the Statistical Distribution of the Heights of Sea Waves," Journal of Marine Research, Vol. XI, No. 3, 1952, pp. 245-266.

National Marine Consultants (1960): "Wave Statistics for Seven Deep-Water Stations Along the California Coast," prepared for Department of the Army Corps of Engineers Districts, Los Angeles and San Francisco, California. Santa Barbara, California, December 1960 (unpublished).

Newman, J. N. (1962): "The Damping of an Oscillating Ellipsoid Near a Free Surface," Journal of Ship Research, Vol. 5, No. 3, December 1961, pp. 44-59.

O'Brien, J. T., and Muga, B. J. (1963): "Sea Tests on a Swing-Moored Aircraft Carrier," Technical Report R-251, U. S. Naval Civil Engineering Laboratory, Port Hueneme, California, March 1963 (unpublished).

O'Brien, J. T., and Muga, B. J. (1964): "Sea Tests on a Spread-Moored Landing Craft," Proceedings of Conference on Coastal Engineering, American Society of Civil Engineers, New York, N. Y., 1964, pp. 765-799.

Pierson, W. J. (1957): "On the Phases of Motions of Ships in Confused Seas," Technical Report No. 9, College of Engineering, Research Division, New York University, 1957.

Pierson, W. J., and Marks, W. (1952): "The Power Spectrum Analysis of Ocean Wave Records," Transactions, American Geophysical Union, Vol. 33, No. 6, Washington, D. C., 1952, pp. 834-844.

Porter, O. J., Urquhart, L. C., McCreary, B. D., and O'Brien, K. H. (1956): "Feasibility Study for Harbor Development, San Clemente Island, California," U. S. Navy Bureau of Yards and Docks, Contract NBy 4226, December 1956 (unpublished).

Prohaska, C. W. (1947): "The Vertical Vibration of Ships," The Shipbuilder and Marine Engine-Builder, October-November, 1947, pp. 542-546, 593-599.

St. Denis, M., and Pierson, W. J. (1953): "On the Motions of Ships in Confused Seas," Transactions, Society of Naval Architects and Marine Engineers, Vol. 61, 1953, pp. 280-357.

Sergius, L. A. (1952): "The Santa Ana," Weatherwise, Vol. 5, 1952, pp. 66-68.

Stoker, J. J. (1950): "Non-Linear Vibrations in Mechanical and Electrical Systems," Interscience Publishers, Inc., New York, 1950.

Thom, H. C. S. (1954): "Frequency of Maximum Wind Speeds," Proceedings of American Society of Civil Engineers, Vol. 80, Separate No. 539, 1954.

Thom, H. C. S. (1960): "Distribution of Extreme Winds in the United States," Paper No. 2433, Journal of the Structural Division, Proceedings of American Society of Civil Engineers, 1960, pp. 11-24.

Tukey, J. W. (1961): "Discussion, Emphasizing the Connection between the Analysis of Variance and Spectrum Analysis," Technical Report No. 41, Department of the Army, Project No. 5B 99-01-004, Princeton, N. J., March 1961 (unpublished).

von Kármán, Th. (1940): "The Engineer Grapples with Non-Linear Problems," Bulletin, American Mathematical Society, Vol. 46, 1940, pp. 615-683.

Vossers, G. (1960): "Fundamentals of the Behavior of Ships in Waves," International Shipbuilding Progress, Vol. 7, No. 65, January 1960, pp. 28-46.

Vossers, G. (1962): "Some Applications of the Slender-Body Theory in Ship Hydrodynamics," The Netherlands Ship Model Basin, Publication No. 214, H. Veenman and Zonen N. V. Wageningen, The Netherlands, 1962.

Wilson, B. W. (1959): "The Energy Problem in the Mooring of Ships Exposed to Waves," Proceedings of Conference on Berthing and Cargo Handling in Exposed Locations, Princeton University, 1958, The Ivy Press, Philadelphia, Pa., 1959, pp. 1-68.

BIBLIOGRAPHY

Bureau of Yards and Docks, Department of the Navy: "Deep Sea Mooring Plan and Typical Moorings Legs and Deep Sea Mooring Details," Drawings No. 896131 and 896132, June 1961 (unpublished).

Dalzell, John F.: "Cross Spectral Analysis of Ship Model Motions: A Destroyer Model in Irregular Long-Crested Head Seas," Report No. 810, Davidson Laboratory, Stevens Institute of Technology, Hoboken, New Jersey, April 1962.

Havelock, T. H.: "The Forces on a Submerged Body Moving Under the Waves," Quarterly Transactions, The Institution of Naval Architects, Vol. 96, No. 2, April 1954, pp. 77-88.

Havelock, T. H.: "The Effect of Speed Advance Upon the Damping of Heave and Pitch," Transactions, The Institution of Naval Architects, Vol. 100, 1958, pp. 131-135.

Holstein, H.: "Untersuchungen an einem Tauchschwingungen Ausführenden Quader," Werft-Reederei-Hafen, 1 December 1936, pp. 385-389.

Jacobs, W. R., Dalzell, J., and Lalangas, P.: "Guide to Computational Procedure for Analytical Evaluation of Ship Bending Moments in Regular Waves," Report No. 791, Davidson Laboratory, Stevens Institute of Technology, ONR Contract Nonr 263-10 DL Proj FX2057, October 1960.

Jasper, N. H.: "Statistical Distribution Patterns of Ocean Waves and of Wave-Induced Ship Stresses and Motions with Engineering Applications," Proceedings of Annual Meeting, New York, The Society of Naval Architects and Marine Engineers, November 1956, pp. 375-415.

Kaplan, Paul, and Hu, Pung Nien: "Virtual Mass and Slender-Body Theory for Bodies in Waves," Proceedings of the sixth Midwest Conference on Fluid and Solid Mechanics, University of Texas, 1959, pp. 183-197.

Korvin-Kroukovsky, B. V.: "Forces Acting on a Submerged Body Moving Under Waves," Experimental Towing Tank, Stevens Institute of Technology, ONR Contract N6onr-24-24704 (unpublished).

Korvin-Kroukovsky, B. V., and Jacobs, W. R.: "Pitching and Heaving Motions of a Ship in Regular Waves," Transactions, The Society of Naval Architects and Marine Engineers, Vol. 65, 1957, pp. 590-632.

Lewis, Edward V., and Dalzell, John F.: "Motion, Bending Moment and Shear Measurements on a Destroyer Model in Waves," Report No. 656, Experimental Towing Tank, Stevens Institute of Technology, April 1958.

Maniar, Naresh M.: "Model Tests of Fishhook Barge," Stevens Institute of Technology, Davidson Laboratory Letter Report No. 1024, Contract NBy-32248 DL Project 2836/479, for U. S. Naval Civil Engineering Laboratory, Port Hueneme, California, May 1964 (unpublished).

Sheehan, Joseph M.: "Behavior of an Anchored C-3 Hull Escort Carrier in Shallow Water Waves," Report 1606, David Taylor Model Basin, Department of the Navy, February 1962.

Walton, Thomas S., and Polachek, Harry: "Calculation of Non-Linear Transient Motion of Cables," Research and Development Report 1279, David Taylor Model Basin, Applied Mathematics Laboratory, Department of the Navy, July 1959.

Wiegel, R. L., Beebe, K., and Dilley, R. A.: "Model Studies of an LSM Moored in Waves," Proceedings of the VIth Coastal Engineering Conference, Berkeley, California, 1957, Engineering Foundation Council on Wave Research, Berkeley, California, 1958, pp. 844-877.